

**Competitive Analysis and Value Proposition of Frozen Silt Mats as an alternative to Crane  
Timber Mats**

by

Ghulam Muhammad Ali

A thesis submitted in partial fulfillment of the requirements for the degree of

Master of Science

in

Construction Engineering and Management

Department of Civil and Environmental Engineering

University of Alberta

©Ghulam Muhammad Ali, 2018

## ABSTRACT

The construction industry is adopting the modular construction paradigm with the integration of heavy crane usage. Because of the weight of the modules that are to be lifted, which currently can reach as much as hundreds of tons, ensuring proper ground integrity under the lifting equipment is paramount since its failure can result in dire consequences for the workers and the project. The traditional method of ground support is to utilize timber or steel mats.

The use of frozen silt (a frozen mixture of water and soil) to prepare crane mats is outside the box idea dispensing with traditional constraints. Artificial ground freezing is a technique used in the construction industry to provide temporary ground support. The mechanical properties of frozen silt are comparable to Coastal Douglas-Fir, but depends upon the temperature attribute. This research contribution aims to investigate the competitive analysis for the use of ice and frozen silt in the form of crane mats to support heavy lifting and hauling. The impact of loading on the crane mats is simulated using ANSYS (FEA platform). Five matting materials (S355, G40.21, Coastal Douglas-Fir, ice, and frozen silt) are investigated using five linear and one non-linear mechanical properties under identical crane loading and boundary conditions.

The required frozen silt mat surface temperature is considered as  $-10^{\circ}\text{C}$  based on the competitive mechanical properties for its practical usage and FEA simulation. The graphical outcome in the form of normal stresses and ground deflection along the crane superstructure slew delivers a conceptual perceptual map for the application of ice and frozen silt in comparison to their traditional competitors (steel and wood). As per FEA simulation, the performance of frozen silt is equal to that of Coastal Douglas-Fir. This similarity promotes the preparation and usage of the frozen silt mat. The conclusion derived from these replications provides a foundation for the estimation of the freezing process in conjunction with ground freezing techniques.

Based on the loading simulations, this contribution also covers the aspects of freezing methods and energy drainage for the mat temperature attainment. The proposed design of the frozen silt mat is integrated with the traditional means of ground freezing, and the freezing process is studied using ANSYS (FEA). Simulation is performed to attain the bottom-up estimate of ground freezing using indirect freezing (brine chillers) and direct freezing (liquid nitrogen). FEA simulation provides the graphical representation of mat freezing with respect to time-lapse using energy equations and viscosity constraints. The outcome from thermal simulation delivers a baseline for the cost estimation for the alternative crane matting solution in the form of capital, operational, and opportunity cost for this novel approach rather than Coastal Douglas-Fir timber mat ground support.

Based on the research presented in this thesis, the frozen silt mat within the assumed constraints offers strong practical value as an environmentally-friendly alternative to crane timber mats and is suitable for the climate of North America with good technical and financial industry benchmarks.

## **Dedication**

This thesis is dedicated to my wife Gulfishan and my two little velociraptors Omer and Mohid for their continuous support from the initial to the final stages of my research.

## **Acknowledgments**

First, I want to thank God for providing me with the strength, thoughts, health, and supportive people needed to finish my research work.

I would like to express my deepest gratitude and sincere appreciation to my supervisors, Dr. Ahmad Bouferguene and Dr. Mohamed Al-Hussein, for their guidance, motivation, immense knowledge, and continuous support throughout the research and writing of this thesis.

My gratitude also goes to Mr. Joseph Kosa of NCSG Crane & Heavy Haul Corporation for helping me in the preparation of the cost estimation and comparison.

## TABLE OF CONTENTS

<b>LIST OF TABLES .....</b>	<b>ix</b>
<b>LIST OF FIGURES .....</b>	<b>x</b>
<b>LIST OF ABBREVIATIONS .....</b>	<b>xv</b>
<b>CHAPTER 1: INTRODUCTION: .....</b>	<b>1</b>
1.1 Research Objective and Scope .....	3
1.2 Thesis Organization.....	5
<b>CHAPTER 2: LITERATURE REVIEW .....</b>	<b>7</b>
2.1. Traditional Method of Calculating GBP under Crane Tracks/Pads.....	8
2.2 Finite Element Analysis for Crane Stability .....	15
2.3. Load Distribution under Mats .....	18
2.4. Allowable Soil Bearing Capacity.....	25
2.5 Finite Element Analysis for Crane Mat Stability. ....	26
2.6 Artificial Ground Freezing (AGF) .....	28
2.7 Practical Approach towards Artificial Ground Freezing.....	31
2.8 Finite Element Analysis for Artificial Ground Freezing (AGF) .....	38
2.9. Basic Definitions for ANSYS Analysis .....	40
2.10 Preliminary Market Research for Ice/Frozen Silt Mat.....	44
<b>CHAPTER 3: RESEARCH METHODOLOGY .....</b>	<b>49</b>
3.1 Problem Statement and selection of FEA .....	49
3.2. ANSYS Solver Usage .....	50
3.3. ANSYS Methodology .....	54
<b>CHAPTER 4: GROUND BEARING PRESSURE AND STRESS ANALYSIS: .....</b>	<b>74</b>
4.1 Ground Bearing Pressure .....	74

4.2. Linear and Non-linear Stress Analysis (ANSYS).....	81
<b>CHAPTER 5: HEAT TRANSFER AND COST ANALYSIS:.....</b>	<b>95</b>
5.1. Conclusion of Mechanical Properties Analysis. ....	95
5.2. Frozen Silt Mat Proposed Design.....	95
5.3. ANSYS Simulation for Frozen Silt Mat (Freezing).....	98
5.4. ANSYS Simulation for Frozen Silt Mat (Thawing).....	106
5.5. Cost Estimation for Indirect Freezing (Brine chiller). ....	108
5.6. Cost Estimation for Direct Freezing (Liquid Nitrogen). ....	113
5.7. Cost Estimation for Timber Mats. ....	115
5.8. Cost Comparison – Traditional Mat versus Frozen Silt Mat .....	115
<b>CHAPTER 6: SUMMARY AND CONCLUSIONS .....</b>	<b>124</b>
6.1. The decision process for artificial ground freezing for heavy cranes .....	124
6.2. Market Approach for Ice/Frozen Silt Mats. ....	124
6.3. SWOT Analysis for New Technology (Frozen Silt Mat for Crane Matting).....	126
6.4. Research Limitations and Assumptions .....	130
6.5. Conclusion.....	131
6.6. Future Research Recommendations.....	133
6.7. Value Proposition for Frozen Silt Mat.....	134
<b>REFERENCES.....</b>	<b>135</b>
<b>Appendix A - Minimum Normal Stress Values for different mat materials Crawler Crane along boom rotation (0° to 90° from Front to Left Rear) .....</b>	<b>148</b>
<b>Appendix B - Minimum Normal Stress Values for different mat materials under Hydraulic Crane along boom rotation (0° to 90° from Rear to Right Front) .....</b>	<b>149</b>
<b>Appendix C – Graphical Representation of Frozen Silt Mat freezing using Brine (30 days) .....</b>	<b>150</b>

**Appendix D - Frozen Silt Mat (Liquid Nitrogen at 10°C Ambient Temperature, 30 days).  
..... 151**

**Appendix E - Frozen Silt Mat (Liquid Nitrogen at 5°C Ambient Temperature, 30 days). 152**

**Appendix F - Frozen Silt Mat (Liquid Nitrogen at 0°C Ambient Temperature, 30 days). 153**

**Appendix G - Cost Estimation for Indirect Freezing (Brine chiller). ..... 155**

**Appendix H - Cost Comparison – Traditional Mat versus Frozen Silt Mat. .... 156**

**Appendix I - Cost Breakeven - Traditional Mat versus Frozen Silt Mat. .... 157**

**Appendix J – Research Path for Ice/Frozen Silt Mat. .... 158**



## LIST OF TABLES

Table 1: Characteristics of LN <sub>2</sub> and brine freezing (Stoss & Valk, 1973) .....	38
Table 2: Major projects in Yellowknife, Dawson Creek, Edmonton, and Fort McMurray.....	46
Table 3: Linear mechanical properties.....	60
Table 4: Non-linear mechanical properties (bilinear isotropic hardening).....	60
Table 5: Thermal properties of materials involved in frozen silt mat thermal process ANSYS analysis.....	64
Table 6: Hypothetical Project Detail (in Numbers) .....	72
Table 7: Crane Configuration for Manitowoc 18000 .....	74
Table 8: Variation of GBP values between Manitowoc, manual, and ANSYS calculation (Manitowoc 18000).....	75
Table 9: The Hydraulic Crane Configuration GMK7550.....	78
Table 10: Minimum Normal Stresses under crane mats along superstructure rotation (0° to 90° from Front to Left Side).....	84
Table 11: Load limit for permanent Coastal Douglas-Fir mat deformation for Crawler Crane. ..	87
Table 12: Graphical Representation of Plastic Deformation of Steel plate under Loading.....	88
Table 13: Minimum Normal Stresses under crane mats along superstructure rotation (0° to 90° from Rear to Right Side).....	92
Table 14: Liquid Nitrogen Velocity for three cases. ....	103
Table 15: Assumed Timber Mat Expenditures (Crawler Crane).....	115
Table 16: Assumed major Cost Figures (\$) for one year (Bottom-up estimation for 8 months at Yellowknife).....	121
Table 17: Perceived Competitive Position of New Research (based on the research in this thesis) .....	126

## LIST OF FIGURES

Figure 1: Contributing factors along fatalities in “Crane Tipped Over” accidents (50). (Adapted from Zhao., 2011) .....	1
Figure 2: Market Research Conducted by Golden Environmental Mat Services in 2014 (Golden Environmental Mat Services, 2015) .....	<b>Error! Bookmark not defined.</b>
Figure 3: Rotating and stationary parts of Crawler Crane and Hydraulic Crane.....	8
Figure 4: Tree diagram for construction site fatalities (Zhao, 2011).....	9
Figure 5: Number of fatality cases and direct causes (Zhao, 2011).....	10
Figure 6: Contributing factors to “Crane tip over” (Zhao, 2011) .....	11
Figure 7: Pressure diagram based on configuration of crane part weights and their respective COGs .....	12
Figure 8: Parameters used for crawler crane GBP calculations.....	13
Figure 9: Parameters used for hydraulic crane GBP calculations.....	14
Figure 10: Three-point loading test for measuring mat strength in bending .....	19
Figure 11: Load distribution under mat (Adapted from David Duerr, 2010).....	20
Figure 12: Graphical representation of effective mat length (liftinglogistics.com, 2017).....	25
Figure 13: Wood description (earlywood and latewood) .....	27
Figure 14: Experimental and finite element load-deflection results (Adapted from Mahamid et al., 2017).....	28
Figure 15: Lateral view of recovery tunnel of the east line (Adapted from Hu and Deng, 2016)	30
Figure 16: Application of artificial ground freezing (Adapted from Moretrench, 2018).....	31
Figure 17: Peripheral artificial ground freezing.....	32
Figure 18: Mass artificial ground freezing.....	33
Figure 19: Schematic diagram of example of mass freezing.....	33
Figure 20: Schematic diagram of indirect freezing (Moretrench, 2018) .....	34

Figure 21: Proposed schematic diagram for primary plant and pumped loop secondary coolant (Moretrench, 2018). .....	35
Figure 22: Proposed schematic diagram for expendable liquid refrigerant (Moretrench, 2018)..	37
Figure 23: Young’s modulus (elastic modulus).....	41
Figure 24: Tensile yield strength .....	41
Figure 25: Compressive strength .....	41
Figure 26: Poisson’s Ratio .....	42
Figure 27: Tangent modulus .....	42
Figure 28: Heat transfer from heat source .....	43
Figure 29: Dynamic viscosity .....	44
Figure 30: Grains of Wood .....	44
Figure 31: Major mines and oil & gas facilities in Canada .....	47
Figure 32: Average monthly ambient temperature (12 months).....	47
Figure 33: Number of days that reach required temperature ( $-10^{\circ}\text{C}$ to $0^{\circ}\text{C}$ ) .....	48
Figure 34: ANSYS problem-solving sequence (ANSYS Mechanical Workbench 17.1).....	51
Figure 35: ANSYS problem-solving sequence (ANSYS Fluid Flow - Fluent).....	53
Figure 36: Bearing length/width and actual length/width of crawler crane track.....	55
Figure 37: Flowchart for crawler/hydraulic crane data flow for crane benchmark .....	57
Figure 38: Traditional versus ANSYS load (compressive stress) distribution under crane tracks	58
Figure 39: Trapezoidal pressure (compressive stress) converted into two parts (Liu et al., 2008) .....	58
Figure 40: Average strength versus temperature relationship for frozen silt in uniaxial compression and tension tests. ....	59
Figure 41: Steel mat (S355 & G40.21-44W).....	61
Figure 42: Test mat (Douglas-fir, ice, and frozen silt) .....	61

Figure 43: Soil properties for mat investigation .....	62
Figure 44: Flowchart for Crane Mat Strength Analysis.....	63
Figure 45: Flowchart for frozen silt mat freezing sequence .....	65
Figure 46: Cost drivers for traditional crane timber mats.....	67
Figure 47: Cost drivers for Frozen Silt Mat (Indirect Freezing).....	68
Figure 48: Cost drivers for Frozen Silt Mat (Direct Freezing). .....	69
Figure 49: Hypothetical Project (Any resemblance with any existing project is coincidence) ....	70
Figure 50: WBS for a Dummy project in Yellowknife, NWT (Timber Mat Use). .....	73
Figure 51: Manitowoc 18000 Model (ANSYS).....	74
Figure 52: GBP (minimum principal stress) values from Manitowoc software (Manitowoc, 2017), manual calculations, and ANSYS simulation calculations on four sides of crawler crane, Manitowoc 18000, along boom slew angle from 0° to 90° from front to left side with load of 50,000 kg (110,231.13 lb) at lifting radius of 25.917 m (85 ft).....	76
Figure 53: GBP (minimum principal stress) values from Manitowoc software (Manitowoc, 2017), manual calculations, and ANSYS simulation calculations on four sides of crawler crane, Manitowoc 18000, along boom slew angle from 0° to 90° from front to left side with load of 75,000 kg (165,346.69 lb) at lifting radius of 21.336 m (70 ft).....	77
Figure 54: GBP (minimum principal stress) values from Manitowoc software (Manitowoc, 2017), manual calculations, and ANSYS simulation calculations on four sides of crawler crane, Manitowoc 18000, along boom slew angle from 0° to 90° from front to left side with load of 100,000 kg (220,462.26 lb) at lifting radius of 19.812 m (65 ft).....	77
Figure 55: Grove 7550 Model in ANSYS Mechanical Workbench.....	78
Figure 56: Pad load values from Grove online application (Grove, 2017) and manual calculations under four outriggers of Grove GMK7550, along boom slew angle from 0° to 360° from rear to right side of crane with load of 40,000 kg (88,185 lb) at lifting radius of 19.812 m (65 ft). .....	79

Figure 57: Pad load values from manual calculations and ANSYS simulation of the four outriggers of the hydraulic crane, Grove GMK7550, along with boom slew angle of 0° to 90° from rear to right side of crane with load of 40,000 kg (88,185 lb) at lifting radius of 19.812 m (65 ft). .....	80
Figure 58: Geometry (crane, load, mat and soil) for analysis.....	81
Figure 59: Normal Minimum Stress under Left Front Mat along with boom slew angle of 0° to 90° from left front to left side (Manitowoc 18000).....	82
Figure 60: Normal Minimum Stress under Left Rear Mat along with boom slew angle of 0° to 90° from left front to left side (Manitowoc 18000).....	82
Figure 61: Left-Front Mat deformation under loading, along boom slew angle of 0° to 90° from left front to left side (Manitowoc 18000).....	83
Figure 62: Steel plate arrangement for permanent deformation example.....	87
Figure 63: Normal Minimum Stress under Right Rear Mat along boom slew angle of 0° to 90° from Right Rear to Right Side (Grove GMK7550) .....	89
Figure 64: Normal Minimum Stress under Right Front Mat along boom slew angle of 0° to 90° from Right Rear to Right Side (Grove GMK7550).....	90
Figure 65: Right Rear Mat deformation under loading. along boom slew angle of 0° to 90° from Right Rear to Right Side (Grove GMK7550).....	90
Figure 66: Proposed Frozen Silt Mat configuration .....	96
Figure 67: Proposed Frozen Silt Mat laying process .....	97
Figure 68: Proposed Frozen Silt Mat Design/layout.....	98
Figure 69: Inlet and Outlet Average Temperature (Brine Solution).....	99
Figure 70: Heat Transfer (Frozen Silt Mat) for Indirect and Direct Freezing .....	100
Figure 71: Mat Surface Average Temperature. ....	101
Figure 72: Heat Removal from Frozen Silt Mat.....	101
Figure 73: Power usage for Ground Freezing.....	102
Figure 74: Liquid Nitrogen Total Flow (L/hr).....	104

Figure 75: Liquid Nitrogen Cumulative Total Flow (L).....	104
Figure 76: Average Mat Surface Temperature (Direct Freezing - Liquid Nitrogen) .....	105
Figure 77: Mat Surface temperature drop at Different Ambient Temperatures (Indirect Freezing/Thawing Process).....	106
Figure 78: Average Mat Surface Temperature at 10°C Ambient Temperature.....	107
Figure 79: Average Mat Surface Temperature at 5°C Ambient Temperature.....	107
Figure 80: Average Mat Surface Temperature at 0°C Ambient Temperature.....	107
Figure 81: Refrigerator Coefficient of Performance (COP) .....	109
Figure 82: Industry Standard for Chiller Efficiency .....	110
Figure 83: Industry Standard for Chiller Efficiency (Adapted from Herbert 2009).....	111
Figure 84: Power usage for the required cooling effect.....	112
Figure 85: Cost Breakdown for Indirect Freezing. ....	113
Figure 86: Cost Estimation for Liquid Nitrogen Use for all three Cases.....	114
Figure 87: Cost Breakdown for Direct Freezing.....	114
Figure 88: Schedule for Brine chiller Frozen Silt Mat (Crawler Crane) .....	117
Figure 89: Schedule for Liquid Nitrogen Frozen Silt Mat (Crawler Crane).....	118
Figure 90: Hybrid System (Liquid Nitrogen and Brine chiller). ....	118
Figure 91: Total Expenditures for seven Case examples (15 years).....	122
Figure 92: Cost Analysis for seven case examples at Yellowknife project (15 years).....	123
Figure 93: Market Segment for New Research.....	125
Figure 94: Load Distribution under Mat.....	131
Figure 95: Normal Stress Distribution under Mats with positive values at the edges.....	132

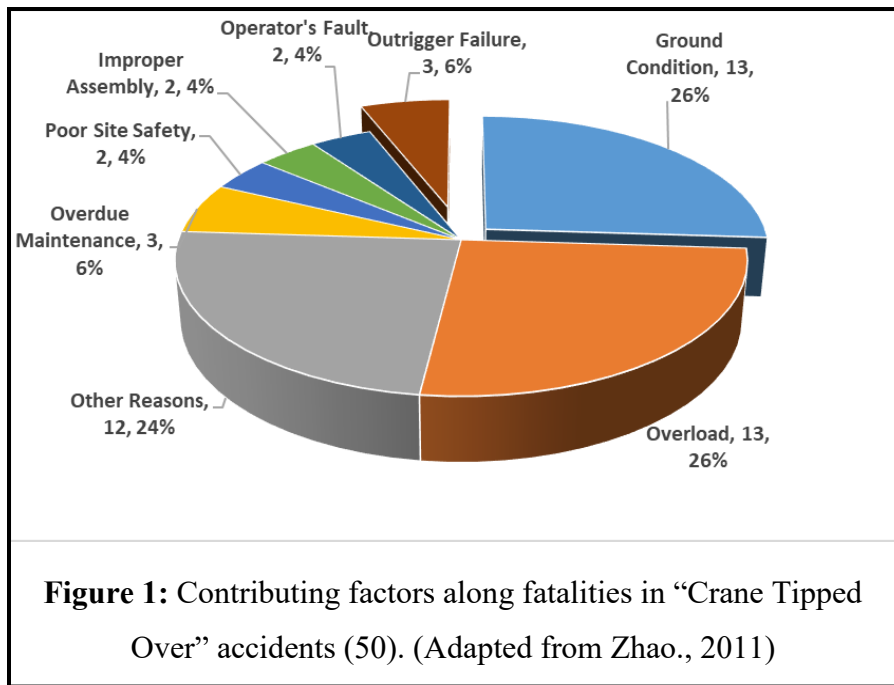
## LIST OF ABBREVIATIONS

AGF	Artificial Ground Freezing
AHRI	Air-Conditioning, Heating, & Refrigeration Institute, USA
ASTM	American Society for Testing and Material
CFD	Computational Fluid Dynamics
CLT	Cross Laminated Timber
COG	Center of Gravity
COP	Coefficient of Performance
FEA	Finite Element Analysis
FS	Factor of Safety
GEMS	Golden Environmental Mat Services
GBP	Ground Bearing Pressure
ISO	The International Organization for Standardization
NCSG	Northern Crane Services Group & Heavy Haul Corporation (mobile crane rental company headquartered in Alberta, Canada).
NDS	National Design Specification
OSHA	Occupational Safety and Health Administration, USA
SWOT	Strength, Weakness, Opportunity and Threats
USRt	US Refrigeration Tonnage = 12,000 BTU/hr
WBS	Work Breakdown Structure

## CHAPTER 1: INTRODUCTION:

The crane manufacturing industry has begun to build heavy cranes due to the fact that the modern heavy construction industry is adopting the concept of modularization to accommodate an increase in the number of heavy and oversized loads to be lifted. The weight of modules has increased from a few metric tons to a few hundreds of metric tons in recent years. With such an increase in weight, the pressure on the ground exerted by the outriggers or the crawler tracks is also amplified thereby making the soil stability a significant high-risk impact factor in the risk matrix. According to the Occupational Safety and Health Administration (OSHA), USA, it is worth noting that from 1997 to 2003 approximately 11% of crane accidents are linked with onsite mobile crane operation. It is also worth noting that approximately 84% of crane/derrick fatalities were of the workers directly related to onsite crane work (Beavers, Moore, Rinehart, & Schriver, 2006).

In another study, according to OSHA, from 2000 to 2009, it was assessed that approximately 12% of fatalities on construction sites were associated with crane work. A total of 587 lives were lost as a result of 571 accidents from crane work during that period, of which 105 were crane operators, 375 were riggers, and eight were signal people. This accounts for about 83% of all the casualties of workers who were linked with crane work. It is estimated that approximately 50 deaths were caused by “Crane Tipped Over”, which is directly connected with poor ground support. Figure 1



presents the contributing factors in detail, underscoring that 13 deaths were due to poor ground conditions (soil settlement) and 3 deaths were from outrigger failure (Zhao, 2011). The cost associated with ground preparation is relatively high, including the direct costs



of the aggregate, compaction, removal of aggregate after the lift, and labor (Shapiro & Shapiro, 2011).

Another widely-used ground support method is using mats under the outriggers or the crawler crane tracks. The competitive advantage is its reusable property, making it superior to the ground preparation. The mats may be comprised of steel or timber. The market for mats is vast. Usually, they are known as access mats. Their major use is to provide ground support for the heavy equipment used in construction and other resource-based activities which may include drilling rigs, camps, tanks, and even helipads. Often, these mats are used as roadways to provide support against unstable and sensitive ground.

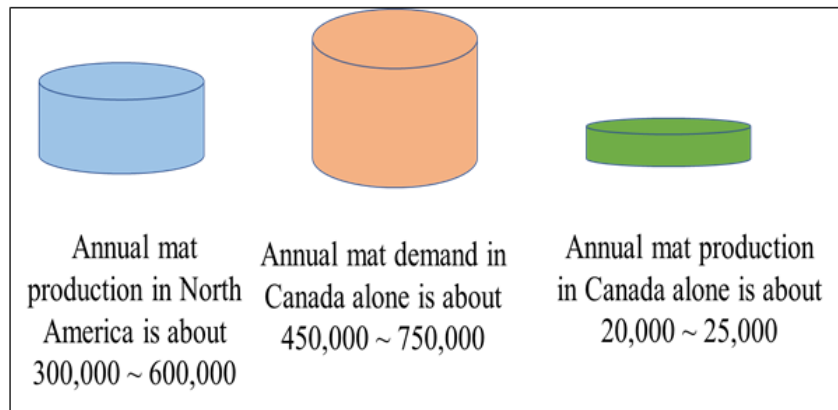


**Figure 2:** Market Research Conducted by Golden Environmental Mat Services in 2014 (Golden Environmental Mat Services, 2015)

Market research was conducted in 2014 by Golden Environmental Mat Services (GEMS) to assess the mat market in Canada for future company growth. According to their market research, in 2014, the total mat demand in Canada alone was approximately 450,000–750,000 mats per annum. Annual mat production in North America in 2014 was approximately 300,000–600,000 mats per annum (see **Error! Reference source not found.**). The number of rig mats produced in Canada in 2014 was approximately 20,000–25,000 mats per annum. Furthermore, in 2004, the industry was small in terms of mats, but the growth was approximately 200% from 2009 to 2014 (Golden Environmental Mat Services, 2015).

The major barrier for customers is the cost of transportation for timber/steel mats. Another difficulty confronted by the mat industry is the durability of timber mats (Golden Environmental Mat Services, 2015).

Inventory management for mats is also a major issue in the mat industry. A significant amount of space is required for stacking and storage of mats, whether at the provider's facility or on a construction site. In general, the mat industry invests significant resources on indirect expenses such as storage space and transportation (Golden Environmental Mat Services, 2015).

Given the costs associated with the ground preparation method and the utilization of mats (steel or timber), the primary objective of this thesis is to develop a novel approach, both technically and financially, toward ground support for heavy mobile cranes in the form of frozen silt or ice.

## **1.1 Research Objective and Scope**

The aim of this research is to develop an alternative solution for ground support for heavy lifting. To achieve this, some guidelines and methodologies are presented in this thesis in order to evaluate the competitive analysis of various mat materials along with ice and frozen silt<sup>1</sup>. The objective is further integrated into the sub-sections based on qualitative and quantitative research analysis:

Discussion about the availability of the market gap which could be fulfilled by using ice/frozen silt mats. The reason behind this approach of using ice/frozen silt mats rather than the traditional method is also discussed in detail. This also covers the qualitative Strength, Weakness, Opportunity, and Threats (SWOT) analysis of new research and its conceptual perceptual status against other methods. Furthermore, the aspects of the Alberta market requirement, where the temperature of the ground and the atmosphere is already at the required stage ( $-10^{\circ}\text{C}$ ) to fabricate these mats without any additional cost, are presented. The objective is to address where and when these mats can be applied for ground support of heavy cranes.

The traditional approach towards ground bearing pressure calculation and mat selection is also explored in this thesis for easy application in comparing the mat performance with respect to different mechanical properties. A brief overview of the conventional measuring approach for Ground Bearing Pressure (GBP) under crawler crane tracks and pad force under hydraulic crane

---

<sup>1</sup> Silt, as a type of soil is a granular material, the size of which is between sand and clay. For ANSYS, the mechanical properties of the frozen silt mats under investigation are taken from the research conducted by Yang, Still, and Ge (2015) on the specimens composed of silt from Campbell Creek Bridge site in Anchorage, AK (seasonally frozen soil) and the CRREL Permafrost Tunnel in Fox, AK (permafrost, frozen for two consecutive seasons). These mechanical properties are assumed within the range provided by Yang et al. (2015). These values are counter checked with the mechanical properties presented in the Master Thesis by Wilson (1982), "Dynamic properties of naturally frozen Fairbanks silt". Details are provided in Section 3.3.2 of the present study.

outriggers is also presented in this thesis. Additionally, the conventional approach for mat selection is discussed to make a case for research in new mat design.

For this research, Finite Element Analysis (FEA) is conducted to evaluate the performance of these mats in a quantitative way. ANSYS workbench version 17.1<sup>1</sup> is used to compare the various mat materials under crane loading. To evaluate these mats, the benchmark for the mobile cranes is developed in ANSYS workbench, and the benchmark is used to build a basis for evaluating the performance of these mats under loading.

Linear and non-linear deformation are observed for these mats under crane loading with the help of ANSYS 17.1 workbench. For linear and non-linear stress analysis, six main mechanical properties (5 linear and 1 non-linear) are compared to develop a competitive and quantitative analysis resulting in GBP and deflection. The key objective of this observation is to predict the requirement of mat thickness for use during crane work. These observations are compared with the traditional mat material results.

Another objective of this thesis is to provide guidelines for the fabrication process of ice/frozen silt mats. The procedures available in the market for ground freezing are discussed along with a brief overview of the equipment required to fabricate ice/frozen silt mats. FEA using ANSYS provides the heat removal requirement in figures (numbers) for the proposed mats. To begin, the energy required for heat removal increases during the freezing phase, but after the freezing phase is achieved, the energy requirement decreases exponentially during the maintenance phase. This research aims to obtain the figures for the freezing phase and the maintenance phase based on conduction from ground/air and radiation from surroundings using FEA.

The decision for adopting these mats can only be evaluated by the cost comparison of the proposed technology to the conventional one. The real figures from the market are difficult to get. As a result, most of the data is assumed in a reasonable and practical way to prepare the quantitative value engineering analysis of this new approach.

Overall, this thesis provides a feasibility report for the use of new technology in the form of ice/frozen silt under mobile cranes in comparison to conventional mats (steel or timber).

---

<sup>1</sup> Finite Element Analysis software.

## 1.2 Thesis Organization

The first chapter (Introduction) covers the problem statement for the use of new research. It also briefly describes the customer challenges for utilizing the conventional method of soil support. The objective of this thesis is discussed in detail in this chapter.

The second chapter (Literature Review) covers the traditional method of calculating the ground bearing pressure under crawler tracks and pad loads under hydraulic crane outriggers. The traditional mat selection criteria and the soil bearing capacity calculation are also presented in this chapter. Usually, the allowable soil bearing capacity value for a construction site is obtained from a geotechnical report. However, a new approach is discussed in this chapter using shallow foundation criteria for the calculations of the allowable soil bearing capacity. This is calculated by using the conservative soil material properties. This chapter also covers the work carried out by several researchers in terms of soil mechanism in relation to crane work. The thermal and mechanical properties are also discussed in this chapter and are used for ANSYS calculations.

The third chapter (Research Methodology) presents the methodology used for the comparison. The first step is to establish a benchmark for crawler and hydraulic cranes. The next step is to develop a methodology for the linear and non-linear stress analysis. The third step is to develop a methodology for the heat transfer. The final step is to develop a guideline for the cost comparison.

The fourth chapter (Ground Bearing Pressure and Stress Analysis) discusses the benchmark for crawler and hydraulic crane ground bearing pressure as per the methodology described in Chapter 3. It provides a base for the mat strength analysis under crane loading. Additionally, this chapter presents case studies under linear and non-linear stress distribution, and also covers the deformation of mat/ground during crane superstructure rotation using ANSYS 17.1. The outcome of Chapter 4 is the comparison between different mat materials under crane loading.

The fifth chapter (Heat Transfer and Cost Analysis) involves the calculations for the energy required for the preparation of frozen silt mats. This chapter estimates the heat transfer for water/silt phase change and outlines the heat addition from the surroundings and the ground to the ice/frozen mats. This chapter also discusses the cost comparison of the frozen silt mats with the conventional soil stabilization techniques and traditional mats. The processes of indirect and direct freezing form the basis of this comparison.

The sixth chapter (Summary and Conclusion) provides a conclusion, key contributions, research limitations, market approach, SWOT analysis, recommendations, and value proposition.

## CHAPTER 2: LITERATURE REVIEW

The main theme of this chapter is to compile the research material regarding crane ground support and use of FEA. To provide some background, the working of the crane and its impact on the ground are first presented. This chapter covers an introduction to the traditional method of calculating the ground bearing pressure under crawler tracks and pad loads under hydraulic crane outriggers. Crawler crane calculations differ from those of hydraulic crane. For crawler cranes, the pressure under the crawler track is obtained using mathematical modelling. On the other hand, the calculations for the hydraulic crane is based on the pad loads. These pad loads are used to calculate the pressure under the outrigger mat based on the surface area and material used for the manufacturing of the crane mat.

Furthermore, the traditional mat selection criteria and the soil bearing capacity calculation are also discussed in this chapter. There are many ways to calculate the suitability of a crane mat, of which two or three aspects of mat selection are observed and used in practice. A brief description of these parameters is presented in this chapter. For soil bearing capacity, in practice, calculations are carried out by the direct<sup>1</sup> or indirect<sup>2</sup> method (Eslami & Gholami, 2005). Onsite, the allowable soil bearing capacity is usually obtained from a geotechnical report prepared by a geotechnical company. The soil bearing capacity calculations are discussed in this chapter, using shallow foundation criteria for the calculations of the allowable soil bearing capacity, which is prepared by using the conservative soil material properties. This chapter also presents various research on soil mechanism in relation to crane works.

This chapter also provides details of mechanical properties used for ANSYS analysis, including five linear mechanical properties and one non-linear property, for the purposes of comparing the response of different mat materials under crane loading with the same parameters.

The heat transfer parameters are also discussed in this chapter. Heat transfer parameters are used for the freezing of silt and are required to calculate the heat removal from silt to make it workable as crane ground support. The thermal analysis of frozen silt mats is conducted using ANSYS Fluent.

---

<sup>1</sup> Cone penetration test.

<sup>2</sup> Friction angle and undrained shear strength calculations.

The final section of this chapter is based on the metrological data of four major mining and oil & gas hubs in North America. The main objective of this data is to analyze the available opportunity for the use of these mats. The average monthly ambient temperature of these four locations (Edmonton, Fort McMurray, Dawson Creek, and Yellowknife) is presented in the form of line charts and bar charts. Major mines and oil & gas E&P are located near these four locations. The outcome is a measurement of the number of days this new technology can be used.

## 2.1. Traditional Method of Calculating GBP under Crane Tracks/Pads

Cranes are used to lift heavy and large objects and move them to their required location. The history of the crane can be dated back to Greek architecture. The process of hoisting and lifting was based on the compound pulley system (Coulton, 1974). The modern era of mobile cranes was invented by William Smith Otis. He invented a steam-powered device to carry out excavation during railroad construction in 1837. Steam-powered excavators performed in a similar manner to

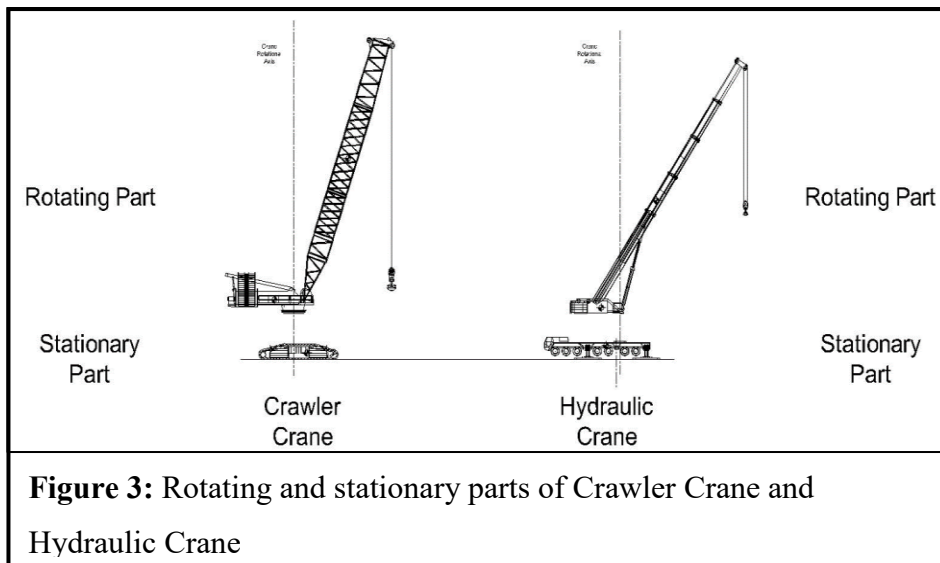


**Figure 3:** Rotating and stationary parts of Crawler Crane and Hydraulic Crane

digging with a shovel. This invention gave birth to the concept of mobile cranes (Stueland, 1994).

In general, there are two types of mobile cranes, crawler cranes and hydraulic cranes, both of which are composed of two

major parts, a moving part (superstructure) and a stationary part (carrier). For crawler cranes, the crane is supported by crawlers; and in the case of hydraulic cranes, the outriggers are used to support the crane (see Figure 3).

A significant amount of academic research has been conducted on crane selection for heavy industrial construction projects (Rodriguez-Ramos & Francis, 1983; Hornaday, Haas, O'Connor, & Wen, 1993; Dharwadkar et al., 1994; Lin & Haas, 1996). Al-Hussein, Alkass, and Moselhi

(2005) developed an algorithm for the onsite selection of mobile cranes as well as the optimization of onsite mobile crane location based on its coordinates for the purpose of obtaining the optimal solution and avoiding any obstacles while remaining within acceptable safety parameters. The database for this algorithm was developed by Al-Hussein, Alkass, and Moselhi (2000), and contains details of various mobile cranes, including crane lifting configurations and respective lifting capacity charts (load charts).

Research in the field of crane selection advanced with the advent of 3D simulation, which provides an enhanced visualization of the actual lift on site (Han, Bouferguene, Al-Hussein, & Herman, 2017; Al-Hussein, Niaz, Yu, & Kim, 2005). Wu, Lin, Wang, and Gao (2011) established a 3D graphical simulation module integrated with crane selection, rigging, and ground bearing pressure. Olearczyk, Lei, Ofrim, Han, and Al-Hussein (2015) included obstacle management within the crane selection algorithm to be shown in 3D visualization; in their study, 3D visualization-based motion planning was presented to optimize crane operation with various design changes. These selection and optimization techniques are based on calculations and path planning algorithms (Olearczyk, Lei, Ofrim, Han, & Al-Hussein, 2015).

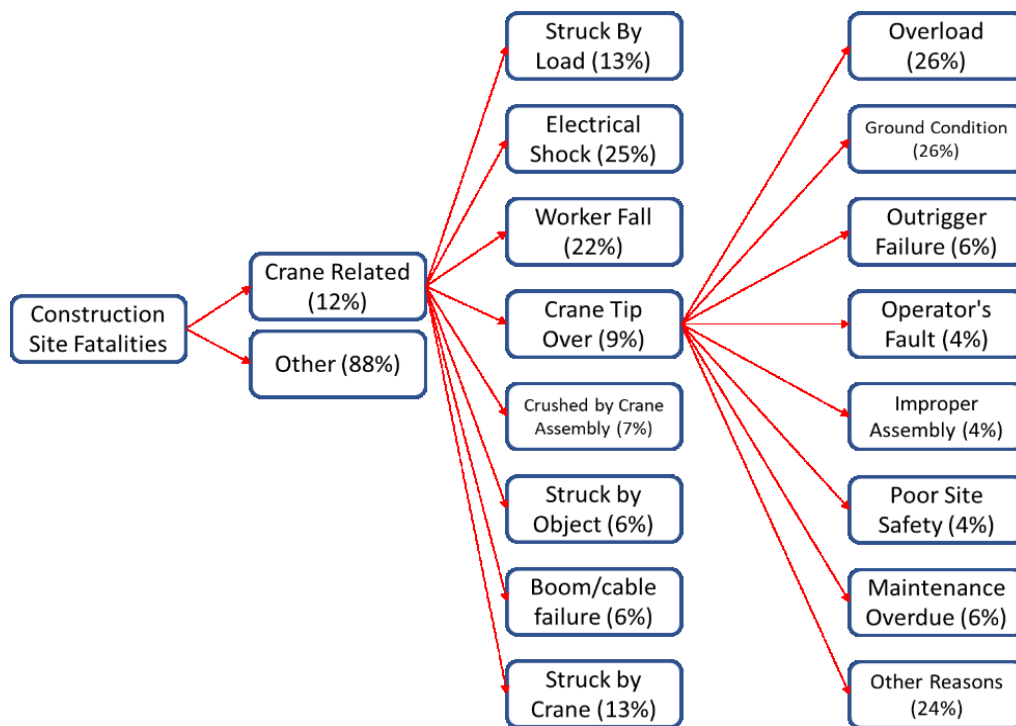


**Figure 4:** Tree diagram for construction site fatalities (Zhao, 2011)



Upon completion of selecting the proper crane and determining the optimized path, the next step is ensuring the stability of the crane during lifting. Most crane-related accidents are related to soil stability (see Figure 1). To address the soil problem, a proper calculation of ground bearing pressure exerted by the crane on the ground must be conducted. In 2001, according to OSHA, the fatality rate of the construction industry (US) reached 13.3 fatalities per 100,000 construction workers. In the case of mobile cranes/derricks, it is estimated that approximately 84% of fatalities are linked with mobile cranes (Beavers et al., 2006). According to OSHA (USA), during the period of 2000 to 2009, approximately 12% of fatalities on construction sites were related to crane work; of 571 accidents, approximately 587 fatalities occurred due to crane work during that period, of which 105 were crane operators, 375 were riggers, and 8 were signal people. Based on these statistics, approximately 83% of all construction site crane related casualties are of workers related to crane work. More specifically, approximately 178 (31.17%) accidents occurred due to being struck by load/object or caught in/between equipment, 140 (24.52%) incidents were related to electrical shock, 126 (22.07%) incidents covered worker falls, and approximately 50 (8.76%) incidents were related to crane tipping. These fatality details are provided in Figure 4 and Figure 5 (Zhao, 2011).

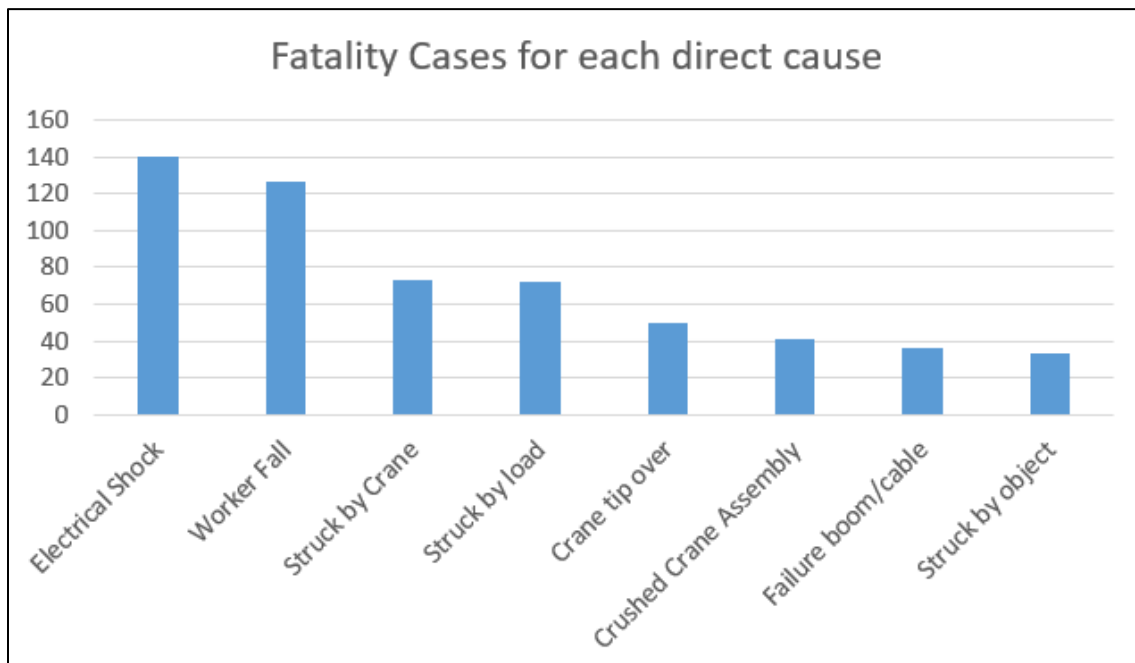
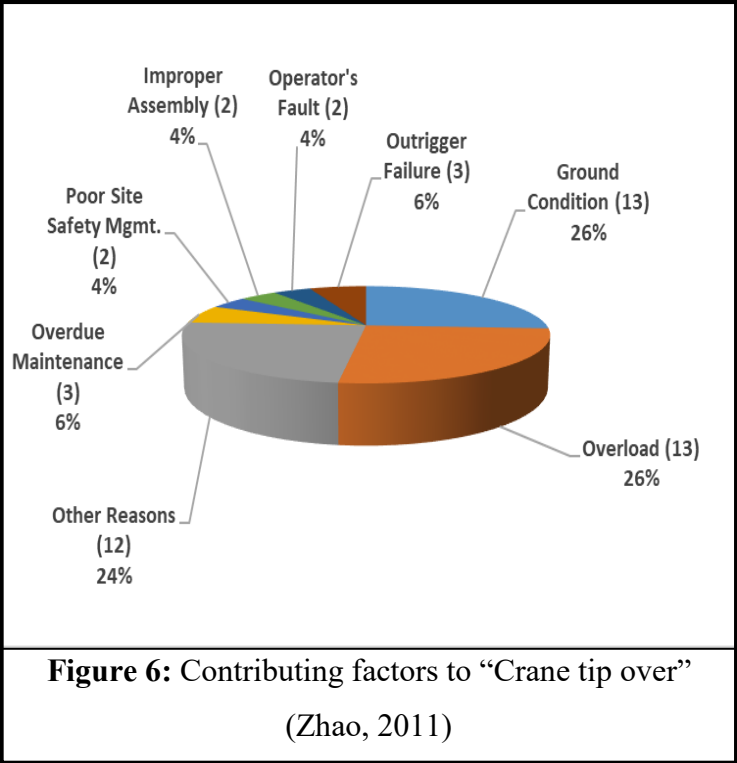


**Figure 5:** Number of fatality cases and direct causes (Zhao, 2011)

The various factors that contribute to the cause of “Crane tip over” are presented in Figure 6. It is clear from the Figure 6 that approximately 13 incidents took place due to poor ground conditions. This is directly related to the calculations of crane stability over available ground conditions. The calculations for allowable ground bearing pressure under mobile cranes are vital to avoid fatal incidents on site.



The modern heavy construction industry is increasingly adopting

modularization as its primary design and project delivery paradigm. One vital reason for this transition is the possibility of shifting a major portion of the work from the construction site to an indoor environment. In this context, projects are broken down into elements (known as modules) that are fabricated independently in a controlled environment, leaving a single activity to be carried out on the construction site, namely the assembly of these modules. Because indoor fabrication can be viewed as a variation of manufacturing, several of the production systems developed for the latter could easily be applied to the fabrication of modules. As a result, the designing and fabricating of modules has become an efficient operation that has encouraged engineers to front-load these modules with an increasing number of functionalities in order to minimize onsite work. On the other hand, the maximizing of functionalities of a module results in a significant increase in weight, from a few tons in past decades to tens if not hundreds of tons in recent years. With the emergence of this new weight constraint, a new generation of lifting equipment characterized by their high capacity has been developed. However, this high capacity is synonymous with increased structural complexity and heavier weights. On construction sites, to ensure that cranes can operate safely, the first order of business is to ensure that the bearing capacity of the ground can accommodate the pressure due to the compounded weights of the crane and the payload.

The traditional method of calculating ground bearing pressure under the crawler/outriggers is based on the methodology where the loads are taken as static forces acting on the ground by the supports in the form of outriggers or crawlers. The carrier has a fixed Center of Gravity (COG), but the COG of the superstructure moves based on the lifting radius, the angle of the boom, and the rotation of the boom. Shapiro and Shapiro (2011) presented the calculations covering all crane weights and their COGs (Shapiro & Shapiro, 2011). Several GBP calculation software programs are available in the market based on these equations (Al-Hussein et al., 2000; Al-Hussein et al., 2005; Manitowoc, 2017; Grove, 2017).

### 2.1.1. Crawler Crane

For the GBP calculations, the key factors include the weights of the stationary and rotating parts of the crawler crane and their COGs. The pressure under the track along the track length may vary from trapezoidal to triangular (see Figure 7) based on the configuration of the part weights and their respective COGs.

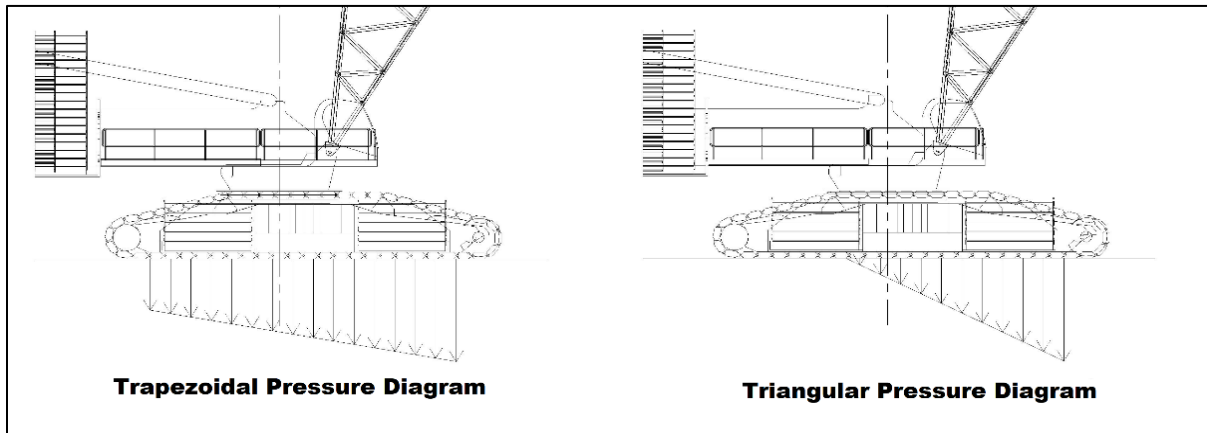


**Figure 7:** Pressure diagram based on configuration of crane part weights and their respective COGs

According to Shapiro and Shapiro (2011), if the sum of the vertical load,  $V$ , and rear moment,  $f_r$ , is greater than front moment,  $f_f$ , the pressure diagram is trapezoidal; and if the sum is less, then the pressure diagram is triangular (Hasan, Al-Hussein, Hermann, & Safouhi, 2010; Shapiro & Shapiro, 2011).

The values of vertical load, rear moment, and front moment can be calculated as:

$$V = \frac{W_c + W_u + W_b + W}{2wd_l} \quad (1)$$

$$f_f = \frac{3((W_b d_b + W d + W_u d_u) \cos \alpha + (W_c + W_u + W_b + W) x_0 + W_c d_c)}{w(d_t)^2} \quad (2)$$

$$f_r = \frac{(W_b d_b + W d + W_u d_u) \sin \alpha}{w d_t} \quad (3)$$

where  $W_c$  = weight of carrier;  $W_u$  = weight of superstructure;  $W$  = weight of payload;  $W_b$  = weight of boom;  $d_c$  = horizontal distance of COG of carrier to the crane rotational axis (positive towards front);  $d_u$  = horizontal distance of COG of superstructure to the crane rotational axis (positive towards front);  $d$  = the lifting radius;  $d_b$  = horizontal distance of boom's (and boom accessories') COG to the crane rotational axis (positive towards front);  $x_0$  = distance between centerline of tracks and the crane rotational axis (positive towards front);  $d_t$  = the bearing length of the track;  $d_t$  = distance between the tracks centerlines;  $w$  = bearing width of the track; and  $\alpha$  = the angle of boom slew from the front to the left side (see Figure 8).

In cases where the pressure diagram is trapezoidal, Equations (1) to (3) can be used to calculate the GBP on the four sides of the tracks as:

$$GBP_{left\ front} = V + f_r + f_f \quad (4)$$

$$GBP_{left\ rear} = V + f_r - f_f \quad (5)$$

$$GBP_{right\ front} = V - f_r + f_f \quad (6)$$

$$GBP_{right\ rear} = V - f_r - f_f \quad (7)$$

In cases where the pressure diagram is triangular,

$GBP_{left\ rear} = 0$  and  $GBP_{right\ rear} = 0$ . The pressure on the left front and right front shall be:

$$GBP_{left\ front} = \frac{(W_c + W_u + W_b + W) d_t + 2((W_b d_b + W d + W_u d_u) \sin \alpha)}{w d_t} \quad (8)$$

$$GBP_{right\ front} = \frac{(W_c + W_u + W_b + W) d_t - 2((W_b d_b + W d + W_u d_u) \sin \alpha)}{w d_t} \quad (9)$$

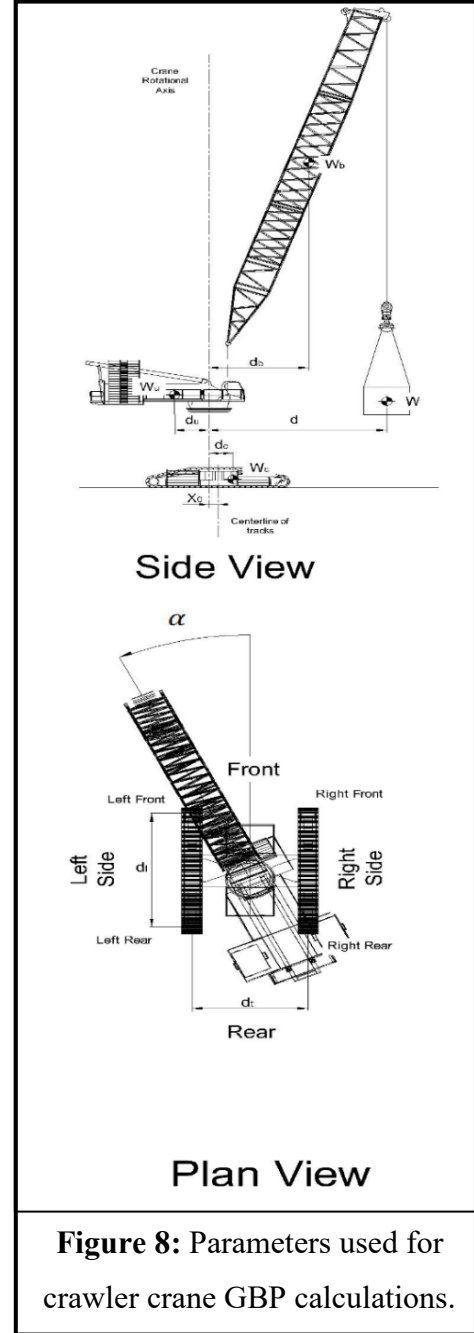


**Figure 8:** Parameters used for crawler crane GBP calculations.

where,

$$l = 1.5d_l - \frac{3((W_b d_b + W d + W_u d_u) \cos \alpha + (W_{cr} + W) x_0 + W_c d_c)}{W_{cr} + W} \quad (10)$$

The pressure variation is taken trapezoidal or triangular along the length of the track (Hasan et al., 2010; Shapiro & Shapiro, 2011). It is clear that the pressure diagram along the width of the crawler will also be trapezoidal in nature; but, for calculation purposes, it is considered uniform as the pressure variation is too small.

### 2.1.2. Hydraulic Crane

The GBP calculation for hydraulic cranes is rather simple and differs from crawler cranes. For crawler cranes, the pressure under the tracks area is calculated. However, for hydraulic cranes, outrigger loads in the form of forces under the outriggers are calculated. The surface area of the outrigger mat is used to calculate the GBP exerted by that outrigger. The reaction force under the outriggers are calculated using the following equations (see Figure 9):

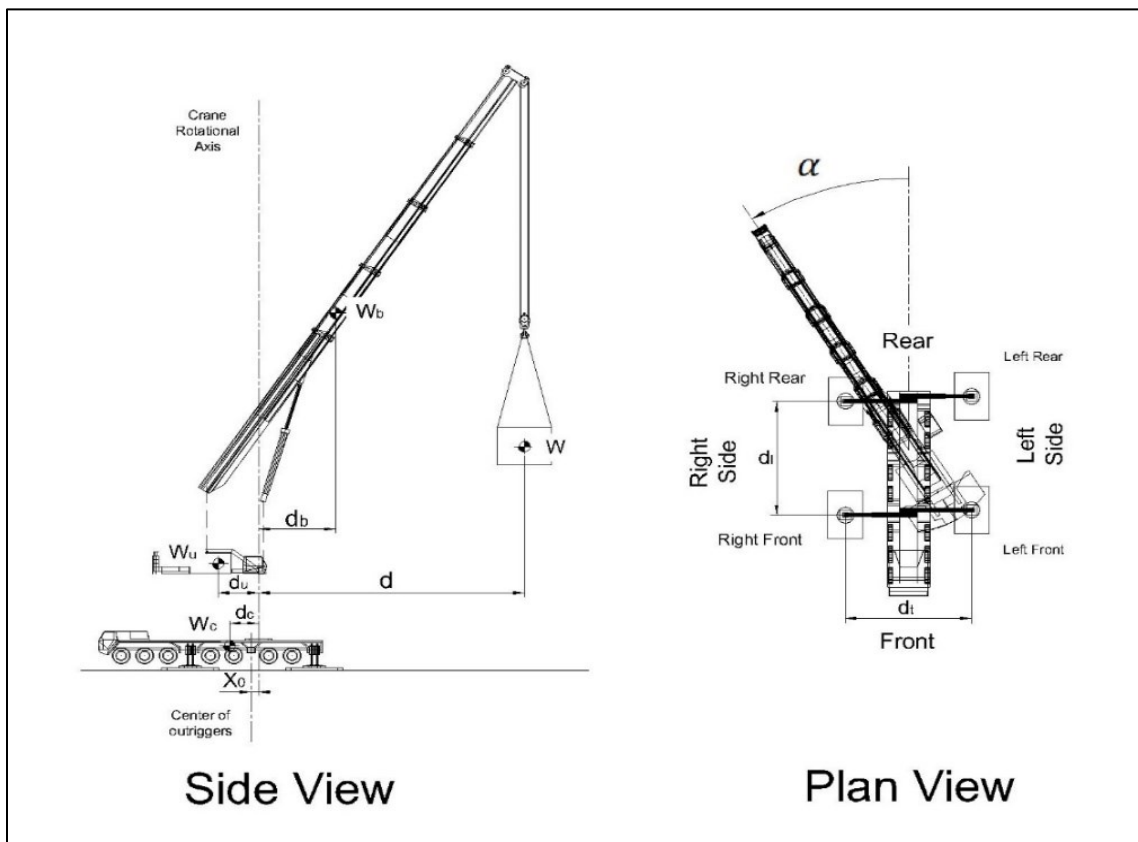


**Figure 9:** Parameters used for hydraulic crane GBP calculations.

$$R_{(right\ front)} = \frac{W_c+W_u+W_b+W}{4} + \frac{1}{2} \left( \frac{(Wd+W_u d_u)\sin\alpha}{dt} - \frac{(Wd+W_u d_u)\cos\alpha+(W_c+W_u+W_b+W)x_0+W_c d_c}{dl} \right) \quad (11)$$

$$R_{(left\ front)} = \frac{W_c+W_u+W_b+W}{4} - \frac{1}{2} \left( \frac{(Wd+W_u d_u)\sin\alpha}{dt} + \frac{(Wd+W_u d_u)\cos\alpha+(W_c+W_u+W_b+W)x_0+W_c d_c}{dl} \right) \quad (12)$$

$$R_{(right\ rear)} = \frac{W_c+W_u+W_b+W}{4} + \frac{1}{2} \left( \frac{(Wd+W_u d_u)\sin\alpha}{dt} + \frac{(Wd+W_u d_u)\cos\alpha+(W_c+W_u+W_b+W)x_0+W_c d_c}{dl} \right) \quad (13)$$

$$R_{(left\ rear)} = \frac{W_c+W_u+W_b+W}{4} - \frac{1}{2} \left( \frac{(Wd+W_u d_u)\sin\alpha}{dt} - \frac{(Wd+W_u d_u)\cos\alpha+(W_c+W_u+W_b+W)x_0+W_c d_c}{dl} \right) \quad (14)$$

where  $W_c$  = weight of carrier;  $W_u$  = weight of superstructure;  $W$  = weight of the load;  $W_b$  = weight of boom;  $d_c$  = horizontal distance of COG of carrier to the crane rotational axis (positive towards front);  $d_u$  = horizontal distance of COG of superstructure to the crane rotational axis (positive towards front);  $d$  = lifting radius;  $d_b$  = horizontal distance of boom's (and boom accessories') COG to the crane rotational axis (positive towards front);  $x_0$  = distance between centroid of outriggers and the crane rotational axis (positive towards front);  $d_l$  = distance between outriggers lengthwise (center to center);  $d_t$  = distance between the outriggers widthwise (center to center); and  $\alpha$  = angle of boom slew from rear to the right front (Hasan et al., 2010; Shapiro & Shapiro, 2011). Furthermore, the pressure is considered to be uniformly distributed under the mats.

## 2.2 Finite Element Analysis for Crane Stability

Cranes as critical construction machinery in heavy construction; as such, the finite element analysis (FEA) of crane structure is not new. The advent of FEA software provided a method to easily analyze the stability of a crane under load. Significant research has been conducted on full-range FEA for the boom structure. Crawler cranes are used to lift heavy loads, so the analysis under static and dynamic loading remains abstract for the researchers. The boom under dynamic loading can lead to crane instability. The change in structure equilibrium can lead to buckling. Many researchers have taken buckling analysis as their main research theme. Some procedures were adopted to analyze the buckling of crane boom structure. Researchers often begin with the linear stability approximation before adding non-linear terms (Anlin, Tao, Yaning, & Fei, 2012). Tower cranes are also investigated for dynamic loading. Static design for large mechanical structures enters the dynamic region when dealing with moving payload under different forces. Fatigue damage is very common. Finite element analysis can be used to evaluate the dynamic loading on a tower crane. The mechanical part under investigation can be loaded with the different

actual site conditions to simulate the behavior. It can reduce the impact of crane failure on site (Yang, Jianzhi, & Junjun, 2011). Mobile cranes are not only crawler crane, but hydraulic cranes also. The stability of telescopic boom of the truck crane (hydraulic crane) can also be monitored in finite element analysis. The research was done to analyze the stability of hydraulic boom under loading (Zhang, Jin, & Zaho, 2013). The manual calculated value was compared with the FEA method. Buckling of the telescopic boom was observed using finite element analysis. The critical values of linear and non-linear buckling were compared using ANSYS. The outcome of the research was that the structural stability of hydraulic boom decreases substantially with the increase in boom length. That is the reason the capacity of crane decreases in an abrupt way with the increase in boom length. Zhang, Jin, and Zaho (2013) recommended that the results from their research can solve the non-linear hydraulic telescopic boom buckling problems on construction site.

FEA was also used to analyze the use of a combinatorial jib<sup>1</sup> on a portal crane. The research conducted by Zhao and Tong (2010) argued that the functionality and efficiency of the combinatorial jib system can be improved using FEA to design a lightweight combinatorial jib section with good reliability (Zhao & Tong, 2010). The same research was further expanded by Zhao et al. (2015) for the design of a lightweight combinatorial jib using FEA<sup>2</sup> (Zhao, Zhao, Li, & Zhao, 2015).

The stability of internal crane parts was also analyzed using FEA. For example, the buckling stability of cable drum on a crane was analyzed using the finite element method and Euler Distribution forces, which reflects realistic loading. The research provided a comparable result to initiate optimized stable design. The stability of the cable drum was investigated using Euler distribution by building a model in FEA<sup>3</sup> and applying respective boundary conditions in the form of forces and angular moment (Qiyu, Yixiao, & Yang, 2016).

Interestingly, FEA can be incorporated into a 3D simulation of crane lifting work. The stability of different parts of the crane can be studied using FEA during a simulated lift. Wu, Wang, Lin and Wang (2008) developed a 3D simulation system which incorporated FEA simulation into the

---

<sup>1</sup> Combinatorial Jib is a combination of different standard jib sections to make one supporting structure.

<sup>2</sup> MATLAB software was used for the finite element analysis.

<sup>3</sup> ANSYS

lifting simulation. The main purpose of their study was to observe the material mechanical properties during lifting and tailing. The developed integrated system was helpful to the site workers to simulate the lift in advance in order to verify and validate the lifting plan based on the site conditions. The main usage of their proposed system is to simulate the impact of forces on the lifting lugs/trunions during lifting/tailing. Additionally, the mechanical properties of lifting accessories can be analyzed under simulated loads, which can identify the weak points in crane lifting. Usually, the stability of rigging accessories are only considered under static loading, but in reality the dynamic loading plays an important role in the failure of rigging accessories (Wu, Wang, Lin, & Wang, 2008).

Unfortunately, few studies have been conducted on the GBP calculations under crawler or hydraulic crane using FEA. In fact, little if any research work incorporating the use of ANSYS for the calculations of GBP under crawler/hydraulic cranes has been carried out to date.

However, the research conducted by Liu, Chan, and Gerbrandt (2008) regarding the calculations of soil bearing capacity for crawler cranes should be noted. According to their study, the soil type and the configuration of crane and mat determines soil capacity for the safe usage of the crane. Calculating from the soil bearing capacity equations only provides a conservative design criteria. One of the soil bearing capacity equations is discussed in later sections of this chapter (Section 2.4). Liu et al. (2008) performed computer simulation using 2D finite difference program<sup>1</sup> and later compared it with field studies using crane and soil deflection due to loading. Using the standard Factor of Safety (FS) of 2 or 3 for the traditional calculations of soil bearing capacity can be misleading in case of crane usage due to load variation and mat configuration. Liu et al. (2008) proposed a new method to calculate the soil bearing capacity under crawler tracks based on the soil type, crane and mat configuration. The field values were used to propose the modification of the traditional soil bearing capacity equations to make it comparable to the computer simulation. The soil types used in their investigation included (1) sand and gravel, (2) soft and medium clay, and (3) stiff clay. The field study deflection values were used to calculate the soil bearing capacity and corresponding ground bearing pressure under the crawler crane track. However, the proposed method by Liu et al. (2008) cannot be used for problematic soil like sensitive clay, loose sand, etc. The moisture content can also impact the results from this proposed method (Liu, Chan, &

---

<sup>1</sup> FLAC4.0



Gerbrandt, 2008). To avoid the gap between field values and the simulation values, the research presented in this thesis uses the material properties to compare within similar boundary conditions. The comparison in this thesis provides the competitive position of ice/frozen silt with respect to other mat materials case by case rather than calculating them individually using complex mat stability equations and material properties.

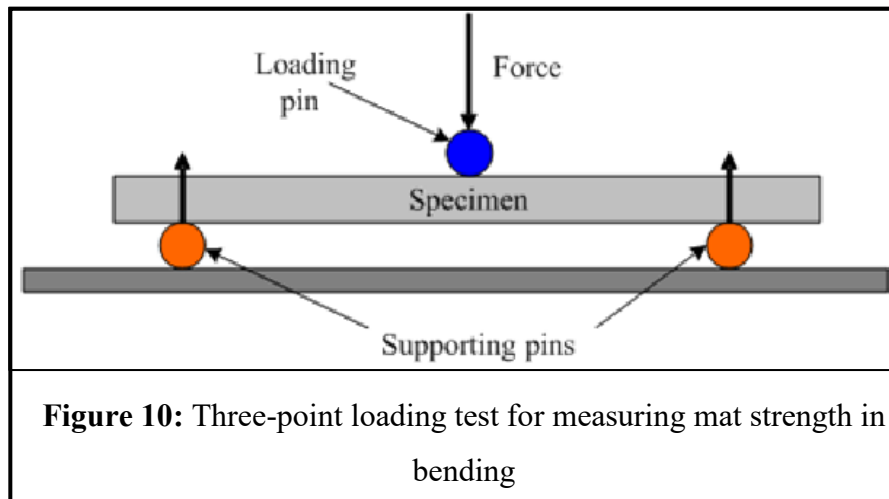
Another interesting study was conducted by Lin et al. (2017) to determine the distribution of mobile crane loads under outrigger. According to their study, area preparation is required to place the crane at the lifting location, and is carried out using the rule of thumb due to the non-availability of actual load distribution under the hydraulic mat. The experimental data was calculated using the traditional method of calculating the load distribution. Furthermore, the investigation was performed using a 2D axisymmetric model through FEA. The outcome of their study indicated that the traditional method can be used considering the outrigger mat as rigid with the increment of 10% (Lin et al., 2017).

### **2.3. Load Distribution under Mats**

Engineers in the crane industry use many different approaches to design and calculate the strength of crane mats (timber/steel). In Section 2.1, the calculated GBP values are used to design the crane supporting mat. Shapiro and Shapiro (2011) provide a guideline for the selection of mats. If the allowable soil bearing capacity is lower than the calculated crane loading, crane mats are used for stabilizing and distributing the load on the ground. In this way, the force exerted by the crane is distributed in such a way as to not exceed the allowable GBP of soil. If the ground bearing pressure exerted by the crane is greater than the allowable soil bearing pressure, the pad will press the ground, which will result in crane tipping. To avoid this, crane rental companies use crane mats (Shapiro & Shapiro, 2011). The main concern is the dynamic loading caused by load movement. This load movement may be the result of wind or the rotation of the superstructure. A simplified method of calculating the simulated dynamic loading was formulated by Zaretsky and Shapiro (1997). The developed system uses linear optimization to calculate the dynamic loading (Zaretsky & Shapiro, 1997).

The major use of timber beside crane matting is for Timber bridges. It includes stringer bridges, timber mats, modular timber truss bridges and stress-laminated deck bridges. These bridges are

typically designed to last 40 to 45 years. One of the advantages of timber bridges is that they can often use local material for the construction. Research was conducted in 1995 to design a portable timber mat bridge, which can be used as per the site requirements on a temporary basis (Taylor, Keliher, Thompson, Ritter, and Murphy, 1995). Many research studies have been conducted to evaluate the comparative performance of timber bridges and the strength of timber mats (Gutkowski & McCutcheon, 1987). B-Jahromi, et al. (2006) presented research which deals with the analysis of the type of cross-section on the strength of the timber beams. In their study, a



comparison was made between static and dynamic loading, and as a result, the boxed I-beam was determined to be the most efficient (B-Jahromi et al., 2006).

In terms of timber mats, a study was conducted

by Howard et al. (2008), which covers the testing of mat strength in the three-point bending according to ASTM 5456 (modified for mats) (see Figure 10). The timber mats appear very ductile and the load transfer behavior varies with the increment of load. Laminated wood was used for the testing and analysis purposes. Their research also paved the way for research on the usage of timber mats for the construction industry (Howard, Saucier, & Shmulsky, 2008).

Timber mats are also vulnerable to fracture. Dourado, de Moura, and Morel (2015) conducted an investigation to observe the mode-1 fracture characteristics of wood. In their study, a single-edge-notched beam was loaded with three-point-bending to observe the fracture. The result indicates the existence of a unique cohesion law which governs the fracture of a wood specimen (Dourado, de Moura, & Morel, 2015).

Duerr (2010) presented the industry practice for the selection of timber mats. Engineers in the crane industry use various approaches. Some of which are based on the allowable deflection of the mat, mat length based on allowable soil capacity, mat length based on the bending stress, and shear stress developed in the mat during loading and compressive strength limit. Hasan et al. (2010) also

included these parameters to develop the required mat design for the maximum pressure exerted by the crane. The crane supporting system design module works alongside the crane database that is specifically designed and compiled for the crane industry (Hasan et al., 2010). However, there are two most commonly used techniques for the design of mats (timber/steel): one depends on the mat length based on the allowable soil bearing capacity, and the other depends upon the strength of the mat under loading (Duerr, 2010).

### 2.3.1. Mat Length based on Allowable Soil Bearing Capacity

Mat design under this method is straightforward. The load is divided by the area of the mat. If the resulting pressure is equal to or lower than the allowable soil bearing capacity, the mat is selected for further calculation. If the value is greater, the mat is rejected. This mat length is later used to calculate bending and shear stresses on the mat. If the bending and shear stresses are within the prescribed limits of the material, the mat is accepted. The problem with this calculation is that

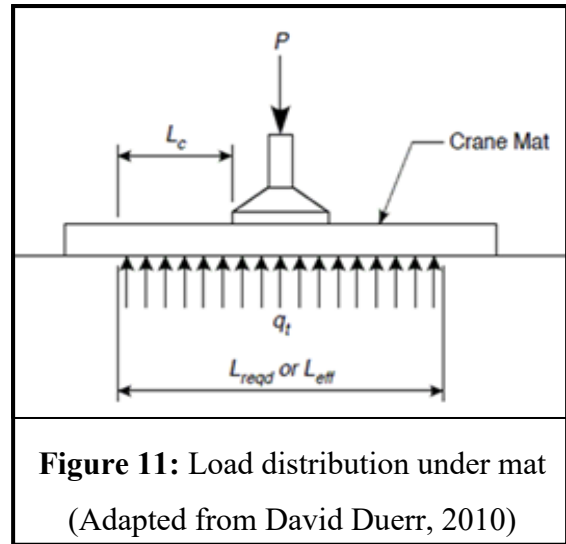


**Figure 11:** Load distribution under mat  
(Adapted from David Duerr, 2010)

it considers a uniform distributed load under the crane mat, which is not accurate. It is not essential to adhere to the above-mentioned parameters, bearing length, bending stress, and shear stress. The allowable deflection and allowable compression stress can also be included in the design parameters for mat selection. The deflection for crane stability is taken as  $\pm 1\%$  (ISO, 1991). However, for the present research, the deflection is taken as 0.75% of the total effective length based on ISO (ISO, 1991). The research presented in this thesis attempts to uncover the variation of load distribution under crawler crane. The mat selection is the same for both crawler crane and hydraulic crane. Once the load on the mat is determined using the crane GBP calculation software, or manually using Equations 1–14, the resulting load value is incorporated in Equations 15–25 to select the correct mat thickness and length. The equations used to calculate the effective length are expressed below (Duerr, 2010):

$$A_{reqd} = \frac{P+W}{q_a} \quad (15)$$

$$L_{reqd} = \frac{A_{reqd}}{B} \quad (16)$$

$$L_c = \frac{L_{reqd} - C}{2} \quad (17)$$

$$q = \frac{P}{L_{reqd}B} \quad (18)$$

$$M = \frac{(qB)L_c^2}{2} \quad (19)$$

$$f_b = \frac{M}{S} \leq F_b \quad (20)$$

$$V = (qB)(L_c - d) \quad (21)$$

$$V = (qB)L_c \quad (22)$$

$$f_v = \frac{1.5V}{Bd} \leq F_v \quad (23)$$

$$f_v = \frac{V}{n_w d t_w} \leq F_v \quad (24)$$

$$P + W \leq f_{cp} (A_{reqd}) \quad (25)$$

where

P = crane load (on one pad);

W = self-weight of the mat;

$q_a$  = allowable ground bearing pressure;

$A_{reqd}$  = required mat bearing area;

B = mat width;

d = mat depth (thickness);

$L_{reqd}$  = mat effective length required;

C = bearing width of track/outrigger;

$L_c$  = cantilevered length of mat;

q = ground bearing pressure due to P;

$M$  = bending moment in the mat;

$S$  = section modulus of mat;

$f_b$  = bending stress due to  $M$ ;

$F_v$  = allowable shear stress;

$n_w$  = number of webs (steel or aluminum design);

$f_{cp}$  = allowable compression stress;

$t_w$  = web thickness.

### 2.3.2. Mat Length based on Allowable Mat Strength

This method is the opposite of the first method (Section 2.3.1.). In this method, the effective length of the mat is assumed initially. The assumed length is adjusted based on the bending stress, shear stress, compression stress, and deflection of the mat. The following equations are used for this calculation (Duerr, 2010):

$$L_c = \frac{L_{eff} - C}{2} \tag{26}$$

$$q = \frac{P}{L_{eff} B} \tag{27}$$

$$M = \frac{(qB)L_c^2}{2} \tag{28}$$

$$f_b = \frac{M}{S} = F_b \tag{29}$$

$$V = (qB)(L_c - d) \tag{30}$$

$$V = (qB)L_c \tag{31}$$

$$f_v = \frac{1.5V}{Bd} = F_v \quad (32)$$

$$f_v = \frac{V}{n_w d t_w} = F_v \quad (33)$$

$$q_t = \frac{P+W}{L_{eff} B} \leq q_a \quad (34)$$

$$P + W = f_{cp} (A_{reqd}) \quad (35)$$

$$P + W = f_{cp} (A_{reqd}) \quad (35)$$

where

$L_{eff}$  = effective mat bearing length;

$q_t$  = actual ground bearing pressure.

This method is iterative because the mat length is assumed first, and based on that length, the mat appropriateness is calculated.

### 2.3.3. Adjustment of Design Values

The strength of the mat also depends upon the design factors. The National Design Specification (NDS, 2018) provides a set of factors to account for the design adjustment. These factors can be incorporated into the equations provided in Sections 2.3.1 and 2.3.2 to make these equations more realistic and workable. The design values of bending stress, shear stress, and compression stress of timber mats are readjusted to counter the service conditions. Some of the factors are outlined below:

- a. Load Duration Factor ( $C_D$ ): Timber mats can withstand maximum load for short duration. Over time, the ability to withstand load decreases; for example, it decreases 30% to 40% after one year under constant and uniform loading (NDS, 2018).
- b. Wet Service Factor ( $C_m$ ): Timber mat strength varies with moisture content (NDS, 2018).
- c. Temperature Factor ( $C_t$ ): The factor which governs the strength of the timber mat due to ambient temperature (NDS, 2018).

- d. Beam Stability Factor ( $C_L$ ): This factor accounts for beam buckling and rotation under bending and loading (NDS, 2018).
- e. Form Factor ( $C_f$ ): It is a shape factor. Round timber mats present different strength as compared to rectangular mats (NDS, 2018).
- f. Bearing Area Factor ( $C_b$ ): The factor which depends upon the bearing area of the mat (NDS, 2018).

If the above 6 factors are added to the values of shear stress and compressive stress, the updated equations will be:

$$\text{Updated } \underline{F}_v = (C_D) (C_m) (C_t) (C_L) (C_f) (C_b) F_v$$

$$\text{Updated } f_{cp} = (C_D) (C_m) (C_t) (C_L) (C_f) (C_b) \cdot f_{cp}$$

#### **2.3.4. Graphical Representation of Bearing Pressure and Mat Strength Chart**

The above exercise can be presented graphically. Crane rental companies often observe only three parameters; but, due to the complexity of the projects and the usage of heavy-duty cranes for extra heavy loads, some additional parameters are used to design the mat requirements for mobile cranes. A sample graphical representation is presented in Figure 12 (liftinglogistics.com, 2017).

The GBP with respect to the length of the mat reaches the effective length of the mat. This becomes the minimum length required to balance the allowable soil bearing capacity. If the bending stress, shear stress, deflection, or compression stress based on the length of the mat reaches earlier, the minimum effective length required starts earlier. The maximum effective length depends upon the remaining parameters, and when they reach their respective allowable limits. The first parameter which reaches its limit determines the effective length of the mat. The remaining length of the mat is considered as waste, as no pressure is supported beyond the effective length. The main purpose of the chart provided in Figure 12 is to calculate the effective and wasted mat length (liftinglogistics.com, 2017).

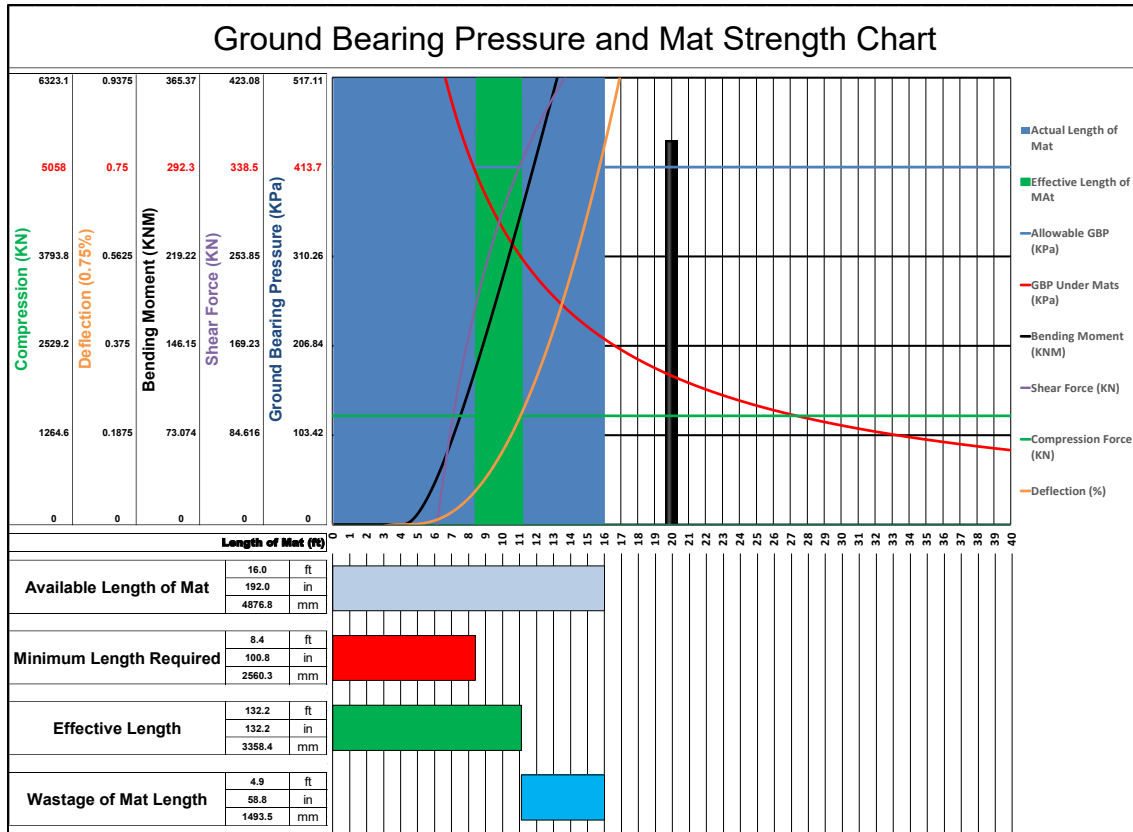


Figure 12: Graphical representation of effective mat length (liftinglogistics.com, 2017).

## 2.4. Allowable Soil Bearing Capacity

The GBP under the tracks/outriggers is calculated using Equations 1 to 14 (presented in Section 2.1.1). The maximum values are used to measure the strength and effective length of the mat; the value of allowable soil strength is also required. The design of the mat is based on two external values, one from the GBP of crane track/outrigger and the other from the allowable soil bearing capacity. The calculations for the allowable soil bearing capacity was first introduced by Terzaghi (1943). According to their study, the failure of the soil occurs when the load moves the soil downward. The ultimate bearing strength of soil under shallow foundation is calculated using Equation 36. The equation for ultimate bearing strength incorporates Terzaghi's bearing capacity factors:  $N_c$ ,  $N_q$ , and  $N_\gamma$ . These capacity factors depend upon the angle of soil internal friction ( $\phi$ )<sup>1</sup>.

<sup>1</sup> Angle of internal friction (friction angle): A measure of the ability of soil to withstand a shear stress. It is the angle ( $\phi$ ) measured between the normal force and resultant force when failure just occurs in response to a shearing stress.



The soil bearing capacity of the same soil varies under foundations of different dimensions. The factors  $B$  and  $z$  are dependent upon the dimension of the shallow foundation. As expressed in Equation 36, the allowable soil bearing pressure under a mat will be high as compared to the soil under bare tracks/outriggers. As the dimensions of the mat increase, so will the allowable soil bearing capacity also increase. Terzaghi (1943) also provided the values of  $N_c$ ,  $N_q$ , and  $N_\gamma$  with respect to the angle of internal friction.

$$q_{ult} = cN_c + \bar{q}zN_q + (0.5)\gamma BN_\gamma \quad (36)$$

where

$$N_c = \cot\phi (N_q - 1)$$

$$N_q = e^2 (3\pi/4 - \phi/2) \tan\phi / [2 \cos^2 (45 + \phi/2)]$$

$$N_\gamma = (1/2) \tan\phi (K_{pr} / \cos^2 \phi - 1)$$

$K_{pr}$  = Passive pressure coefficient (pressure exerted by soil horizontally)

Terzaghi's equation in its basic form is used widely in construction industry to measure the allowable soil bearing capacity of the soil. Unfortunately, few full-scale tests have been conducted to verify the accuracy and precision of these equations. Several research projects have been conducted to simplify the equation for easier use on site with fewer factors (Elfass, Norris & Vimalaraj, 2007). The variation of these factors with respect to the internal angle of friction was also observed. The variation of these factors from Terzaghi involves that values increase with the increase of internal soil friction angle. The values of  $N_c$  and  $N_q$  can be determined, but the value of  $N_\gamma$  requires some approximation. Numerical procedure and evaluation are widely adopted to approximate the value of  $N_\gamma$  (Dewaiker & Mohapatro, 2003; Kumbhojkar, 1993).

## 2.5 Finite Element Analysis for Crane Mat Stability.

Timber mats are most commonly made of Coastal Douglas-Fir. FEA complements experimental work and is useful since it provides an analytical framework for understanding and exploring the physics underlying the mechanics of deformation/stress under load. The main reason behind this approach was to check the stability of wood for the use as construction material.

Wood strands are composed of the earlywood layers and latewood layers of trees (see Figure 13).

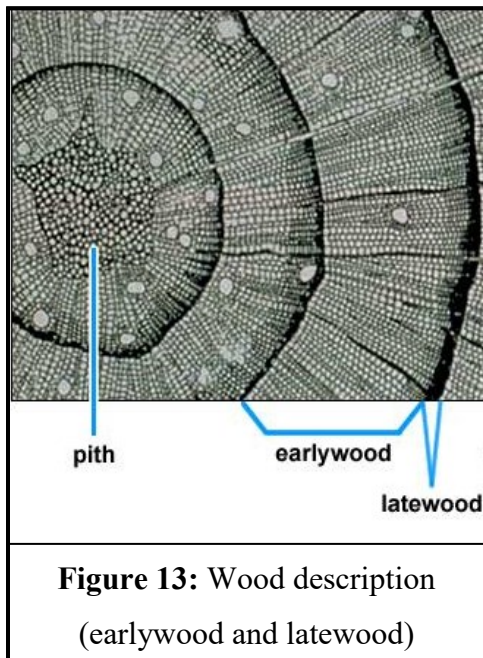


**Figure 13:** Wood description  
(earlywood and latewood)

Past research demonstrates that latewood is better in terms of mechanical properties as compared to early wood. Hindman and Lee (2007) built FEA models of wood strands in order to observe the impact of loading on the wood. ANSYS was used in their study to simulate the behaviour of strands under stress, and the modelling was conducted at a cellular level to make it more realistic. Experimental testing was carried out to retrieve the strength and stiffness of the wood under investigation, and as such, the models contain different layers of earlywood and latewood (Hindman & Lee, 2007).

Timber beams were often used in the past in bridge construction. The main issue with these beams is their propensity to crack. Research was conducted by Kováčiková, Ekevad, Berg, and Ivánková (2016) to observe the behaviour of timber beams with flaws under different loading conditions. It was carried out using timber beams with flaws and loading the model in finite element simulator<sup>1</sup>. The simulation was conducted with appropriate boundary conditions to observe different conditions (Kováčiková, Ekevad, Berg, & Ivánková., 2016). The first beam without flaws was loaded with forces; the second beam was loaded with a central flaw, the third with an oblique crack, and the fourth with a round hole. Sawn timber was used for the incorporation of mechanical properties. It was observed that simulating wood is more complicated as compared to steel or plastic due to the anisotropic<sup>2</sup> nature of wood. On the other hand, steel or plastic material is isotropic<sup>3</sup> in nature (Kováčiková et al., 2016).

Timber mats are bonded together using glue. The glue-laminated beams are held together with prestressed steel bars. When the force is exerted on the beams, the laminated pieces try to slip. Ekevad, Jacobsson, and Forsberg (2011) conducted research using FEA to monitor the slippage of glue-laminated timber beams observing both vertical and horizontal frictional slippage. The FEA result of their study indicated that vertical slippage can withstand a higher load but immediate failure

<sup>1</sup> ABAQUS Finite Element Analysis software.

<sup>2</sup> Different mechanical properties in different directions.

<sup>3</sup> Same mechanical properties in all directions.

occurs. The slip usually generates permanent deformation. In the case of horizontal slippage, the beam starts to slip at a low load, but withstands immediate failure (Ekevad, Jacobsson, & Forsberg, 2011).

Mahamid, Brindley, Triandafilou, and Domagala (2017) conducted research on the stability of cross-laminated timber (CLT) mats. Mats of various dimensions were loaded and observed. The deflection and cracking of these mats were observed in a laboratory setting. The same specimen was built in ANSYS, and as such the test mats were also loaded with the same configuration to obtain bending and shear parameters. These

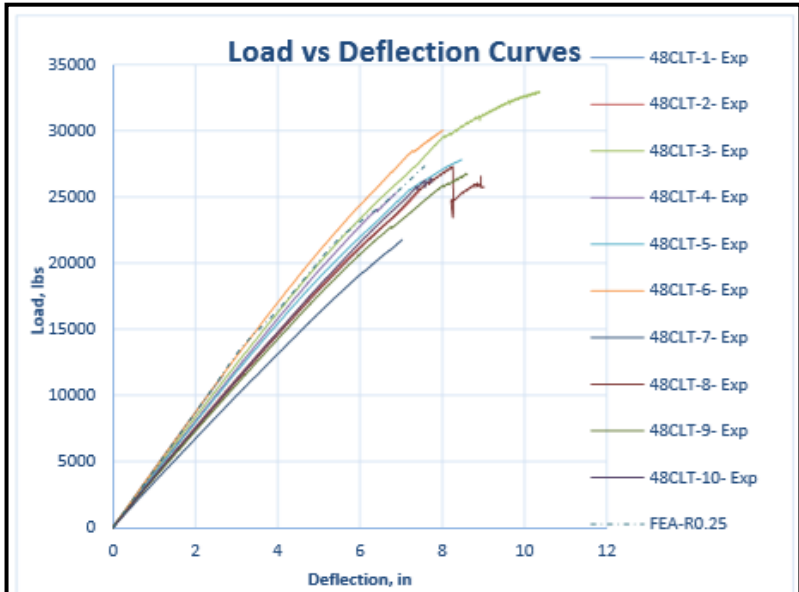


**Figure 14:** Experimental and finite element load-deflection results (Adapted from Mahamid et al., 2017)

*(Sources: Reprinted from "Behavior and Strength Characteristics of Cross-Laminated Timber Mats: Experimental and Numerical Study" by Mahamid, Mustafa, Tom Brindley, Nicholas Triandafilou, and Slawomir Domagala. 2017, Structures Congress 2017 254-268. Copyright 1996-2018 by ASCE)*

results were compared with the actual laboratory testing. The graphical representation indicated that the ANSYS results were similar to the actual test results (see Figure 14). These timber mats were build using Southern Yellow Pine. As a result of the study, Mahamid et al. (2011) provided recommendations for the design of access timber mats (Mahamid, Brindley, Triandafilou, & Domagala, 2017).

## 2.6 Artificial Ground Freezing (AGF)

The concept of Artificial Ground Freezing (AGF) is not new. The earliest documented application of AGF was in a mine shaft near Swansea, South Wales, in 1862. Later, this freezing method was patented by F. H. Poetsch, a German engineer, in 1883 with some major improvements (Sanger & Sayles, 1979). In 1884, excavation of a tunnel in Stockholm was aided with a frozen stabilized arch (Cauer, 1885).

The principle of AGF is simple in nature, involving lowering the temperature of the soil until the water content freezes and converts the soil into a solid block of frozen silt (Jessberger & Vyalov, 1979). The water particles in the form of ice work as the bonding agent between the soil particles, and thus increase the strength of the soil. The soil works as a separate and independent element. The barrier of this strong watertight frozen earth enables excavation and other work to proceed safely within its proximity (Andersland & Ladanyi, 2004). The benefits of AGF include its environmental-friendliness, its applicability on different soil and rock types, its ease of application in difficult ground conditions, and the ease with which the integrity of the frozen ground conditions can be monitored. AGF applications include various geotechnical applications, including groundwater cut off, ground stabilization, and temporary excavation supports (Tang, Ahmed, & Lu, 2004).

The primary utilization of AGF is to freeze the ground for tunneling projects. Along with many case studies, there are several publications regarding the application of ground freezing for construction work. Usually, the purpose of ground freezing is to contain water movement by creating a solid soil barrier in addition to supporting heavy structures (Jones, 1981). Some projects use ground freezing for tunneling work (Harris, 1995; Braun & Macchi, 1974; Gail, 1972; Wind, 1979). The artificial ground freezing is more used for shaft tunneling (Jones, 1981).

The first known use of AGF in Canada was deployed for geological purposes and involved the sample collection of the loose sand beneath the Duncan Dam in British Columbia at a depth greater than 10 m in an effort to obtain an undisturbed soil sample. For this ground freezing project, liquid nitrogen was used as the cooling agent. The main purpose was to get the undisturbed soil sample (Sego, Robertson, Sasitharan, Kilpatrick, & Pillai, 1994).

In recent years, AGF has evolved significantly. Its primary application continues to be to create a water barrier and provide support. The meltdown that occurred at the Fukushima Daiichi nuclear power plant in Japan was a major catastrophic event (March 11, 2011). The engineers discovered seepage of contaminated underground water into the surroundings of the plant. The selected solution was to freeze the ground to curtail the movement of the contaminated water. This is a good example of using ground freezing for creating a barrier for the groundwater movement (Morrison, 2013).

According to Leung, Leung, Cheung, and Chan (2012), in 2009, AGF was effectively deployed to strengthen the soil around tunneling construction in Singapore. The Tunnel Boring Machine (TBM) tunneling method was used for the construction of the sewage system. The impact of ground freezing was to strengthen the soil and to stop the water movement from the construction area. The ground condition was assessed before the application of AGF, and as a result, indirect freezing was the method used. Brine chillers were used as the main source of cooling agent. The design temperature was  $-15^{\circ}\text{C}$ , and was achieved within 14 days, well before the estimated time (45 days). During this project, it was assessed that the effectiveness of the artificial ground freezing depends mainly on the maintenance stage (Leung, Leung, Cheung, & Chan, 2012).

AGF has been used successfully in various projects. Hu and Deng (2016) described a process in which ground freezing was successfully used for an intake installation to an under-river tunnel (see Figure 15). AGF using brine enabled a good construction environment for the intake installation to the under-river tunnels. With the AGF system, it was possible to make the intake installation from a working platform above the river instead of jacking the intake upward to the river surface from the under-river tunnel (Hu & Deng, 2016).

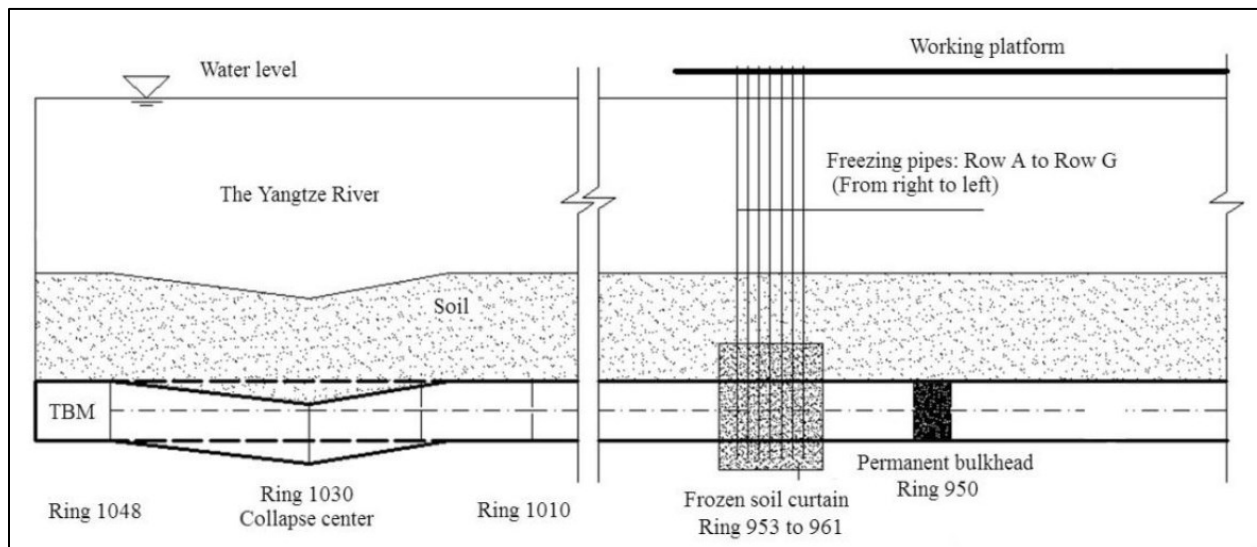


**Figure 15:** Lateral view of recovery tunnel of the east line (Adapted from Hu and Deng, 2016)

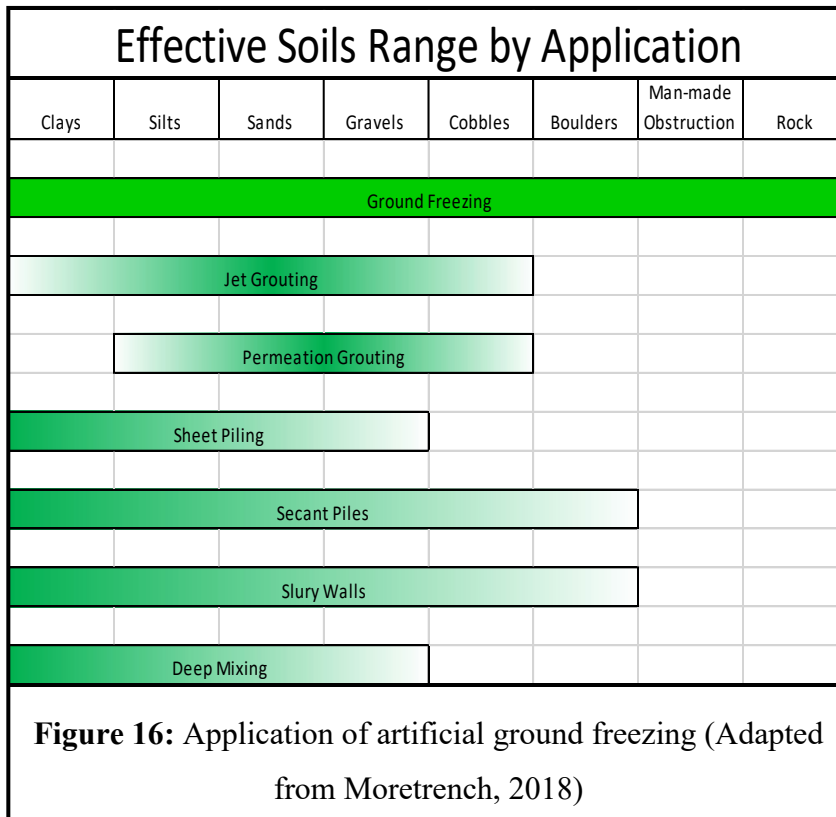
(Sources: Reprinted from “Ground freezing application of intake installing construction of an underwater tunnel.” By Hu, Xiangdong, and Shengjun Deng. 2016. Procedia Engineering. 633-640, Copyright 2016 by The Authors)

In Canada, AGF is not new to the construction industry. It has recently been applied as the best-practice method for water control and stability at uranium mines in northern Saskatchewan. Brine chiller was utilized to achieve the required temperature between  $-25^{\circ}\text{C}$  and  $-35^{\circ}\text{C}$  (Newman, Newman, Chapman, & Harbicht, 2011).

Ground freezing for cranes was first adopted in the state of Georgia when a temporary foundation for a 450-Ton crane was required for the installation of a reactor. Due to the sandy ground in the region, during boring the sand in rushed the bore hole. Ground freezing was used to freeze the sand around the holes, and later a temporary foundation was constructed over the frozen piles of sand. The crane was placed, and the work was carried out according to plan (Stoss & Valk, 1973).

## 2.7 Practical Approach towards Artificial Ground Freezing

### 2.7.1 Artificial Ground Freezing Procedure and Material Requirement



AGF may be used with any soil or rock formation, regardless of structure, grain size, or permeability. Figure 16 presents the feasibility of AGF with respect to other soil stabilizing options. The mechanical properties of frozen ground are more dependent on time and temperature than on the geology of the strata. Only lateral groundwater flow requires additional considerations. Freezing may

be used for any size, shape, or depth of soil, and the same refrigeration plant can be reused for multiple projects. The actual direct cost of freezing for a specific project—excluding the contractor’s capabilities—will depend largely on ground conditions, including groundwater flow

and impurities, the spacing of freezing elements, time available, and type of refrigeration system (indirect or direct freezing systems) used (Andersland & Ladanyi, 2004).

## 2.7.2 Freezing Methods and System Installation

A standard soil freezing installation involves a refrigeration source, a distribution system, and cooling pipes for freezing which are called freeze pipes<sup>1</sup> (Moretrench, 2018). The distribution system circulates the cooling agent<sup>2</sup> from the refrigeration source to the freeze pipes which extract the heat from the soil. In general, there are two main types of cooling agents widely used on job sites: brine solution and liquid nitrogen. Liquid nitrogen is sometimes replaced by carbon dioxide but works on the same principle. Both types of cooling agents have their own specifications, advantages, and disadvantages and are applied depending on the circumstances of the project. The selection of the cooling system depends upon several constraints (Implenja, 2017):

- time required for freezing
- duration of frozen ground
- volume of the frozen soil
- operating cost
- rigidity of frozen soil
- groundwater flow
- site constraints (accessibility for boring and placing freeze pipes)

Based on the above constraints, the cooling systems are divided into two main categories (Terratest, 2018): indirect freezing and direct freezing (move reference here).



**Figure 17:** Peripheral artificial ground freezing

There are two types of ground freezing in the construction industry, namely peripheral freezing and mass freezing (Powers, Corwin, Schmall, & Kaeck, 2007).

---

<sup>1</sup> Pipes used for the freezing of soil.

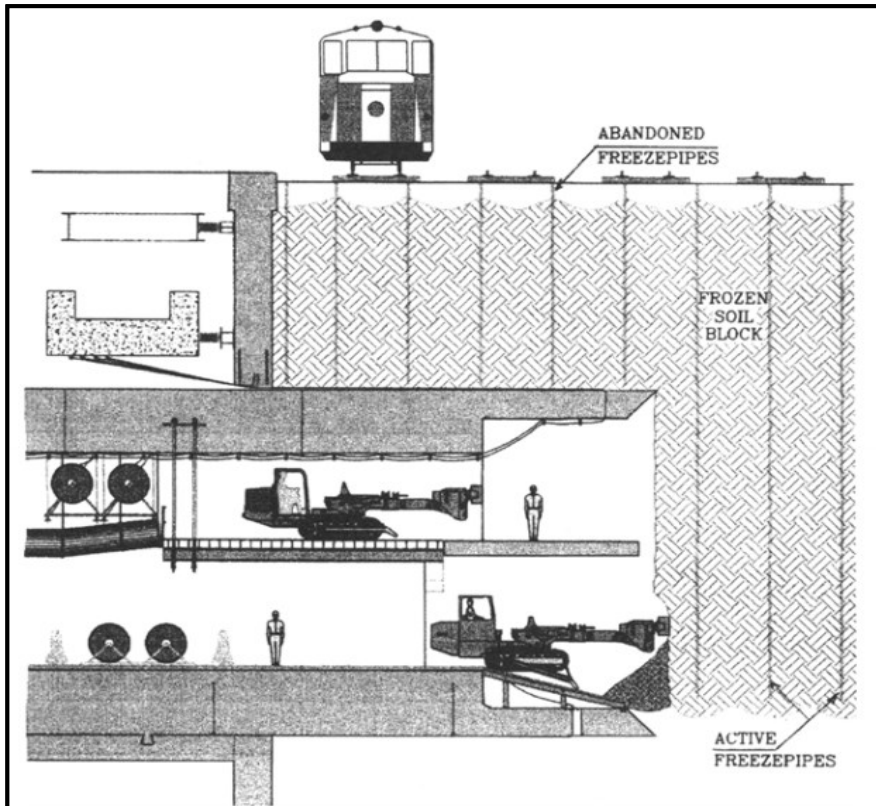
<sup>2</sup> Coolant used for the freezing of the soil.

Figure 17 presents an example of peripheral freezing, which is often used in the process of shaft tunneling. The soil around the shaft excavation is frozen to obtain a solid soil stability for the tunnel construction work. The main purpose of peripheral ground freezing is to develop a wall of frozen soil around an excavation or tunneling process. The frozen wall of soil works as a support for the excavation area, and also helps to control the groundwater



**Figure 18:** Mass artificial ground freezing

from entering the excavation area. It can be achieved vertically, horizontally, or at an incline. Mass freezing is used to maintain a wall of solid frozen soil or a block of frozen soil to support a structure. Unlike peripheral freezing, in mass freezing, the entire area is being frozen as per the



**Figure 19:** Schematic diagram of example of mass freezing

site requirements (see Figure 18). The main purpose of mass freezing is to provide support to the structures. Particularly during the tunneling process under the existing structure, mass freezing provides feasible ground support (Powers et al., 2007). For crane work, mass freezing can be used to support the weight of the ground. Figure 19 provides an example of mass freezing.



### 2.7.3 Primary Plant and Pumped Loop Secondary Coolant (Indirect Freezing)

A commonly used refrigeration source is a one- or two-stage refrigeration plant. A two-stage plant<sup>1</sup> is used when the required temperature ranges from  $-25^{\circ}\text{C}$  to  $-35^{\circ}\text{C}$ . These plants are widespread and available in a wide range of capacities. They are powered by diesel or electric engines and have a high thermal efficiency. The schematic diagram presented in Figure 20 illustrates the mechanics of a system with a primary plant (freezing agent<sup>2</sup>) and a pumped loop secondary coolant (cooling agent) (brine system).

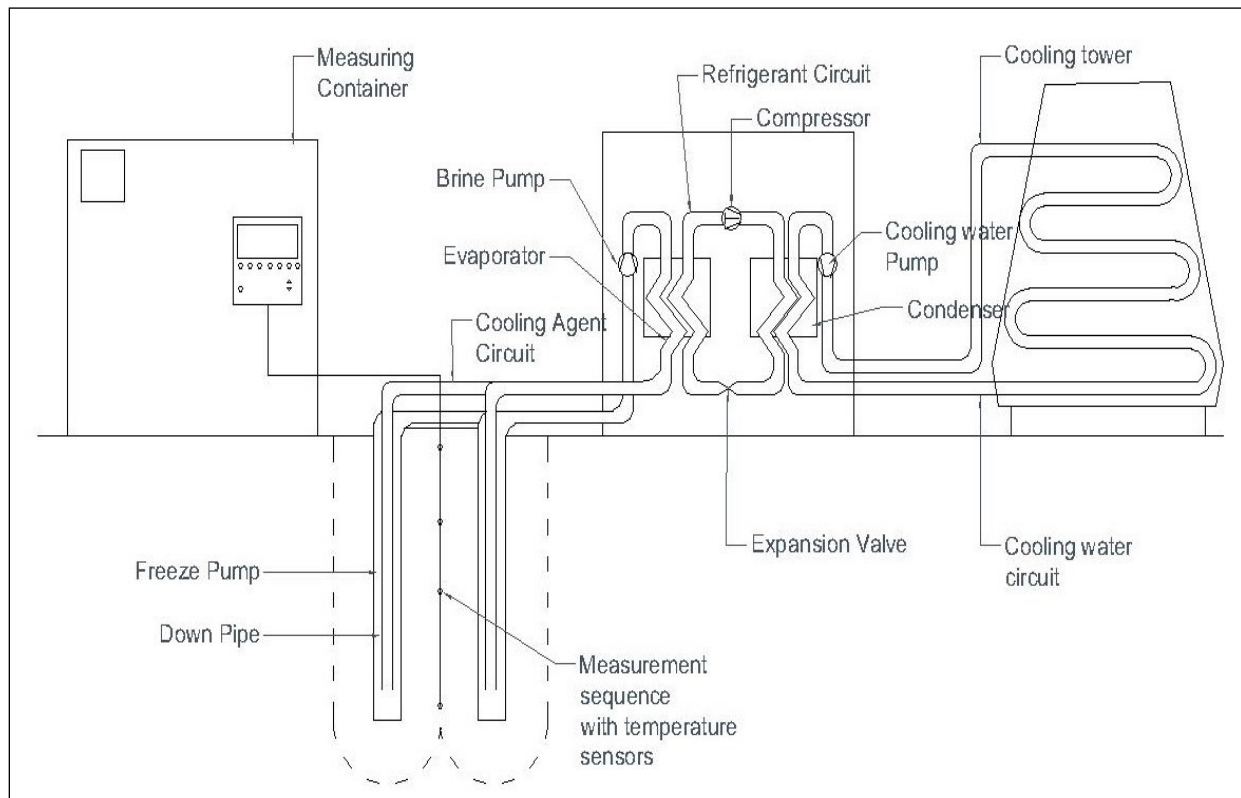


**Figure 20:** Schematic diagram of indirect freezing (Moretrench, 2018)

(Sources: Reprinted from “Ground Freezing Brochure” by Moretrench. 2018, Accessed 05 11, 2018. <http://www.moretrench.com/brochures/>. Copyright 2018 by MORETRENCH)

Usually, chilled calcium chloride ( $\text{CaCl}_2$ ) or magnesium chloride ( $\text{MgCl}_2$ ) is used as a cooling agent to freeze the ground and is typically cooled to temperatures between  $-15^{\circ}\text{C}$  to  $-25^{\circ}\text{C}$ . The

<sup>1</sup> Two compressors working in series.

<sup>2</sup> Refrigerant used for the lowering the temperature of cooling agent.

cooling agent is then pumped down by the drop tube in the freezing pipe, and then it flows upward withdrawing the heat from the soil. The temperature of the brine solution increases by approximately 2°C to 3°C during the process. The brine solution returns to the refrigeration unit to remove the heat and cool it again. The refrigeration unit can be installed on site along with the cooling tower, which may be water cooled or air cooled, depending on the site environment.

The whole ground freezing process occurs in three phases. The first phase is known as the **Freezing Phase**. In this phase, the ground is frozen to achieve the required strength. The energy drainage required to freeze the ground is more as compared to the energy drainage required sustaining the frozen ground (Jessberger & Vyalov, 1979).

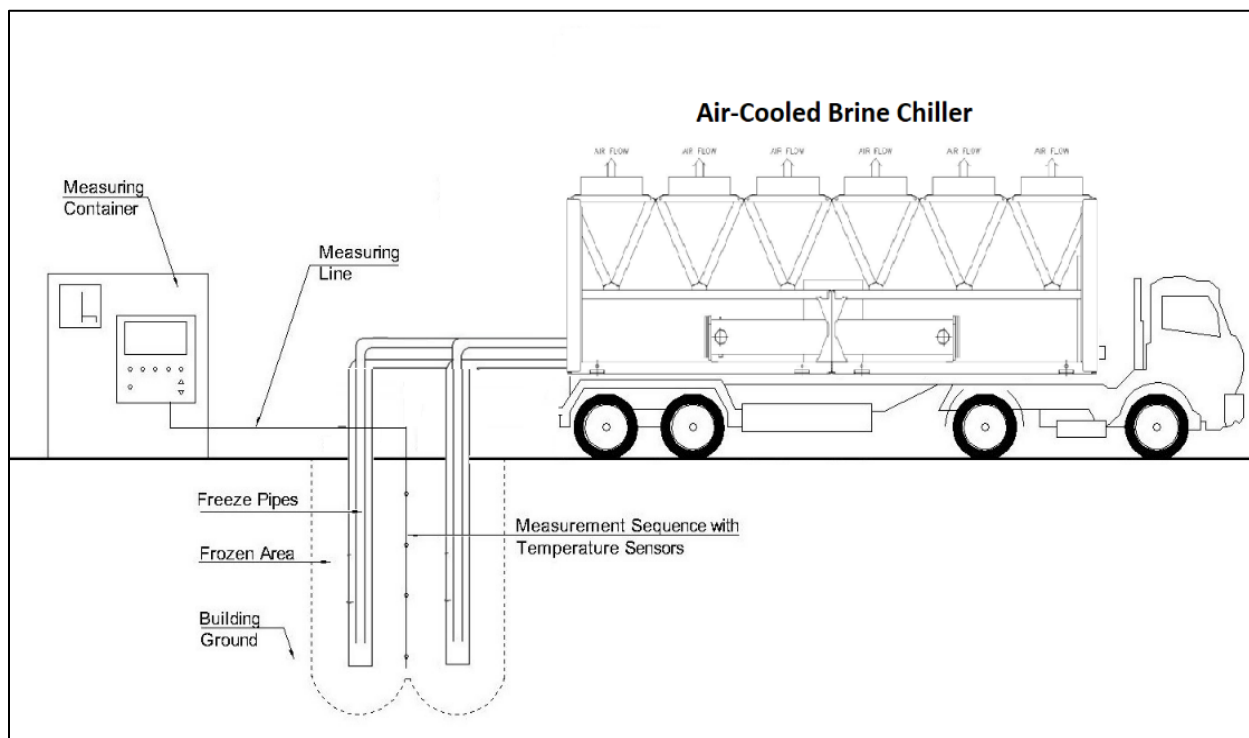


**Figure 21:** Proposed schematic diagram for primary plant and pumped loop secondary coolant (Moretrench, 2018).

The next step is to maintain the temperature of the frozen soil. This is known as the **Maintenance Phase**. As previously stated, less energy is required to maintain the frozen soil than to freeze the soil initially. The energy required for freezing is approximately 0.14 KW per meter of pipe. After the soil has been frozen, the power usage decreases exponentially (Newman et al., 2011).

The final phase is to terminate the freezing project, known as the **Thaw Phase**. In this phase, the ground is left to thaw by means of the surrounding ground heat (Implenia, 2017). The proposed layout of brine solution chiller for mat freezing is presented in Figure 21.

**Advantages of Indirect Freezing** (Implenia, 2017):

- The operating cost of indirect freezing is lower than direct freezing.
- Cooling process is slow, thus it is easy to control.
- Brine is reusable, thus there is no wastage as compared to direct freezing.

**Disadvantages of Indirect Freezing** (Implenia, 2017):

- The process is slow as compared to direct freezing.
- The frozen soil is less rigid as compared to direct freezing due to lower temperature.
- The setup is complex in nature since it requires various pieces of equipment.
- High initial cost (owned/rental) as refrigeration unit has to be arranged for the freezing.

#### **2.7.4 Expandable Refrigerant (Direct Freezing)**

As indicated by its name, in the direct freezing process the soil is directly cooled by the freezing agent. Primarily liquid nitrogen is used to freeze the ground in this process. It also involves three stages: the freezing stage, maintenance stage, and thaw stage. The coolant is supplied to the system directly from the storage tank. The continuous flow of the coolant through the freeze pipes at the desired temperature transforms the pore water in the soil into ice, the rate of which depends on the size, spacing, and orientation of the pipes. The soil around each freeze pipe freezes radially. The volume of the frozen soil column around adjacent freeze pipes slowly increases and merges, resulting in a continuous watertight frozen medium. The amount of nitrogen required for the freezing is maintained by using temperature sensing valve. As the valve opens, nitrogen escapes into the atmosphere at a rate that is not dangerous to the environment. Figure 22 illustrates the proposed process. The main disadvantage of this method is its operation cost.

**Advantages of Direct Freezing** (Implenia, 2017):

- Quick formation of frozen soil and well-frozen mass rigidity.
- Less equipment is involved and thus covers less space.

- Liquid nitrogen is safe for the environment.
- Can sustain high groundwater flow.

**Disadvantages of Direct Freezing (Implenia, 2017):**

- High cost in the long run.
- Very low temperature, which may result in frostbite in case worker touches it barehand.
- Ventilation is required in closed areas.

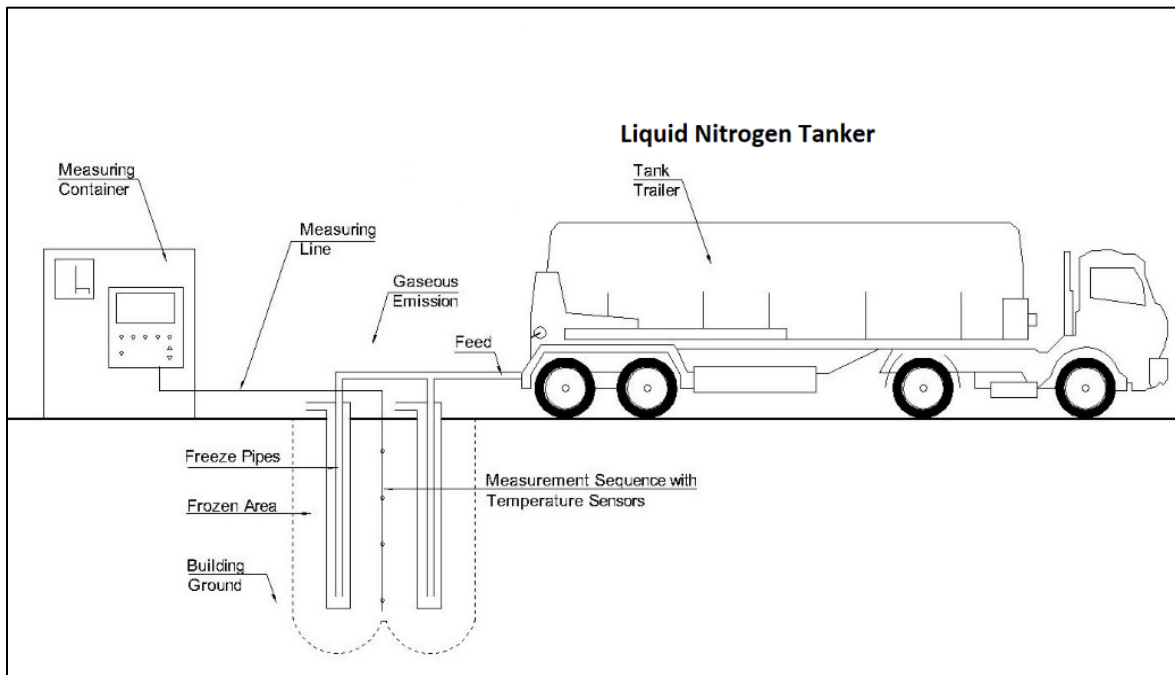


**Figure 22:** Proposed schematic diagram for expendable liquid refrigerant (Moretrench, 2018).

**2.7.5 Comparison of Direct and Indirect Freezing Costs**

An expendable refrigerant such as liquid nitrogen or carbon dioxide is attractive for a single project of short duration or for the projects where the cost of delay is high. The characteristics and relevant differences between liquid nitrogen freezing and brine freezing are presented in Table 1. Over time, the cost of direct freezing increases compared to indirect freezing. At the onset, indirect freezing may be costly, but over time, indirect freezing is a more cost-effective option. If ground freezing is required for a heavy crane over an extended period, indirect freezing may offer a good solution. In the case of 1 to 2 lifts (short duration), direct freezing may offer a good solution for soil stabilization (Stoss & Valk, 1973).

**Table 1:** Characteristics of LN<sub>2</sub> and brine freezing (Stoss & Valk, 1973)

Item		LN <sub>2</sub>	Brine
<b>Site Installation</b>	Electric power	Not required	Required
	Water for cooling	Not required	Required
	Refrigeration plant	Not required	Required
	Storage tank	Required	Required
	Circulation Pumps	Not required	Required
	A pipe system for distribution of coolant	Supply only	Supply and return
	Low-temp. material for surface, pipes, valves, etc.	Required	Not required
	Low-temperature material for freeze pipes	Not required	Not required
<b>Execution of freezing</b>	The physical condition of the coolant	Liquid/vapor	Liquid
	Minimum temp. achievable (in theoretical)	-196°C	-34°C (MgCl <sub>2</sub> ) -55°C (CaCl <sub>2</sub> )
	Reuse of coolant	Impracticable	Standard
	Control of system	Difficult	Easy
	The shape of the freeze wall	Often irregular	Regular
	The temperature profile in freeze wall	Great differences	Small differences
	Frost penetration	Fast	Slow
	Impact on freeze wall in case of damaged freeze pipe	None	Thawing effect
	Noise	None	Little

## 2.8 Finite Element Analysis for Artificial Ground Freezing (AGF)

The freezing of soil cannot be completed without an understanding of the concept of soil mechanics under loading. Several studies have been carried out to estimate the impact of reinforcement on the bearing strength of soil. Research was carried out by Belal, Nagy, and

Elshesheny (2015) which includes a numerical model developed in ANSYS to investigate the performance of foundation under loading. It was observed that tensile strength plays an important role in determining the strength of the soil. The ANSYS values were compared with the experimental values, and the results indicated that ANSYS can be used to simulate the behavior of soil under footing (Belal, Nagy, & Elshesheny, 2015).

The usage of FEA for AGF is a new concept that is gaining strength with the recent development of FEA simulators. Padilla, Villeneuve, and Stein (1997) compared FEA-based numerical and experimental values for the frost heaves in soil columns and found a 5% variation in the results. The finite element one-dimensional simulator<sup>1</sup> was used to predict the time required for ground freezing (Padilla, Villeneuve, & Stein, 1997). Padilla and Villeneuve (1992) also conducted a study which includes the modelling and experimental studies of frost heaves. For this purpose, the model<sup>2</sup> proposed in this thesis was built on Miller's theory.

Computational modelling of the frozen soil and pipe interaction are key in cold regions due to the frosting of soil around pipes; the volume of soil increases as it freezes, which impacts the strength of a pipe buried underground. A 3D model simulation can be used to predict the impact of frosting on the life and durability of buried pipes (Selvadurai, Hu, & Konuk, 1999).

Kudryavtsev (2004) presented a method for the numerical modelling of deep seasonal ground freezing. The numerical queries were solved by using thermal equations in accordance with phase change. The numerical results indicated that the magnitude of the ground freezing can be predicted using numerical methods. Kudryavtsev (2003) also presented a proposed numerical model for the thermophysical process of freezing and thawing. The model was based on the temperature distribution and moisture field.

Many researchers have presented freeze numerical codes to predict the freezing of the soil. One was derived from thermos-hydraulic software developed at ETH Zurich that covers the basic design features of artificial freezing, which includes pipe sizes, pipe spacing, the flow of cooling agent, the thermal conductivity of soil, and the time variation of soil freezing. The developed

---

<sup>1</sup> MELEF model (Modèle d'ÉLÉments Fluides).

<sup>2</sup> MELEF V-3.

application, “Freeze”, is a powerful tool for the simulation and estimation of freezing (Papakonstantinou, Anagnostou, & Pimentel, 2013).

Ground freezing is complex due to the estimation of time required for the freezing of the ground as well as the estimation of the maintenance phase. Researchers attempt to minimize the gap between the numerical simulation and the actual freezing data by introducing various approaches using FEA. SMAP-T2 is a specially designed numerical tool for the geotechnical application of heat transfer, which can be used to estimate the various aspects of soil freezing (Kim, Kang, Lee, Hong, & Kim, 2012).

Artificial ground freezing was utilized as the soil stabilizing technique during the construction of the Shanghai Metro Line No.13 (Song, Cai, Yao, Rong, & Wang, 2016). The values from the actual project were used to compare with the FEA of the same model with equal physical properties. A study was conducted in 2016 to evaluate the accuracy and precision of ABAQUS finite element program with respect to the actual project pertaining to artificial ground freezing. The results indicated that FEA is a reliable addition to the simulation of artificial ground freezing (Song et al., 2016).

Hu, Liu, Wei, and Wang (2017) conducted a research where artificial ground freezing was used in the tunnel project of the Nanjing Subway Line 10. Horizontal ground freezing was deployed to stabilize the soil. The finite element software ADINA was used for the feasibility of the artificial ground freezing project. ADINA was also used for the estimation of artificial ground freezing for Xi’anmen station on Nanjing’s Subway Line 2. The results indicated that the formation of a frozen soil wall depends upon the soil properties and the water content in the soil. The best results are found using cement-admixed sandy soil. The strength and the stability of frozen silt increase with additives (cement-admixed) (Hu, Liu, Wei, & Wang, 2017).

## **2.9. Basic Definitions for ANSYS Analysis**

### **2.9.1. Linear Mechanical Properties**

When a force/load is applied to a structural material, it will cause the material to change shape in the form of elongation, shrinkage, or shearing. This change in shape is called deformation. A temporary shape change that returns to its original shape after the force is removed is called elastic

deformation or linear deformation. When the stress is sufficient to permanently deform the metal, it is called plastic deformation or non-linear deformation.

Five linear and one non-linear mechanical properties are observed in the present research.

### 2.9.1.1. *Young's Modulus*

Young's modulus is the measure of the stiffness of a material. It is also known as elastic modulus. The units are equal to the stress (force/area). This describes the amount of stress required to get a unit strain. The higher the value of Young's Modulus, the higher the force required to reach the same unit strain (see Figure 23).

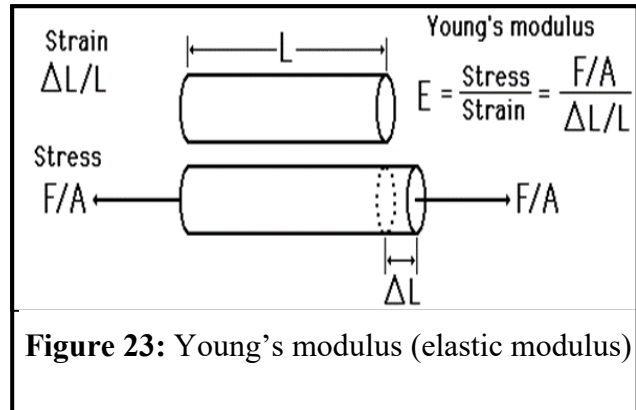


**Figure 23:** Young's modulus (elastic modulus)

### 2.9.1.2. *Tensile Yield Strength and Ultimate strength*

Tensile strength is the capacity of the material to withstand loads tending to increase its size in length or try to elongate it. Tensile yield strength is the maximum stress a material can withstand before reaching plastic deformation. Tensile ultimate strength is the maximum stress a material can bear before rupture. These are measured in force per unit area. If the yield strength is higher, the material can sustain higher loads without reaching the plastic deformation threshold. For tensile ultimate strength, the higher the value, the greater the force it can sustain before rupture (see Figure 24).

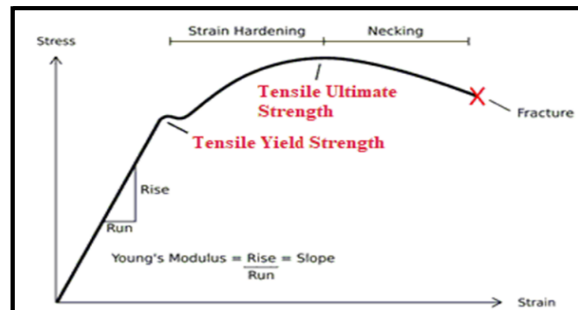


**Figure 24:** Tensile yield strength

### 2.9.1.3. *Compressive strength*

Compressive strength is the opposite of tensile strength. Compressive strength is the capacity of the material to

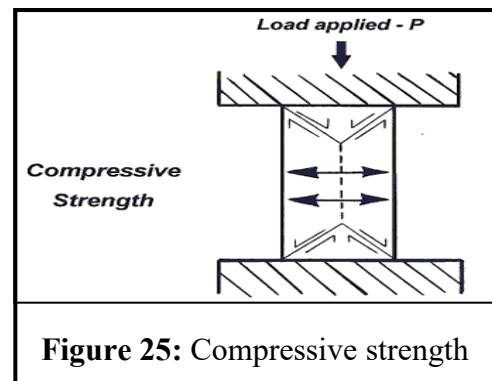


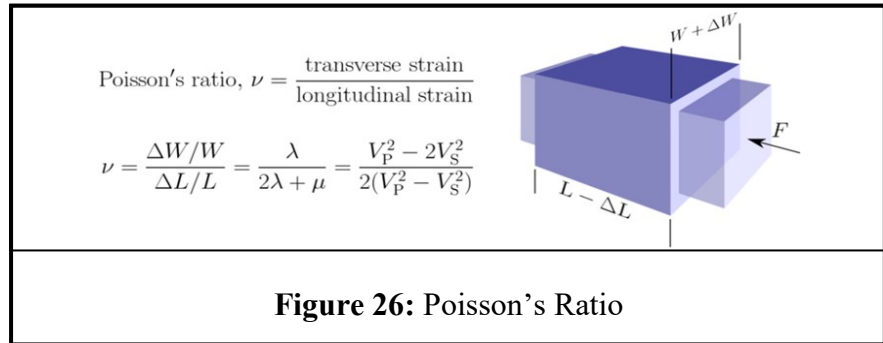
**Figure 25:** Compressive strength



withstand loads tending to reduce its size. Its units are same as Tensile Strength. The greater the compressive strength, the greater its ability to withstand pressure against buckling and rupture (see Figure 25).

### 2.9.1.4. Poisson's Ratio

Poisson's ratio is the ratio between transverse strain and longitudinal strain. It is a unitless quantity. Poisson's ratio for ice is 0.330; for Coastal Douglas-Fir is 0.449; and

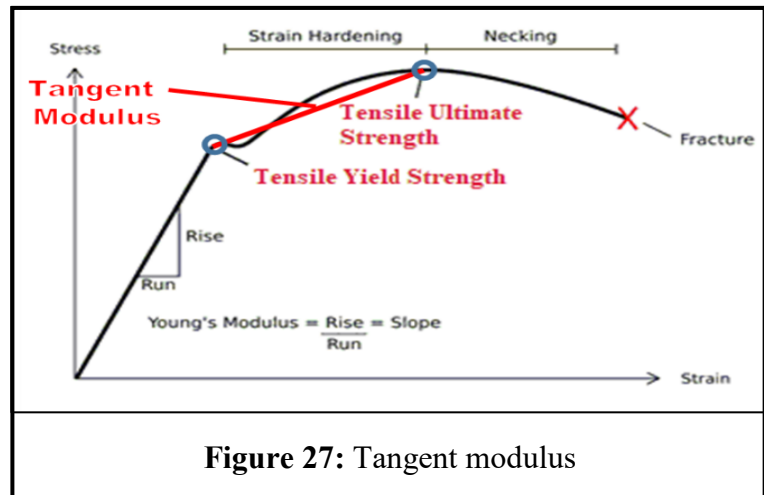


for steel is 0.300 (see Figure 26). Poisson's ratio is important for calculating the bending deflection of a beam in 3D.

## 2.9.2. Non-Linear Mechanical Properties (Bilinear Isotropic Hardening)

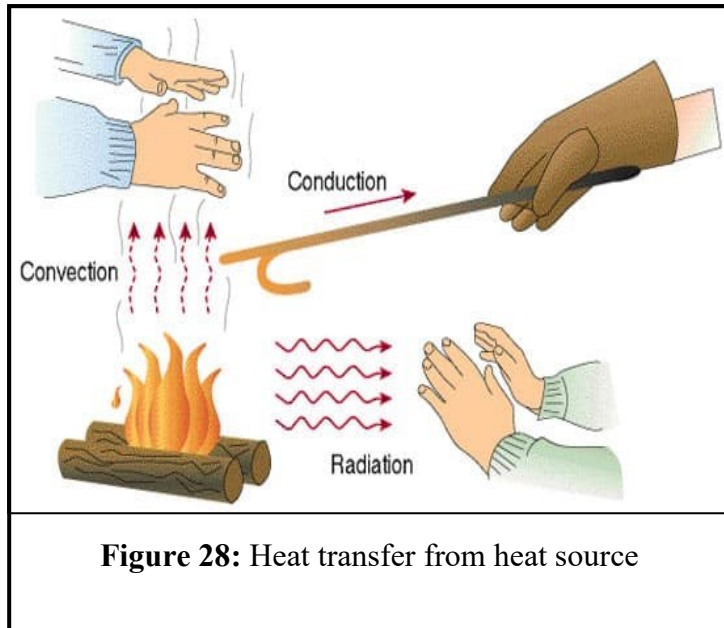
### 2.9.2.1. Tangent Modulus

In solid mechanics, the tangent modulus is the slope of the stress-strain curve at any specified stress or strain. For research purposes, plastic deformation is input in the form of tangent modulus for the ANSYS simulation. Its units are the same as the unit for Young's Modulus (see Figure 27). If these values are not used, any stress greater than tensile yield strength will result in an error in ANSYS simulation since the system considers it as infinite elongation.



### 2.9.3. Heat Transfer and Fluid Flow

Specific heat capacity or thermal capacity are defined as the amount of heat required to raise the temperature of a unit mass of a substance by 1 Kelvin or 1°C. The greater the value, the greater



the amount of heat required to raise the temperature. This value must be added to FEA software in order to calculate the heat removal from the soil and the heat addition to the cooling agent (brine or liquid nitrogen).

If a cold body of matter is near a source of heat, the heat is transferred to the cold body in three ways: conduction, convection, and radiation (see Figure 28). This heat transfer will continue until the cold body reaches thermal

equilibrium with the source of heat.

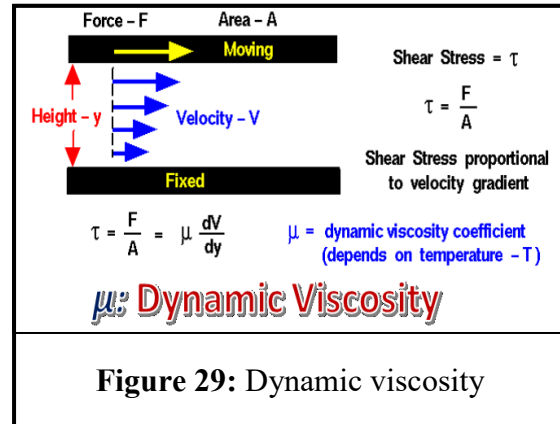
Thermal conductivity (conduction) is the property of a material to conduct heat. It is calculated using Fourier's Law of Conduction. Thermal conductivity is measured in watts per meter-kelvin ( $W/(m \cdot K)$ ).

Convection is the heat transfer that results from the mass motion of fluid such as air or water when the heated fluid moves away from the heat source. It is also known as heat transfer coefficient. Heat transfer convection is measured in watts per square meter Kelvin ( $W/(m^2K)$ ).

Heat transfer through radiation takes place in the form of electromagnetic waves (primarily infrared). Thermal radiation occurs through a vacuum or any transparent medium. It is the transfer of heat energy by means of photons in electromagnetic waves. It is based on Stefan-Boltzmann's law of radiation, i.e., based on emissivity and the Stefan-Boltzmann constant. Emissivity depends upon the reflection of heat, where 0 indicates the perfect reflector and 1 indicates a black body. The value of the Stefan-Boltzmann constant is  $5.668 \times 10^{-8} W/(m^2 \cdot K^4)$ .

### 2.9.3.3. *Dynamic (absolute) Viscosity*

The coefficient of absolute viscosity is the measure of a fluid's internal resistance to flow. It is the tangential force per unit area required to move one layer of fluid with respect to another. The units of dynamic viscosity are Poise (P). This helps to determine the flow of cooling medium during mat freezing. The heat transfer from the freeze pipe to the cooling medium occurs more rapidly on the outer layer of fluid versus the inner layer of fluid. The temperature gradient from the fluid center to the fluid outer layer depends upon the viscosity of the fluid.



## 2.10 Preliminary Market Research for Ice/Frozen Silt Mat

### 2.10.1 Usage of Timber Mats

In terms of the heavy industrial construction industry, there are two main types of cranes, crawler cranes and hydraulic cranes. The Liebherr LTM 11200-9.1 is the largest telescopic crane (hydraulic crane) in the world, with a capacity of nearly 1,500 Ton (1 metric Ton = 2,204.62 lb). As mentioned in Chapter 1, heavy cranes with loads exert pressure on the ground, thus, the ground must be compacted, and special mats are used to distribute the load to avoid earth settling. Timber mats are used in the crane industry to provide cost-effective and lightweight ground support compared to steel mats.



**Figure 30: Grains of Wood**

Usually, timber mats are made of Coastal Douglas-Fir (Golden Environmental Mat Services, 2015). The tensile strength of Coastal Douglas-Fir with 12% moisture is approximately 2.3 MPa perpendicular to the grain. If terms of parallel to the grain, the tensile strength of Coastal Douglas-Fir is approximately 107.6 MPa. The compressive strength of green, clear wood specimen of Coastal Douglas-Fir (12% moisture content) is 5.5 MPa (perpendicular to grain) (Kretschmann,

2010). The modulus of elasticity of timber (wood) is between 9 GPa to 14.5 GPa (Zhiyong & Robert, 2010). For this reason, the use of wood is advantageous for crane matting. It can withstand heavy loads without plastic deformation. When the crawlers of a crane exert pressure on the ground, the ground also exerts pressure on the timber mats, and the mats dissipate the load over the area without plastic deformation.

Timber mats are not only being used for load bearing, but also for crawler crane traveling, and super lift counterweight support. During the heavy crawler crane movements, timber mats are used as a support for the crane. This increase in mat use leads to an increase in cost for the project. Below is a list of the main issues customers face when using timber mats:

- Cost of timber mats. The usage of such mats is getting more and more attention in the construction industry. A few decades ago, there was lack of interest in using timber mats in the construction industry. But, the industry has grown 200% from 2009 to 2014. Mats are not only used in cranes, but also in other industries (Golden Environmental Mat Services, 2015).
- Transportation cost. Transportation of mats from the provider to the site, and later back to the provider's storage facility is a major cost driver.
- Storage and stacking cost. Inventory management is time-consuming and costly; timber mats must be stored and stacked both at the provider's facility and on the construction site. An area is used with respect to the size of the project.
- Durability and lifespan. These mats can be used for 2 to 3 years (Golden Environmental Mat Services, 2015). The lifespan is only 2~3 years as they warp, rot, splinter and break down over time (Miniat, 2017).

### **2.10.2 Climate Data for Edmonton, Fort McMurray, Dawson Creek, and Yellowknife**

Four locations are used as the test locations for frozen silt mats. The selected locations are Edmonton (Alberta) and Fort McMurray (Alberta), Dawson Creek (British Columbia), and Yellowknife (Northwest Territories). The purpose of selecting these locations is to show the usage of this new technology throughout Western Canada. These locations are in close proximity to major mine/oil & gas points as shown in Figure 31. Some of the major projects in the selected locations are listed in Table 2. Climate data (1981–2010) were obtained from the Canadian

Government Weather website (Canada, 2018). Figure 32 presents the variation of monthly average ambient temperature over a 12-month period. Figure 33 indicates the number of days in one month that reach the required ambient temperature ( $-10^{\circ}\text{C}$  and  $0^{\circ}\text{C}$ ).

**Table 2:** Major projects in Yellowknife, Dawson Creek, Edmonton, and Fort McMurray

	Project Name	Short Description
<b>Yellowknife (Northwest Territories)</b>		
1.	Diavik Diamond Mine	Diamond Mine Production: 7 million carats of diamonds/year (RioTinto, 2018)
2.	Ekati Diamond Mine	Diamond Mine 7.5 million carats of diamonds per year (Zimnisky, 2013)
<b>Dawson Creek (British Columbia)</b>		
1.	Willow Creek Coal Mine	Coal Mine 900,000 ton of coal per year (Jan, 2018)
2.	Brule Coal Mine	Coal Mine 1.3 million tons of coal annually (The-Canadian-Press, 2016)
3.	Wolverine Coal Mine	Coal Mine 1.5 million tons of coal annually (The-Canadian-Press, 2016)
4.	Pembina Pipeline	Pipeline Construction Total Value: \$320 million (Pembina, 2017)
<b>Edmonton (Alberta)</b>		
1.	CleanSEAS Demonstration Plant	Oil & Gas Total Estimated Value \$100 Million (Alberta-Government, 2018)
2.	Hi-Q Pilot Plant	Oil & Gas Total Estimated Value: \$125.0 Million (Alberta-Government, 2018)
3.	Gascana Liquefied Natural Gas Facility	Oil & Gas Total Estimated Value: \$4.0B (Commencing in 2020) (Alberta-Government, 2018)
4.	Sturgeon Refinery	Oil & Gas Total Estimated Value: \$9.7B (Schedule 2013-2018) (Alberta-Government, 2018)
<b>Fort McMurray (Alberta)</b>		
1.	Meadow Creek East SAGD Project	Oil & Gas Total Estimated Value: \$1.5B (Schedule 2019-2023) (Alberta-Government, 2018)
2.	Voyageur South Mine	Oil & Gas Total Estimated Value: \$4.4B (Alberta-Government, 2018)
3.	Aspen Oil Sands Project	Oil & Gas Total Estimated Value: \$4.0B (Alberta-Government, 2018)



**Figure 31: Major mines and oil & gas facilities in Canada**

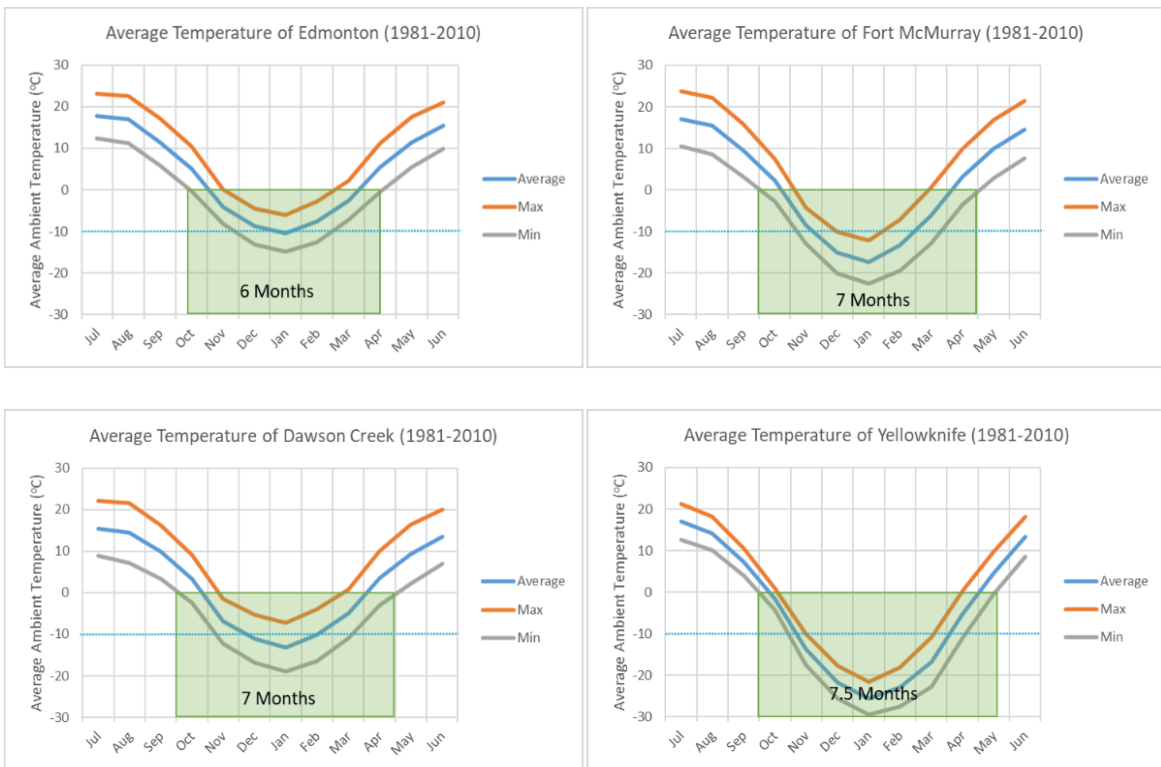


**Figure 32: Average monthly ambient temperature (12 months)**

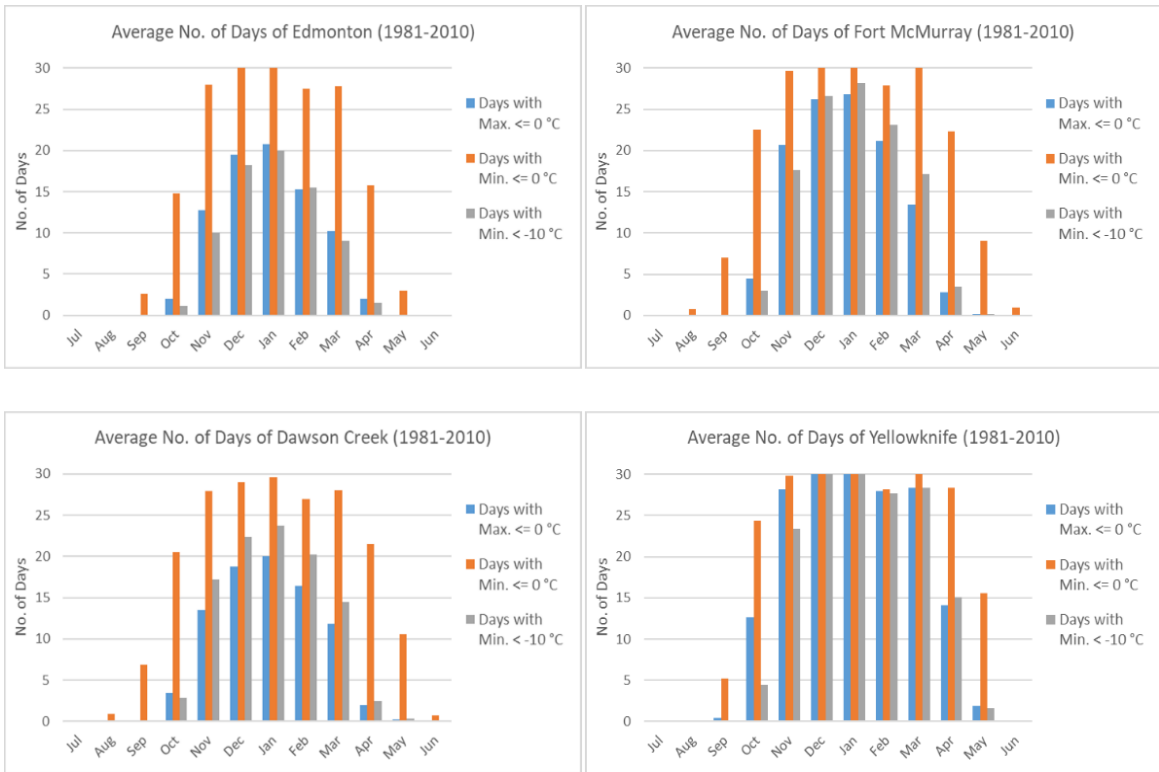


**Figure 33:** Number of days that reach required temperature (−10°C to 0°C)

## CHAPTER 3: RESEARCH METHODOLOGY

### 3.1 Problem Statement and selection of FEA

The aim of the proposed reasearch is to design a frozen silt mat which can compete with the traditional crane mats currently used in practice. There are several methods to achieve this design goal, some of which are described below:

1. Build prototype model and later apply the loads in a laboratory.
2. Build an actual model of frozen silt mat and conduct field study.
3. Build a miniature model to analyze the mechanical and thermal properties.
4. Use FEA to carry out competitive analysis of frozen silt mat versus traditional mat material under same boundary conditions.

The use of FEA to conduct competitive analysis by simulating the loading behaviour is selected in this research. The main reason is that it can provide a base for future practical application and field experimentation. The simulation conducted using FEA is similar to the actual field application. The use of FEA with conservative figures can help to build a prototype for field testing with minimal error or failure.

Turner, Clough, Martin, and Topp (1956) introduced finite element method. They converted complex structural problems into small simple trusses and joints to calculate and analyze the bending and load distribution (Turner, Clough, Martin, & Topp, 1956). Since its inception, many books and papers have been published to develop the basic FEA into the current-state complex FEA software available in the market. Today, FEA is a major player in the designing and simulation of various complex engineering models. The basis of FEA is to subdivide the whole problem into small finite elements. Decomposing irregular elements into small finite and regular elements makes it easier to observe and analyze. FEA involves the following key stages (Madenci & Guven, 2015):

1. Divide domain into small infinite elements.
2. Select required functions.
3. Develop respective finite element matrix.
4. Join small finite element matrices to form a large matrix for the whole domain.
5. Apply boundary conditions.



6. Solve.
7. Results and further computation (if required).

The above-mentioned sequence is used by most FEA software programs. Based on these steps, there are 3 primary approaches to FEA: direct approach, weighted residual approach, and variational approach (Madenci & Guven, 2015).

### **3.2. ANSYS Solver Usage**

The proposed research on frozen silt mats can be divided into two parts with respect to FEA usage:

1. Mechanical Simulation
  - a. GBP calculations under crane track/outrigger;
  - b. mechanical Properties competitive analysis under similar boundary conditions.
2. Thermal Simulation
  - a. heat transfer to/from proposed frozen silt mat;
  - b. usage of cooling agent for the freezing of proposed silt mat for cost comparison.

ANSYS workbench (version 17.1) is used for this research. For mechanical simulation, mechanical workbench “Static Structural”<sup>1</sup> is available in ANSYS which can simulate the load variation along the slew of the crane superstructure. For thermal simulation, “Fluid Flow (Fluent)”<sup>2</sup> solver is available in ANSYS to simulate the computational fluid mechanics (CFD) and thermal variation. The framework and processes of this software is described below:

#### **3.2.1. Mechanical Workbench “Static Structural”.**

For the mat deformation analysis using the mechanical workbench, the following methodology is adopted:

##### **Step 1 (Define Material Properties):**

In step one, the material of the mat and the soil under the mat are defined; only 6 mechanical properties (5 linear and 1 non-linear) are investigated. The properties of the material are taken from the literature review (see Section 3.3.2.).

---

<sup>1</sup> Module in ANSYS which deals with static structural mechanics. Finite Element Analysis is performed without any transition of the structures.

<sup>2</sup> Module in ANSYS which deals with computational fluid mechanics and thermal analysis.

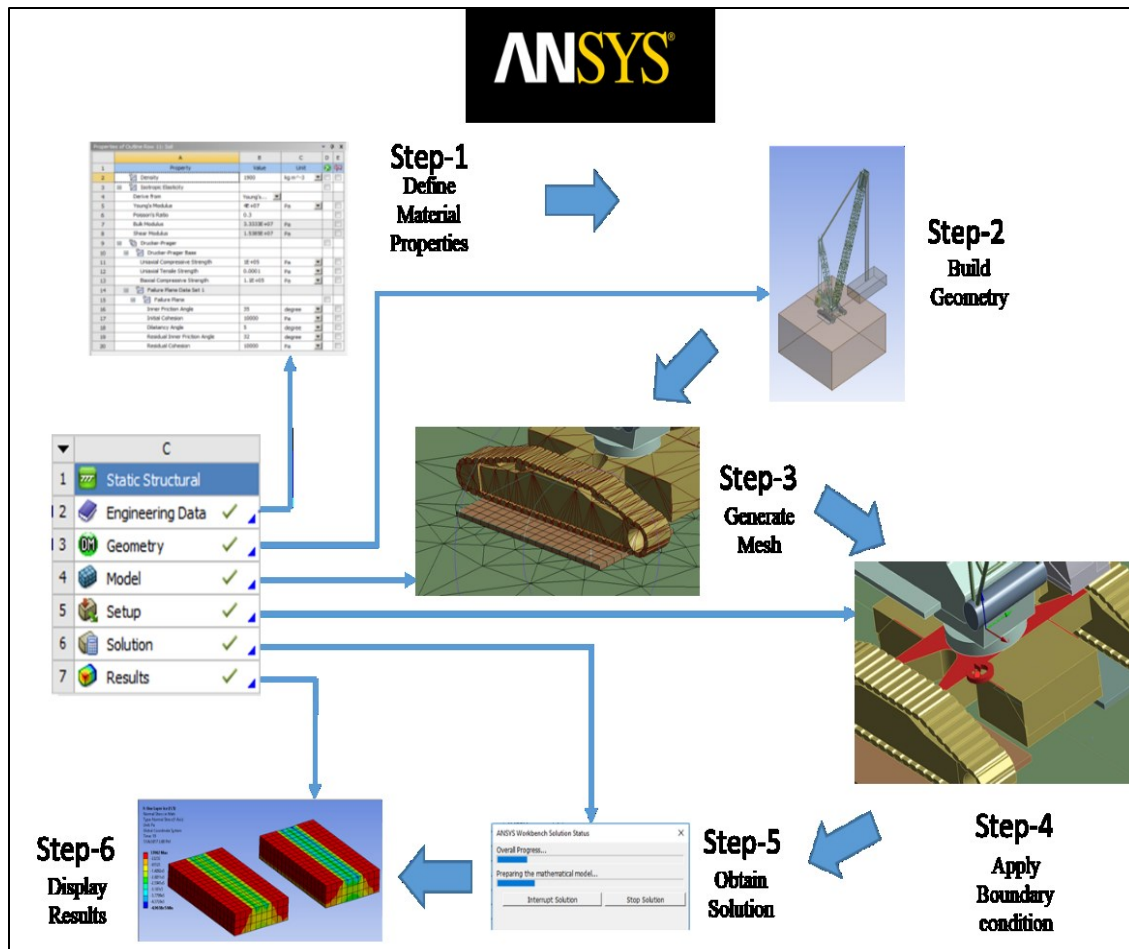


Figure 34: ANSYS problem-solving sequence (ANSYS Mechanical Workbench 17.1)

### Step 2 (Geometry<sup>1</sup> Build):

In this step, the geometry of the object or structure to be investigated is built. The geometry can also be imported from the 3D AutoCAD file of that model. The smaller the number of geometry parts, the faster the ANSYS mechanical solver can analyze and implement the mesh.

### Step 3 (Generate Mesh):

In this step, the model is uploaded in ANSYS Mechanical Solver “Model”. Each geometry part is assigned to its respective material. The density of the material is adjusted to achieve the required weight of that particular part. Also, the contact that is made between the different parts of the

<sup>1</sup> Term used for the structure or object in ANSYS. It is the module which deals with building the 3D model of the structure or object for FEA.

model is assigned. This step also includes meshing<sup>1</sup> of the model to small elements for FEA. The type and conditions of meshing are described in this section.

#### **Step 4 (Apply Boundary Condition):**

The next step is to apply the boundary condition. The boundary condition includes (but is not limited to) fixed support, rotation of the joint, gravity, forces, pressure, etc. It also includes the rotation of the superstructure of the crane with respect to time.

#### **Step 5 (Obtain Solution):**

The next step is to define the parameters of the solution. It includes (but is not limited to) number of time steps, iteration per time step, FE connection visibility, linear and non-linear controls, etc. Once all of the parameters have been assigned correctly, ANSYS Mechanical APDL is initiated to solve the problem.

#### **Step 6 (Display Results):**

The final step is to display the results. The results can be displayed in many forms, including normal stresses, principal stresses, forces, energy, deformation, etc. The results can also be displayed in the form of a video which shows the changes in values with respect to boundary conditions.

### **3.2.2. Fluid Flow (Fluent) Solver**

For frozen silt mat thermo analysis, ANSYS Fluid Flow (Fluent) is used. The following steps are taken to observe the heat transfer.

#### **Step 1 (Geometry Build):**

In this step, the geometry of the object or structure is drafted or imported from a 3D AutoCAD file. The smaller the number of geometry parts, the faster the ANSYS fluid flow solver can analyze and implement the mesh. As the number of parts of a geometry increases, the time required by ANSYS solution increases exponentially.

---

<sup>1</sup> Meshing is defined as the process of dividing the whole component into number of elements so that whenever the load is applied on the component it distributes the load uniformly.

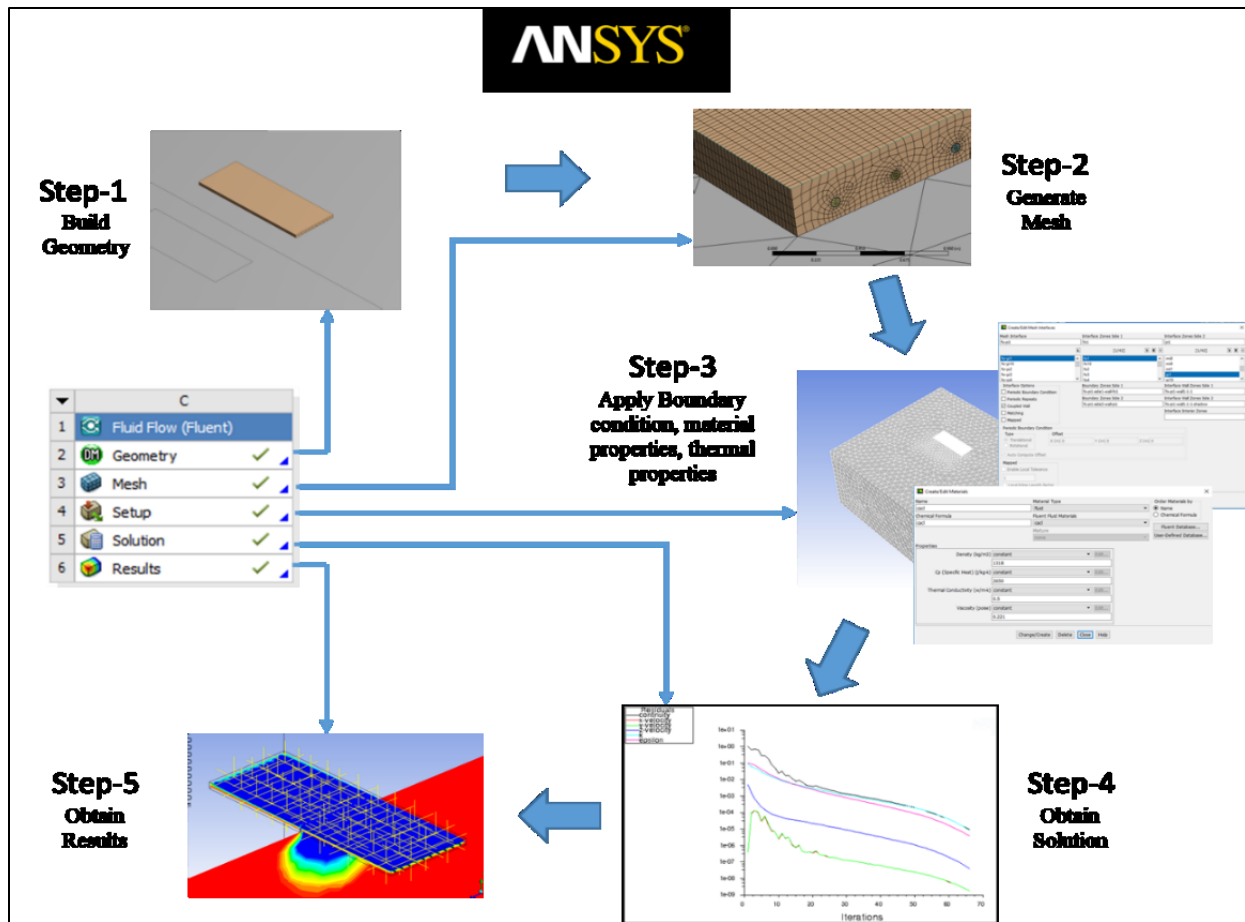


**Figure 35:** ANSYS problem-solving sequence (ANSYS Fluid Flow - Fluent)

### Step 2 (Generate Mesh):

In this step, the model is uploaded to ANSYS Fluid Flow (Fluent) solver “Mesh”. This part includes meshing of the model to small elements for FEA. The type and conditions of meshing are described in this section. The smallest the meshing element, the better it is. But the accuracy and precision must be monitored to make it workable. It is better to give each surface a separate named selection. These name selections make step 4 easier.

### Step 3 (Apply Boundary Conditions):

In this step, the previously determined energy equations are applied to the geometry, and thermal and viscous properties of the fluids are assigned. The interference between different body surfaces is also assigned in this step as well as cell zone conditions. Finally, the inlet and outlet temperature and fluid velocity are assigned accordingly.

#### **Step 4 (Obtain Solution):**

After obtaining the geometry and assigning the required boundary conditions, the solution of the problem is initiated. The solution depends upon the solution initialization, number of time steps, duration of time steps, and maximum iterations per time step.

#### **Step 5 (Display Results):**

The final step is to obtain the results. Fluid dynamics is the basis of these results. Heat transfer with respect to time is obtained in this step. The results can be shown in the form of graphs, colour variation, or various charts and sheets. The data can be exported to different file formats as necessary for further investigation.

### **3.3. ANSYS Methodology**

#### **3.3.1. Crane Ground Bearing Pressure**

The first thing that is required to be done is to make the ANSYS model which can provide GBP for the crane. Usually, the GBP values are obtained from the crane manufacturer. These values can also be calculated using the equations presented in Chapter 2. To obtain a realistic model, the values from ANSYS should be equal to the manual calculations.

To make this research versatile, both crawler and hydraulic cranes are considered for the ANSYS benchmark. One crane model is used for the analysis of crawler cranes and one crane model is used for the analysis of hydraulic cranes.

**Step 1:** To develop the FEA model, the weights of various parts of the crane and their Center of Gravity (COG) location are required, which are provided by the manufacturer of the selected crane. For crawler cranes, this data is used to develop an algorithm for manual calculations using Eq. 1 to Eq. 14 in Chapter 2 for the GBP calculations under crawler with respect to the angle of the boom slew from the front to the left side of the crane. Boom slew angle increments are recorded every  $5^\circ$  from  $0^\circ$  to  $90^\circ$ . The obtained values are verified using the GBP software provided by the crane manufacturer. This prerequisite check is carried out to ensure the validation of the available data. For hydraulic cranes, similar to the crawler crane, the weights and the COGs of all the major parts of the hydraulic crane are required. These are provided by the hydraulic crane manufacturer.

**Step 2:** The next step is to develop a crane model (crawler crane or hydraulic crane). For this, all the major dimensions of the crane under investigation are obtained from the 3D AutoCAD drawing of the model. The user can also design the model in the Geometry module of ANSYS. All parts (carrier, superstructure, boom, and load) are selected to be rigid (only forces, no stresses, no deformation) in the “Stiffness”<sup>1</sup> section of ANSYS Mechanical Workbench. For crawler cranes, in general, the load-bearing length of the track is smaller as compared to the actual length of the track and, in the case of a solid surface, the effective width is also shorter as compared to the actual width of the track (see Figure 36) (Shapiro & Shapiro, 2011).

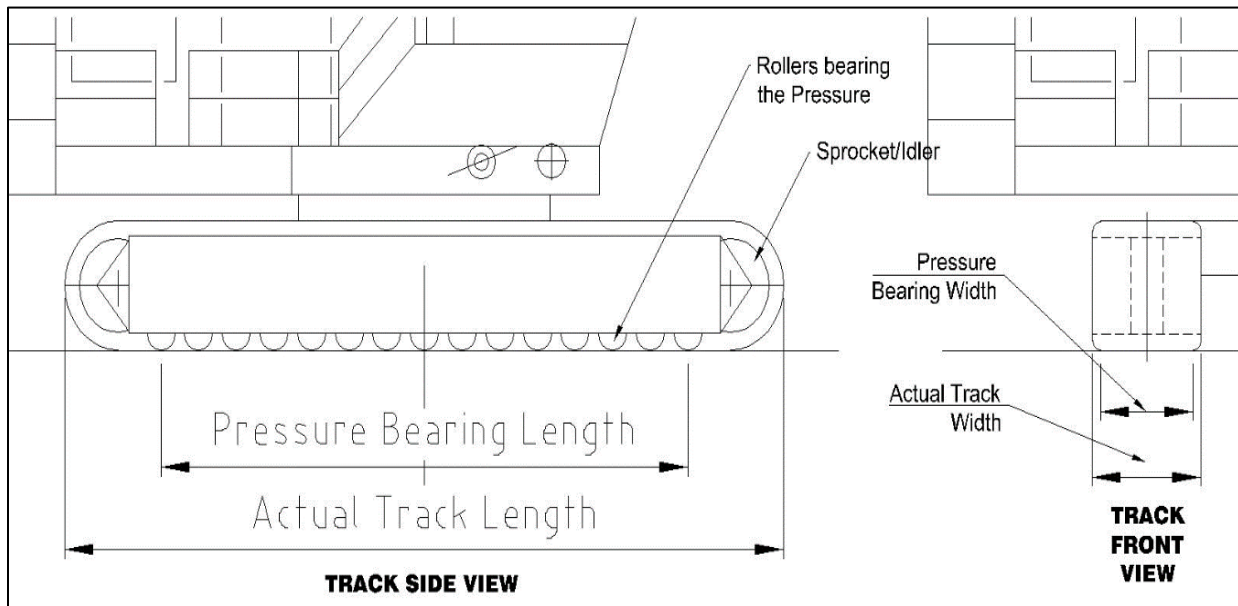


**Figure 36:** Bearing length/width and actual length/width of crawler crane track

It is standard protocol of ANSYS simulation that ANSYS does not provide any stress or deformation values over rigid body. To obtain these readings, a thin plate (25-mm thick) of dimensions equal to the bearing length and the bearing width is placed under each track. This thin plate functions as a sensor to obtain the stress and deformation values for the pressure exerted by the tracks due to crane weight and the payload. The “Stiffness” of this plate is selected as “Flexible”.

<sup>1</sup> ANSYS term for material elastic/plastic behaviour of material is “Stiffness”. The program’s GUI allows the user to select stiffness as “Rigid” (only forces) and “Flexible” (elastic/plastic behaviour). If the user selects “Rigid”, no stress/deformation values pertaining to that model can be obtained after the simulation.

For hydraulic cranes, all crane parts (carrier, superstructure, hydraulic boom, and load) are assumed to be rigid. Given that only the reaction forces are required, rather than using a thin plate, crane mats are used for crane ground support and load reading. The “Stiffness” of these crane mats is selected as “Flexible”.

**Step 3:** The developed crane geometry is uploaded to a static structural mechanical workbench. For crawler cranes, the lowermost surface of the plate is loaded with fixed support<sup>1</sup>. The weights and location of COGs of the various crane parts are adjusted by adding material blocks until the overall weight and COG of each part corresponds to the available data<sup>2</sup>. The model is then loaded with gravity<sup>3</sup>. After the model is solved, the results are obtained in the form of normal stress and minimum principal stress<sup>4</sup>. ANSYS provides negative values of principal stresses due to compression. The top surface of the thin plate and the lower surface of the track are assumed to be bonded<sup>5</sup>. In the case of triangular pressure distribution, ANSYS provides negative values within the triangular region (I) (Eq. 10) and positive values outside the triangular region ( $d_1 - l$ ) considering it as tension rather than compression. The positive values are ignored and the values within the region ( $d_1 - l$ ) are considered to be zero.

For hydraulic cranes, the lowermost surface of the outrigger mats is loaded with fixed ground support. All parts of the cranes are assigned with their respective weights and COG locations, which are then adjusted by adding material blocks with various density and location to the particular part until the overall weight and COG location of the part corresponds to the given data. Once the model is solved, the solution is applied in the form of reaction forces on all four outriggers.

---

<sup>1</sup> Fixed support functions as ground support for these mats. Therefore, this fixed support functions as a reaction force for the applied load and crane weight.

<sup>2</sup> The actual weight of each part is different from the 3D drawing. To match the values, extra blocks of material are added to the geometry part with the adjusted density and location until the required weight and COG location are achieved.

<sup>3</sup> Boundary condition for the Earth’s gravity in one direction.

<sup>4</sup> When only the three normal stresses remain, and all the shear stresses are zero by converting them to the three normal stresses, these normal stresses are known as principal stresses.

<sup>5</sup> Contact relationship between two surfaces in ANSYS.

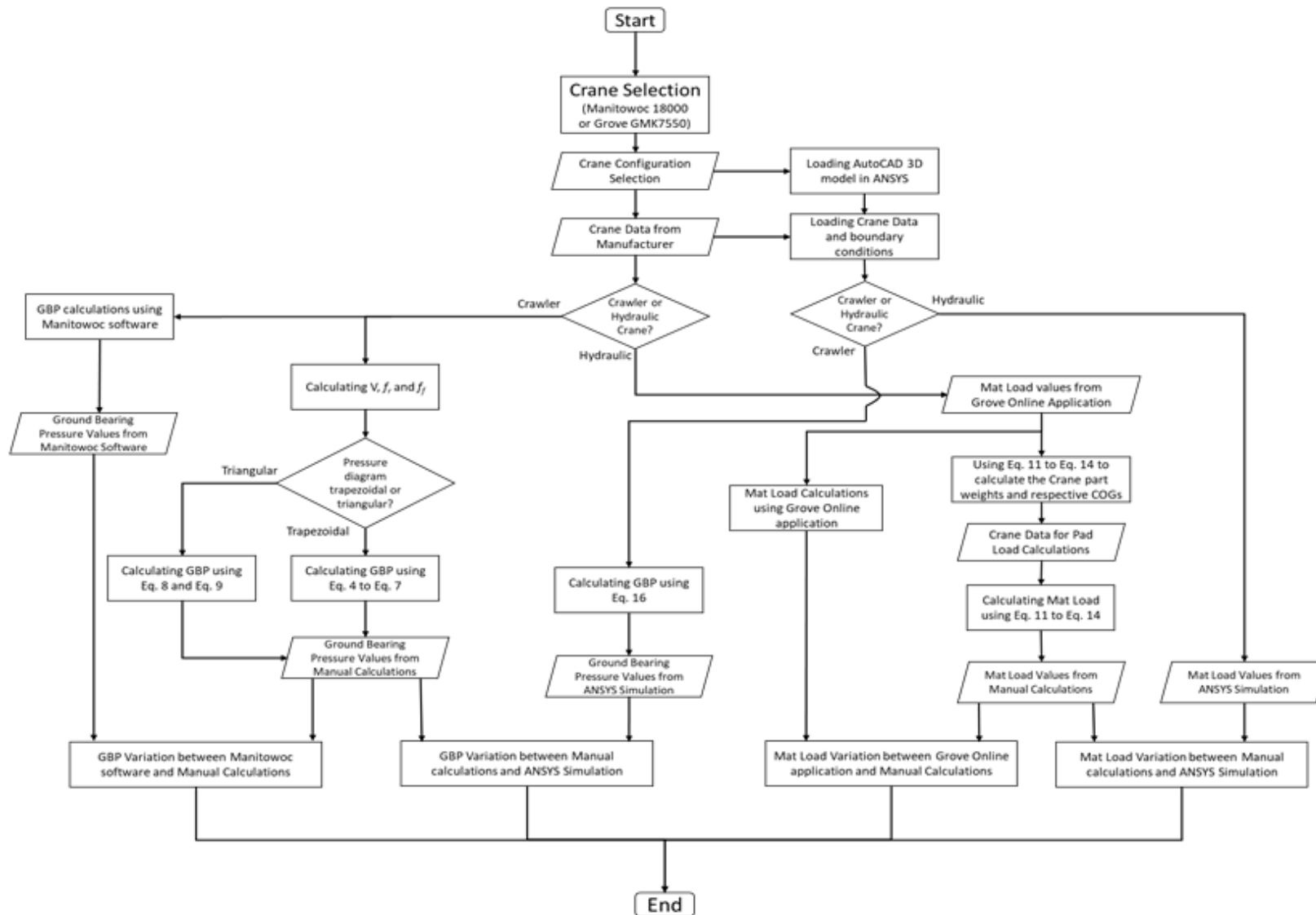


**Figure 37:** Flowchart for crawler/hydraulic crane data flow for crane benchmark



**Step 4:** The final step is to compare the results from ANSYS and the values from the manual calculations using the algorithms provided in the literature. Traditionally, for crawler cranes, widthwise pressure distribution under the track of the crane is considered uniform (Shapiro & Shapiro 2011). But in reality, the widthwise pressure distribution diagram is trapezoidal in nature (see Figure 38). For this reason, ANSYS provides two values for each side of the track, one maximum and one minimum. To compare with the traditional calculations, only one value is required from ANSYS. This is achieved by dividing the trapezoidal pressure diagram into two parts, as can be seen in Figure 39, rectangular uniform stress in the form of a rectangular pressure diagram, and two triangular pressure diagrams with maximum and minimum stresses in opposite directions. The total compressive stress can be written as (Liu, Chan & Gerbrandt, 2008),

$$\text{Total Compressive Stress} = \frac{(b+a)}{2} - \frac{(b-a)}{2} + \frac{(b-a)}{2} \quad (37)$$

$$\text{Total Compressive Stress} = \frac{(b+a)}{2} \quad (38)$$

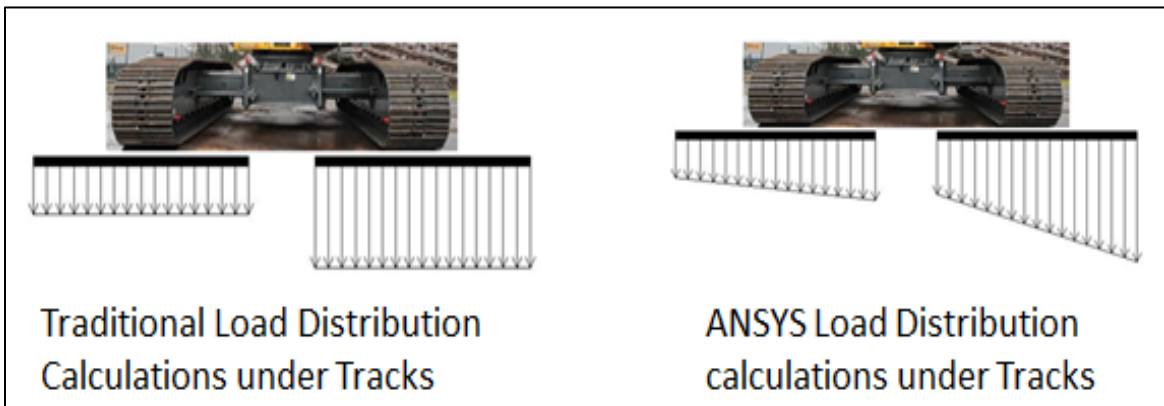


**Figure 38:** Traditional versus ANSYS load (compressive stress) distribution under crane tracks

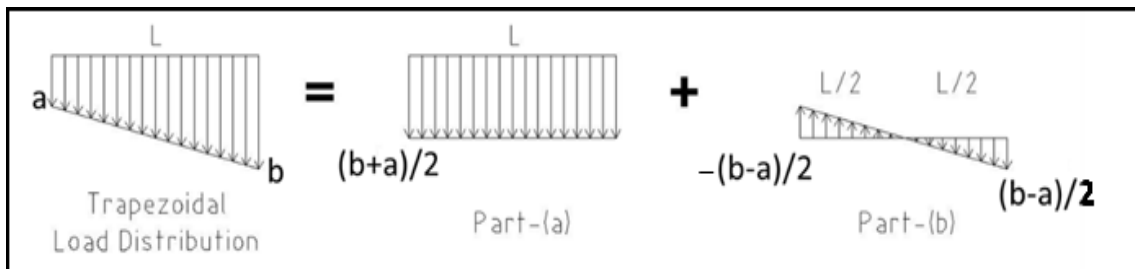


**Figure 39:** Trapezoidal pressure (compressive stress) converted into two parts (Liu et al., 2008)

The value obtained from Eq. 38 is compared with the traditional calculations (Liu et al., 2008). The entire process creates three sets of values: (1) from the manufacturer’s software, (2) from the manual calculations, and (3) from ANSYS analysis. The first two sets of values are based on Eq. 1 to Eq. 14 (found in Chapter 2), but the third set of values does not rely on these equations since they are obtained using FEA calculations of the pressures under the tracks.

For hydraulic cranes, ANSYS can provide stress values (minimum and maximum) as well as values of the load on each outrigger. For the comparison, the load (force) values are required since the manufacturer software and the manual calculations only provide the value of force exerted by each outrigger. The entire process also creates three sets of values. Figure 37 presents the data flow for a crawler and hydraulic crane.

### 3.3.2. Mat Material and Mechanical Properties

For the mat strength, the first thing to consider is the material properties. For the purpose of this research, five materials (G40.21-44W, S355, Coastal Douglas-Fir, ice, and frozen silt) are selected. For each mat material, 5 linear and 1 non-linear mechanical properties are selected for FEA.

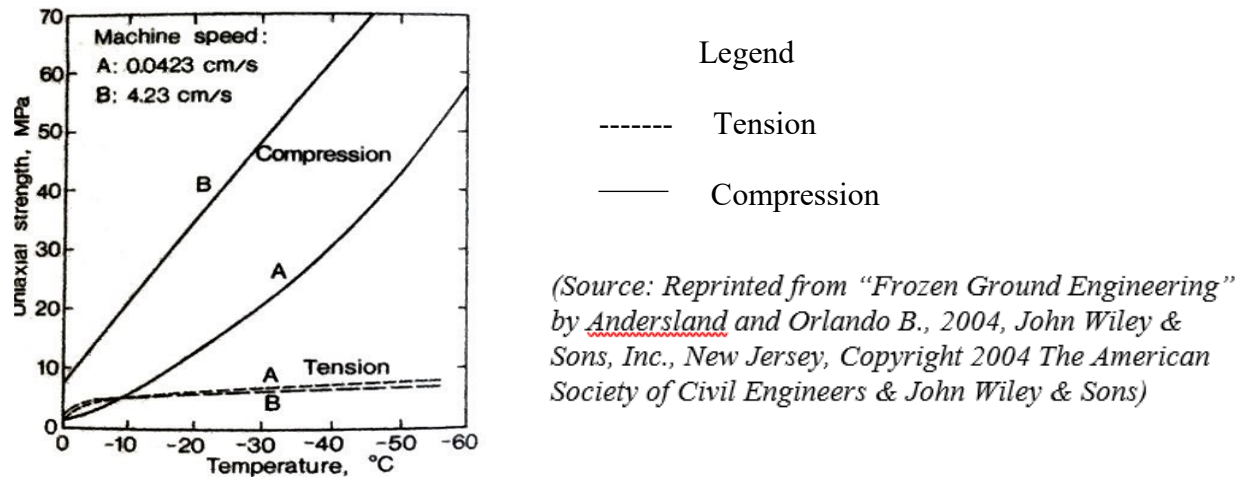


**Figure 40:** Average strength versus temperature relationship for frozen silt in uniaxial compression and tension tests.

For the research analysis, ice is considered as a material which can be used for the manufacturing of crane mats. The temperature of the frozen silt and ice is considered as  $-10^{\circ}\text{C}$  for analysis purposes (see Figure 40 for frozen silt). The values of the mechanical properties of these materials are presented in Table 3 and Table 4.

**Table 3:** Linear mechanical properties

		Units	G40.21-44W	S355	Coastal Douglas-Fir	Ice	Frozen Silt
1.	Young's Modulus	MPa	200,000 <sup>1</sup>	210,000 <sup>2</sup>	13,400 <sup>3</sup>	9.0 <sup>4</sup>	10,000 <sup>5,3,6</sup>
2.	Poisson's Ratio		0.3 <sup>29</sup>	0.3 <sup>30</sup>	0.449 <sup>6</sup>	0.33 <sup>3,2</sup>	0.3 <sup>39</sup>
3.	Tensile Yield Strength	MPa	350 <sup>29</sup>	355 <sup>30</sup>	2.3 <sup>31</sup>	3.1 <sup>7</sup>	5.1 <sup>8</sup>
4.	Compressive Yield Strength	MPa	152 <sup>9</sup>	546 <sup>10</sup>	5.0 <sup>31</sup>	25 <sup>32</sup>	5.0 <sup>36</sup>
5.	Tensile Ultimate Strength	MPa	450 <sup>29</sup>	460 <sup>30</sup>	5.0 <sup>31</sup>	3.1 <sup>32</sup>	5.1 <sup>36</sup>

**Table 4:** Non-linear mechanical properties (bilinear isotropic hardening)

		Units	G40.21-44W	S355	Coastal Douglas-Fir	Ice	Frozen Silt
1.	Tangent Modulus	MPa	504 <sup>11</sup>	504 <sup>39</sup>	110 <sup>34</sup>	0 <sup>12</sup>	0 <sup>40</sup>

<sup>1</sup> CISC. 2017. Handbook of Steel Construction. Canadian Institute of Steel Construction, 11th edition. Accessed 03 16, 2018. <http://www.webcivil.com/frmsteelproperty.aspx>.

<sup>2</sup> MEADinfo. 2015. Material Properties of S355 Steel - An Overview. 08 23. Accessed 03 16, 2018. <http://www.meadinfo.org/2015/08/s355-steel-properties.html>.

<sup>3</sup> Kretschmann, David. E. 2010. "Mechanical Properties of Wood, Chapter 5." In Wood Handbook, 5.1-46. U.S. Dept. of Agriculture, Forest Service, Forest Products Laboratory.

<sup>4</sup> Schulson, Erland M. 1999. "The Structure and Mechanical Behavior of Ice." JOM (Springer-Verlag) 51 (2): 21-27. doi:<https://doi.org/10.1007/s11837-999-0206-4>.

<sup>5</sup> Wilson, Charles Ralph. 1982. "Dynamic Properties of Naturally Frozen Fairbanks Silt." Master of Science Thesis in Civil Engineering. Corvallis: Oregon State University, April 22.

<sup>6</sup> Green, David W., Jerrold E. Winandy, and David E. Kretschmann. 1999. "Mechanical Properties of Wood." In Wood Handbook, 4.1-45. U.S. Dept. of Agriculture, Forest Service, Forest Products Laboratory.

<sup>7</sup> Petrovic, J. J. 2003. "Review Mechanical properties of ice and snow." JOURNAL OF MATERIALS SCIENCE (Kluwer Academic Publishers) 38 (1): 1-6. doi:<https://doi.org/10.1023/A:1021134128038>.

<sup>8</sup> Yang, Zhaohui (Joey), Benjamin Still, and Ziaoxuan Ge. 2015. "Mechanical properties of seasonally frozen and permafrost soils at high strain rate." Cold Region Science and Technology 113: 12-19. doi:[doi:10.1016/j.coldregions.2015.02.008](https://doi.org/10.1016/j.coldregions.2015.02.008).

<sup>9</sup> Boyer, Howard E., and Timothy L. Gall. 1985. Metals Handbook. OH: American Society for Metals, Materials Park.

<sup>10</sup> Singh, N. K., E. Cadoni, M. K. Singha, and N. K. Gupta. 2013. "Dynamic Tensile and Compressive Behaviors of Mild Steel at Wide Range of Strain Rates." JOURNAL OF ENGINEERING MECHANICS (ASCE) 139 (9): 1197-1206. doi:[10.1061/\(ASCE\)EM.1943-7889.0000557](https://doi.org/10.1061/(ASCE)EM.1943-7889.0000557).

<sup>11</sup> Andersland, Orlando B., and Branko Ladanyi. 2004. Frozen Ground Engineering. New Jersey: Wiley.

<sup>12</sup> Assumed brittle in nature

### 3.3.3. Mat Sizes

There are five test materials utilized for the mat strength. For steel mats, the mat illustrated in Figure 41, which is the most commonly used design by crane rental company NCSG in Alberta, is used for the present analysis. The length and the size of the mat are as below:

- Length = 3.6449 m
- Width = 2.4384 m
- Height (thickness) = 0.2032 m
- 1. Material = G40.21-44W
- 2. Material = S355

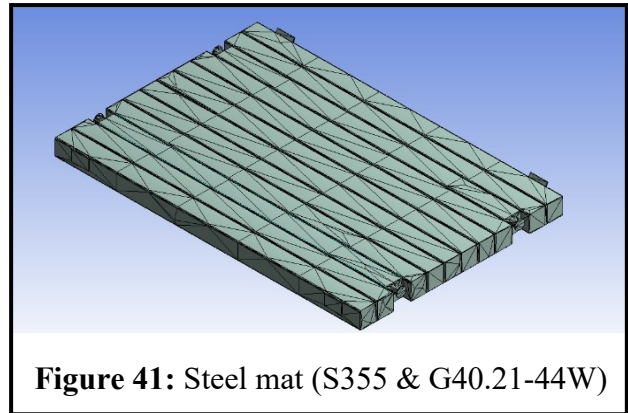


**Figure 41:** Steel mat (S355 & G40.21-44W)

For Coastal Douglas-Fir, ice, and frozen silt mats, the test mat depicted in Figure 42 is used for the analysis. The size is similar to the previously mentioned mat, but the thickness is different for ice. The dimensions are as below:

- Length = 3.6449 m
- Width = 2.4384 m
- Height (thickness):
  - 1. Material = Coastal Douglas-Fir (0.2032 m)
  - 2. Material = Frozen silt (0.2032 m)
  - 3. Material = Ice (0.8 m and 1.3 m)

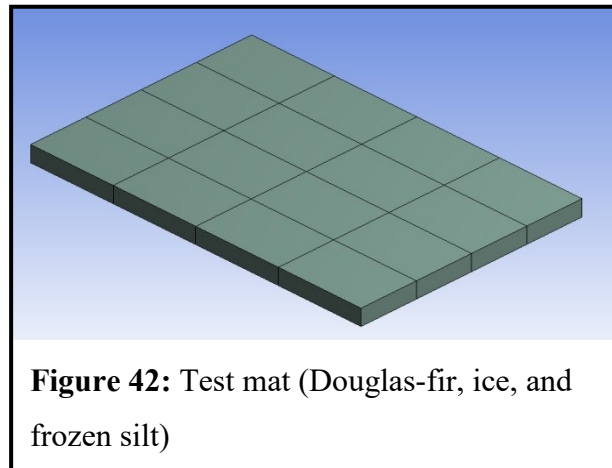


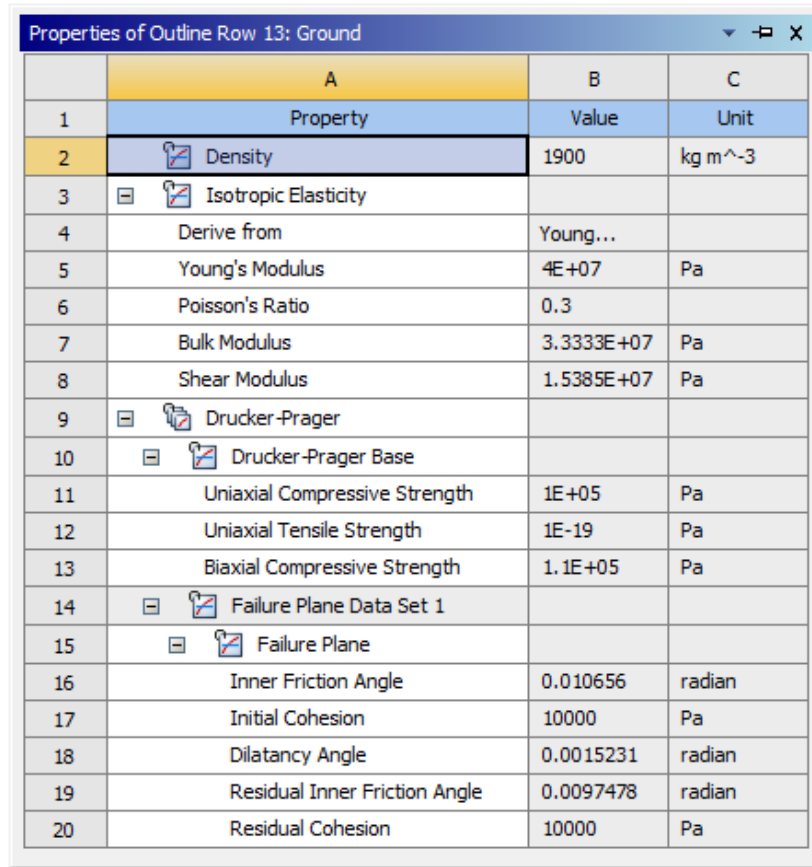
**Figure 42:** Test mat (Douglas-fir, ice, and frozen silt)

### 3.3.4. Soil Properties

The target of this research is to find a better solution for crane matting. These mats are required in heavy industrial projects to provide stable ground support in situations where the soil bearing strength is weak. The soil parameters are included in this research. The bearing strength of the soil with respect to the length of the mat has already been discussed in the previous chapter (Section

2.3.4). The soil parameters considered for this research are listed in Figure 43 (Yang, Xiu, Zhang, & Yan, 2010).

The soil under the mats is modelled as per Drucker-Prager theory (Badry & Satyam, 2013)<sup>1</sup>. The model was first presented by D. C. Drucker in 1952 and is based on the elastic-plastic constitutive relationship. It is a pressure-dependent model to estimate the failure or permanent deformation under loading (Drucker & Prager, 1952).



Properties of Outline Row 13: Ground			
	A	B	C
1	Property	Value	Unit
2	Density	1900	kg m <sup>-3</sup>
3	Isotropic Elasticity		
4	Derive from	Young...	
5	Young's Modulus	4E+07	Pa
6	Poisson's Ratio	0.3	
7	Bulk Modulus	3.3333E+07	Pa
8	Shear Modulus	1.5385E+07	Pa
9	Drucker-Prager		
10	Drucker-Prager Base		
11	Uniaxial Compressive Strength	1E+05	Pa
12	Uniaxial Tensile Strength	1E-19	Pa
13	Biaxial Compressive Strength	1.1E+05	Pa
14	Failure Plane Data Set 1		
15	Failure Plane		
16	Inner Friction Angle	0.010656	radian
17	Initial Cohesion	10000	Pa
18	Dilatancy Angle	0.0015231	radian
19	Residual Inner Friction Angle	0.0097478	radian
20	Residual Cohesion	10000	Pa

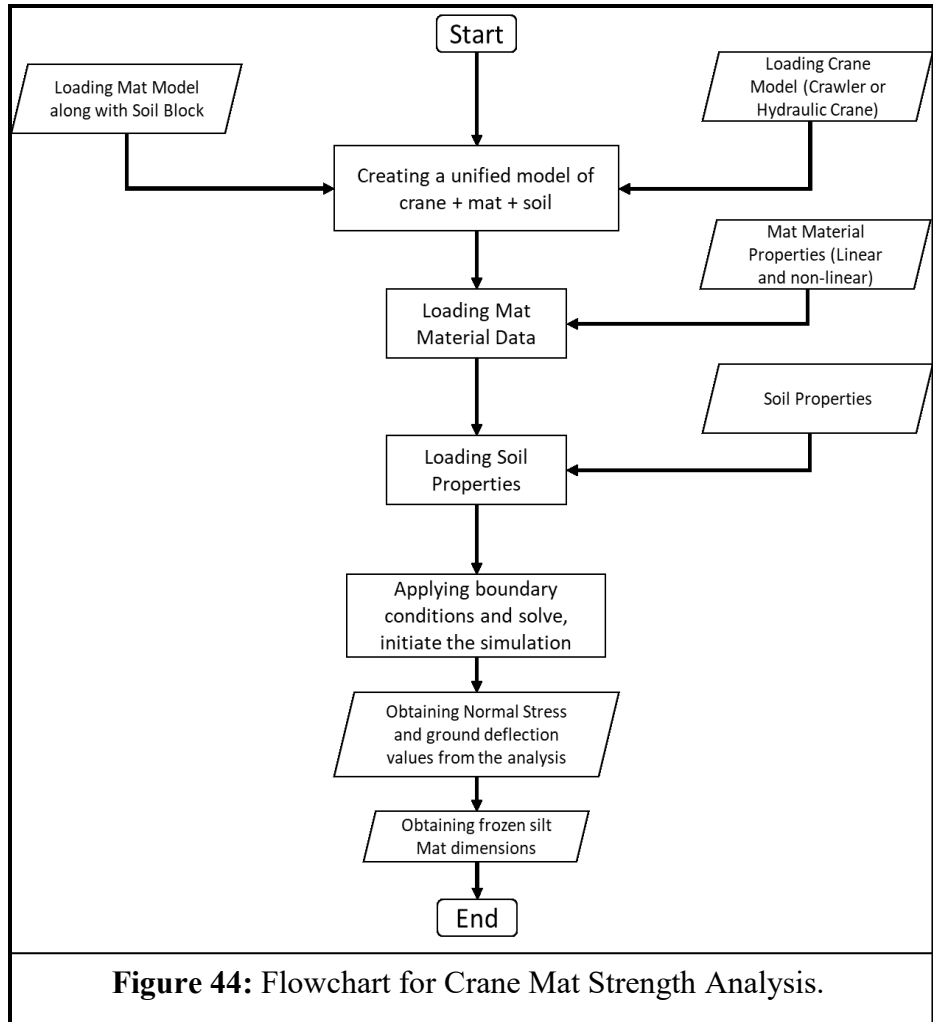
**Figure 43:** Soil properties for mat investigation

### 3.3.5. Mat Strength Analysis Methodology

The mat model is placed under the crane. The crane benchmark (Section 3.3.1.) paves the way for the mat strength stability. The material properties of the mat material are uploaded to ANSYS mechanical workbench. For the mat material strength simulation, both the linear and non-linear

<sup>1</sup> Module available in ANSYS to simulate soil behavior under pressure.

material properties are considered. The details of the mechanical properties are discussed in Chapter 2. For analysis purposes, only the normal stresses under the mat are considered. Usually, the normal stresses are similar to minimum principal stresses. The purpose of the analysis is to determine the relationship between different mat materials under similar circumstances. The



The main normal stress values are not compared with some manual calculations. Rather, they are compared with each other to define whether an ice or frozen silt mats can replace or perform equally to the traditional method. Therefore, all 5 materials are tested under similar conditions. Along with normal stresses, the ground deflection is also considered for the comparative analysis. The deflection is low for steel as compared to timber mats and ice/frozen silt mats.

For the analysis, only one crane configuration was selected for the crawler crane and the hydraulic crane. The data flowchart is presented in Figure 44. The values of normal stresses under the crane mat and the ground deflection for each mat material are obtained to analyze and compare. The data obtained from this exercise is used to obtain the strength of ice and frozen silt under loading, observing similar circumstances used for timber mats and steel mats.

### 3.3.6. Thermal Properties

For the thermal analysis, the thermal properties of the material for ANSYS simulation are tabulated in Table 5.

**Table 5:** Thermal properties of materials involved in frozen silt mat thermal process ANSYS analysis.

Sr.	Description	Density (kg/m <sup>3</sup> )	C <sub>p</sub> (j/kg•°C)	Thermal Conductivity (W/m•K)	Viscosity (Poise)
1.	Steel	7,500	500	43	0
2.	Frozen Silt (120%)	1,100 <sup>1</sup>	1,360 <sup>42</sup>	1 <sup>42</sup>	0
3.	Ice	900	2,090	0.08	0
4.	CaCl <sub>2</sub> (30%)	1,318 <sup>2</sup>	2,650 <sup>43</sup>	0.5 <sup>3</sup>	0.221 <sup>44</sup>
5	Liquid Nitrogen (-150°C)	808.5 <sup>4</sup>	2,040 <sup>5</sup>	0.1396 <sup>46</sup>	0.00068 <sup>6</sup>

### 3.3.7. Heat Transfer Analysis Method

The data from the mat strength analysis provide the basis for the heat transfer analysis. For heat transfer analysis, ANSYS Fluid Flow (Fluent) solver is used in order to simulate the cooling of frozen silt mat to convert it into frozen silt mat (solid). Two processes are used for this purpose,

<sup>1</sup> Andersland, Orlando B., and Branko Ladanyi. 2004. *Frozen Ground Engineering*. New Jersey: Wiley.

<sup>2</sup> OXYChem. 2018. "Calcium Chloride - A Guide to Physical Properties." OXYChem Publisher.

<sup>3</sup> DYNALENE. 2018. "Calcium Chloride Series Brine." Dynalene.

<sup>4</sup> Itterbeek, A. Van, and O. Verbeke. 1960. "Density of Liquid Nitrogen and argon as a function of pressure and temperature." *Physica (Elsevier)* 26(11): 931-938.

<sup>5</sup> Jensen, J. E., W. A. Tuttle, R. B. Stewart, H. Brechna, and A. G. Prodell. 1980. VI - Properties of Nitrogen. Vol. 1, in *BROOKHAVEN NATIONAL LABORATORY SELECTED CRYOGENIC DATA NOTEBOOK*, by J. E. Jensen, W. A. Tuttle, R. B. Stewart, H. Brechna and A. G. Prodell, 45. New York: Brookhaven National Laboratory.

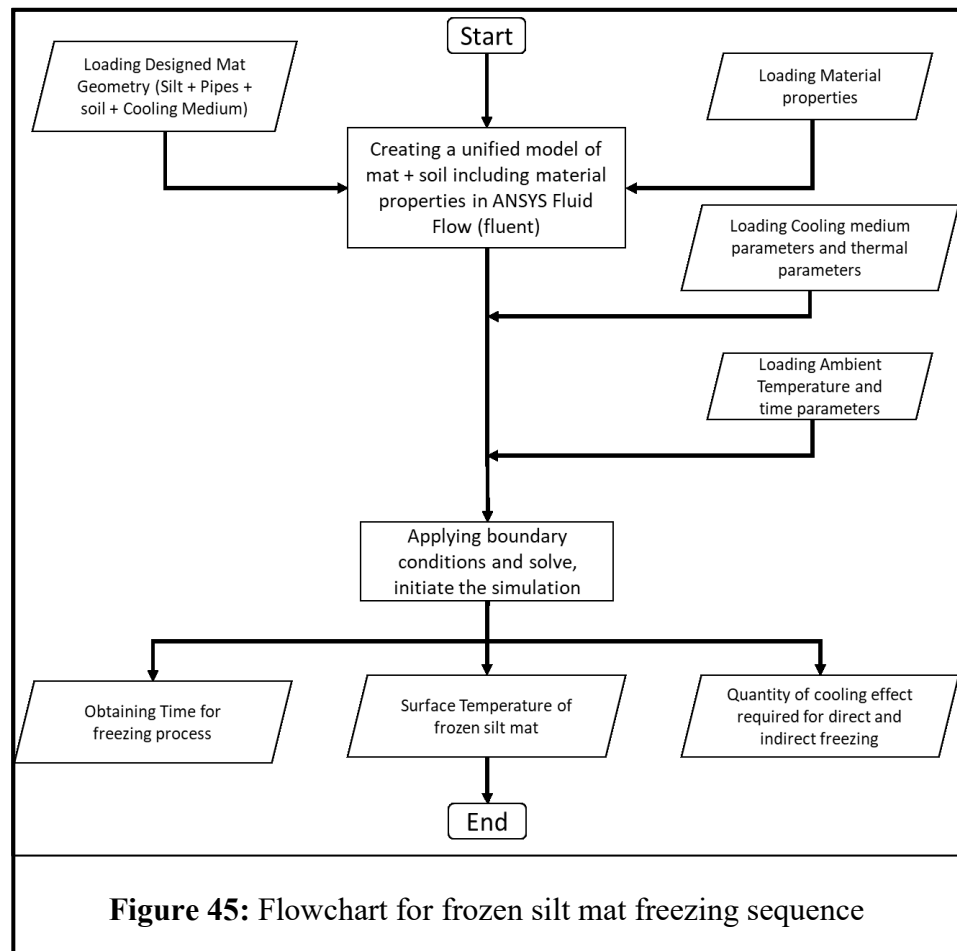
<sup>6</sup> Grevendonk, W., W. Herreman, and A. De Bock. 1970. "Measurement on the Viscosity of Liquid Nitrogen." *Physica (Elsevier B.V.)* 46 (4): 600-604.

indirect freezing and direct freezing, which were presented in Chapter 2. The process is summarized in the following steps:

Step 1: The mat dimensions obtained from the mat strength analysis are used to propose the design of the frozen silt mat. The freeze pipes are added to the frozen silt mat for the purpose of freezing the soil around the freeze pipes, resulting in a solid frozen silt mat. The design of the mat with the addition of freeze pipes is uploaded in ANSYS Flow (Fluent) Geometry Module. The mat is placed on the same soil model which is being used for the mat strength analysis. The parameters of soil

and the frozen silt mat are considered to be equal with the exception of the differences in the internal temperature of the frozen silt after cooling and the ambient temperature of the loose soil beneath the frozen silt mat.

Step 2: One end of the pipe is considered to be an inlet for the cooling agent, and the other



end as the outlet for the cooling agent. For indirect freezing, CaCl<sub>2</sub> is used as the cooling agent. The velocity and temperature of the cooling agent are adjusted to obtain the heat transfer. For direct freezing, the flow of liquid nitrogen is used to monitor the freezing of the mat. The temperature of the inlet of the cooling agent is adjusted as per the cooling parameters.

Step 3: The heat transfer rate along the flow of the liquid provides the data of heat transfer for cost calculations. The cooling administered by the cooling agent is used to determine the capital cost



of the freezing refrigeration unit for indirect freezing. For direct freezing, the amount of liquid flow provides the quantity of liquid nitrogen used for the freezing of the mat. The time required for the freezing of the mat surface is also recorded for further analysis.

Step 4: The ambient temperature and the boundary conditions are applied to the model. Prior to this, the geometry is subdivided into smaller elements by applying “meshing”. Meshing is carried out to break the whole model into small finite elements for analysis. The time steps and iterations per step are applied to the solver.

Step 5: The solution is uploaded to the results section of the solver. The required data is used to obtain the figures for cost comparison. The heat transfer with respect to time is obtained for the operating cost of the whole system. The surface temperature of the mat is observed and recorded to check the feasibility of required frozen silt mat temperature. For indirect freezing, there are three main variables obtained from this exercise: the temperature difference between inlet and outlet temperature of cooling medium; the time required for cooling; and surface temperature of the frozen silt mat. For direct freezing, there are three main variables: the flow of liquid nitrogen; the time required for cooling; and the surface temperature of the frozen silt mat.

The above-mentioned methodology is presented in the form of a data flowchart in Figure 45.

### **3.3.8. Cost Driver**

To conduct the cost analysis, the estimation of cost drivers is essential. The cost comparison can be divided into three main categories of cost drivers: traditional crane timber mats, frozen silt mats (indirect freezing), and frozen silt mats (direct freezing).

#### **3.3.8.1. *Traditional Crane Timber Mats***

The mind map of the cost drivers is shown in Figure 46. The major cost drivers are the timber mat, transportation, labor, and equipment for laying/removal of the timber mats on site. Values for all these cost drivers are obtained from industry experts<sup>1</sup>. These values are used for the cost comparison in the present research. It should be noted that it is assumed that silt is available free of cost.

---

<sup>1</sup> NCSG Crane & Heavy Haul Corporation, Engineering Department

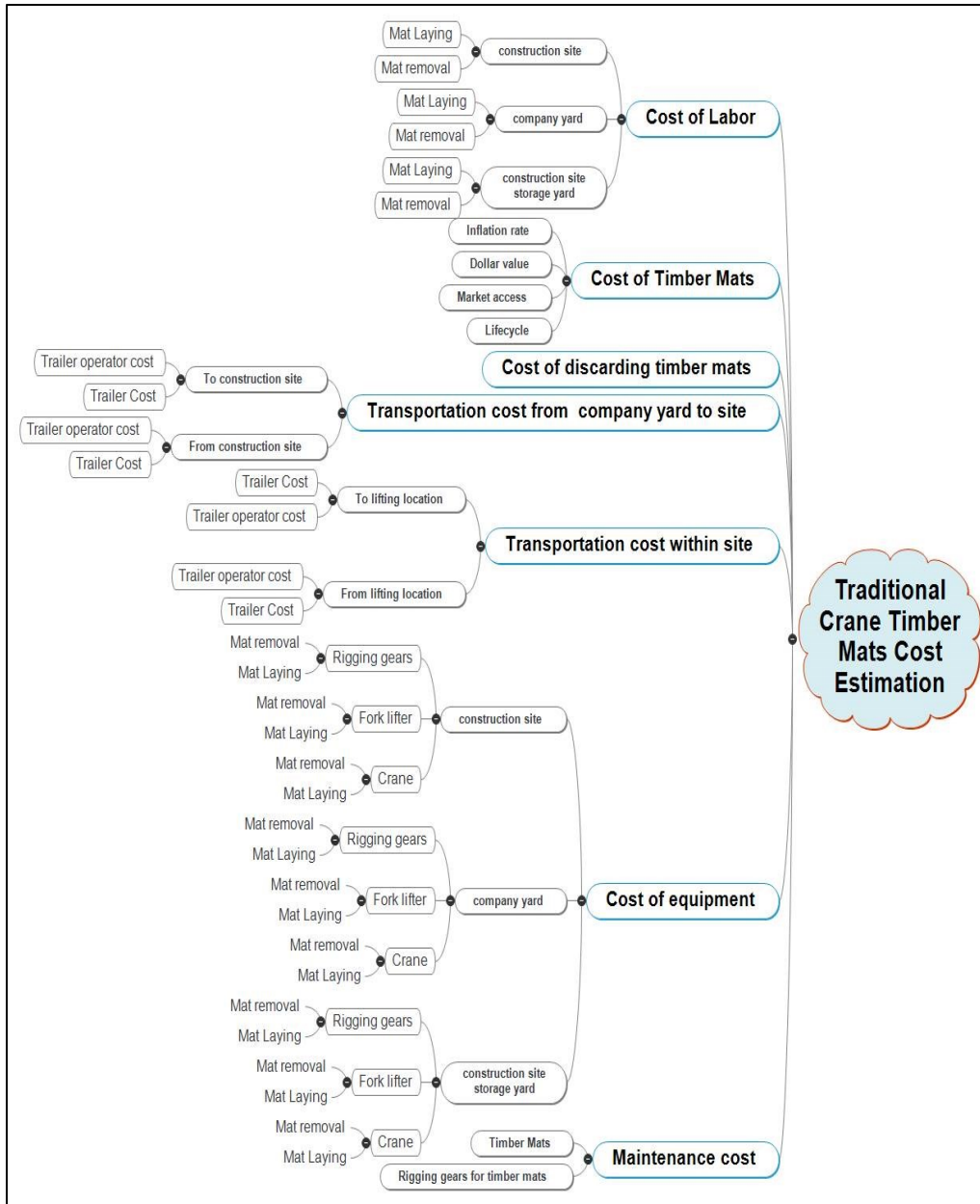


**Figure 46:** Cost drivers for traditional crane timber mats

### 3.3.8.2. *Frozen Silt Mat (Indirect Freezing)*

Brine chiller is used for indirect freezing. The main cost driver for indirect freezing is the cost of the brine chiller, although here the case company already owns a chiller. On the other hand, if the chiller is a rental, the rental cost becomes the main cost driver. A mind map diagram of cost drivers is shown in Figure 47. The present research assumes that the silt for the mat is readily available on site and that the mechanical and thermal properties of the soil on site are close to the assumed silt

mechanical properties used for this research. It is assumed, as noted above, that silt is available free of cost. In the interest of simplicity, some of the cost drivers (chiller breakdown, pipe rupture, etc.) are omitted from the map diagram. The detailed cost drivers can be incorporated in future research optimizing this newly designed frozen silt mat along with the field testing.

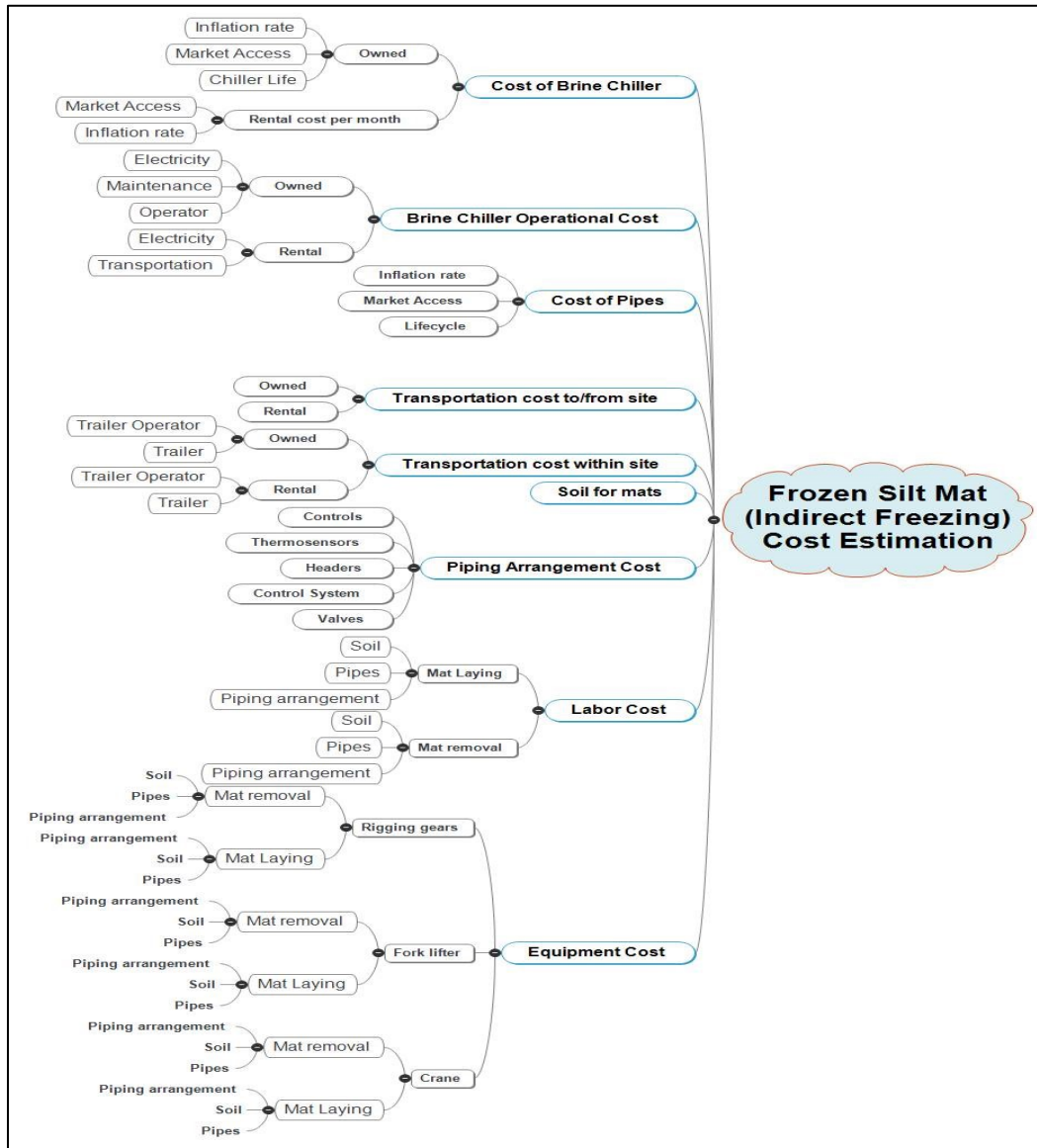


**Figure 47:** Cost drivers for Frozen Silt Mat (Indirect Freezing).

**3.3.8.3. Frozen Silt Mat (Direct Freezing)**

In indirect freezing, the main cost driver is the cost of the liquid nitrogen used for the freezing. The liquid nitrogen is dispersed into the air again as gas after freezing of the mat. Figure 48 shows

the mind map of the cost drivers of direct freezing. The present research considers that the silt for the mat is readily available on site and the mechanical and thermal properties of soil on site are close to the assumed silt mechanical properties used for this research. It is assumed that the project site is accessible for the transportation of liquid nitrogen. The complexity of the rear project site will be captured in future research.

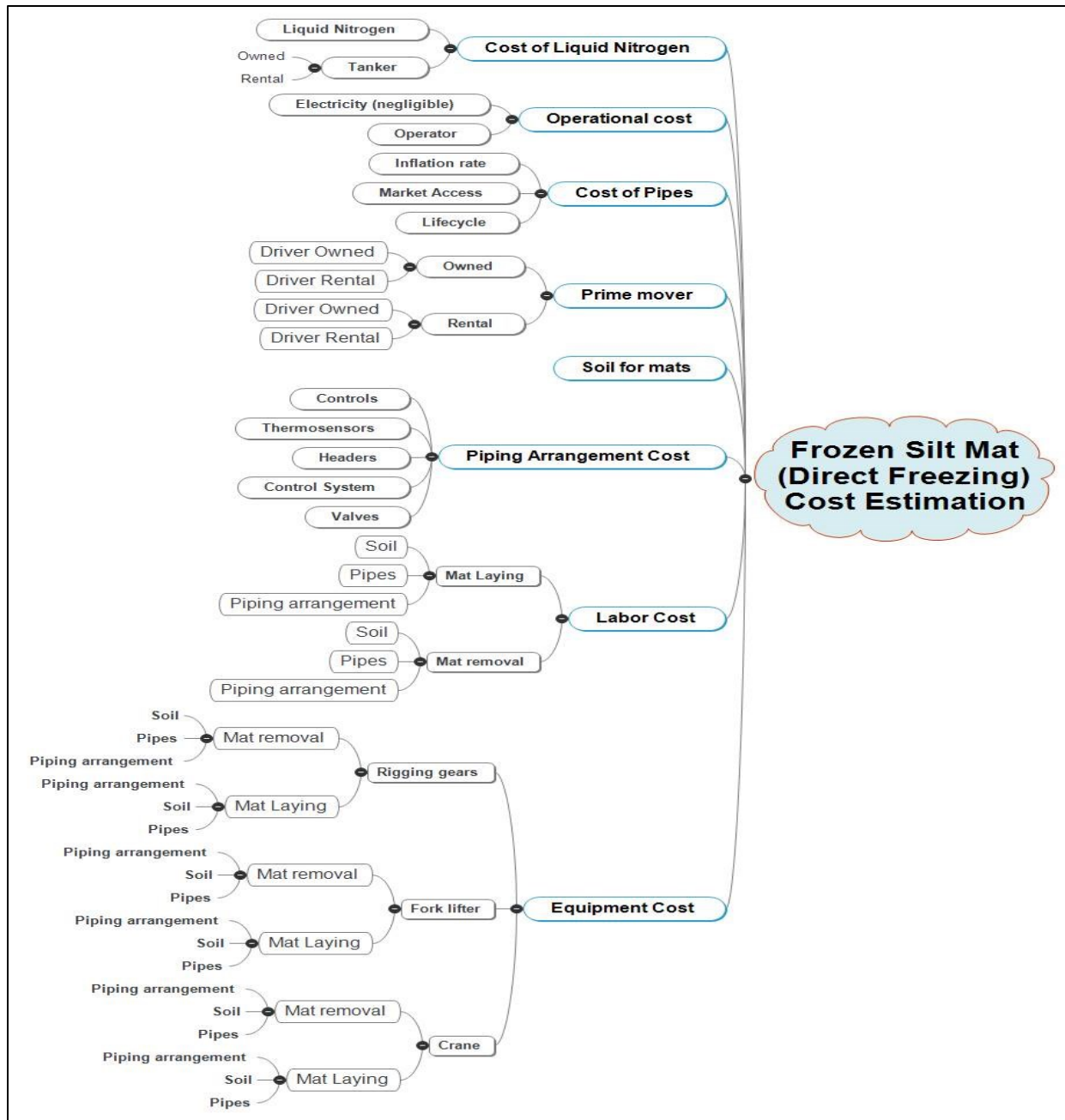


**Figure 48:** Cost drivers for Frozen Silt Mat (Direct Freezing).

### 3.3.9. Cost Comparison Analysis Method

For the cost comparison, values of the cost drivers are required which are to be applied to a real-time project to predict the cost estimation for these three investments. Due to the complexity of actual projects, it is difficult to apply these cost parameters in practice. A solution to this complexity is to assume a hypothetical project where these three categories are applied simultaneously within the same environment subject to the same conditions. There is one more category assumed where the hybrid system is applied to prepare the cost comparison.

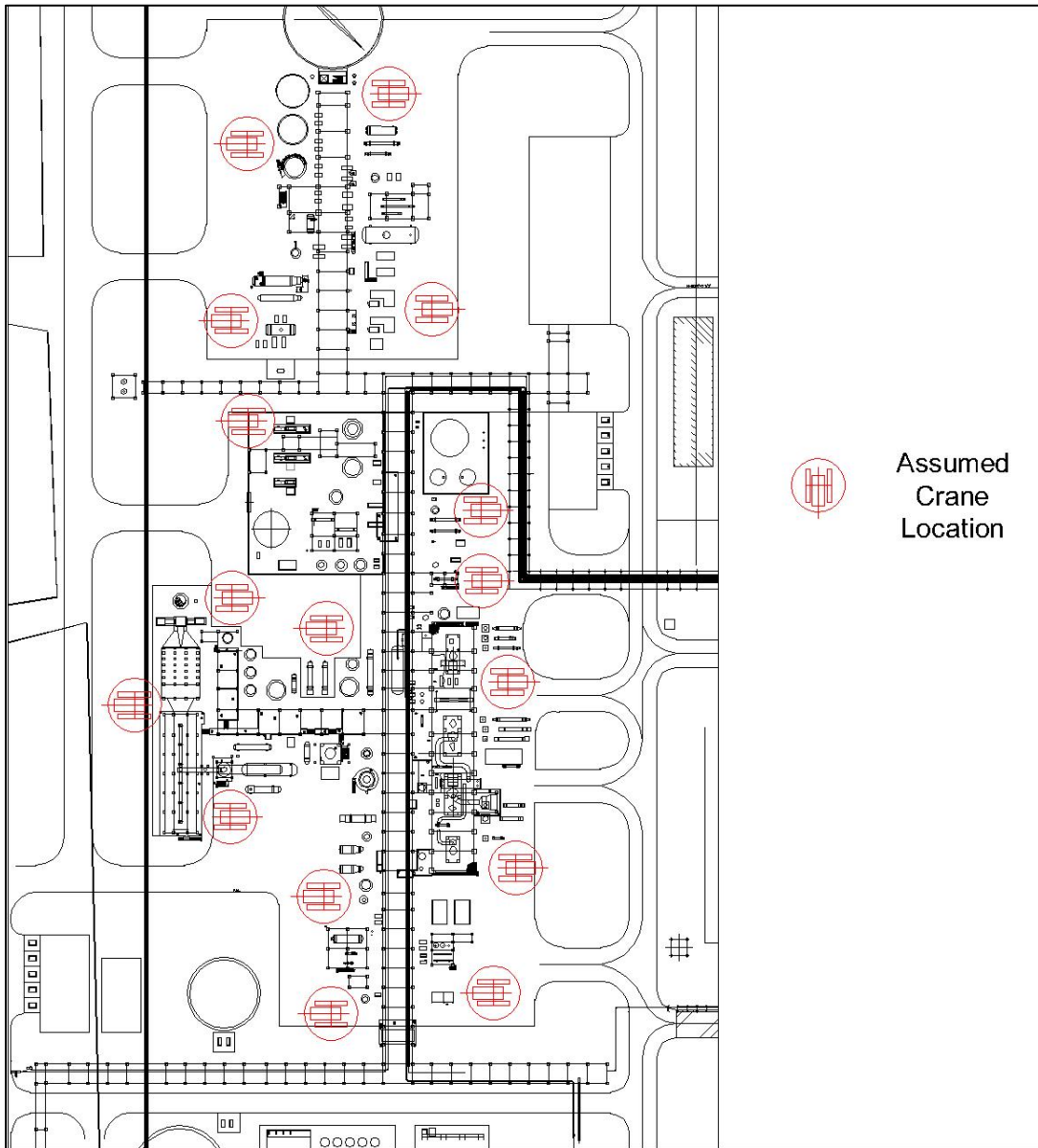


**Figure 49:** Hypothetical Project (Any resemblance with any existing project is coincidence)

The project considered in this research is located north of Yellowknife, NWT, Canada. There are already two diamond mines north of Yellowknife (see Section 2.10.2). The duration of the project is 8 months. The assumed average ambient temperature of each month is shown as below (based on meteorological data for Yellowknife):

A. Month-1	March	-10°C
B. Month-2	April	0°C
C. Month-3	May	5°C
D. Month-4	June	10°C
E. Month-5	July	10°C
F. Month-6	August	10°C
G. Month-7	September	5°C
H. Month-8	October	0°C

It is assumed that the total number of crane lifting locations is 16. The assumed crane usage at one location is 7 days. As such, there is a gap of 8 days between two locations. It is assumed that at each location, about 1.5 pieces of equipment (pipe racks, exchangers, columns, vessels, etc.) is installed in a given day (based on market experts' opinion<sup>1</sup>). For the cost comparison, only one crane (Crawler Crane Manitowoc 18000) is used for the analysis. The work breakdown structure (WBS) of each option is provided below:

### **3.3.9.1. WBS of Traditional Timber Mat**

The WBS of traditional timber mat is very simple. The timbers must be transported from the company yard to the construction site before the start of the project and are returned to the company yard after the project is complete. This involves a one-time cost for each project. It is assumed that matting is transported and placed under the crane in one day. The crane operates for seven days, then moves to another location. Mat removal and transportation are assumed to take 1 day more. There is also transportation cost associated with the shifting of timber mats within a given construction site. There is a gap of 8 days between two locations which figures as waiting time for the equipment arrival. Each month has 14 days of work and 16 days of waiting. The total number of lifts in 240 days is assumed to be 168, involving 21 pieces of equipment in one month (average

---

<sup>1</sup> Northern Crane Services Group Engineering Department.

1.5 lifts per day on a single location). It is assumed that the crane remains stationary at one position throughout its stay on one lifting location. Table 6 shows the assumed project details in numbers.

**Table 6:** Hypothetical Project Detail (in Numbers)

Number of Crane Lifting locations	16.00	Nos.
Days of Crane usage on one location	7.00	Days
Lifts per Location	10.50	Nos.
Days Gap between two locations	8.00	Days
Total Lifts in 240 days (one year)	168.00	Nos.

The assumed project is developed in consultation with crane rental industry experts<sup>1</sup>. The project details and schedule for timber mats is shown in Figure 50.

### **3.3.9.2. WBS of Brine chiller (Indirect Freezing)**

For frozen silt mat preparations, first, it is proposed that the soil with water is to be placed on the ground with the freezing pipes in between. The duration of the project remains the same. It is expected that freezing of soil will take some time. This time calculation using ANSYS is done in later chapters. At the end of the project, the soil is left to thaw and removed from the site later. In this process, only the brine chiller is assumed to be used for the freezing and maintenance phase of the frozen silt mat. The calculations are based on the cost driver for indirect freezing. The brine chiller can be owned or rented. Both options are analyzed in this research.

### **3.3.9.3. WBS of Liquid Nitrogen (Direct Freezing)**

Direct freezing is similar to indirect freezing, with the notable difference that, instead of brine chiller, liquid nitrogen is used for the freezing. After the lifting operations are done, again it is assumed that the frozen silt mat will be left to thaw and removed subsequently.

### **3.3.9.4. WBS of Hybrid System (Liquid Nitrogen and Brine chiller)**

The hybrid process is a combination of direct freezing and indirect freezing. The time required for each phase (direct and indirect), as per the ambient temperature, is calculated in later chapters. As

---

<sup>1</sup> Northern Crane Services Group Engineering Department

in the approaches described above, after the lifting is done, the frozen silt mat is left to thaw and is removed later.

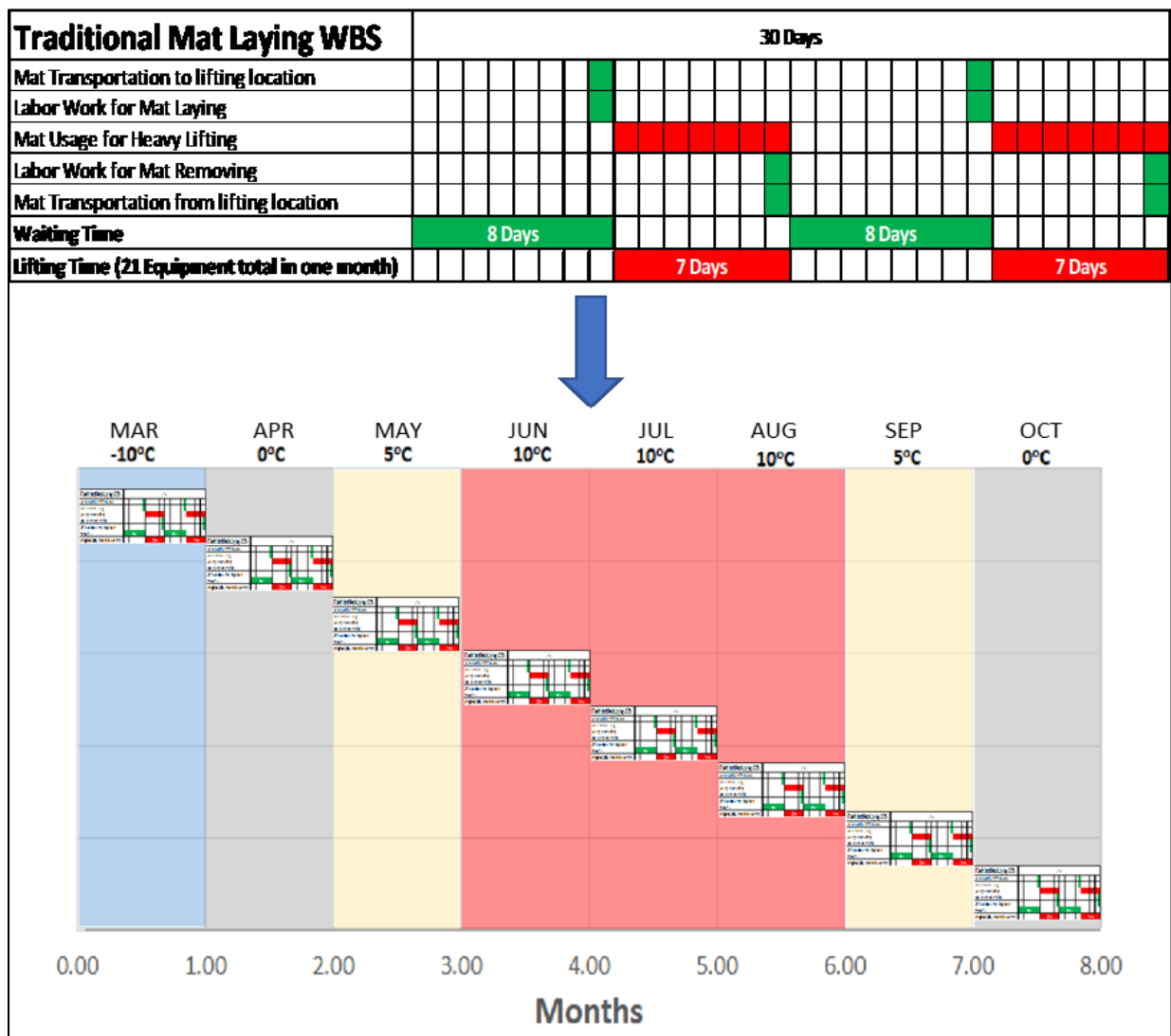


Figure 50: WBS for a Dummy project in Yellowknife, NWT (Timber Mat Use).



## CHAPTER 4: GROUND BEARING PRESSURE AND STRESS ANALYSIS:

### 4.1 Ground Bearing Pressure

#### 4.1.1. Crawler Crane (Manitowoc 18000).

The configuration of the crane is outlined in Table 7. For this case study, three different loads at three different lifting radii are tested using ANSYS. The AutoCAD 3D model is imported into the ANSYS geometry module (see Figure 51). The parts of the crane are segregated into three major parts: upper, lower, and steel plates (stress sensors). The upper part of the crane contains the load. As the

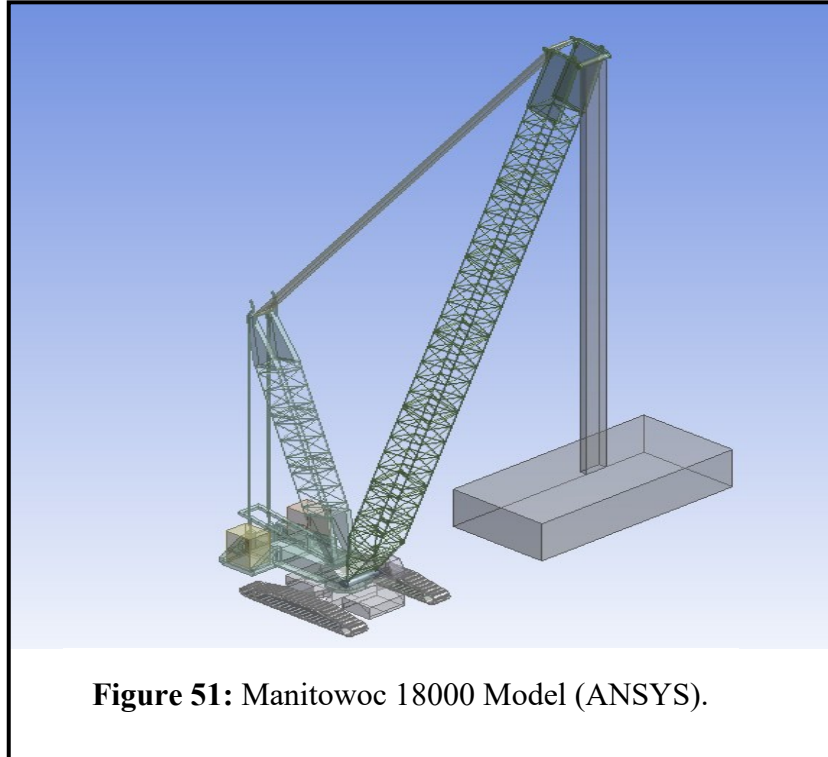


**Figure 51:** Manitowoc 18000 Model (ANSYS).

superstructure rotates, the load rotates with it. The boom angle with the ground's surface is adjusted to obtain the required lifting radius. A dummy block of material is used as the load for this crane, and the density of the dummy block is altered to obtain the required weight of the subject load. Given that the investigation is carried out for the three different loads with three different radii, three different geometries are developed, respectively<sup>1</sup>.

**Table 7:** Crane Configuration for Manitowoc 18000

	Description	Configuration
1.	Boom	85.344 m (280 ft) #55 OR #55A
2.	Carboy Counterweight	145,150 kg (320,000 lb)
3.	Superstructure Counterweight	239,500 kg (528,000 lb)

<sup>1</sup> Geometry consists of crane, mats, ground and load. The whole model under investigation in ANSYS is named Geometry in ANSYS. User can modify the same Geometry for each case study. To avoid rework by back and forth from one case example to the other, same geometry is copied thrice with different radius and loads.

Each geometry is uploaded to the static structural mechanical workbench solver. Identical weights and respective COGs are used for the algorithm to obtain a manual set of GBP data for the boom slew angle in the range 0° to 90° (crane front to crane left side). The same configuration is used to obtain the GBP values from the manufacturer’s software, “Manitowoc Ground Bearing Pressure Estimator Version: 1.0.6.0”, which is available as freeware from Manitowoc’s official website (Manitowoc, 2017). This process is carried out to obtain two sets of values, one from manual calculations and one from company-provided software (see Figure 37).

**Table 8:** Variation of GBP values between Manitowoc, manual, and ANSYS calculation (Manitowoc 18000)

Manual calculation input values			ANSYS input values		
Description	Weight (Ton)	COG distance (m) from CL of rotation	Weight (Ton)	COG distance (m) from CL of rotation	
Boom	118.358	11.256	118.360	11.270	
Upper	346.351	-5.985	346.350	-5.985	
Crawler	249.719	-0.176	249.720	-0.176	
Length of Bearing Crawler		8.839		8.840	
Distance Between Crawler		8.534		8.534	
Load 1	50.000	25.917	49.998	25.917	
Load 2	75.000	21.336	74.996	21.358	
Load 3	100.000	19.812	99.996	19.812	
Variation (%)			Load 1	Load 2	Load 3
Variation (%) between manual and Manitowoc Software Calculations			0.054	0.049	0.036
Variation (%) between manual and ANSYS Calculations			0.518	0.506	0.473

The next task is to obtain the GBP values from ANSYS solver. The first crane geometry is taken at the lifting radius of 25.917 m (85 ft) with the load of 50,000 kg (110,231.13 lb). Table 8 presents the crane configuration details for each case example. The geometry of the crane model is loaded as described in Step 3 for crawler cranes in Section 3.1. The model is loaded with the boundary conditions. The upper part of the crane is rotated from 0° to 90°. The model is then solved using

the static structural mechanical workbench solver. The top surface of the thin plate under the tracks is used as a sensor for the stresses in the form of normal or minimum principal stresses. All major crane parts are assumed to be rigid; thus, the minimum principal stresses are similar to normal stresses. For comparison, minimum principal stresses are utilized instead of normal stresses. Eq. 38 is applied to obtain the single value along the track.

The differences between the manual calculations and Manitowoc software values are noted. The percentage of variation is measured against the largest value. The percentage variation error between the manual calculations and Manitowoc software is found to be approximately 0.054%, (i.e., < 1%). The values of GBP from ANSYS are also obtained. Using Eq. 38, one set of ANSYS values is obtained and compared against the manual calculations. The percentage of error between ANSYS and the manual calculations is found to be approximately 0.518% (again, less than 1%). The GBP values from all three sets with respect to the boom slew angle from 0° to 90° from the front to the left side of the crane are presented in Figure 52.

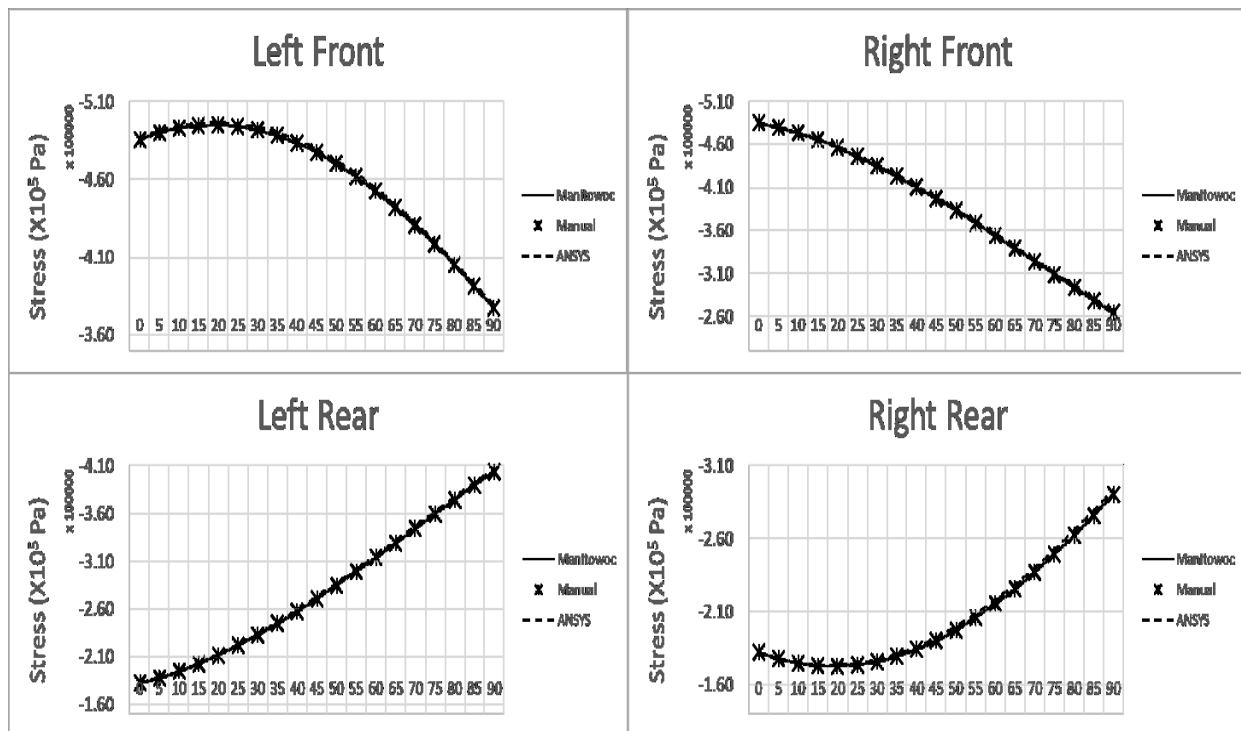


**Figure 52:** GBP (minimum principal stress) values from Manitowoc software (Manitowoc, 2017), manual calculations, and ANSYS simulation calculations on four sides of crawler crane, Manitowoc 18000, along boom slew angle from 0° to 90° from front to left side with load of 50,000 kg (110,231.13 lb) at lifting radius of 25.917 m (85 ft)

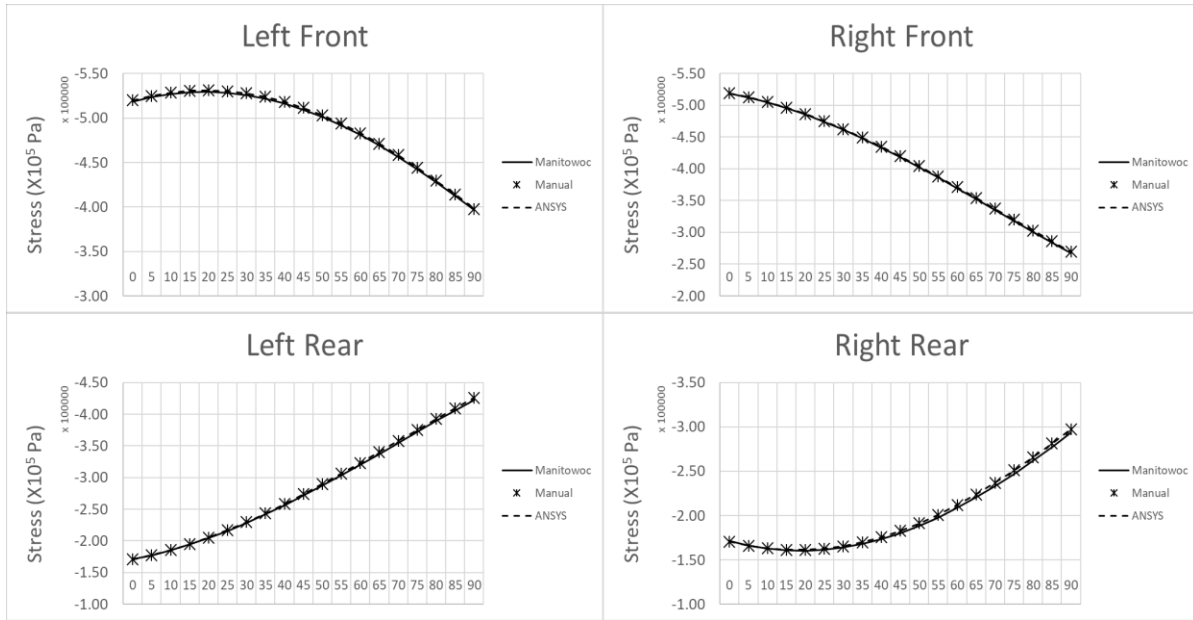


**Figure 53:** GBP (minimum principal stress) values from Manitowoc software (Manitowoc, 2017), manual calculations, and ANSYS simulation calculations on four sides of crawler crane, Manitowoc 18000, along boom slew angle from 0° to 90° from front to left side with load of 75,000 kg (165,346.69 lb) at lifting radius of 21.336 m (70 ft)

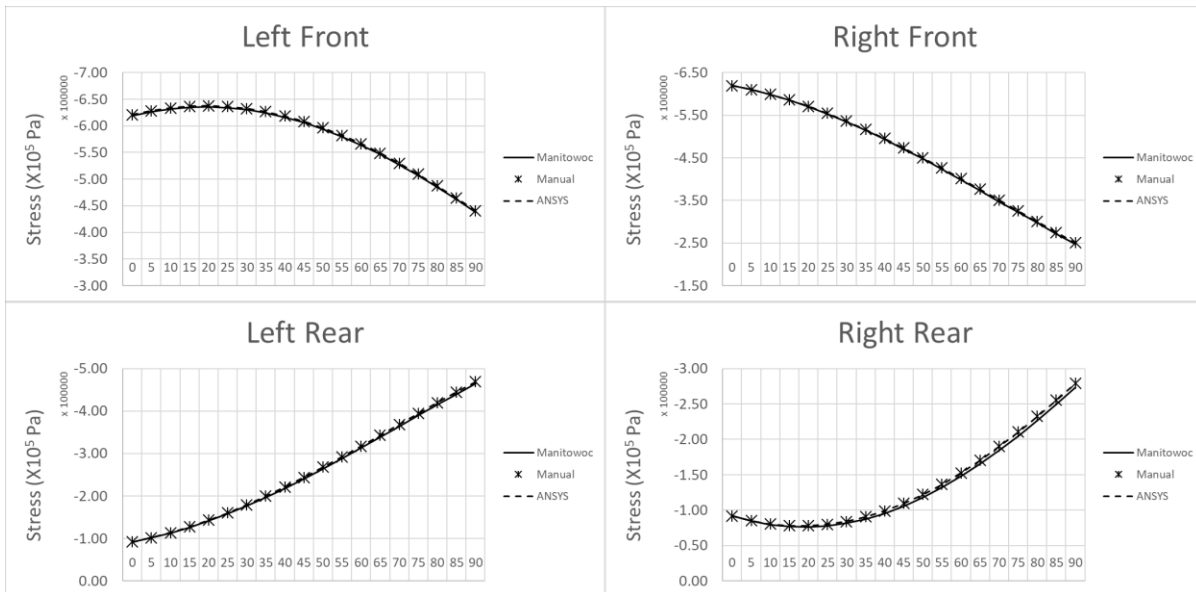


**Figure 54:** GBP (minimum principal stress) values from Manitowoc software (Manitowoc, 2017), manual calculations, and ANSYS simulation calculations on four sides of crawler crane, Manitowoc 18000, along boom slew angle from 0° to 90° from front to left side with load of 100,000 kg (220,462.26 lb) at lifting radius of 19.812 m (65 ft)

For the second load example, the crane geometry is inputted for a lifting radius of 21.336 m (70 ft) with a load of 75,000 kg (165,346.69 lb). The percentage variation between the manual calculations and the Manitowoc software is found to be approximately 0.049% (less than 1%). The percentage of error between ANSYS and the manual calculations is approximately 0.506%, also less than 1%. Figure 53 shows the GBP variation for the second load example.

For the third load example, crawler crane geometry is inputted for a lifting radius of 19.812 m (65 ft) with a load of 100,000 kg (220,462.26 lb). The percentage variation between the manual calculations and Manitowoc software is found to be approximately 0.036% and the percentage of error between ANSYS and the manual calculations is found to be approximately 0.473%. Figure 54 shows the GBP variation for the third load example.

#### 4.1.2. Hydraulic Crane (Grove GMK 7550)

Grove GMK7550 is selected for the second case example. Grove GMK7550 is a hydraulic all-terrain crane (see Figure 55). The crane configuration is shown in Table 9. In the case of hydraulic cranes, the manufacturer’s software and manual calculations only provide the load in the form of force on each outrigger. This reaction force is divided by the area of the mat to obtain the GBP in order to compare it with the soil capacity.

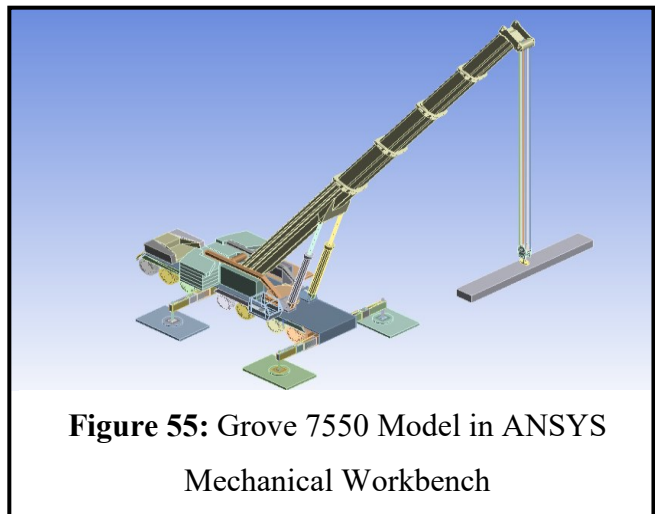


**Figure 55:** Grove 7550 Model in ANSYS Mechanical Workbench

**Table 9:** The Hydraulic Crane Configuration GMK7550.

	Description	Detail
1.	Boom Length	38.13 m (125.1 ft)
2.	Boom Configuration	[0-100-100-0]
3.	Superstructure Counterweights	119,975 kg (264,500 lb)
4.	Lifting radius	19.812 m (65 ft)
5.	Lifting Load	40,000 kg (88,185 lb)
6.	Outrigger Span	28.7 ft × 29.2 ft
7.	Surface Operating Condition	Solid

In this section, only the mat loads are compared rather than the GBP. An online application for pad/mat load calculations is available from the hydraulic crane manufacturer (Grove, 2017); however, this application only provides outrigger loads at particular angles in increments of 45°. For this case example, the superstructure slew angle is taken from 0° to 360° from the rear to the right side at an increment of 45° for the purpose of comparing the manual calculations with the online software (Figure 56).

The manual calculations are obtained from Eq. 11 to Eq. 14. These values are then compared with the online Grove application calculations. The percentage variation between the manual calculations and the Grove online application values is found to be approximately 1.66%. The reason for the higher variation is that the weights of parts and their respective COGs are not available from the manufacturer, but rather the pad loads are available from the online Grove application at various angles. By utilizing these pad load values against different angles and the use of Eq. 11 to Eq. 14 with weights and COGs as unknown variables, the required data is obtained (see Figure 37). The values of weights and COGs are adjusted to minimize the error (1.66% with respect to the largest value). The values of manual calculations and Grove online application values are then plotted against the angle of the superstructure slew in the range 0° to 360° (from the rear to the right side of the crane) at increments of 45° (see Figure 56).

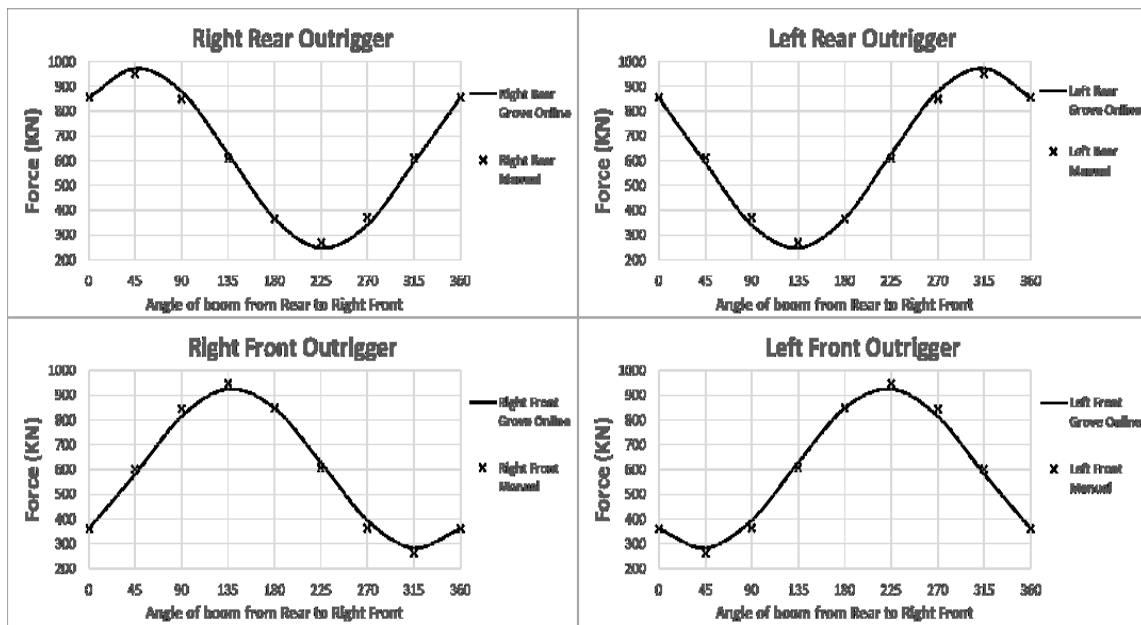


**Figure 56:** Pad load values from Grove online application (Grove, 2017) and manual calculations under four outriggers of Grove GMK7550, along boom slew angle from 0° to 360°

from rear to right side of crane with load of 40,000 kg (88,185 lb) at lifting radius of 19.812 m (65 ft).

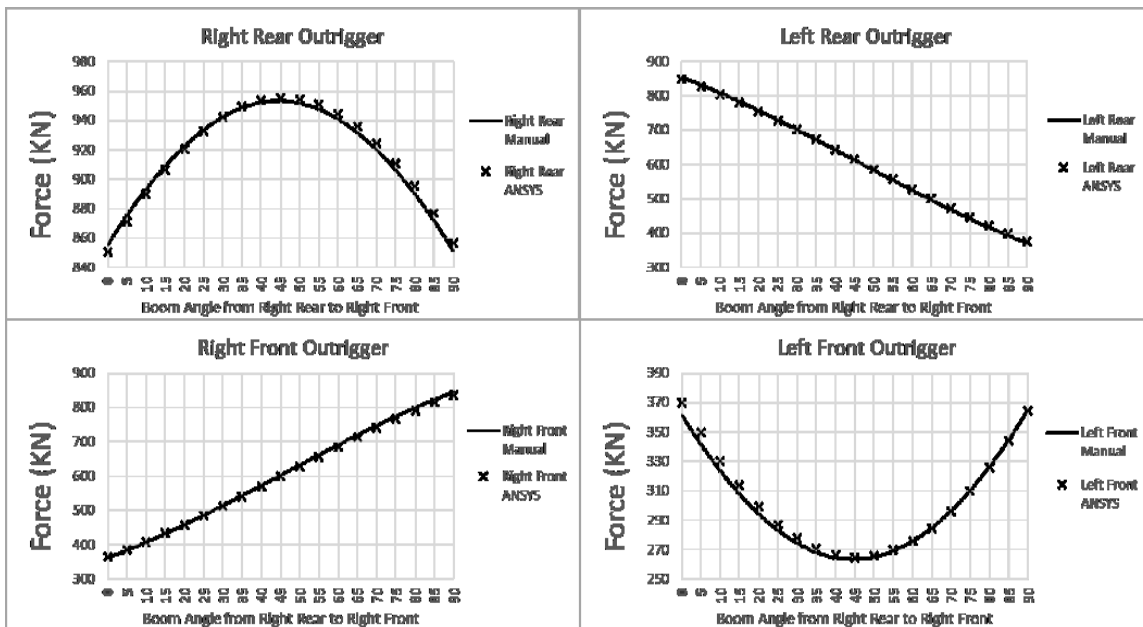


**Figure 57:** Pad load values from manual calculations and ANSYS simulation of the four outriggers of the hydraulic crane, Grove GMK7550, along with boom slew angle of 0° to 90° from rear to right side of crane with load of 40,000 kg (88,185 lb) at lifting radius of 19.812 m (65 ft).

The values of part weights and their respective COGs are used to develop the ANSYS geometry. The density of the dummy load block is altered to obtain the required weight of the subject load. The geometry of the crane model is loaded with the respective weights and COGs as described in Step 3 for hydraulic cranes (Section 3.3.1.). The model is loaded with the boundary conditions. The upper part of the crane is then rotated from 0° to 90°, and the model is solved using the static structural mechanical solver. The top surface of the mats is utilized as a sensor for reaction forces. The values from ANSYS are plotted against manual calculations as presented in Figure 57. The variation in the values is found to be approximately 0.37% (with respect to the largest value), which is less than 1%. Figure 57 shows the pad load values for manual calculations versus ANSYS.

#### 4.1.3. Summary of Crane Benchmark (Crawler and Hydraulic Crane)

This exercise provides a benchmark for the cranes used for the mat load testing and analysis. The crane model with the load used in the above exercise is also used later for the mat material

comparison analysis. The compressive pressure on the mat also changes with the change of boom slew angle. In the case of the crawler crane, as the boom slew from the left front to the left rear, the value of compressive stress increases as the load moves. The compressive stress value reaches its maximum when the load is directly over the left front track. When the load moves further, the value of compressive stress decreases correspondingly until the load comes directly over the crawler left side track. For mat material analysis, the same crane configuration with a load of 50,000 kg (110,231.13 lb) at a lifting radius of 25.917 m (85 ft) is considered. The geometry used is modified by adding mat and soil under the crawler.

The same is the case with the hydraulic crane: as the load moves from the rear to the right side, the value of compressive stress under the right rear outrigger mat increases until the load comes directly over the right rear outrigger. As the load moves away from the right rear outrigger, the value of compressive stress decreases. For mat material analysis, the same hydraulic crane configuration, with a lifting radius of 19.812 m (65 ft) and a load of 40,000 kg (88,185 lb), is considered. The geometry of the hydraulic crane is added with the mat and soil under the outrigger.

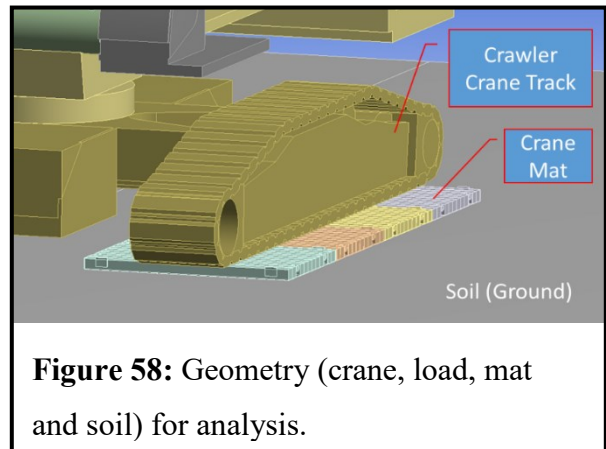
## 4.2. Linear and Non-linear Stress Analysis (ANSYS)

### 4.2.1 Crawler Crane (Manitowoc 18000).

For ANSYS, a case example of a Manitowoc 18000 crane with boom slew angles ranging from 0° to 90° from the front to the left side and with a load of 50,000 kg (110,231.13 lb) at a lifting radius of 25.917 m (85 ft) is considered. Figure 44 shows the data flowchart for the crane mat strength analysis.

Crane steel mats and test mats are placed under the crawler tracks. Figure 58 shows the geometry with crane, load, mat, and soil (ground). Figure 41 and

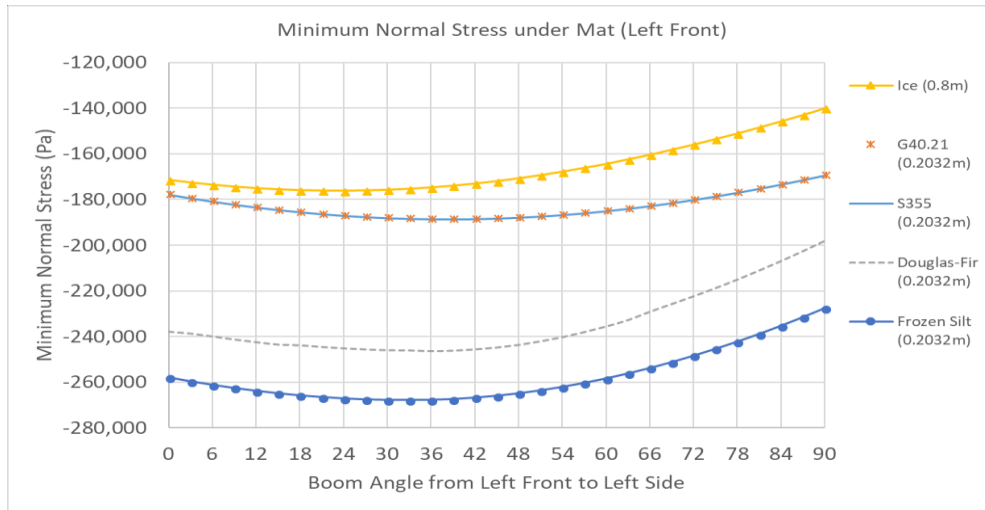
Figure 42 show the dimensions of the mat under investigation. A block of soil is placed under the mats as ground support. The properties of soil are incorporated in ANSYS and assigned to this soil block. For this analysis, only the linear properties of soil are selected (see Section 3.3.4.). However, for mat strength analysis, both linear and non-linear properties are selected (see Section 3.3.2.).



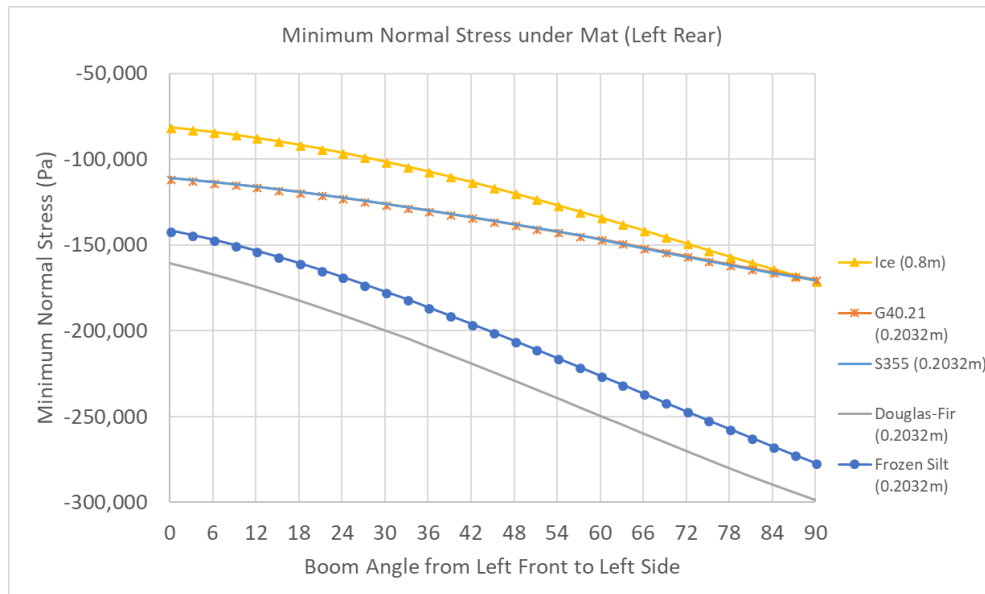
**Figure 58:** Geometry (crane, load, mat and soil) for analysis.



After loading the geometry with the material properties for mat and soil, the crane superstructure rotation is simulated using Mechanical solver in ANSYS Workbench. During the rotation of the superstructure, the ground bearing pressure under the crawler track varies with the change in boom slew angle. Figure 59 shows the minimum normal stress under the left front mat. Figure 60 shows the minimum normal stress under the left rear mat.

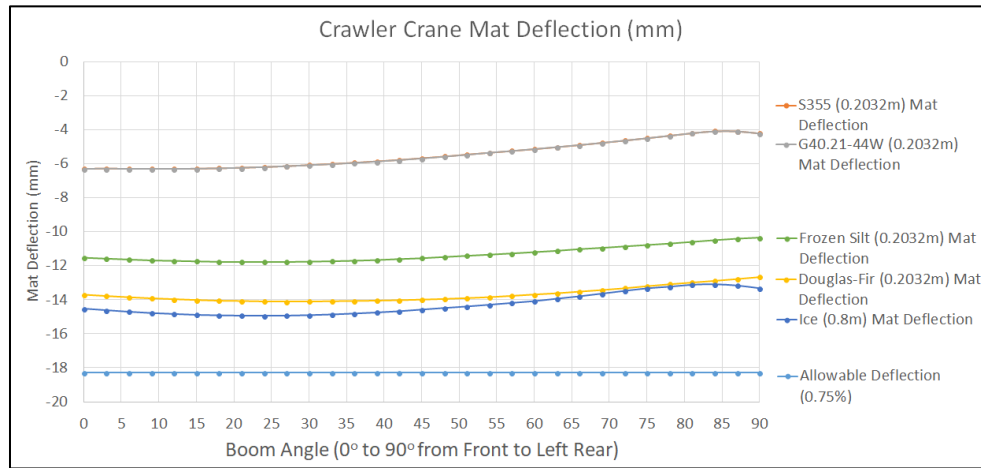


**Figure 59:** Normal Minimum Stress under Left Front Mat along with boom slew angle of 0° to 90° from left front to left side (Manitowoc 18000).



**Figure 60:** Normal Minimum Stress under Left Rear Mat along with boom slew angle of 0° to 90° from left front to left side (Manitowoc 18000).

Figure 61 shows the mat deflection under loading. Under loading condition, the maximum deflection is of the ice mat. The best performers are found to be S355 and G40.21. The deflection is taken as 0.75% of the original length. The analysis shows that all the different material mats fall within an acceptable range according to industry standards. In this mat deflection analysis, the frozen silt (0.2032 m) and Coastal Douglas-Fir (0.2032 m) are comparable to each other. This means that frozen silt can be used as an alternative to timber (i.e., Coastal Douglas-Fir), as the mechanical properties of both are close to one another.

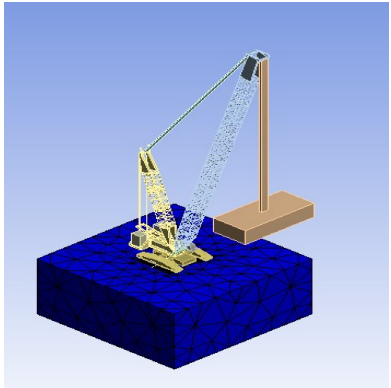
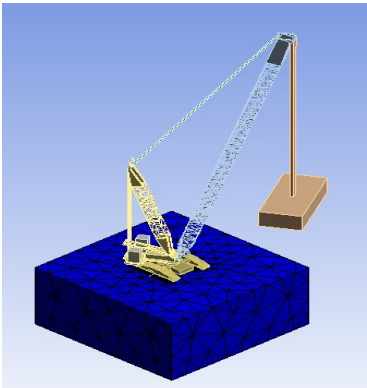
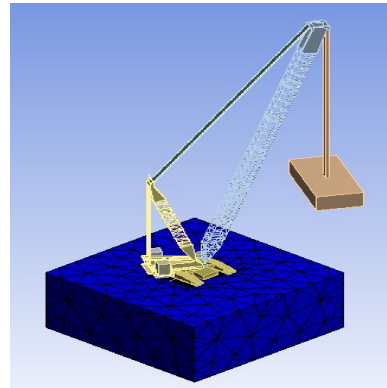
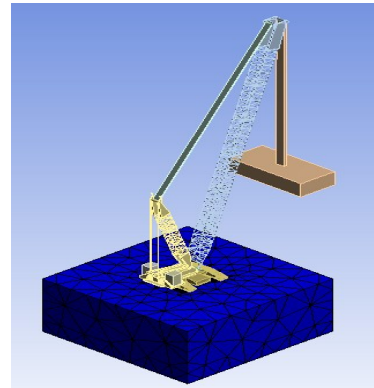
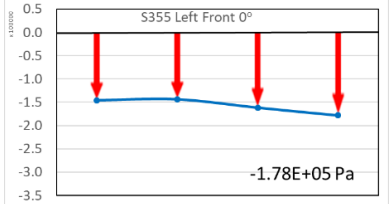
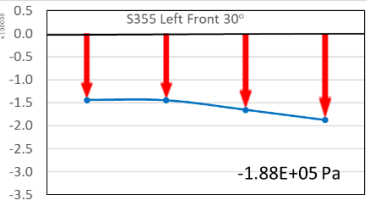
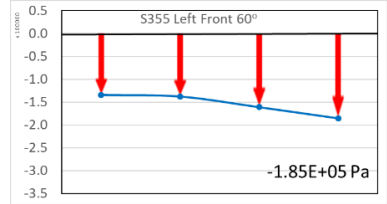
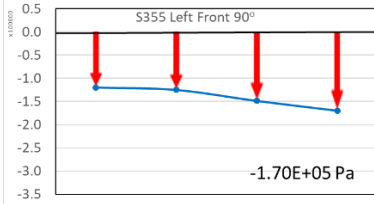
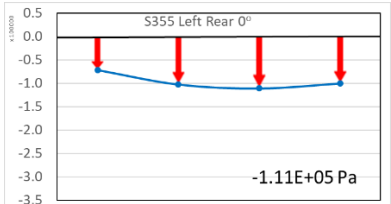
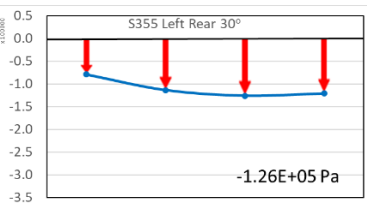
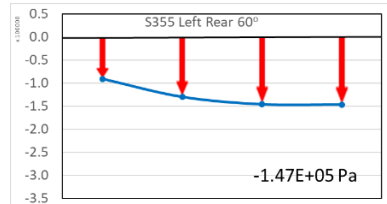
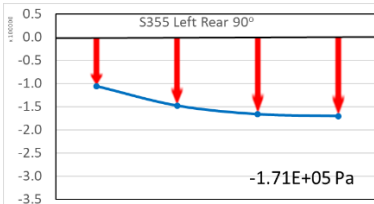


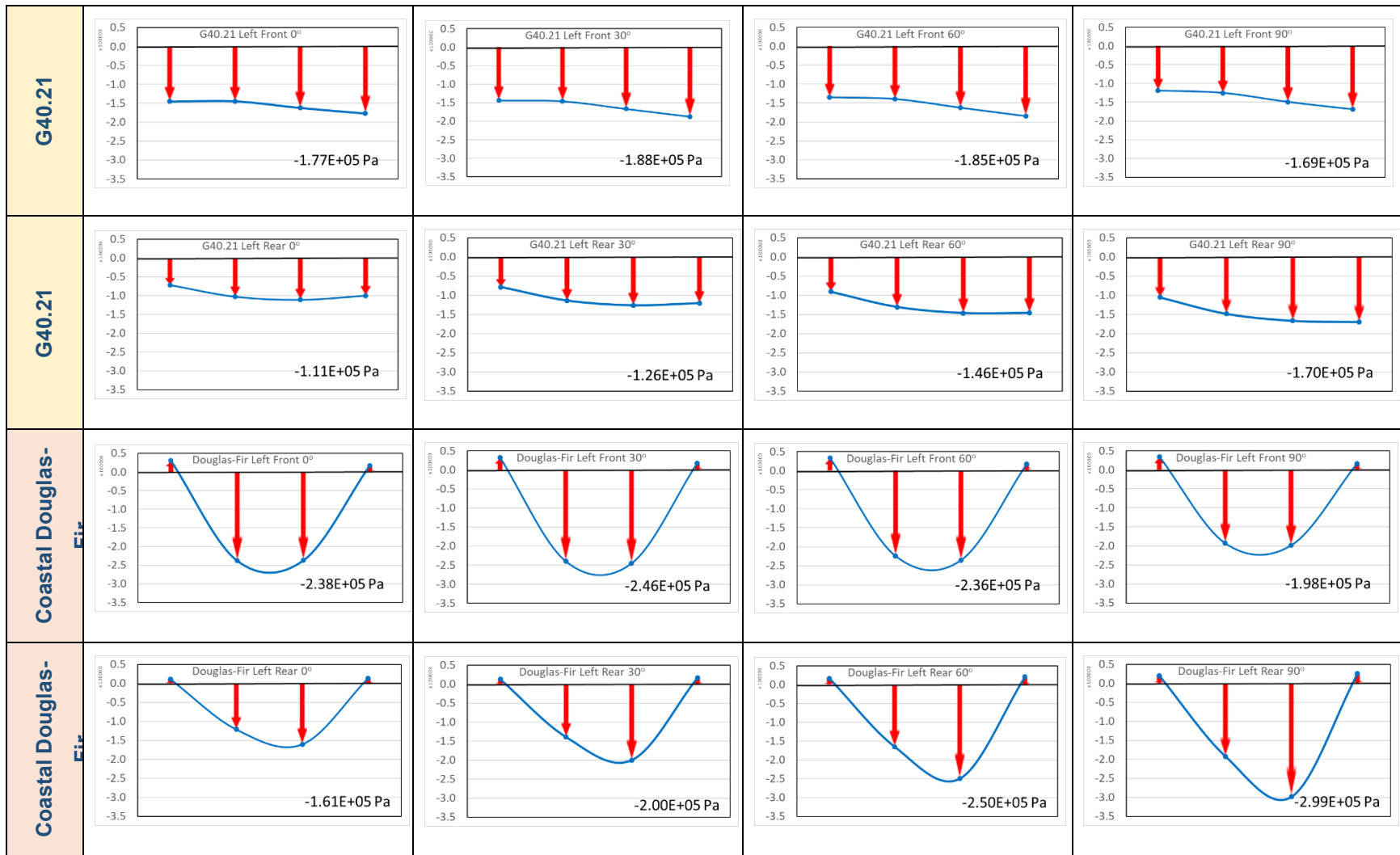
**Figure 61:** Left-Front Mat deformation under loading, along boom slew angle of 0° to 90° from left front to left side (Manitowoc 18000).

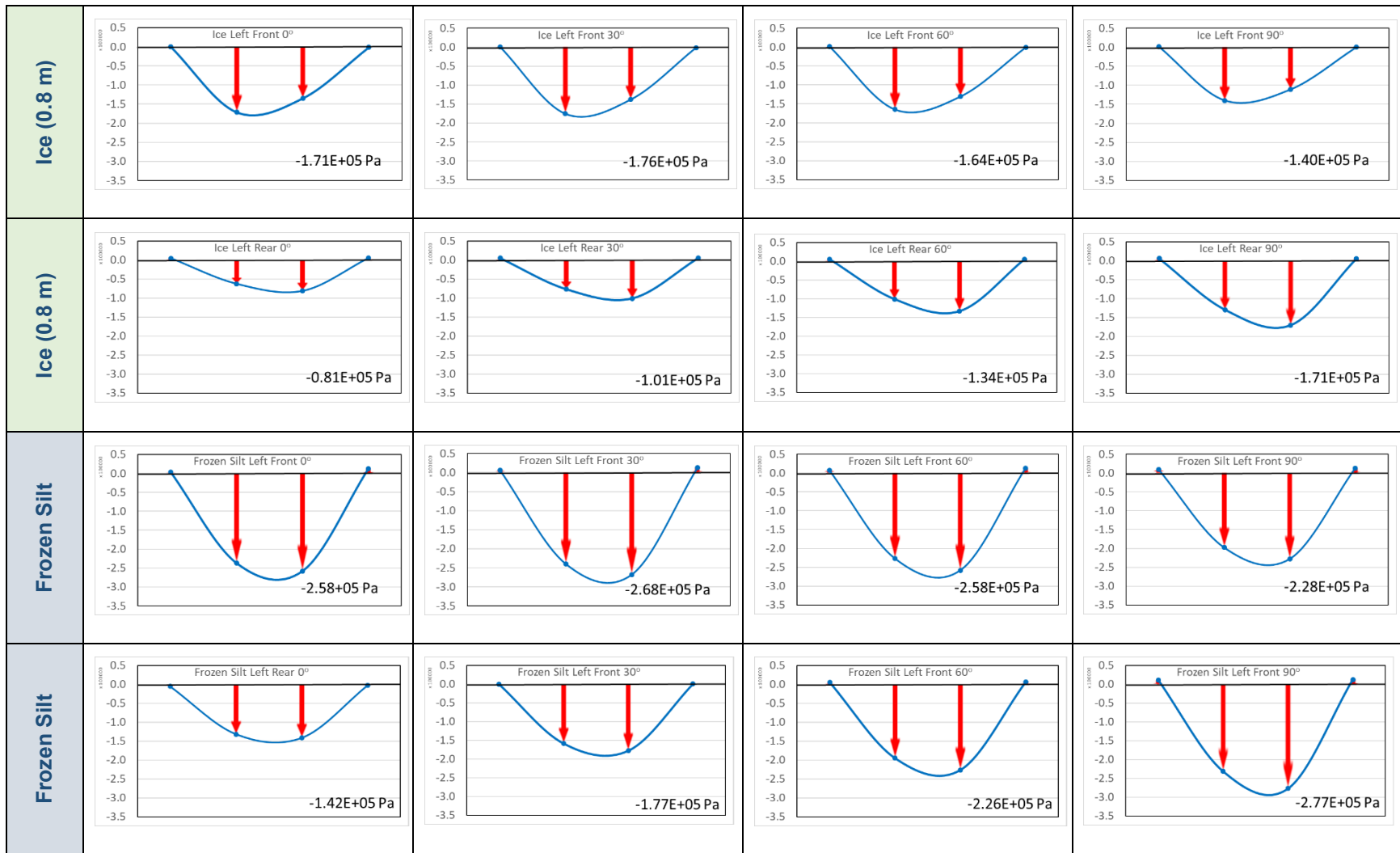
Table 10 shows the normal stress variation under the subject mat on the left front and left rear. For steel, the variation is less as compared to other materials, and the stress is uniform throughout the length of the steel mat under crawler track pressure. The compressive strength and the value of the Young’s modulus of steel is higher as compared to those of Coastal Douglas-Fir, ice, and frozen silt.

The figures in Table 10 show that the strength of ice is greater as compared to S355 or G40.21. The main reason for this is the mat thickness. For all other specimens, the mat thickness is 0.2032 m, but, to make ice compatible, the ice mat thickness is taken as 0.8 m (see Section 3.3.3.). If the thickness of ice were 0.2032 m, the normal stress would be lower than that of frozen silt mat (0.2032 m).

**Table 10:** Minimum Normal Stresses under crane mats along superstructure rotation (0° to 90° from Front to Left Side)

	0°	30°	60°	90°
				
<b>S355</b>	 <p>S355 Left Front 0° -1.78E+05 Pa</p>	 <p>S355 Left Front 30° -1.88E+05 Pa</p>	 <p>S355 Left Front 60° -1.85E+05 Pa</p>	 <p>S355 Left Front 90° -1.70E+05 Pa</p>
<b>S355</b>	 <p>S355 Left Rear 0° -1.11E+05 Pa</p>	 <p>S355 Left Rear 30° -1.26E+05 Pa</p>	 <p>S355 Left Rear 60° -1.47E+05 Pa</p>	 <p>S355 Left Rear 90° -1.71E+05 Pa</p>





The same is the case with left rear, the values of S355 and G40.21 are better as compared to Coastal Douglas-Fir and frozen silt. As the boom slew angle changes, the compressive stress increases as the load moves close to the left rear. For this analysis, only five linear properties and one non-linear property of the materials are used (section 3.3.2). It is also observed that the stresses at the edge of the Coastal Douglas-Fir, frozen silt, and ice mats (lengthwise) are positive, showing that the stress is not fully distributed over the length of the mat. The area bearing the pressure is less than the surface area of the mat. The edges of the mat leave the ground and show as positive instead of negative, indicating that the edges are not under compression and are not bearing the crane load.

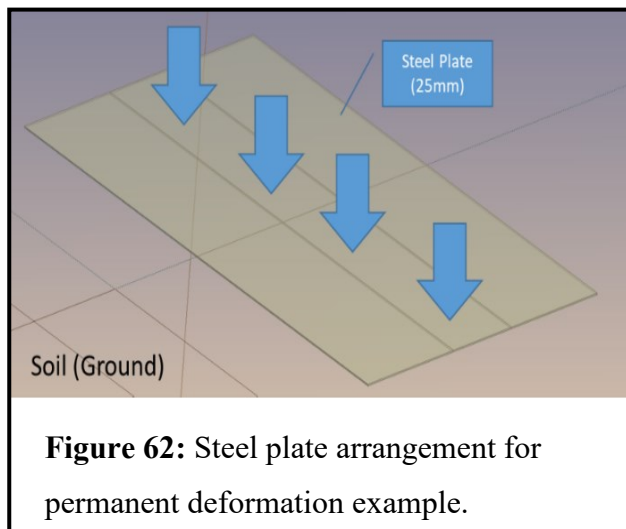
#### 4.2.2. Impact of Non-Linear Mechanical Properties.

The impact of non-linear mechanical properties comes into effect when the stress surpasses the tensile yield strength. All the case studies in this research are conducted within the limits of tensile yield strength. The question then arises how much payload is required to initiate mat failure.

**Table 11:** Load limit for permanent Coastal Douglas-Fir mat deformation for Crawler Crane.

	Boom (ft)	Radius (m)	Capacity (mTon)	Load Limit (mTon)	GBP (Pa)	Non-Elastic Deformation Stress (Pa)	Load Moment (mTon.m)
1	280	19.812	169.7	239.6	-5.00E+06	-5.00E+06	4,747
2	280	21.336	143.8	214.9	-5.00E+06	-5.00E+06	4,585
3	280	25.917	133.7	160.8	-5.00E+06	-5.00E+06	4,168
Average							4,500

Table 11 provides the details of three case examples performed in ANSYS, where the crawler crane geometry is loaded with the load exceeding the capacity of the crane in order to observe the limit of the Coastal Douglas-Fir mat failure.

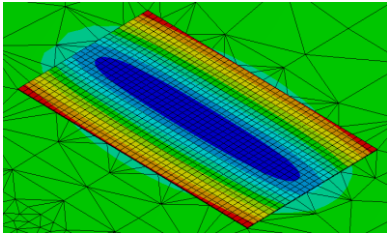
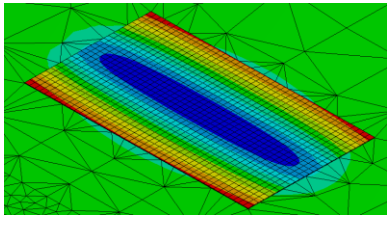
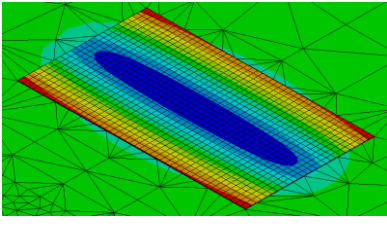
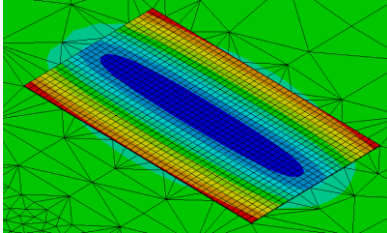
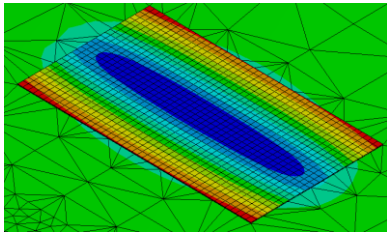
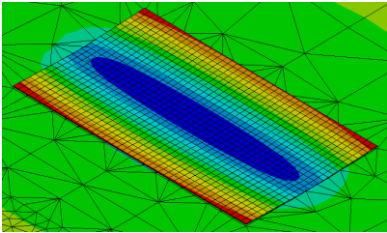
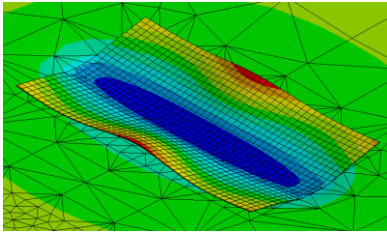
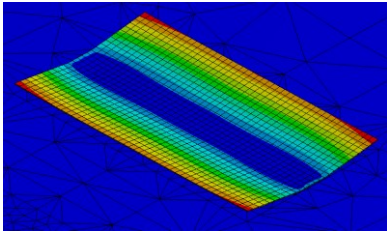


where the crawler crane geometry is loaded with the load exceeding the capacity of the crane in order to observe the limit of the Coastal Douglas-Fir mat failure. If the stress value enters the tangent modulus, the material begins to show plastic deformation. The column “Load Limit (mTon<sup>1</sup>)” in Table 16 provides the load limit at which the plastic deformation of the Coastal Douglas-Fir mat begins.

<sup>1</sup> Metric Ton = 1,000 kg = 2204.62 lb.

One more case example is performed to observe the elastic and plastic deformation of steel (S355) plate under loading. The steel plate (25 mm) is placed on the soil with the soil properties mentioned in Section 3.3.4. The length of the steel plate is 3.6449 m and its width<sup>1</sup> is 2.4384 m. The pressure is applied on the area (3.6449 m × 1.270 m) in the center of the plate as shown in Figure 62 (bearing length and bearing width of crawler track of Manitowoc 18000). The pressure is exerted starting from zero to the maximum value of  $1.00 \times 10^7$  Pa in order to observe the plastic deformation of the steel plate. Table 12 provides a graphical representation of the example.

**Table 12:** Graphical Representation of Plastic Deformation of Steel plate under Loading.

		
0 Pa	100 Pa	1000 Pa
		
10000 Pa	1.00E+05 Pa	1.00E+06 Pa
		
1.00E+07Pa	0 Pa	

<sup>1</sup> Similar to the dimensions of the test mat.

#### 4.2.2. Hydraulic Crane (Grove GMK7550).

For hydraulic crane analysis, the Grove GMK7550 is selected for simulation and investigation. The configuration of the crane is given in Table 9, with the methodology described in Section 3.3.5 used for the analysis. Figure 44 shows the data flowchart for the crane mat strength analysis. The main difference between this hydraulic crane and the crawler crane GBP is the way calculations are done, as described in Sections 2.1 and 4.1. For hydraulic cranes, the pad loads/forces are divided by the mat area in order to obtain the GBP under crane mats.

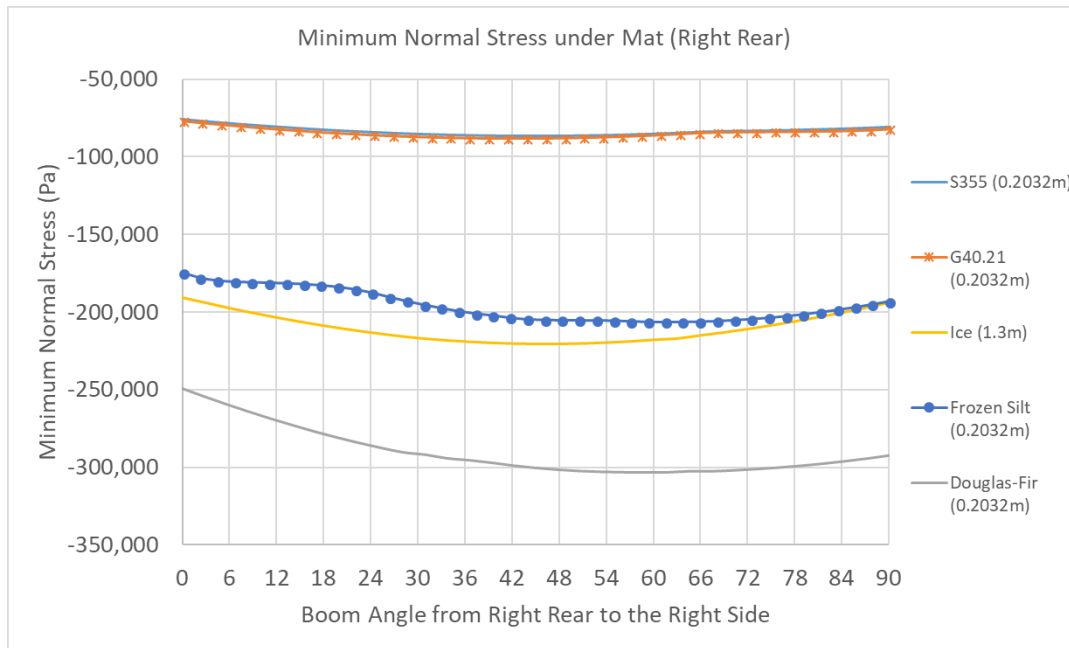
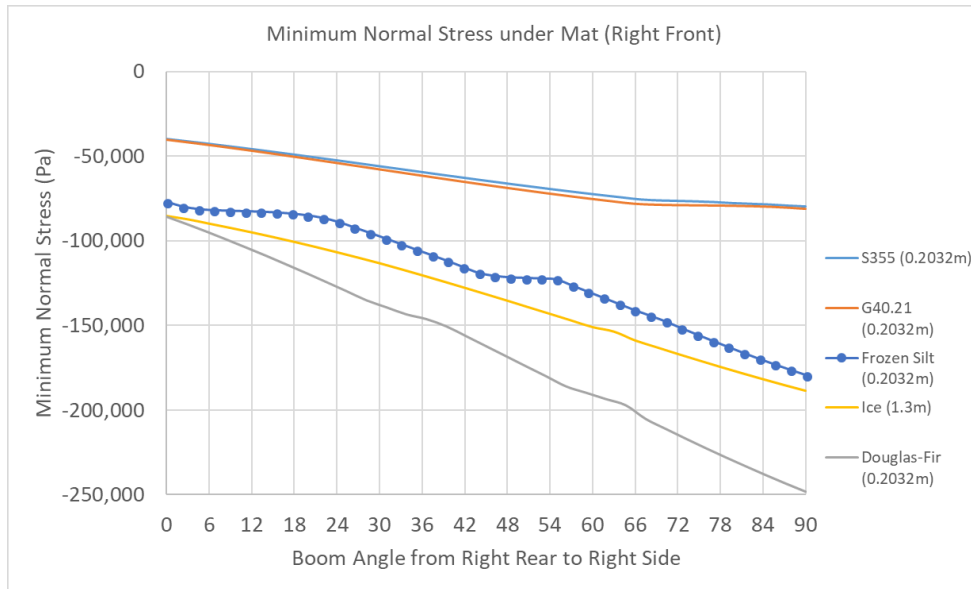


**Figure 63:** Normal Minimum Stress under Right Rear Mat along boom slew angle of 0° to 90° from Right Rear to Right Side (Grove GMK7550)

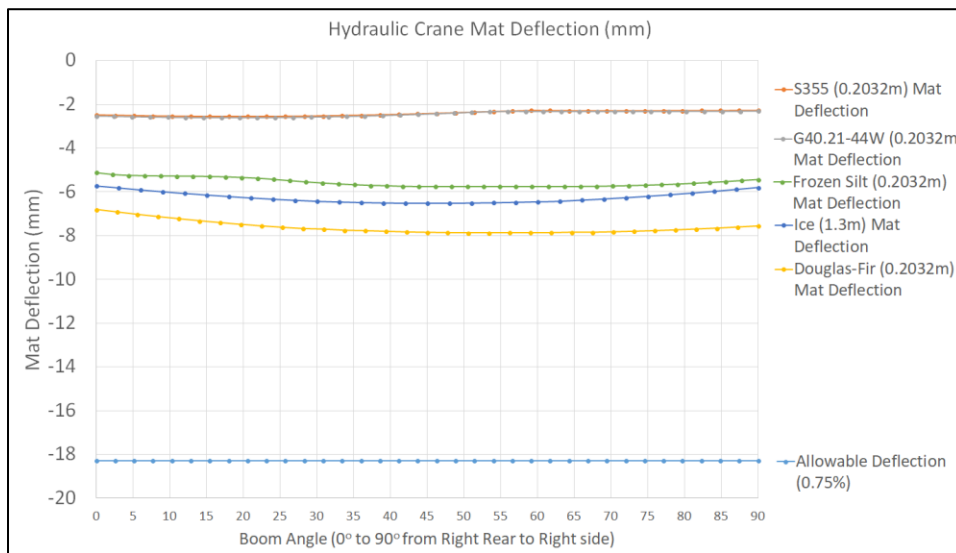
For mat strength analysis, the normal stresses under the mat are obtained from ANSYS simulation. The superstructure is rotated in ANSYS Workbench, creating pressure on the outriggers. The pressure on the outrigger is transferred to the mat under investigation. During the rotation of the superstructure, the resulting forces on the outrigger mats vary with the change in boom slew angle. During the simulation, the boom slews from right rear to the right side. This is the reason stress analysis values are taken for the right rear and right front outrigger mats. For the right rear outrigger, as the load moves from right rear to right side, the value increases initially but decreases later. The maximum value is achieved when the boom is directly over the outrigger during boom



rotation. After this point, the value decreases as the load moves away from the outrigger. Figure 63 shows the normal stress under the right rear outrigger mat. Considering the same load pattern, the mat analysis is performed using mat under the outriggers. Figure 64 shows the normal stress under the right front outrigger mat. From these two figures, it can be concluded that frozen silt is better in terms of stress values when compared to the Coastal Douglas-Fir material.



**Figure 64:** Normal Minimum Stress under Right Front Mat along boom slew angle of 0° to 90° from Right Rear to Right Side (Grove GMK7550).

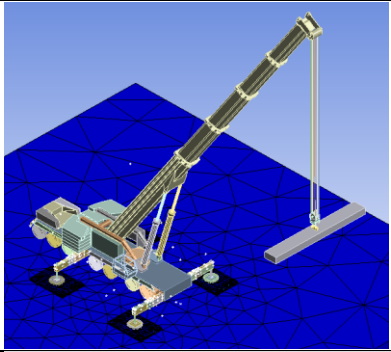
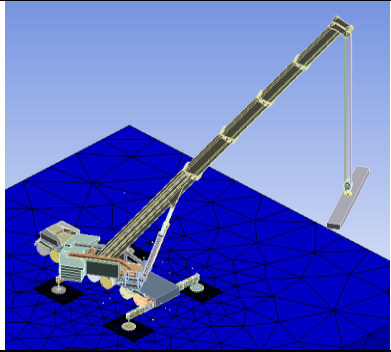
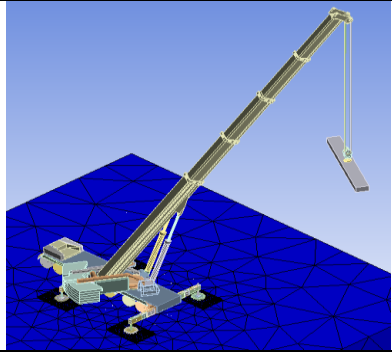
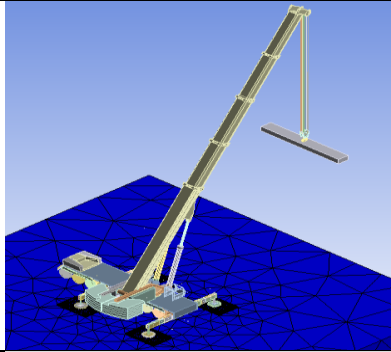
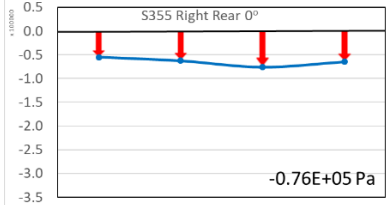
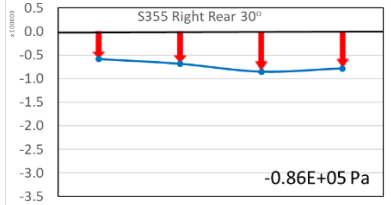
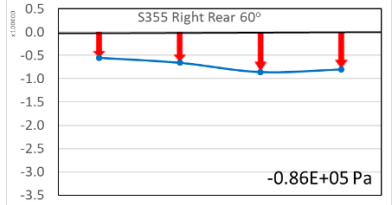
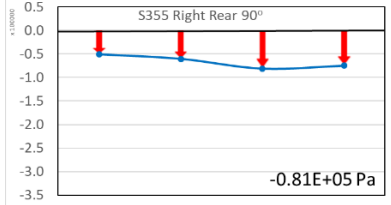
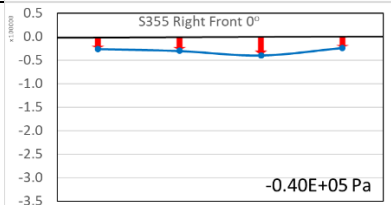
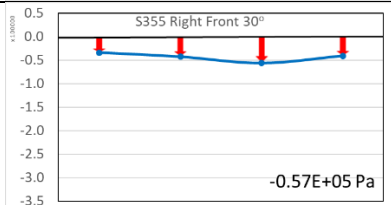
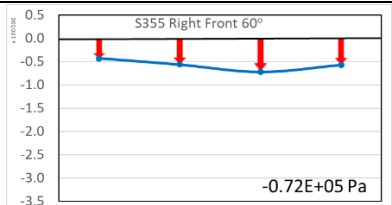
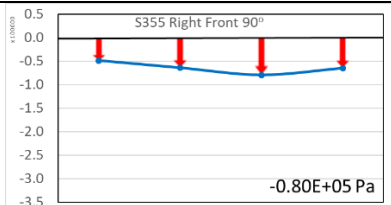
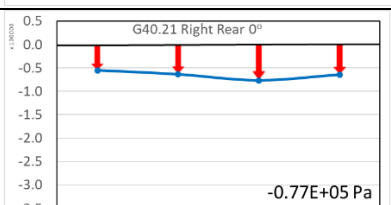
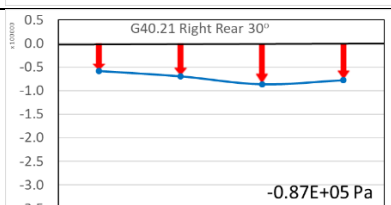
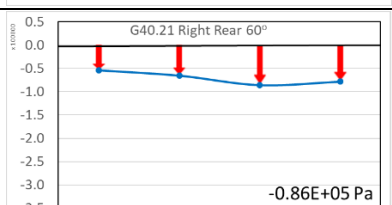
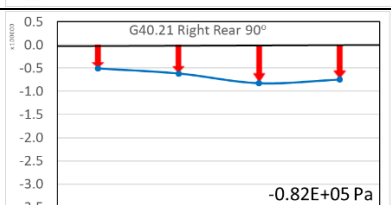


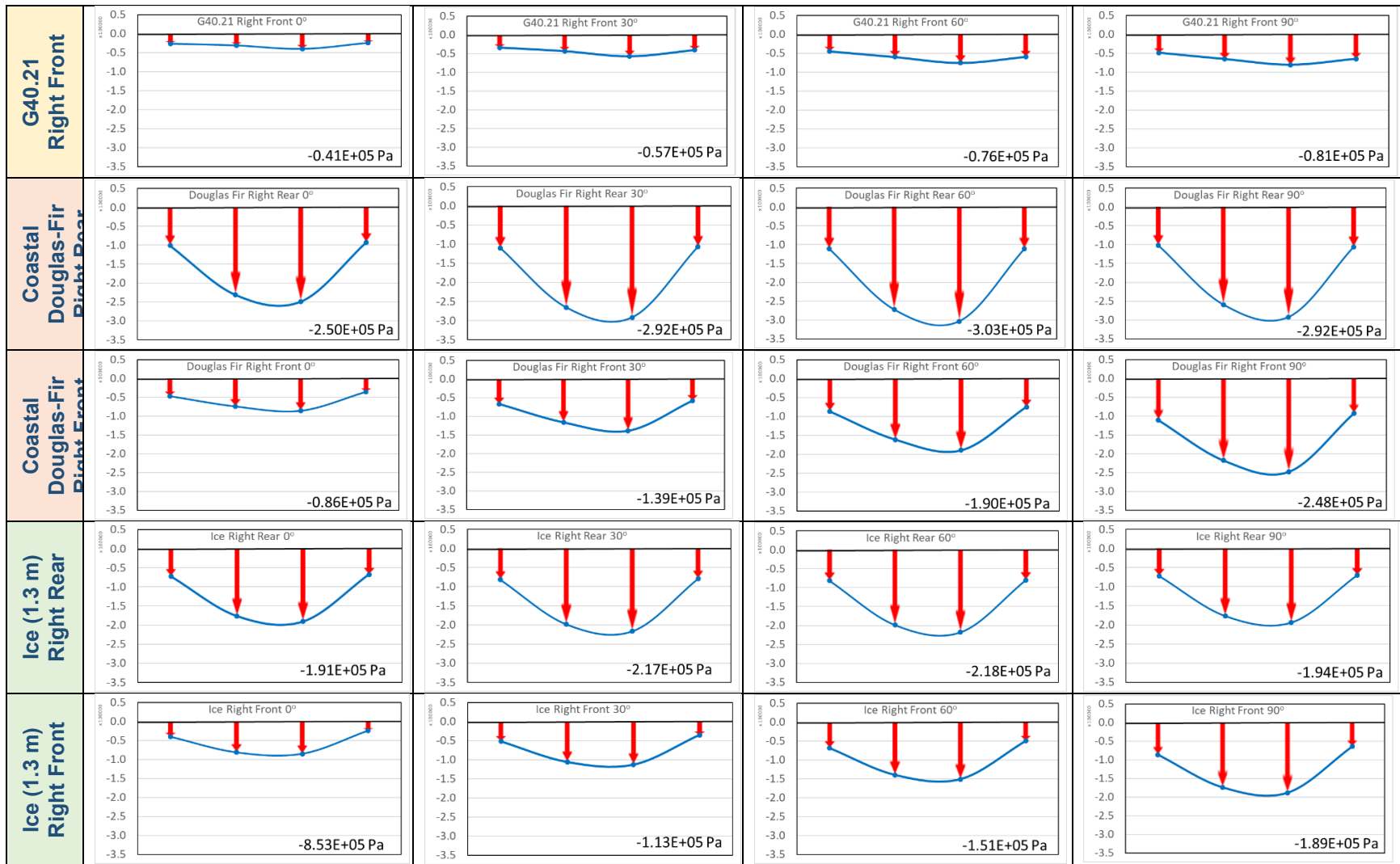
**Figure 65:** Right Rear Mat deformation under loading. along boom slew angle of 0° to 90° from Right Rear to Right Side (Grove GMK7550).

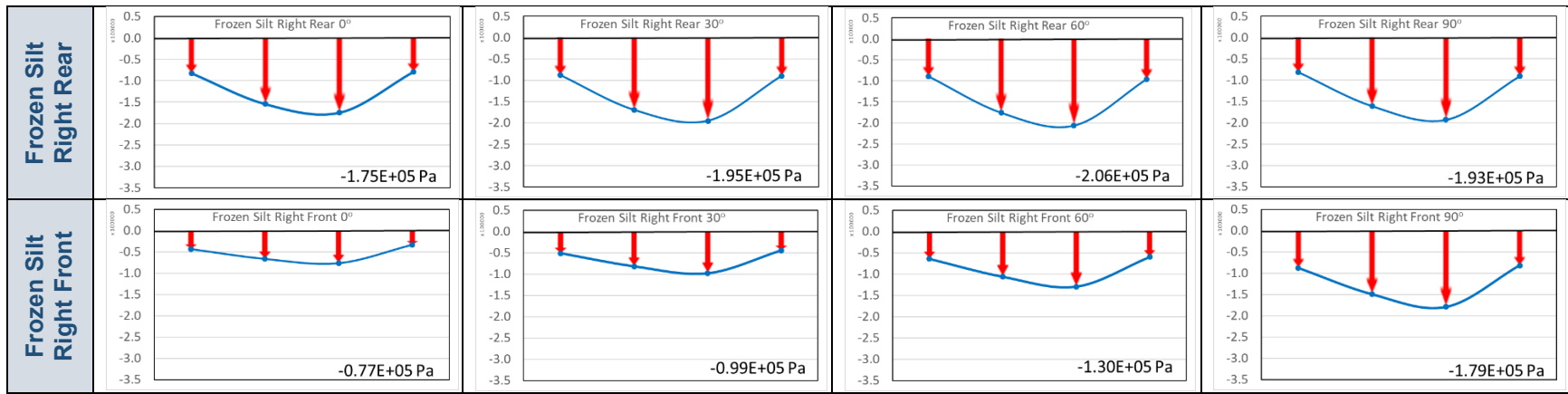
Figure 65 shows the mat deflection under the right rear outrigger. It is found that the industry benchmark is much lower as compared to all the mat material specimens considered. It can thus be concluded that all the mats are capable of easily withstanding the pressure due to crane loading with minimal deformation/bending.

Table 13 shows the stress distribution along the width of the mat. The location of the stress line is in the center of the mat. In the case of crawler cranes, the stress line is taken at the edge, but, for hydraulic crane, the stress line spans the center, as the outrigger exerts maximum pressure on the center of the mat. Appendix B shows the minimum values along the stress line at different boom angles. From Table 13 and Appendix B, it is observed that the mat made of frozen silt is similar to the Coastal Douglas-Fir with respect to the mechanical properties. The pressure exerted by the outrigger is the same for all the mat materials under investigation. However, S355 and G40.21 distribute pressure evenly throughout the mat length. In the cases of Coastal Douglas-Fir, ice, and frozen silt, the distribution is not even, but instead is still concentrated in the center. For hydraulic cranes, the compressive stress value is higher (minimum in terms of normal tensile stress) in the center of the mat. For crawler cranes, the stress values reach maximum at the edge of the mat close to the load.

**Table 13:** Minimum Normal Stresses under crane mats along superstructure rotation (0° to 90° from Rear to Right Side)

	0°	30°	60°	90°
				
<b>S355 Right Rear</b>	 <p>S355 Right Rear 0°</p> <p>-0.76E+05 Pa</p>	 <p>S355 Right Rear 30°</p> <p>-0.86E+05 Pa</p>	 <p>S355 Right Rear 60°</p> <p>-0.86E+05 Pa</p>	 <p>S355 Right Rear 90°</p> <p>-0.81E+05 Pa</p>
<b>S355 Right Front</b>	 <p>S355 Right Front 0°</p> <p>-0.40E+05 Pa</p>	 <p>S355 Right Front 30°</p> <p>-0.57E+05 Pa</p>	 <p>S355 Right Front 60°</p> <p>-0.72E+05 Pa</p>	 <p>S355 Right Front 90°</p> <p>-0.80E+05 Pa</p>
<b>G40.21 Right Rear</b>	 <p>G40.21 Right Rear 0°</p> <p>-0.77E+05 Pa</p>	 <p>G40.21 Right Rear 30°</p> <p>-0.87E+05 Pa</p>	 <p>G40.21 Right Rear 60°</p> <p>-0.86E+05 Pa</p>	 <p>G40.21 Right Rear 90°</p> <p>-0.82E+05 Pa</p>





## **CHAPTER 5: HEAT TRANSFER AND COST ANALYSIS:**

### **5.1. Conclusion of Mechanical Properties Analysis.**

From the mechanical property analysis in Chapter 4, it is inferred that frozen silt mat can be used as an alternative to the timber mat for crane support. Mats made of frozen silt can sustain the GBP if the mat temperature is below  $-10^{\circ}\text{C}$ . The mechanical properties of the frozen silt mat under investigation, it should be noted, are taken from the research done by Yang, Still, and Ge (2015), and by Wilson (1982) (see Section 3.3.2 for details). The value of the Young's modulus ranges from  $0.7 \text{ GN/m}^2$  to  $16.5 \text{ GN/m}^2$  with the temperature ranging from  $0^{\circ}\text{C}$  to  $-10^{\circ}\text{C}$ . The dry density of frozen silt is found to vary from  $320 \text{ kg/m}^3$  to  $941 \text{ kg/m}^3$ , while the water/moisture content varies from 62% to 225% (Yang, Still, & Ge, 2015). Based on the above data, the compressive strength of the frozen silt varies from 1.7 MPa to 7.1 MPa (Yang, Still, & Ge, 2015).

For the present analysis, a Young's modulus of 10 GPa, tensile strength of 5.1 MPa, compressive yield strength of 5.0 MPa, and tensile ultimate strength of 5.1 MPa are considered. The results from Chapter 4 are based on these values. Figure 40 shows the data selection for the frozen silt mat.

### **5.2. Frozen Silt Mat Proposed Design.**

As the comparison of the frozen silt is concluded from Chapter 4, the next step is to provide a preliminary conceptual design for the frozen silt mat. Based on the data available and ANSYS simulation for mechanical properties, a conceptual silt mat design is initiated in this chapter for ANSYS heat transfer simulation. The work presented in this chapter is conducted using ANSYS workbench.

As per the dimensions of the mat, four frozen silt mats are proposed to be used for the hydraulic crane. But for the crawler crane, eight frozen silt mats are proposed to be used (four for each track). For analysis purposes, only the crawler crane is selected for the heat transfer analysis. The mat strength for frozen silt required for the crawler crane, it should be noted, is the same as for the hydraulic crane. The aim is to perform the simulation for the freezing process of silt mats until the surface temperature reaches or drops below  $-10^{\circ}\text{C}$ .

Figure 66 & Figure 67 shows the placement of the proposed four frozen silt mats under one track of a crawler crane. For the freezing purpose, conceptually, 10 freezing pipes are used. In the proposed layout, the pipes are placed evenly inside the soil perpendicular to the length of the mat but parallel to the crawler track. It is assumed that each pipe crosses all the four mats under one crawler track. The cooling agent enters one end of these pipes and exits from the other end. The mats are required to be insulated, and the most cost-effective insulation material available on construction sites is typically soil or wood. For insulation purposes, the soil itself can be used as the mat cushion (insulation), where the thickness of the mat is increased in order to create a mat cushion that functions as insulation.

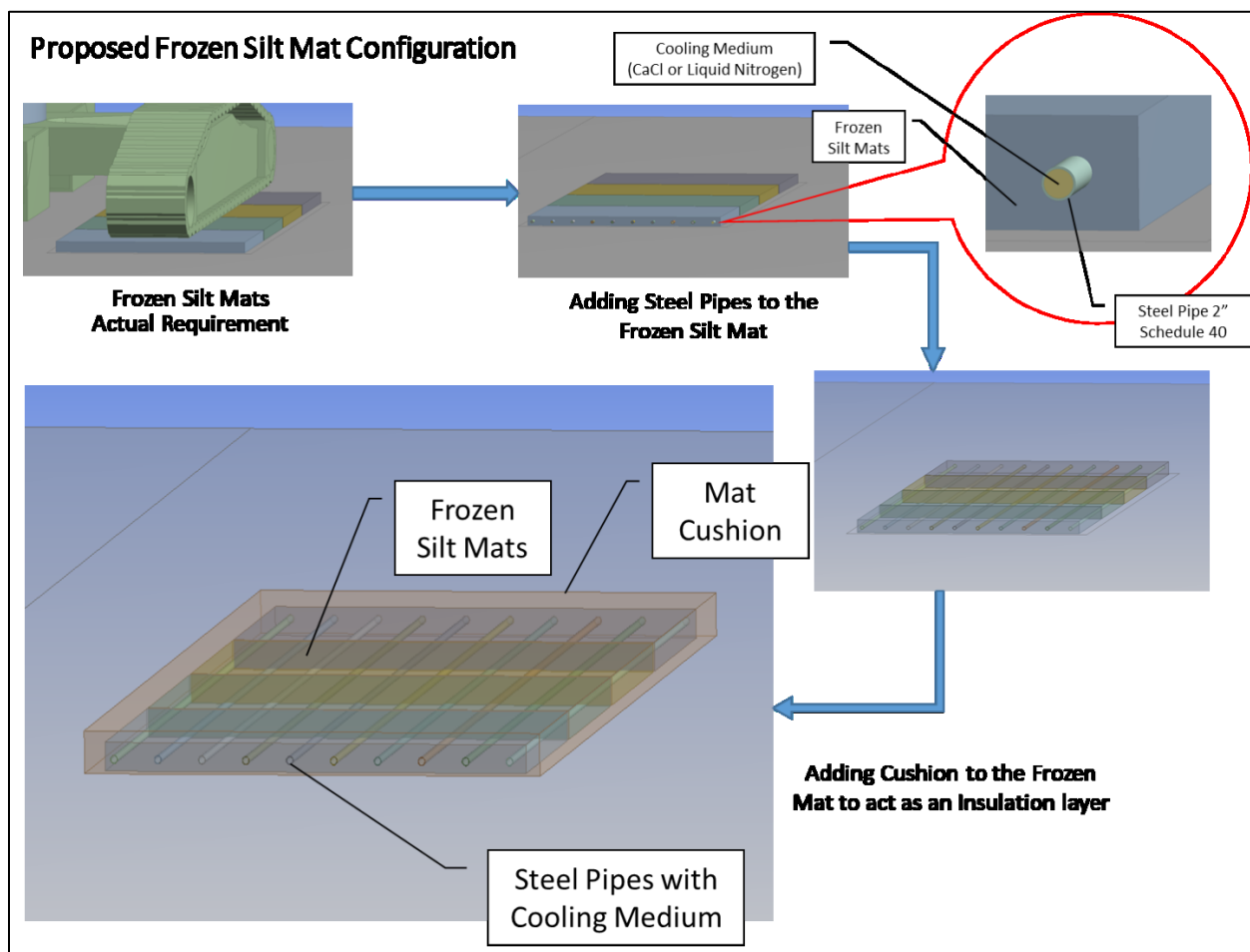


**Figure 66:** Proposed Frozen Silt Mat configuration

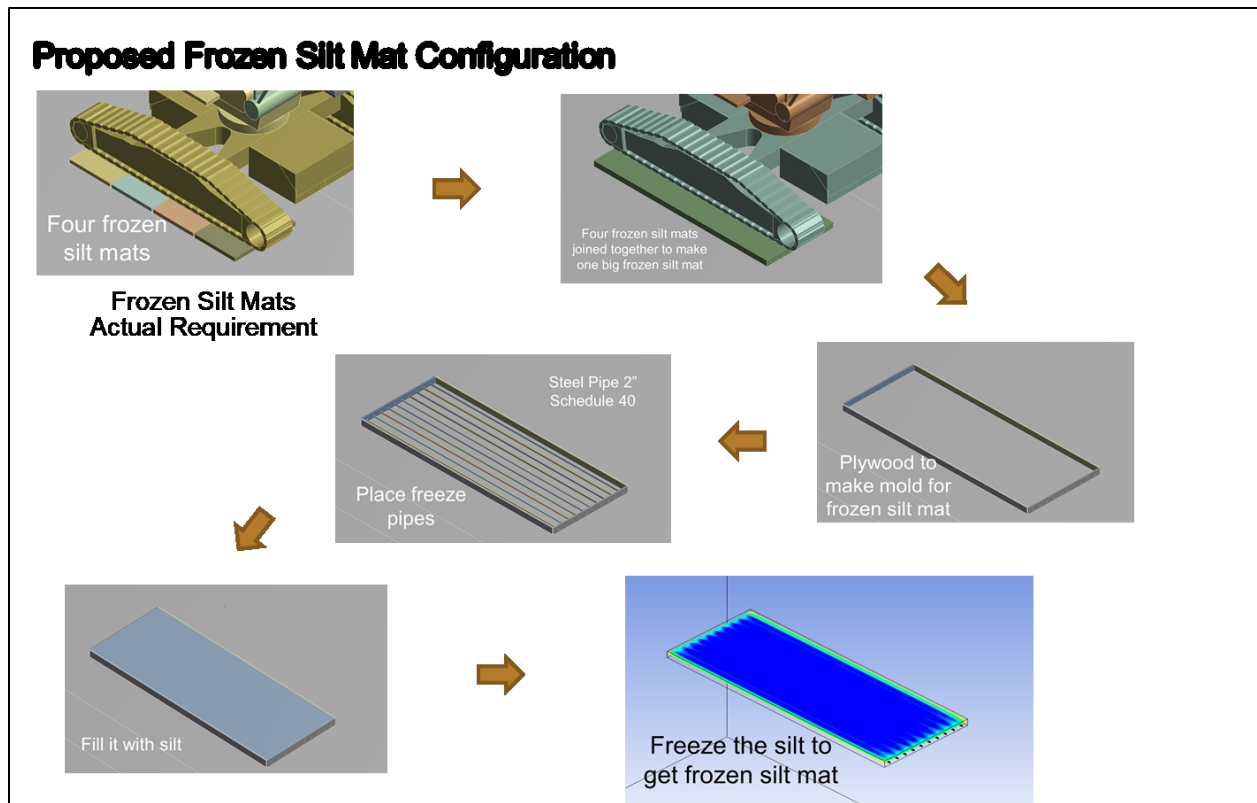


**Figure 67:** Proposed Frozen Silt Mat laying process

The proposed design with dimensions is shown in Figure 68. The four silt mats combine to form one long frozen silt mat with mat cushion (insulation). The length of the whole mat (consisting of four frozen silt mats) is considered to be approximately 10.5 m, with a width of 4 m. Figure 68 shows that the proposed height (0.303 m) of the mat exceeds the practical requirement of mat height (0.203 m) used in the ANSYS simulation in Chapter 4. The extra height provides the mat cushion which functions as insulation. If this insulation is not provided, the surface temperature of the mat drops rapidly. A freezing temperature of  $-10^{\circ}\text{C}$  throughout the mat is required (including the mat surface). 2" steel pipe schedule 40 is used as freeze pipes for the frozen silt mats. These steel pipes work as a conducting material to transfer heat from silt to the cooling agent. The cooling agent for this investigation is either brine or liquid nitrogen. The basics of the mat design are derived from the steel mat dimensions given in Section 3.3.3. Section 3.3.6 provides the thermal properties of the material used in the freezing of silt.



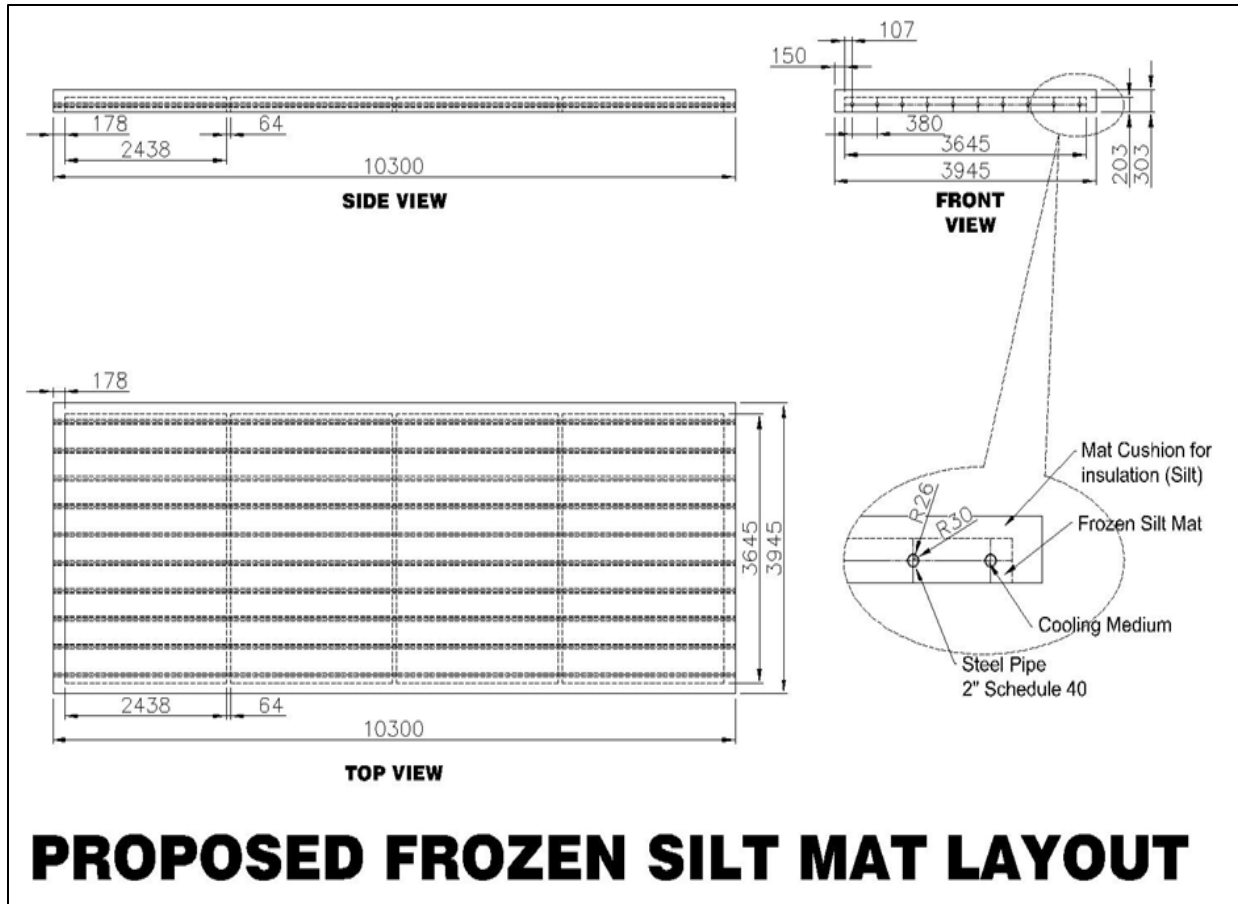


**Figure 68:** Proposed Frozen Silt Mat Design/layout

**5.3. ANSYS Simulation for Frozen Silt Mat (Freezing).**

For heat transfer analysis, ANSYS Fluid Flow (Fluent) Solver is used. The requirement is to simulate the freezing of silt mat to convert soil to frozen silt (solid). Two processes are used for this purpose—indirect freezing and direct freezing.

**5.3.1. Indirect Freezing (Brine Solution CaCl<sub>2</sub>).**

For the indirect freezing, calcium chloride (CaCl<sub>2</sub>) is used as a cooling agent. A detailed description of indirect freezing is provided in Section 2.7.3. For ANSYS simulation purposes, the mat design is placed on the ground without the crane (ANSYS Geometry). The whole geometry is uploaded to ANSYS Fluid Flow (Fluent) solver, with three case examples are taken into consideration. The first case is at 10°C ambient temperature, the second case is at 5°C ambient temperature, and the third case example is at 0°C. The time span for these simulations is 30 days.

The thermal properties involved in this simulation are provided in Section 3.3.6. Given these conditions, heat transfer occurs in the following manner:

- Heat transfer from the pipes to the cooling agent through conduction and convection. The thermal properties and the viscosity of the cooling agent cover the estimation for heat rejection from the geometry (frozen silt mat, pipes, air, ground).
- Heat transfer from the mat to the pipes through conduction.
- Heat transfer from ground to the freezing mat. During the mat freezing process, the soil under the mat also gets frozen with the passage of time and later functions as insulation.
- Heat transfer from the air to the silt mat in the form of convection ( $2 \text{ W/m}^2\cdot\text{K}$ , assumption) and radiation (external emissivity 0.98, assumption) is also taken into consideration in this simulation (Farouki, 1986; The Engineering Toolbox, 2018).

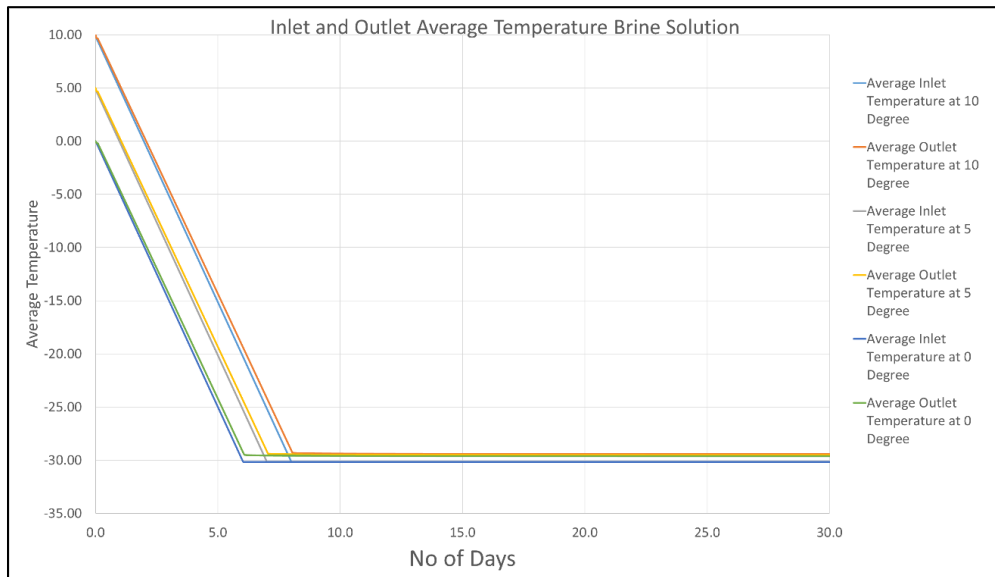


**Figure 69:** Inlet and Outlet Average Temperature (Brine Solution)

For indirect freezing, the velocity of  $\text{CaCl}_2$  is assumed to be 0.29 ft/s (0.088392 m/s). The inlet temperature of  $\text{CaCl}_2$  at the start of the analysis is same as the ambient temperature, but it drops gradually until it reaches  $-30.15^\circ\text{C}$ . To avoid complexity, it is assumed that the temperature drop is  $5^\circ\text{C}$  over a 24-hour period. Figure 69 shows the variation of the inlet temperature of brine with respect to time over a 30-day period. In order to avoid complexity, the decline is assumed to be smooth.

To avoid complexity, the heat generated from the crane engine is not considered, nor is the heat transfer from the crawler track. For this reason, the crane model is not included in this simulation. Figure 70 shows the process of heat transfer, where the cooling agent enters the pipes from one end and exits from the other.

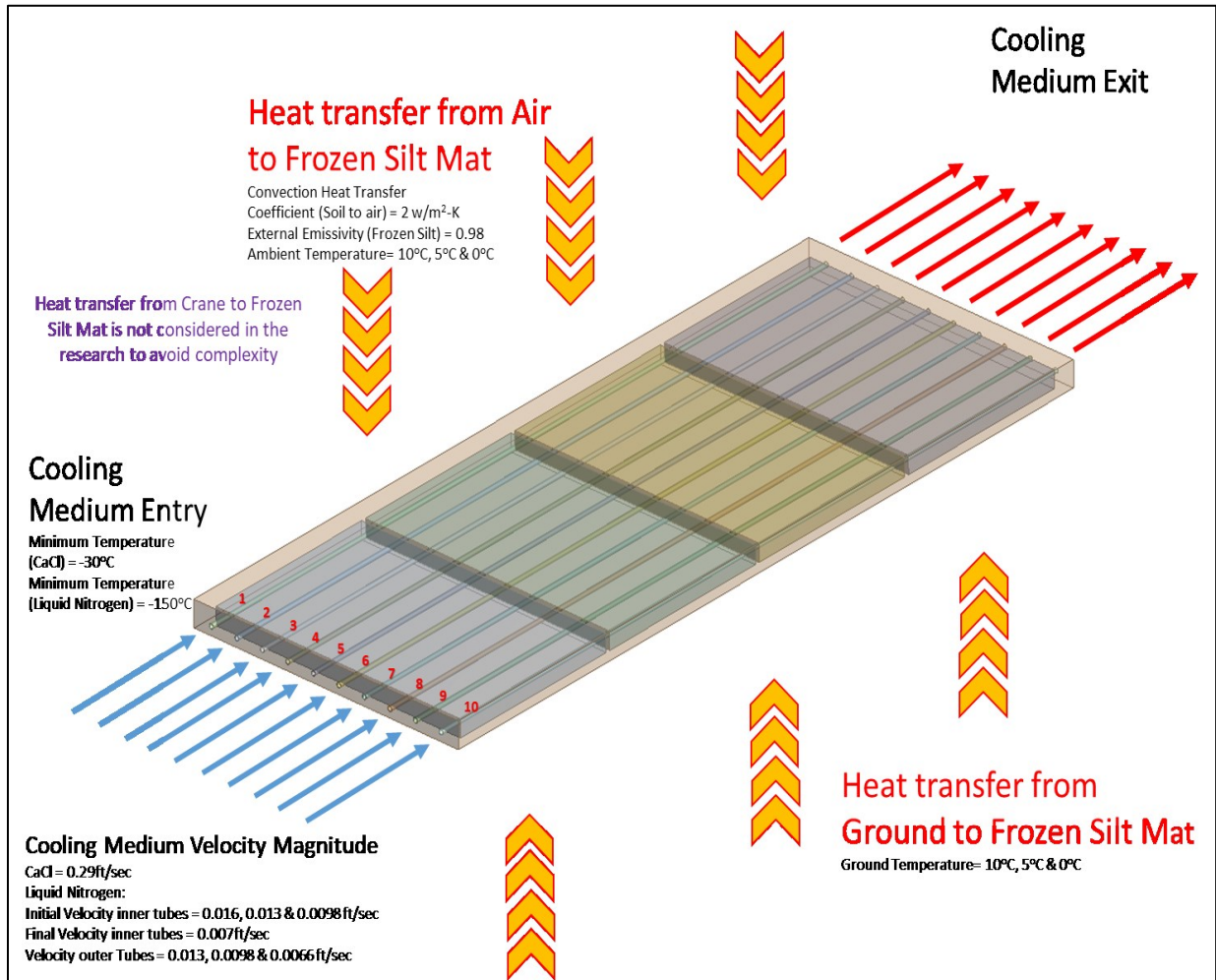
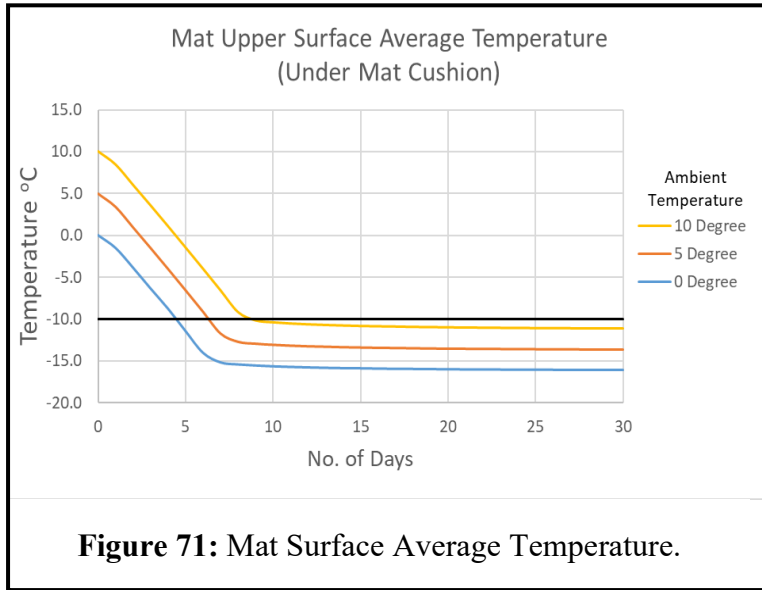


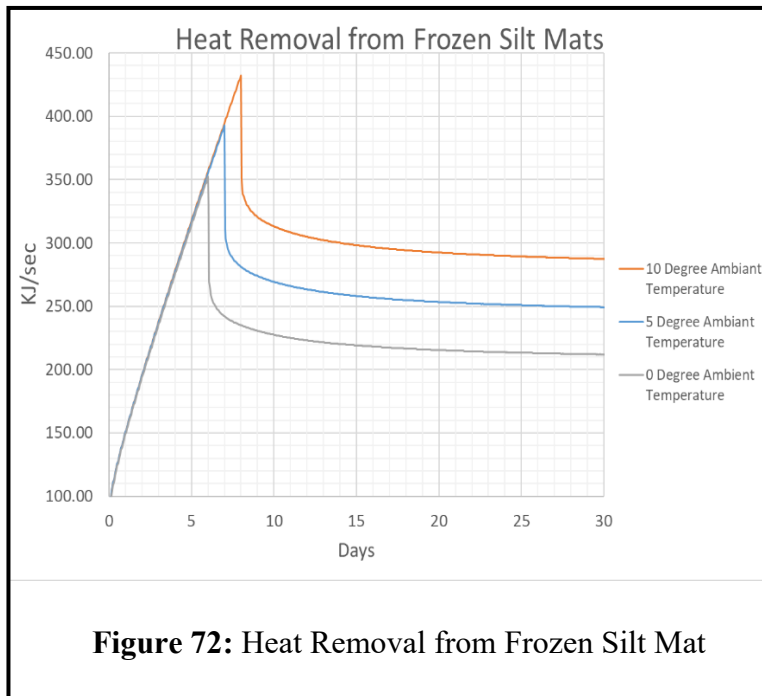
**Figure 70:** Heat Transfer (Frozen Silt Mat) for Indirect and Direct Freezing

Section 3.2.2 provides details about the ANSYS Fluent process. Each step is composed of 3,600 seconds and data is collected at each step. The number of iterations<sup>1</sup> is taken as 200, while the number of steps is taken as 720. Hence, the total time for the simulation is 30 days.

<sup>1</sup> Iteration means the act of repeating a process with the aim of approaching a desired goal, target or result. In ANSYS iterations are done to converge the solution to the best possible solution.



The temperature of the mat surface (under the mat cushion) is recorded and plotted against time (days) in Figure 71. As per the simulation, the surface temperature of the frozen silt mat is close to  $-10^{\circ}\text{C}$  with the ambient temperature of  $10^{\circ}\text{C}$ . According to the simulation, it takes 8 to 9 days to freeze the silt sufficiently to create a frozen silt mat for crane use if the ambient temperature is near  $10^{\circ}\text{C}$ . In the case of an ambient temperature of  $5^{\circ}\text{C}$ , it takes less than seven days to freeze the silt sufficiently. For an ambient temperature of  $0^{\circ}\text{C}$ , the time required for freezing is less than 5 days. The surface temperature of the mat (under mat cushion) ranges



between  $-10^{\circ}\text{C}$  and  $-15^{\circ}\text{C}$  for case-II ( $5^{\circ}\text{C}$ ) and it is below  $-15^{\circ}\text{C}$  in case-III ( $0^{\circ}\text{C}$ ).

The heat removal from the proposed frozen silt mat in the simulation is shown in Figure 72. The heat removal value for case-I (ambient temperature  $10^{\circ}\text{C}$ ) is higher as compared to the other two case examples. The first part of the graph (the linear part)

shows the freezing phase while the later stable straight line shows the maintenance phase. This graph is similar to the energy removal graph (see Figure 73) presented by Newman et al. (2011). Figure 73 shows the relationship between work

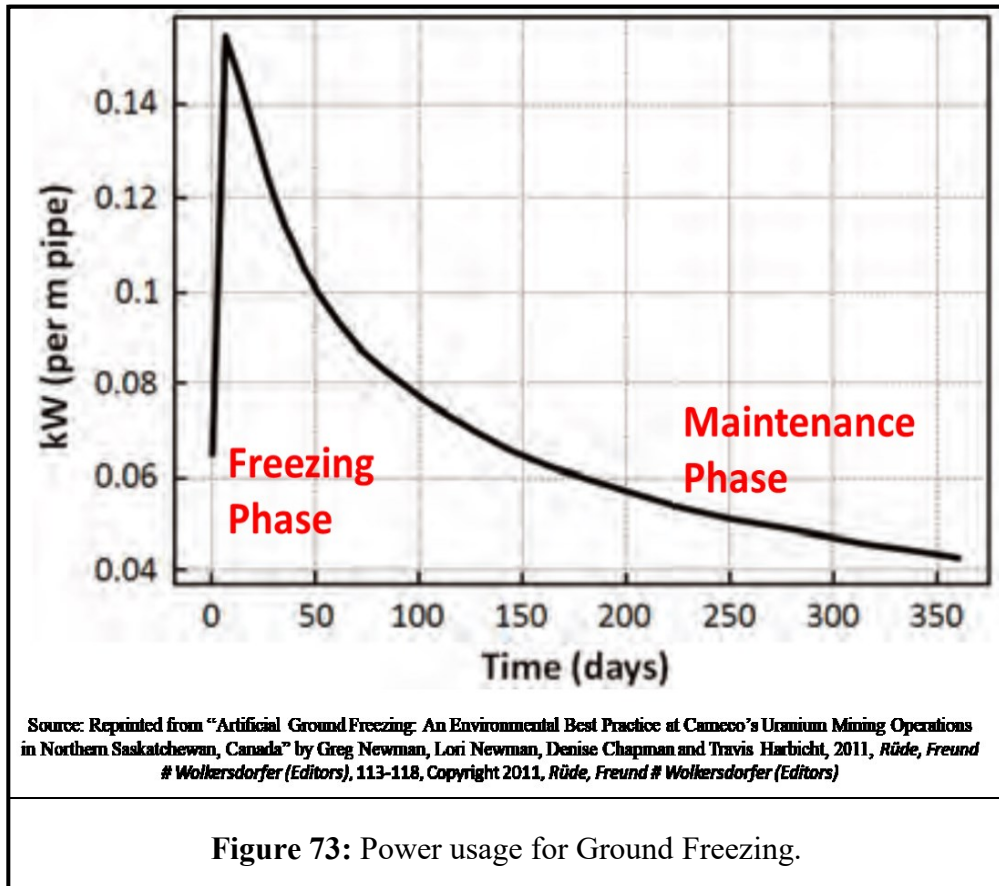


**Figure 73:** Power usage for Ground Freezing.

done (KJ/s) versus the time required for artificial ground freezing (AGF) (Newman et al., 2011). It should be noted that there is a possibility that the actual heat transfer quantity and the rate of energy transfer will be different depending on the site conditions. For simulation and design purposes, a few parameters are taken into consideration for this research. The ANSYS simulation results are based on these select parameters along with the theoretical approach. As shown in Figure 72, the maximum value for each case example is used to determine the cost of the refrigeration system required for the freezing process. The maintenance phase, meanwhile, provides the operational cost of the refrigeration unit. The cost comparison for indirect and direct freezing will be discussed in later sections.

Appendix C provides a graphical representation of freezing simulation for frozen silt mats using brine (indirect freezing), where the dark-blue colour represents mat surface temperatures below  $-10^{\circ}\text{C}$ . The graphical representation shows that, at  $0^{\circ}\text{C}$  ambient temperature, the surface temperature of the mat drops to the  $-10^{\circ}\text{C}$  threshold sooner as compared to the  $5^{\circ}\text{C}$  or  $10^{\circ}\text{C}$

ambient temperature scenarios. Less energy draining is required in the case of 0°C ambient temperature as compared to 5°C and 10°C ambient temperatures.

### 5.3.2. Direct Freezing (Liquid Nitrogen N<sub>2</sub>).

Direct freezing is different from indirect freezing, as discussed in Chapter 2. The thermal properties are taken from Section 3.3.6. The method described in Section 3.3.7 is used for the heat transfer analysis, while the thermal properties of liquid nitrogen are used for the ANSYS analysis (see Section 3.3.6). The flow of the liquid nitrogen is the main cost driver for the cost estimation. The actual frozen silt mat still being in the conceptual phase of development, the freezing of the silt mat in the analysis is carried out using ANSYS with different case scenarios to capture the freezing process. For the analysis purpose, three assumed cases are taken into consideration based on different flow velocities of liquid nitrogen. As per the design of frozen silt mat, there are 10 pipes for each frozen silt mat. The velocity of liquid nitrogen for the outer pipes (pipe 1 and pipe 10)<sup>1</sup> is taken constant (see Figure 70). The velocity of liquid nitrogen for the inner pipes (pipe 2 to pipe 9) is considered variable with respect to time. For pipe 2 to pipe 9, for the first 24 hours (freezing phase), the velocity remains constant, but later it drops gradually (maintenance phase). The liquid nitrogen enters one end of the pipe and exits to the ambient environment through the other. Table 14 shows the details of these cases.

**Table 14:** Liquid Nitrogen Velocity for three cases.

	Pipe-1	Pipe-2 to Pipe-9		Pipe-10
Case-1	0.005 m/s (0.016 ft/s)	0 to 24 hr	0.005 m/s (0.016 ft/s)	0.005 m/s (0.016 ft/s)
		24 to 720 hr	0.005 m/s (0.016 ft/s) linearly decreasing to 0.002 (0.0056 ft/s)	
Case-2	0.004 m/s (0.013 ft/s)	0 to 24 hr	0.004 m/s (0.013 ft/s)	0.004 m/s (0.013 ft/s)
		24 to 720 hr	0.004 m/s (0.013 ft/s) linearly decreasing to 0.0015 (0.0049 ft/s)	
Case-3	0.003 m/s (0.0098 ft/s)	0 to 24 hr	0.003 m/s (0.0098 ft/s)	0.003 m/s (0.0098 ft/s)
		24 to 720 hr	0.003 m/s (0.0098 ft/s) linearly decreasing to 0.001 (0.0033 ft/s)	

<sup>1</sup> The outer pipes (1 and 10) are close to ‘two’ surfaces open to air (top surface and side surface). The inner pipes (2 to 9) are only close to ‘one’ surface (top surface). The heat transfer from these outer pipes (1 and 10) is assumed to be greater as compared to the inner pipes (2 to 9).

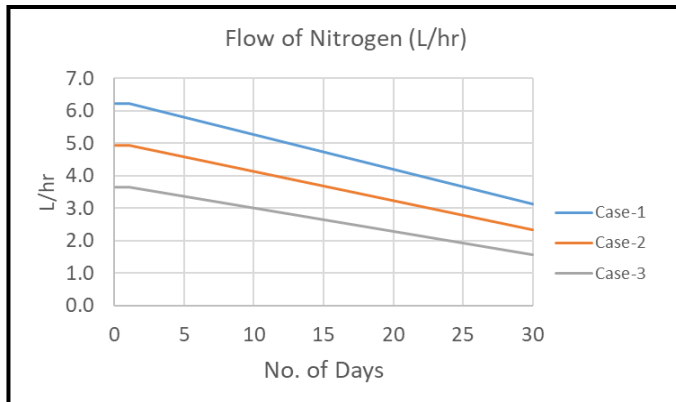


**Figure 74:** Liquid Nitrogen Total Flow (L/hr)

to be maximum for case-1 and minimum for case-3. With every case analyzed under each of the three ambient temperature scenarios, in total nine case examples are simulated for freezing silt mat in ANSYS.

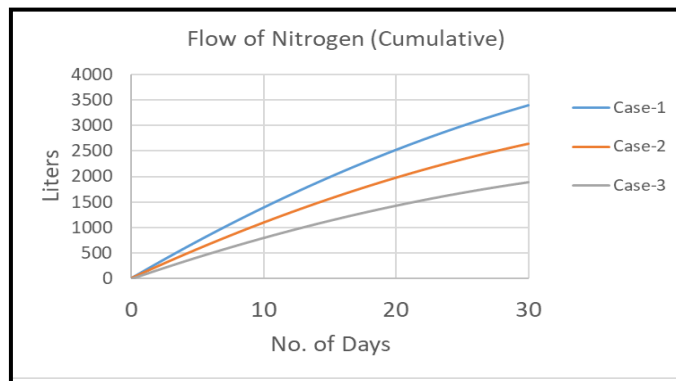


**Figure 75:** Liquid Nitrogen Cumulative Total Flow

Each assumed case study is simulated at three different ambient temperatures 10°C, 5°C, and 0°C. All the remaining parameters are similar to those described in Section 5.3.1. The use of liquid nitrogen with respect to time for all three cases is shown in Figure 74, while the quantity of liquid nitrogen versus the number of days is shown in Figure 75. The flow is found to be maximum for case-1 and minimum for case-3. With every case analyzed under each of the three ambient temperature scenarios, in total nine case examples are simulated for freezing silt mat in ANSYS.

The average surface temperature of the mat decreases rapidly due to the low temperature of liquid nitrogen as compared to brine (the boiling point of nitrogen is -195.8°C at atmospheric pressure). When the liquid nitrogen enters the pipe, it expands, and its temperature decreases rapidly. It is assumed for the

ANSYS simulation that the temperature of liquid nitrogen (LN<sub>2</sub>) entering the pipe is -150°C. Due to this low-temperature flow, the temperature of the mat material (silt) decreases rapidly.

The graphical representation of the mat surface temperature with respect to time is shown in Appendix D for 10°C ambient temperature, Appendix E for 5°C ambient temperature, and Appendix F for 0°C ambient temperature for all three cases.

From this simulation exercise, case-1 is found to perform well at every ambient temperature as compared to case-2 and case-3. The surface of the frozen silt mat reaches -10°C faster if the usage of liquid nitrogen is increased in the form of velocity flow of liquid nitrogen (case-1). Figure 76 shows the average surface temperature of the mat, where the surface temperature for case-1 is lower as compared to those of case-2 and case-3.

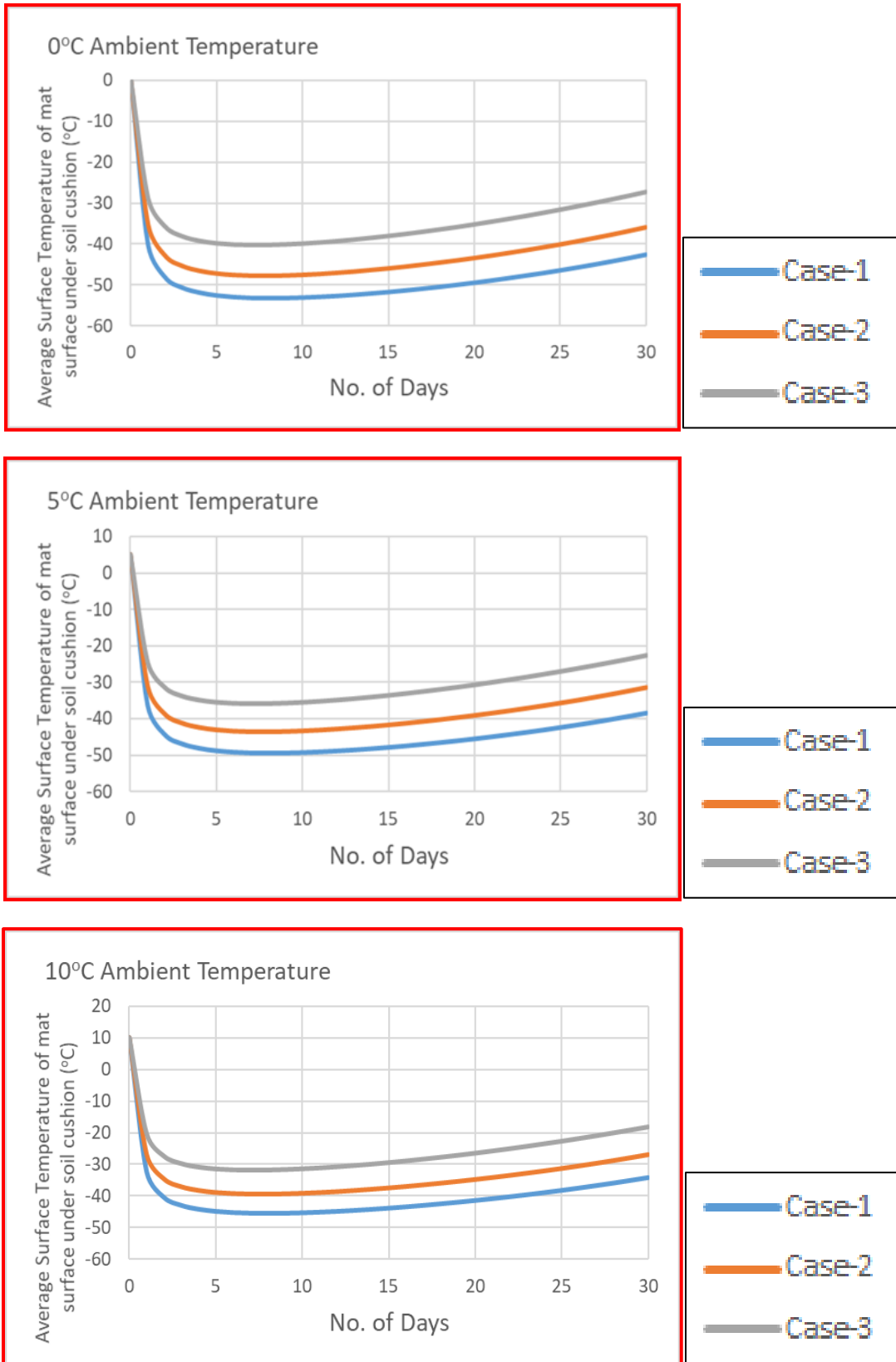


**Figure 76:** Average Mat Surface Temperature (Direct Freezing - Liquid Nitrogen)



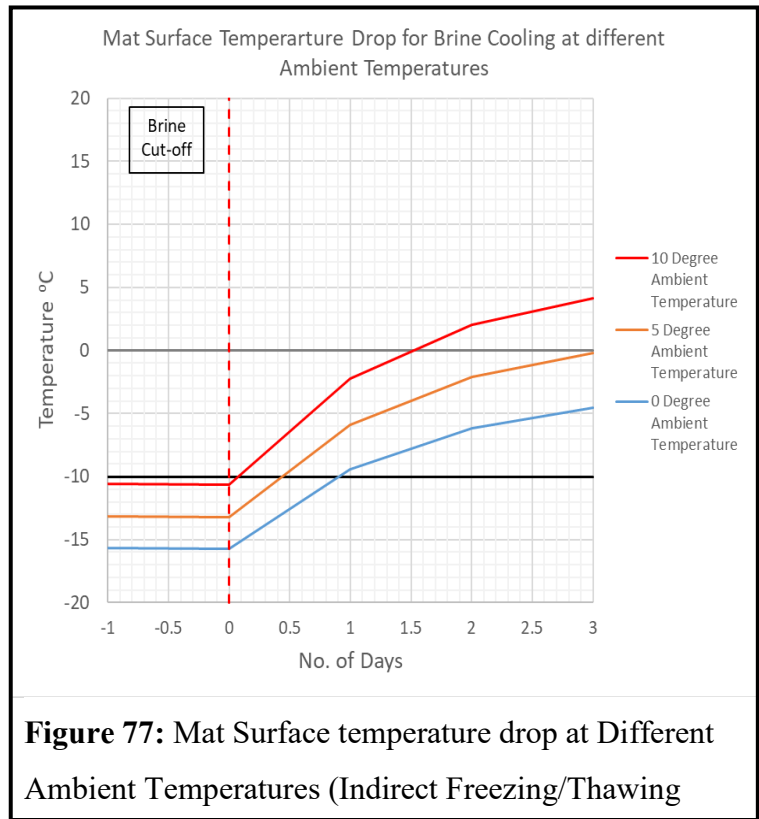
The quantity of liquid nitrogen used for the freezing is used to calculate the cost of liquid nitrogen for further cost comparison purposes, as well as the capital and operational costs of any equipment associated with the direct freezing.

#### 5.4. ANSYS Simulation for Frozen Silt Mat (Thawing).

The next step is to calculate the time required for thawing of the frozen silt for all these cases. This helps with estimating the total time for the use of the frozen mat. This is used to determine how much time the mat can survive without the power input. Both indirect freezing and direct freezing are considered in the ANSYS simulation. The mat surface temperature for indirect freezing, it should be noted, is different from that of direct freezing. The idea is to stop the flow of the cooling agent and measure the time required for the mat to sustain the strength (based on frozen silt mat surface temperature).

##### 5.4.1. Indirect Freezing Thawing Process.

For this analysis, the velocity of brine is dropped to 0 when the average temperature of the mat surface is stable and uniform. Figure 77 shows the temperature drop for indirect freezing (brine solution) at three different ambient temperatures. For ANSYS simulation and analysis, the flow of brine is cut off after 10 days of indirect freezing. Day-10 of the freezing process is taken as Day-0 of the thawing process. The data retrieved from ANSYS simulation shows that, if the ambient temperature is 0°C, the mat can survive one more



day, as the surface temperature requirement is  $-10^{\circ}\text{C}$ . For  $5^{\circ}\text{C}$ , it takes a half day to reach  $-10^{\circ}\text{C}$ . For  $10^{\circ}\text{C}$ , the temperature rises above  $-10^{\circ}\text{C}$  as soon as the brine solution flow is cut off.

### 5.4.2. Direct Freezing Thawing Process.

For liquid nitrogen case studies, it is assumed that the flow of the liquid nitrogen is cut off on Day-3 of the direct freezing process simulation. Usually, as per ANSYS simulation, the surface temperature of the mat reaches the required state within two days of direct freezing (see Section 5.3.2). Three cases are observed under three ambient temperatures: 10°C, 5°C, and 0°C. Figure 78 shows the temperature drop at 10°C ambient temperature, while Figure 79 shows the temperature drops at 5°C ambient temperature and Figure 80 shows the mat surface temperature drop at 0°C. For analysis purposes, Day-3 (liquid nitrogen flow cut-off) of direct freezing is taken as Day-0 of thawing.

The frozen silt mat with liquid nitrogen in case-1 takes one day to reach -10°C with 10°C ambient temperature. The same case example takes two days to reach -10°C with 0°C ambient temperature. For Case-3, with 10°C ambient temperature, the mat surface can only sustain 12 hours. But with the same flow velocity (case-3) with 0°C ambient temperature, it can sustain for 24 hours.

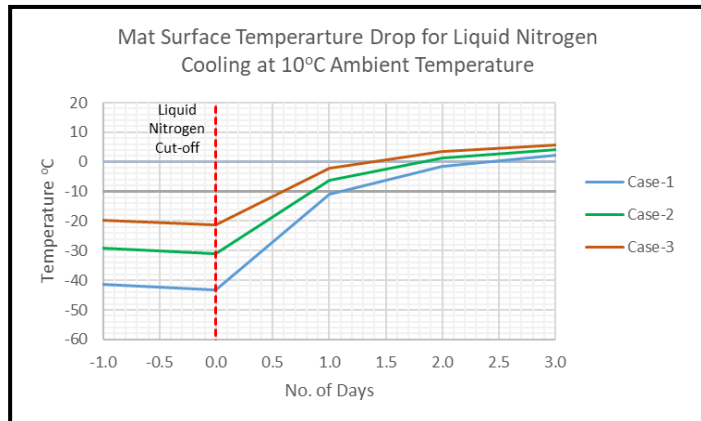


**Figure 78:** Average Mat Surface Temperature at 10°C Ambient Temperature.

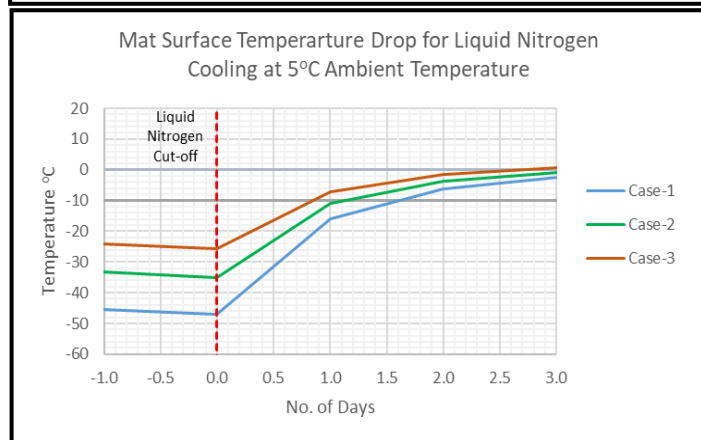


**Figure 79:** Average Mat Surface Temperature at 5°C Ambient Temperature.

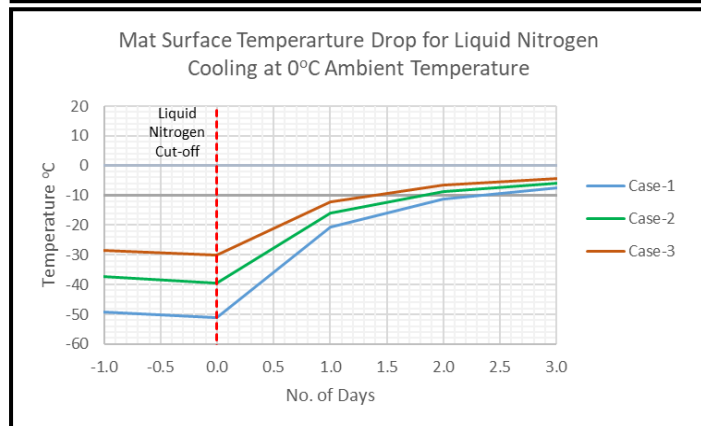


**Figure 80:** Average Mat Surface Temperature at 0°C Ambient Temperature.

From the above exercise it can be seen that the thawing depends upon the initial mat surface temperature. With the high cooling agent flow velocity (case-1) in the freeze pipes, the mat surface temperature drops lower, so the thawing process takes more time to reach  $-10^{\circ}\text{C}$ .

### **5.5. Cost Estimation for Indirect Freezing (Brine chiller).**

A brine chiller is required for the freezing process. The main part of a brine chiller is the refrigeration unit. The freezing agent in the refrigeration cycle cools the cooling agent, which in turn freezes the silt mat. In turn, there are three main components of the refrigeration unit: the evaporator section, condenser section, and the compressor. As such, the estimation of the brine chiller depends upon the power input (compressor), cooling capacity (evaporator), and ambient temperature (condenser). For the frozen silt mat, the ambient temperatures considered are  $10^{\circ}\text{C}$ ,  $5^{\circ}\text{C}$ , and  $0^{\circ}\text{C}$ . The evaporating temperature for the brine inlet is assumed to be  $-30^{\circ}\text{C}$  (brine temperature entering freeze pipes). The cost of the indirect freezing consists of two portions: the cost of the unit refrigeration unit and the operating cost of the unit. The cost of the unit is dependent upon the maximum cooling requirement. The operating cost depends upon the power inputted to produce the required cooling. To avoid complexity, the capital cost and operational cost of the pump required for cooling agent circulation is not considered.

Brine chillers are custom-designed chillers, so the capital cost of a brine chiller is not easy to ascertain. To overcome this challenge, the industry design standard is compared with the frozen silt mat freezing requirement. AHRI-550/590(I-P)-2015 (2015)<sup>1</sup> provides the design standards for water chillers. As per the design standard, the cooling agent temperature is  $6.67^{\circ}\text{C}$  ( $44^{\circ}\text{F}$ ) and the air-cooled condenser temperature is  $35^{\circ}\text{C}$  ( $95^{\circ}\text{F}$ ) (AHRI-550/590(I-P)-2015, 2015). It is assumed that the cost of a brine chiller is close to the cost of the water chiller. To estimate the cost of the brine chiller, the actual cooling capacity of the requirement is converted to the industry standard, with the Coefficient of Performance (COP) formula used to calculate the power input.

---

<sup>1</sup> AHRI = Air-Conditioning, Heating, and Refrigeration Institute, USA

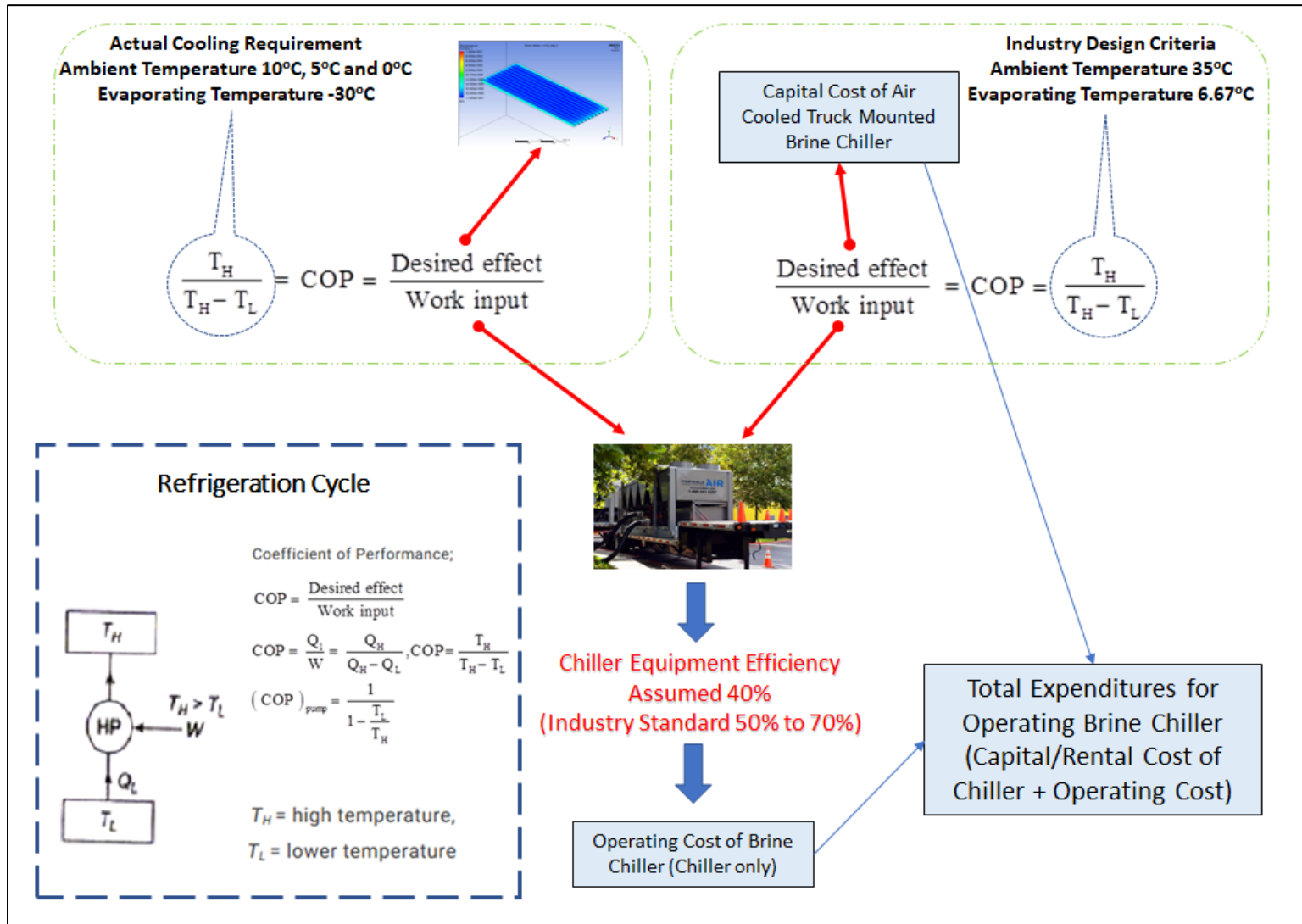
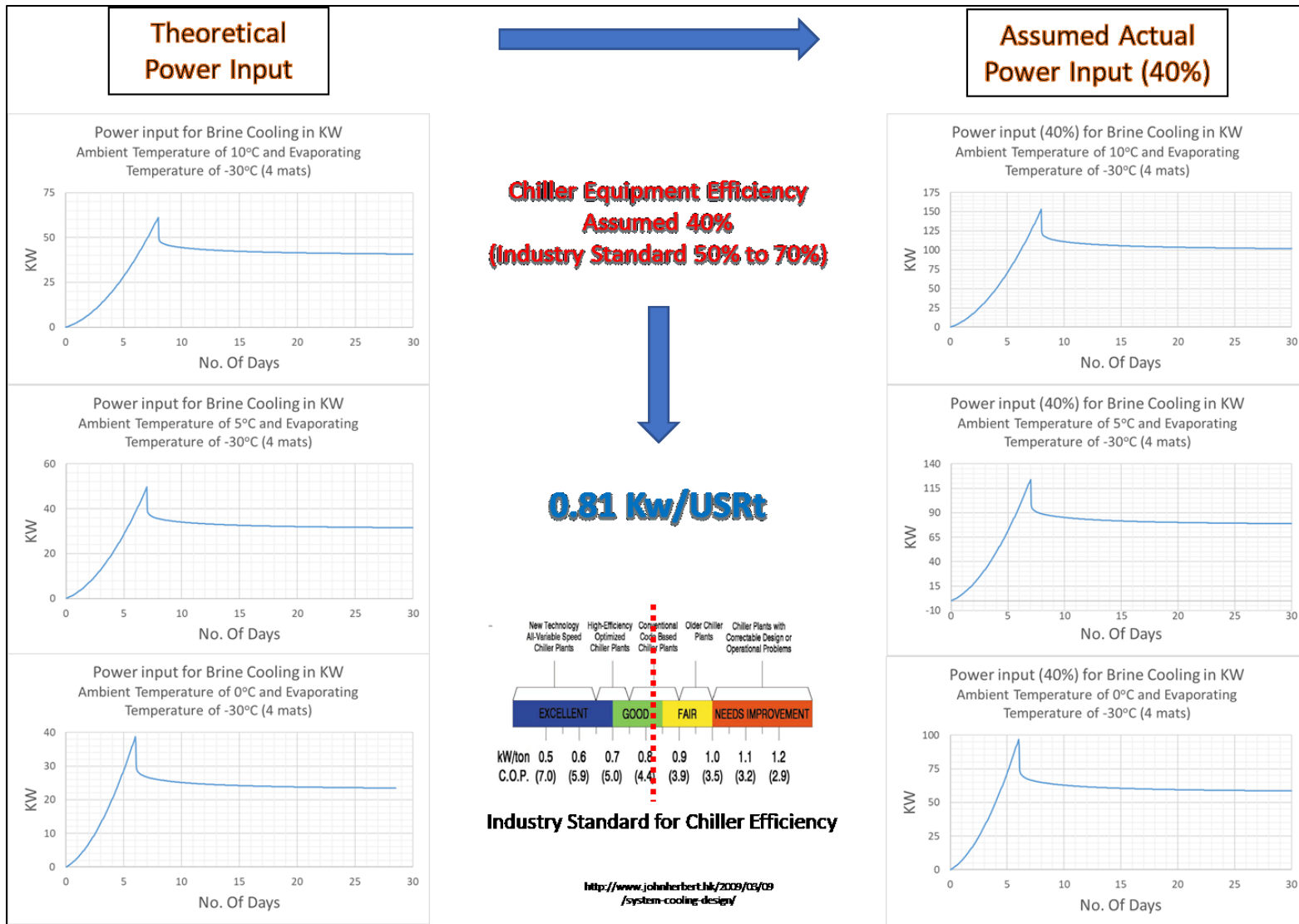


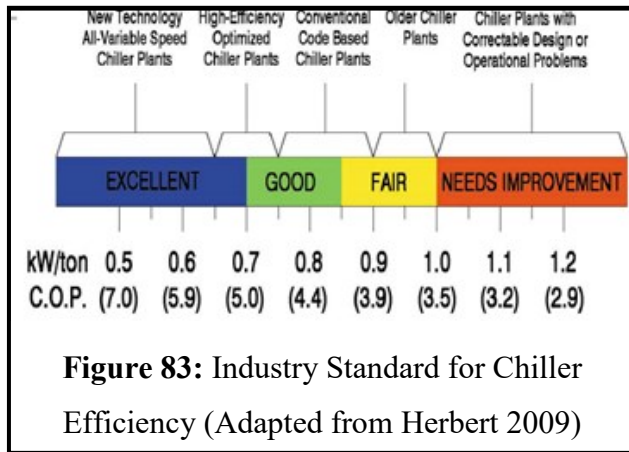
Figure 81: Refrigerator Coefficient of Performance (COP)



**Figure 82: Industry Standard for Chiller Efficiency**

Figure 81 describes the relationship between COP and temperature of the evaporating side and the condenser side. The COP of the mat freezing refrigeration unit is used to calculate the work input by the compressor. The same compressor input is used to calculate the desired effect (cooling) at standard industry design practice using the COP based on a 6.67°C evaporating temperature and a 35°C condenser temperature. The cooling effect value obtained from the industry standard is used to estimate the cost of the brine chiller required for the freezing of silt mats. Figure 81 and Figure 82 illustrate the calculation process in detail.

A 377.73USRt<sup>1</sup> industrial chiller can be used to freeze eight silt mats at an ambient temperature of 10°C with an evaporating temperature of -30°C (brine inlet temperature). A 305.64USRt industrial



chiller can be used to freeze the silt mats at the ambient temperature of 5°C. For the ambient temperature of 0°C, a 239.36USRt industrial chiller can be used to freeze the silt mat. The capacity of the chiller is required in order to calculate its capital cost. Usually, the price of an air-cooled chiller ranges from \$450 to \$700 per USRt<sup>2</sup> (Enersion, 2017). For the cost

comparison, \$450 is taken for one USRt. For the rental chiller, the rental price is assumed to be \$46 per USRt (Trane, 2012).

The next step is to calculate the cost of the electricity for the operation of the brine chiller for indirect freezing. For the operating cost, the power input to the unit is used to calculate the cost of electricity used to operate the unit. The calculations mentioned earlier are based on the theoretical power input; however, in reality, the theoretical power input is less than the actual power input. With the actual efficiency typically ranging between 50% and 70% (Herbert, 2009). For the cost comparison, the brine chiller efficiency is considered to be 40% (a conservative figure). Figure 83 provides the details pertaining to chiller efficiency in terms of cooling effect and power input (Herbert, 2009).

<sup>1</sup> 1 USRt = 12,000BTU/hr

<sup>2</sup> \$ = US Dollars

For the cost comparison, the power input for the freezing and maintenance phases is calculated for the operating cost estimation. Figure 82 describes the process in detail, where the assumed theoretical power input is converted to actual power input with the machine efficiency of 40%.

Power use (KW) per USRt is found to be about 0.81 (KW/USRt), which is considered ‘Good’ for an air-cooled chiller (see Figure 83) (Herbert, 2009). The maintenance cost of the chiller is taken as \$40 per year per USRt. Usually, the maintenance cost varies with the capacity of the chiller. In this case it is within the range \$45 to \$30 (Commercial Energy Library, 2018). The main factor in the calculation of operating cost of chiller is the cost of electricity. In Alberta, the average cost of one kWh of power is about \$0.05 (AUC, 2018). Figure 84 shows the power use in terms of dollars required to achieve the specified cooling effect.

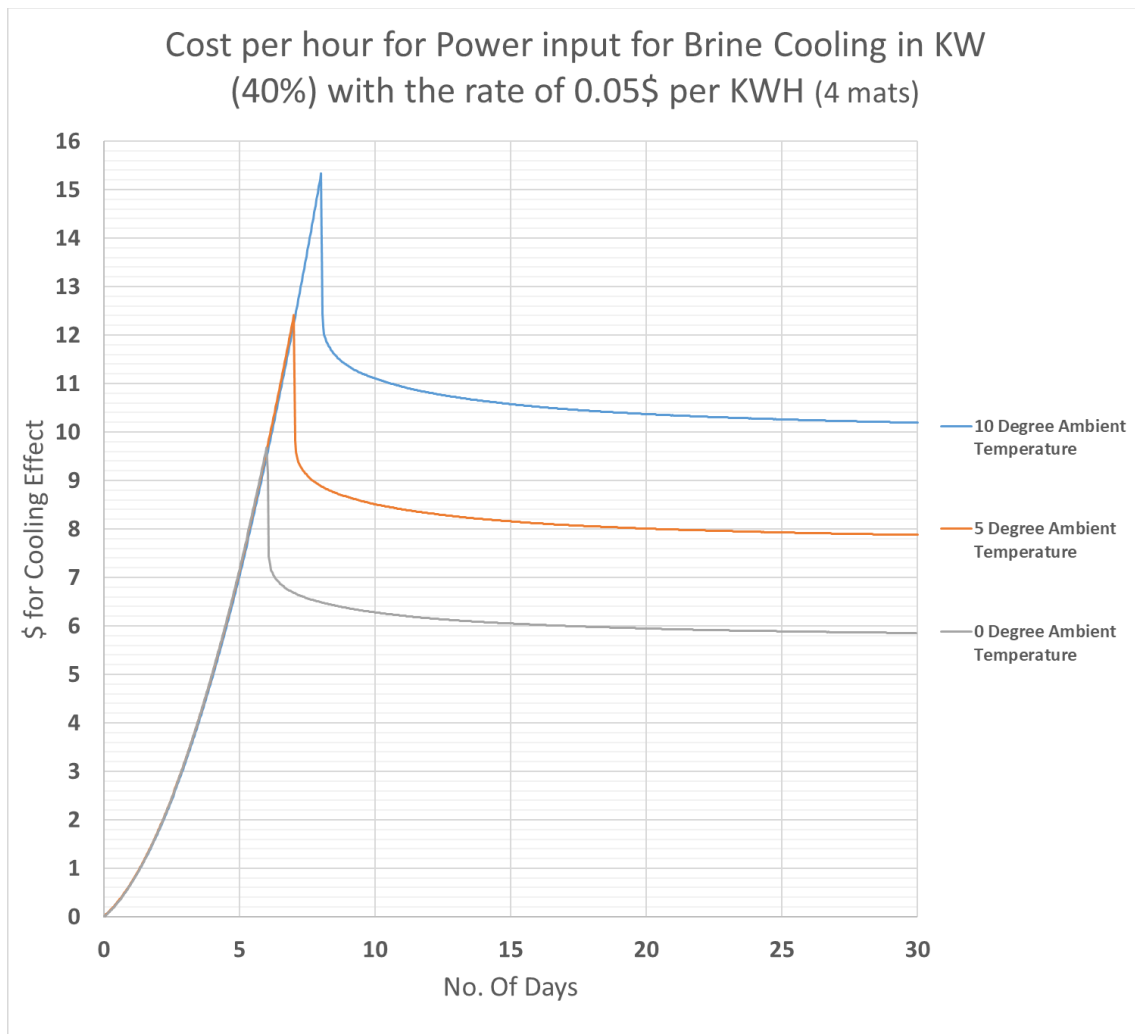


**Figure 84:** Power usage for the required cooling effect.

The chiller operator costs for the respective ambient temperature scenarios are assumed to be \$80 (10°C), \$60 (5°C), and \$40 (0°C). The operator’s cost is assumed to depend upon the size of the brine chiller. The maintenance cost of the chiller (owned<sup>1</sup>) is about \$40 per year per USRt (Commercial Energy Library, 2018). The assumed cost of piping arrangement (pipes, valves, thermo-sensors, chiller control) is \$30,000 (one time in a 15-year period). Figure 85 shows the cost breakdown for indirect freezing, where the lifespan of a chiller is assumed to be 15 years.

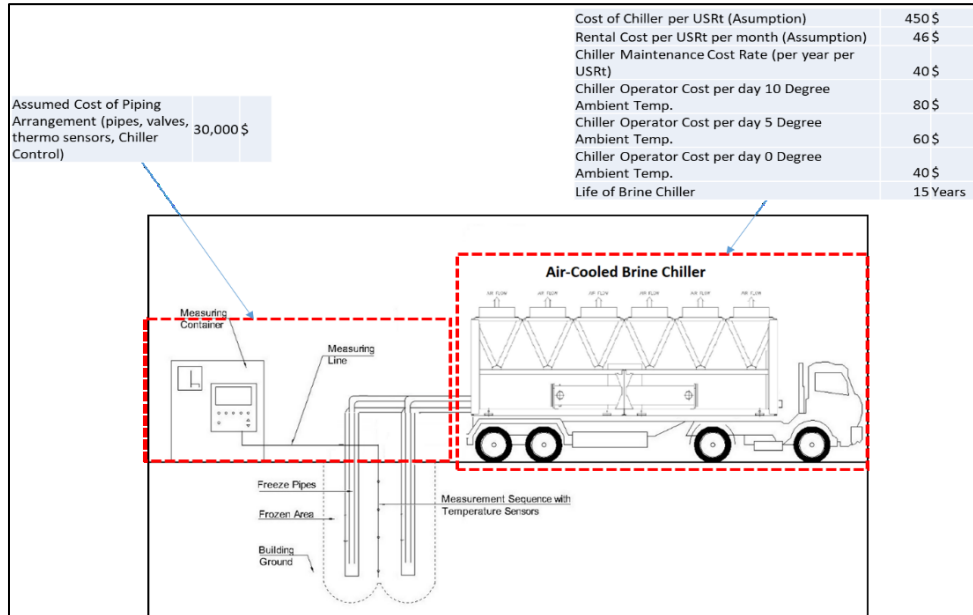


**Figure 85:** Cost Breakdown for Indirect Freezing.

### 5.6. Cost Estimation for Direct Freezing (Liquid Nitrogen).

The cost breakdown for direct freezing is very simple in nature. The flow of nitrogen for the freezing has already been calculated using ANSYS. The same values are used for the cost of liquid nitrogen used, assumed as \$2/L (U of T, 2018).

The use of liquid nitrogen is based on the case studies, where the flow rate of nitrogen is higher for Case-1 as compared to Case-2 and Case-3. The flow of liquid nitrogen is lowest in Case-3. In the same way, the dollar values change (see Figure 86 for further detail).

<sup>1</sup> Assumed to be owned by the Crane Company.



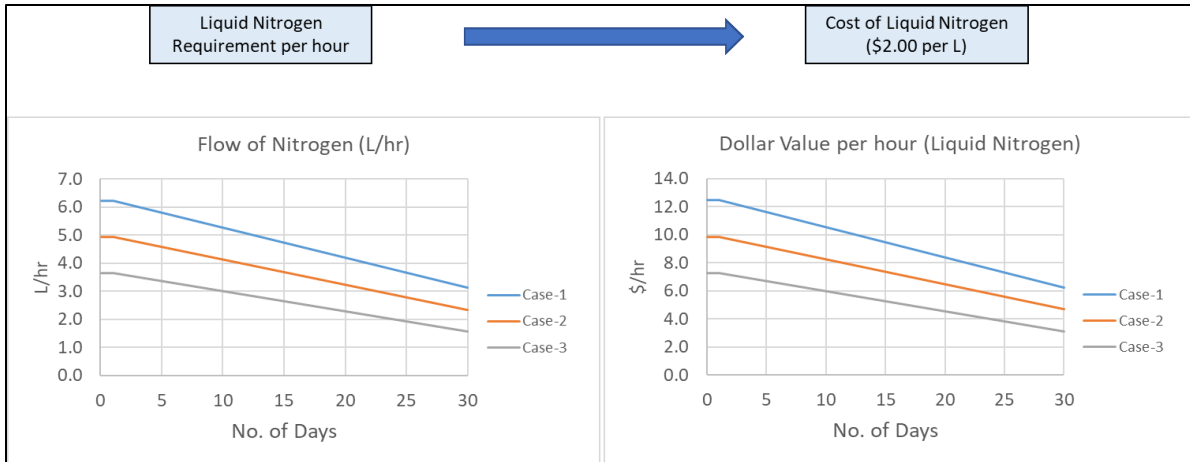


**Figure 86:** Cost Estimation for Liquid Nitrogen Use for all three Cases.

The reasonable rental cost of the liquid nitrogen tanker is assumed to be \$3,000 per month. The rental cost for the prime mover is considered as \$200 for moving the liquid nitrogen tanker from one location to the other, while the cost of the liquid nitrogen plant operator is assumed to be \$80 per day. The assumed cost of the piping arrangement (pipes, valves, thermo-sensors, liquid nitrogen control system) is \$50,000, while the lifespan of the piping arrangement is considered as 15 years. Figure 87 shows the cost breakdown for direct freezing.

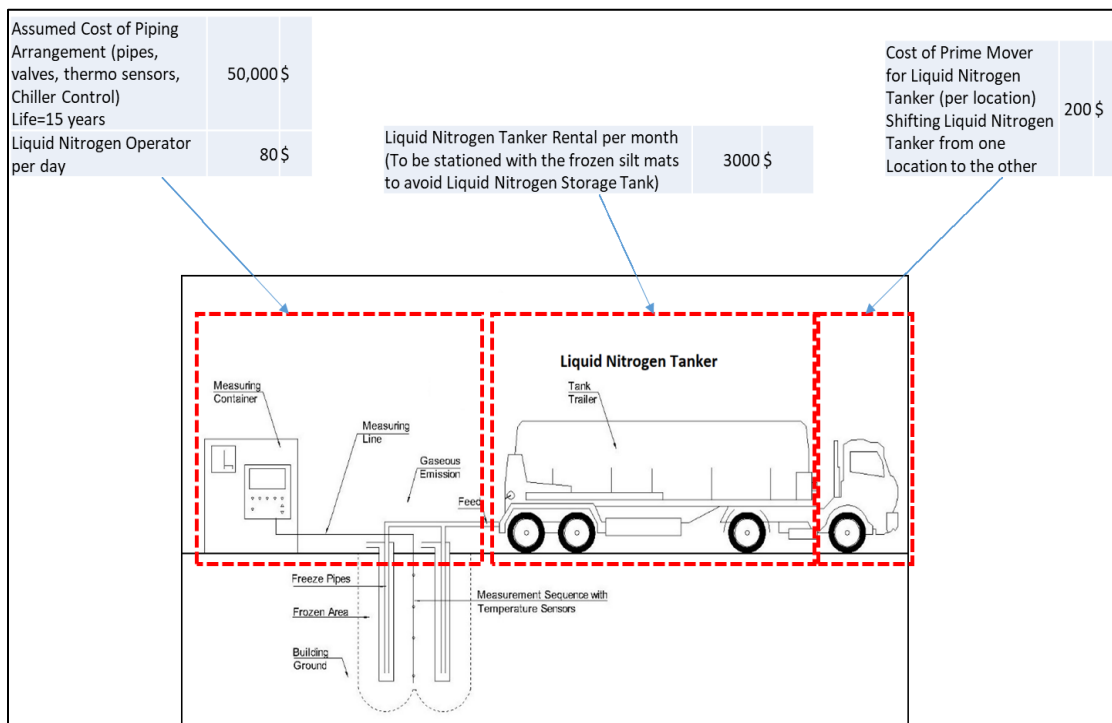


**Figure 87:** Cost Breakdown for Direct Freezing.

## 5.7. Cost Estimation for Timber Mats.

The assumed cost estimation for timber mat use on site is summarized in Table 15, where the lifespan of one timber mat is assumed to be three years. After three years, the mats are considered unusable due to wear and tear, and a new set of timber mats must be purchased for the crane work (Golden Environmental Mat Services, 2015). For the case project in Yellowknife (see Section 3.3.9.), the mats are required to be transported from the company yard to the construction site. At the end of the project, the mats are transported back to the company yard. Other major cost drivers are the cost of mat laying (equipment and labor), cost of mat removal from lifting location (equipment and labor), and transportation of mat within site. As the author lacks the available data regarding stacking/storage cost, in the interest of simplicity it is considered that the stacking/storage of timber mats at the company yard is free of cost. It is also assumed that the stacking/storage of timber mats at a construction site is free of cost. These values can be incorporated in future research.

**Table 15: Assumed Timber Mat Expenditures (Crawler Crane)**

Timber Mat Expenditures (Crawler Crane)		
Timber Mat Cost (per Piece)	1,700.00	\$
Timber Mat life	3.00	Years
Cost for Timber mat discarding	100.00	\$
Timber Mats for Crawler Crane	36.00	Nos.
Cost of Mat Transportation to/from site	2,571.43	\$
Cost of Mat Transportation to/from lifting location	960.00	\$
Cost of Rigger for mat laying/removal	1,280.00	\$
Total Cost of Timber Mats (36 nos.)	61,200.00	\$
Total Cost of Mat Transportation to/from the site for one year	5,142.86	\$
Total Cost of Mat Transportation to/from lifting location for one year	30,720.00	\$
Total Cost of Riggers for mat laying/removing for one year	40,960.00	\$

## 5.8. Cost Comparison – Traditional Mat versus Frozen Silt Mat

What follow are the assumptions taken for the cost comparison:

1. The inflation rate is considered as 2% per year (Taborda, 2018).
2. Frozen silt mat setup/removal cost per location: This includes the use of equipment for the transportation of soil to the mat location and removal after the work is done. It also includes the transportation of cooling equipment from one location to other. The

configuration of the pipe is 2" schedule 40, while the cost of the steel pipe is about \$3.40 per ft (FederalMetals, 2018). The total length of steel pipe for eight mats is about 787.40 ft. It is assumed that the lifespan of these pipes is about one year due to the corrosive characteristics of brine solution. The same one-year lifespan is considered for liquid nitrogen use.

3. Cost of riggers for frozen silt mat laying/removal (one side): This includes the use of manpower for the laying of pipes and setting up the cooling system, as well as the labor cost for the setting up of the frozen silt mat.
4. Chiller Operator cost: Typically, the chillers available in the market are automatic and self-controlled, with the operator merely required to check the readings at a specified interval.
5. Assumed Cost of Piping Arrangement (pipes, valves, thermo-sensors) for Brine chillers: This includes the headers for piping, valves, thermo-sensors, etc. for the brine chiller arrangement, including the control and monitoring system in between the chiller and the frozen silt mat pipes. It is assumed that this complete system is made of corrosion-resistant material and has a lifespan of 15 years.
6. Assumed Cost of Piping Arrangement (pipes, valves, thermo-sensors) for Liquid Nitrogen: This is the control and monitoring system between the liquid nitrogen and the frozen silt mat pipes. This system is assumed to have a 15-year lifespan.
7. For rental chillers, the cost of chiller maintenance and chiller operator are not included in the estimation. The cost of the operator and the maintenance cost are included in the rental cost.
8. In the interest of simplicity, system breakdown cost is not included in the cost comparison.

To perform the value engineering, there are four main approaches to the crane matting problem.

1. **Traditional Timber Mats.** It is composed of using timber mats for crane matting. The schedule is provided in Section 3.3.9.4 (the reader may refer to Figure 50).
2. **Indirect Freezing – Brine chiller.** The duration of the project remains the same. The assumed schedule is shown in Figure 50. As per the ANSYS simulation, at 10°C ambient temperature eight days are required for the brine chiller to bring the temperature of the

frozen silt to the required level for crane support. For 5°C ambient temperature, it takes seven days and for 0°C it takes six days. The same brine chiller is used for the maintenance phase (the cost drivers are available in Section 3.3.8). The schedule for the three ambient temperatures is shown in Figure 88. The estimate is for one month which can be bottom up to get for 8 months, and later for 15 years (bottom-up estimation). The duration remains the same whether the chiller is owned or rented (assumed).

3. **Direct Freezing - Liquid Nitrogen:** The duration of the project remains the same. The advantage of liquid nitrogen is that it takes only one day for the silt to be sufficiently frozen. The cost is based on the use of liquid nitrogen and the liquid nitrogen tanker rental cost (the schedule is shown in Figure 89). The cost of the prime mover is also included in the estimation.



Figure 88: Schedule for Brine chiller Frozen Silt Mat (Crawler Crane)



1. **Traditional Timber Mats:** This is the traditional approach using timber mats. This includes the cost related to the use of timber matting at the case project in Yellowknife.
2. **One Project Brine Chiller Owned:** This describes the use of a brine chiller for the freezing of the mat. The chiller is used for only one case project at a time in Yellowknife. The chiller is assumed to be owned by the company (capital cost of chiller is included in the cost comparison).
3. **One Project Liquid Nitrogen:** This example involves the use of liquid nitrogen for the freezing of the mats. The use is only for one project.
4. **One Project Hybrid System (Owned Chiller):** For this option, the hybrid system is used at only one project. Liquid nitrogen is used for the freezing phase and a brine chiller is used during the maintenance phase (see Figure 90). For this option, the brine chiller is owned by the company.
5. **One Project Hybrid System (Rental Chiller):** For this option, the hybrid system is used for one project. Liquid nitrogen is used for the freezing phase and brine chiller is used during the maintenance phase. For this option, the brine chiller is a rental (per month rental cost is incorporated in the cost comparison).
6. **Two Project Hybrid System (Owned Chiller):** For this option, the hybrid system is used at two projects with similar figures simultaneously, which entails dividing the cost of the chiller between two projects instead of one. As per one project schedule, the brine chiller remains idle during the gap between two lifting locations. The chiller during this idle time can be used at another project with similar requirements. To avoid heavy transportation cost, it is assumed that the second project is close to the first project. The cost of the chiller is divided evenly between two projects.
7. **Two Projects Hybrid System (Rental Chiller):** For this option, the hybrid system is used at two similar projects at the same time. In this case, the chiller considered is a monthly rental. The monthly rent is evenly divided between two similar projects.

For the cost estimation and comparison, most of the figures are determined in consultation with an industry expert<sup>1</sup>. These figures are bottom-up to build one-year cost estimation for all seven case examples. The cost figures for the first year are further extended to 15 years with the addition of

---

<sup>1</sup> NCSG Crane & Heavy Haul Corporation, Engineering Department.

an inflation rate of 2%. The breakdown of cost for the first year for each case example is shown in Table 16.

Figure 91 shows the total expenditures for 15 years for all seven case examples (line chart). Figure 92 shows the bar chart for the total expenditures for these 7 case examples. After 15 years of brine chiller life, based on the assumed figures and ANSYS simulation, it is concluded that the new technology of frozen silt mat can be cost-effective for three case examples: (1) one-project hybrid system (chiller owned), (2) two-project hybrid system (chiller owned), and (3) two-project hybrid system (rental chillers).

The hybrid system looks feasible as per the assumed calculated values and ANSYS simulation. The owned chiller hybrid system is cost-effective in both the cases (one project and two similar projects). In the case of the one chiller (owned) hybrid system at one project only with the chiller remaining idle for 16 days in a month, the cost breakeven point falls between 10 and 11 years. If the chiller (owned) is utilized at another similar project during the idle period, the cost breakeven point is between 4 to 5 years.

In the case in which a rental chiller hybrid system is being used at two similar projects (utilizing chiller on another similar project during the idle period), the option is cost-effective from the fourth year. The figures for these seven case examples are shown in Appendix H. The cost breakeven point with respect to the traditional mat expenditure is shown in Appendix I.

The cost-effectiveness is maximum (\$266,820 after 15 years), in the case of an owned chiller with the hybrid system at two similar projects.

**Table 16:** Assumed major Cost Figures (\$) for one year (Bottom-up estimation for 8 months at Yellowknife)

	Description	Traditional Timber Mats	One Project Brine Chiller Owned	One Project Liquid Nitrogen	One Project Hybrid System (Owned Chiller)	One Project Hybrid System (Rental Chiller)	Two Projects Hybrid System (Owned Chiller)	Two Projects Hybrid System (Rental Chiller)
1	Cost of Timber Mats (36)	61,200	0	0	0	0	0	0
2	Timber Mat transportation and laying cost	76,822	0	0	0	0	0	0
3	Freezing Pipe Cost	0	2,677	2,677	2,677	2,677	2,677	2,677
4	Piping Arrangement (pipes, valves, thermo-sensors)	0	30,000	50,000	50,000	50,000	50,000	50,000
5	Cost of Chiller	0	169,976	0	114,295	0	57,148	0
6	Chiller rent	0	0	0	0	67,329	0	33,665
7	Silt Mat Laying (Rigger and Equipment)	0	22,400	22,400	22,400	22,400	22,400	22,400
8	Operator Cost	0	12,640	11,520	12,640	0	12,640	0
9	Chiller Maintenance Cost	0	10,802	0	15,109	0	7,555	0
10	Liquid Nitrogen Tanker Rental and Prime Mover	0	0	20,800	3,600	3,600	3,600	3,600
11	Liquid Nitrogen Cost	0	0	63,818	6,186	6,186	6,186	6,186
12	Operating Cost of Brine chiller	0	66,633		19,820	19,820	19,820	19,820



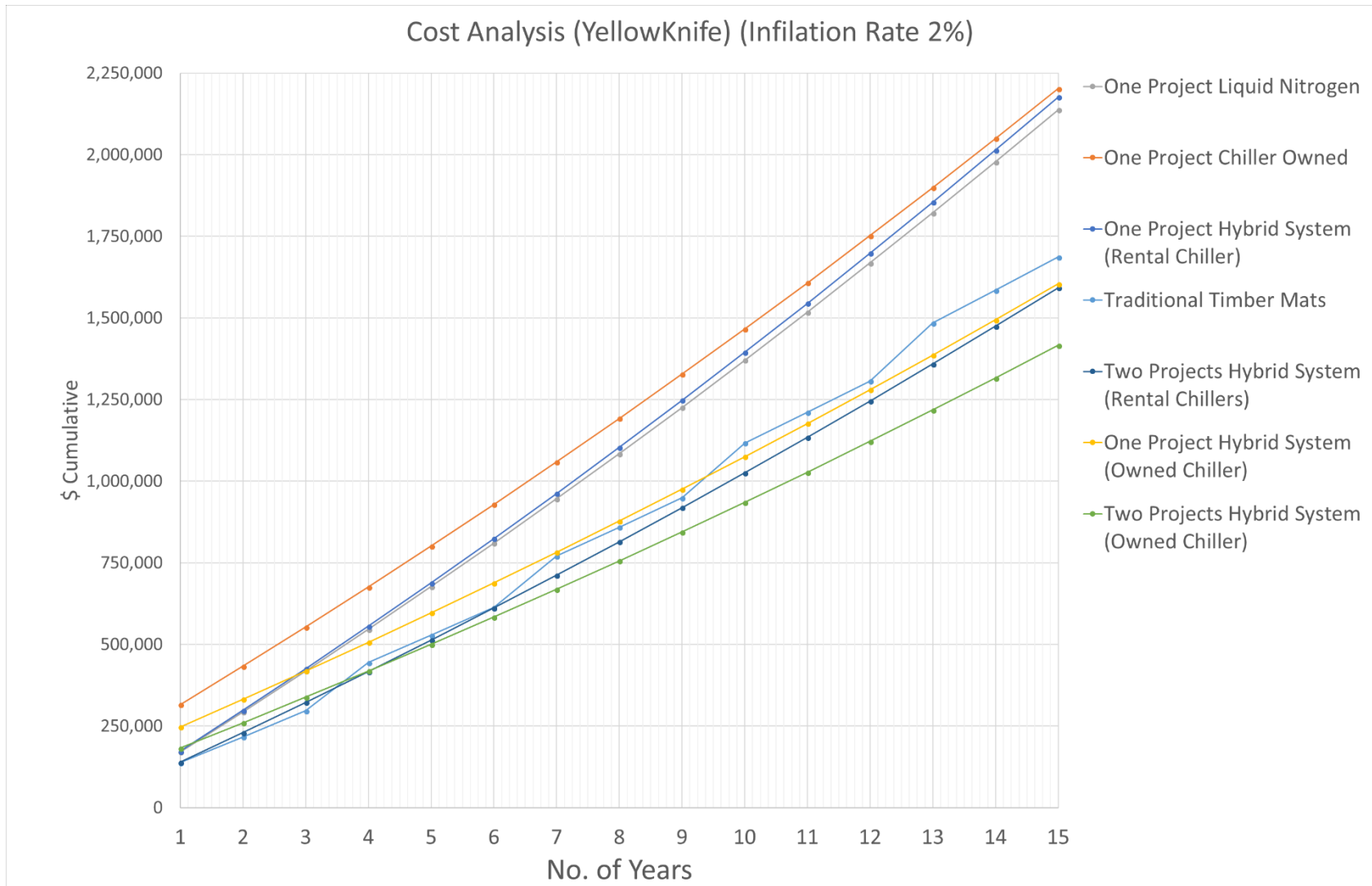


**Figure 91:** Total Expenditures for seven Case examples (15 years)

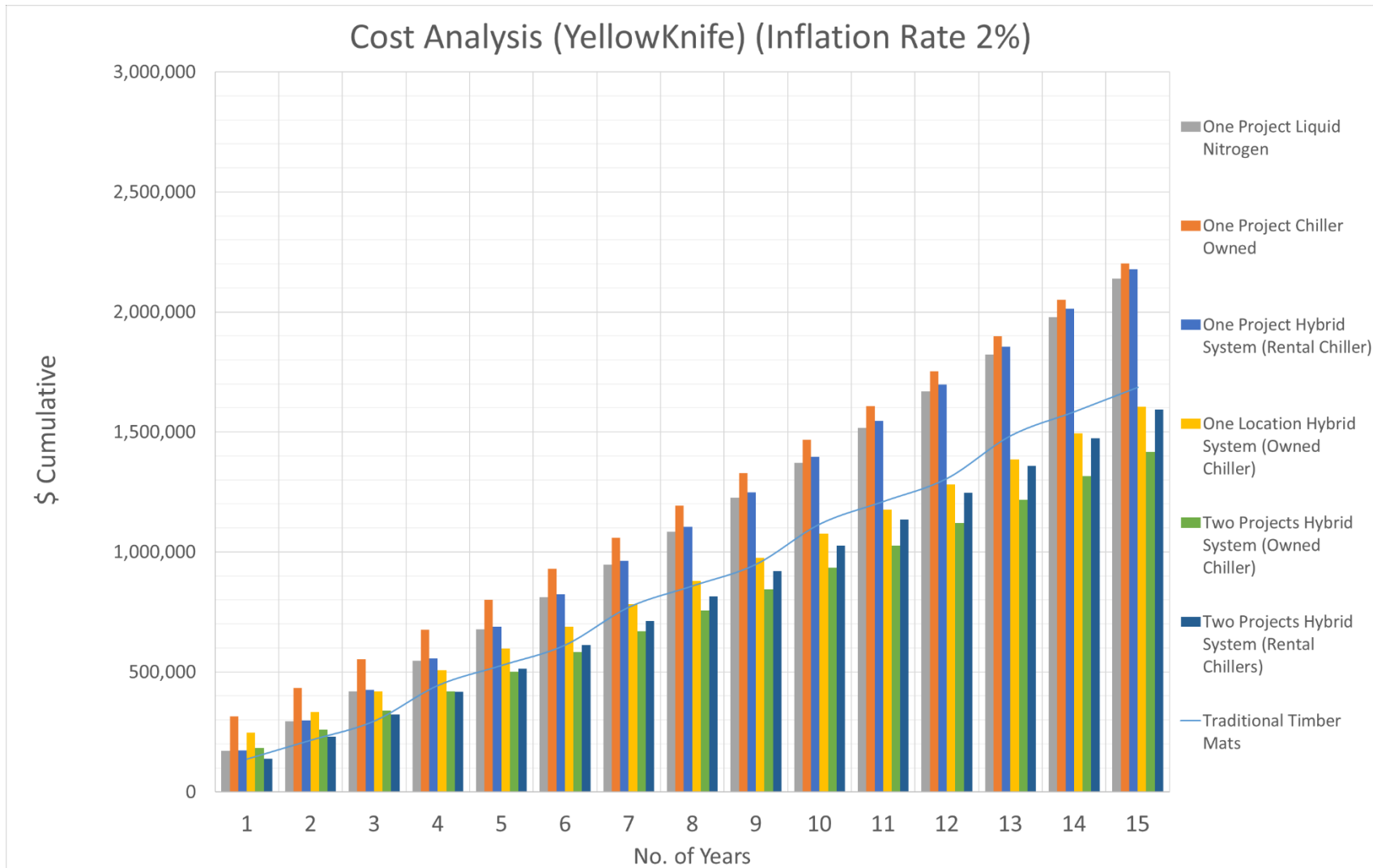


**Figure 92:** Cost Analysis for seven case examples at Yellowknife project (15 years)

## CHAPTER 6: SUMMARY AND CONCLUSIONS

### 6.1. The decision process for artificial ground freezing for heavy cranes

Before embarking on artificial ground freezing for frozen silt mat, there is a need to first decide if frozen silt mat is necessary or not. After site investigation and soil testing, the bearing capacity of the soil should be evaluated. If the soil bearing capacity can effectively support the expected crane load, then the frozen silt mat is not required. However, if the soil bearing capacity is not able to support the expected load, there is a need to evaluate the moisture content of the soil to see if it is sufficient to produce an adequate frozen silt mat that will support the expected load (Andersland & Ladanyi, 2004). If the moisture content of the soil is enough to produce the desired frozen strength, it must be determined whether the cost of freezing is reasonable in comparison with other crane-supporting methods such as timber or steel mats. If the cost of freezing is reasonable, we proceed to prepare the frozen silt mat design, freeze the silt, and monitor the strength of the frozen silt mat by measuring the surface temperature. If the design surface temperature is achieved, the crane can be mobilized to the site.

### 6.2. Market Approach for Ice/Frozen Silt Mats.

The present research shows that ice/frozen silt mats can be used in place of timber mats for load distribution under crane track/outrigger. This technology can be used widely in cold regions where the temperature is already below zero for much of the year. Ice has very high tensile strength and compressive strength, with the tensile strength of ice lying in the range 0.7 MPa to 3.1 MPa. The average tensile strength of ice is about 1.43 MPa for the temperature range  $-10^{\circ}\text{C}$  to  $-20^{\circ}\text{C}$  (Petrovic, 2003), meaning that there is very little variation in tensile strength as the temperature fluctuates. The tensile strength decreases with the increase of grain size<sup>1</sup>(Petrovic, 2003). The tensile strength of ice is a maximum of 3.3070 MPa at  $-40^{\circ}\text{C}$  (Wenyuan & Yingkui, 2015).

Ice has a very high compressive strength as compared to timber mats, ranging from 5 MPa to 25 MPa over the temperature range of  $-10^{\circ}\text{C}$  to  $-20^{\circ}\text{C}$  (Wenyuan & Yingkui, 2015). The compressive strength of ice increases as the temperature drops and the strain rate<sup>2</sup> increases. The compressive

---

<sup>1</sup> In metallurgy the grain size is a precise, standardized measurement of the size of the crystals inside a metallic, crystalline solid.

<sup>2</sup> Strain rate is the change in strain (deformation) of a material with respect to time.

strength of frozen silt fluctuates with the change in the temperature, water content, and strain rate (see Figure 40). In this regard, Goughnour and Andersland (1968) studied the variation of the compressive strength of naturally frozen silt with the change of water content. The compressive strength of artificially frozen ground can be increased by dropping the temperature to  $-60^{\circ}\text{C}$  using liquid nitrogen. In this condition, the compressive strength of ice can surpass the compressive strength of standard 3,000 psi concrete (20.68 MPa) (see Figure 40) (Andersland & Ladanyi, 2004).

The beachhead market for ice/frozen silt mats can be crawler cranes in cold regions of North America. Figure 93 shows the concept of mat market to the beachhead crawler crane mat market. As described above, mats are used for the support of crawler cranes. When a construction crew is moving a crawler crane within a site, there is a requirement for timber mats to cover the route of the crane. Furthermore, during crane operation, timber mats are required to support the weight of the crane. In this context, the construction industry has seen many workplace accidents where the crane has tilted as a result of poor ground preparation (refer to Chapter 1). Frozen silt mats could be a good alternative for crane ground support, with a beachhead market of construction sites in cold regions, as matting in these sites is temperature-sensitive. Transportation and storage of timber mats, it should be noted, is costly (Section 5.7). It is assumed (based on the research described above) that the transportation and storage of frozen silt mats will be negligible as compared to the timber mats (Section 5.8). The basic ingredient of frozen silt mat is soil, which is

readily available and can easily be disposed of. For this reason, it is difficult to describe or illustrate the lifecycle of this new technology. In this approach, the use of storage area on site and at the provider's facility will be minimal, but space on site will be required for the freezing system.

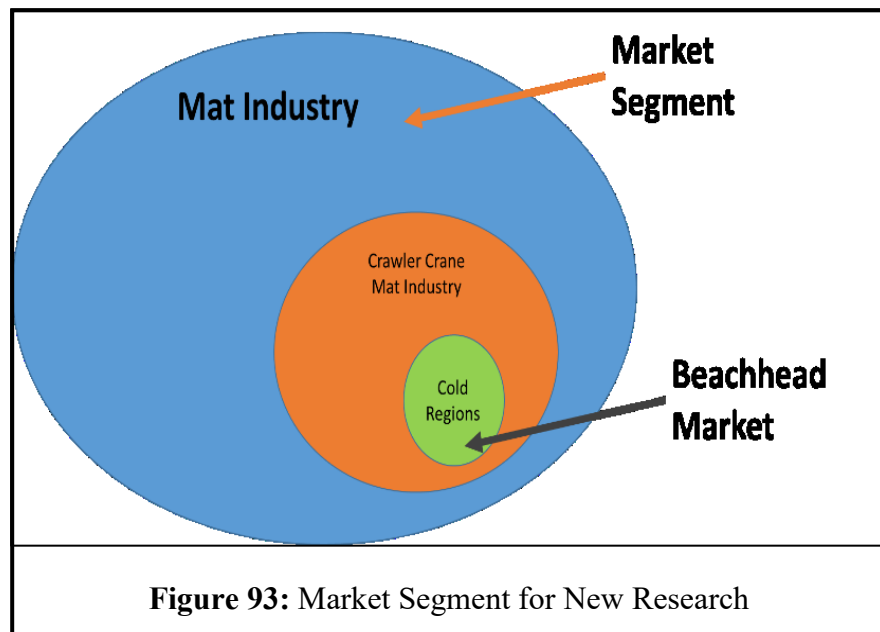


**Table 17:** Perceived Competitive Position of New Research (based on the research in this thesis)

	<b>Description</b>	<b>Timber Mats</b>	<b>Steel Mats</b>	<b>new research</b>
1	Cost of transportation	High	High	Very low
2	Cost of inventory management	High	High	Very low
3	Standard sizes	Limited	Limited	Can be produced in any size
4	Tensile Strength	Low	High	Medium
5	Compressive strength	Low	High	Medium
6	Fracture toughness	Medium	High	Low
7	Modulus of elasticity	Medium	High	Low
8	Flexural Strength (Modulus of Rupture)	Medium	High	low
9	Initial Cost	Medium	High	High
10	Operating cost	Medium	Low	Low (project dependable)
11	Durability	Low	High	Not applicable
12	Temperature sensitivity	Minor	Minor	Highly temperature-sensitive
13	Environmentally-friendly	Medium	Low	High
14	Lifecycle	Short	long	Not applicable

### 6.3. SWOT Analysis for New Technology (Frozen Silt Mat for Crane Matting)

Use of SWOT analysis is common before the launch of a new product or business. It captures strengths, weaknesses, opportunities, and threats related to a new product or business. Same criteria are used in this section for a competitive analysis of the use of frozen silt matting versus traditional methods of ground support for heavy cranes (i.e., steel or timber mats). In terms of mechanical properties, frozen silt performs better as compared to ice (Andersland and Ladanyi, 2004). To be conservative, the mechanical properties of ice are also discussed along with the frozen silt within the same framework. The SWOT analysis is based on previous academic research on the thermal and mechanical properties of ice/frozen silt (McNutt, 1991).

#### Internal - Strength:

1. **Good Tensile Strength:** The tensile strength of ice falls within the range 0.7 MPa to 3.1 MPa. The average tensile strength is about 1.43 MPa for the temperature range  $-10^{\circ}\text{C}$  to  $-20^{\circ}\text{C}$ . The tensile strength decreases with the increase of grain size (Petrovic, 2003). The tensile strength of ice reaches a maximum of 3.3070 MPa at  $-40^{\circ}\text{C}$  (Wenyuan & Yingkui,

2015). The tensile strength of Coastal Douglas-Fir with 12% moisture content is about 2.3 MPa perpendicular to the grain, and 107.6 MPa parallel to the grain (Kretschmann, 2010). The tensile strength of artificially frozen silt, meanwhile, is more than 5 MPa if the temperature drops below  $-10^{\circ}\text{C}$  (Andersland & Ladanyi, 2004). The tensile strength varies with the temperature and the strain rate. The tensile strength of concrete lies between 2 MPa and 5 MPa (The Engineering Toolbox, 2017).

2. **High compression strength:** The advantage of ice is that it achieves a high compressive strength (5 to 25 MPa over the temperature range of  $-10^{\circ}\text{C}$  to  $-20^{\circ}\text{C}$ ). The compressive strength of ice increases with a temperature drop and strain rate increase. An ice-soil mixture also increases the compression strength (see Figure 40) (Petrovic, 2003). The compressive strength of a green and clear wood specimen of Coastal Douglas-Fir (12% moisture content) is 5.5 MPa (perpendicular to grain) (Kretschmann, 2010). The crane mats are able to stand heavy loads. As such, ice stands as a promising matting solution due to its ability to withstand compression. With the temperature drop, the strength can be increased further to the required level. The advantage of artificial ground freezing is that it achieves a very high compression strength. Furthermore, the strength of frozen silt increases as the temperature drops below the freezing point of ice (Andersland & Ladanyi, 2004).
3. **Cheap as compared to other available solutions:** Ice/frozen silt matting requires a one-time investment (capital cost of refrigeration system). If a mesh is used to increase the bearing strength, then the mesh could be reused several times. The fabric reinforcement can increase the modulus of rupture of ice up to 31%. Furthermore, using steel bars or cables as reinforcement increases the flexural strength by six times (Haynes, Collins, & Olson, 1992).
4. **Environmentally-friendly:** There is no waste of wood in this technology, so it is environmentally-friendly as compared to timber mats. The raw material for these mats is assumed to be water and soil (Miniat, 2017).
5. **Can be prepared in any size:** Typically, wood mats are available in standard dimensions (Mats, 2017). If the site is confined, it becomes difficult to adjust these mats to the site requirements. It is assumed that ice/frozen silt mats can be prepared in any size as per the construction site requirement.

6. **Can be prepared on the site as per the site requirement:** The proposed mats can be prepared on site. The basic ingredients are water and soil, so it can be prepared anywhere, anytime.
7. **Transportation is cheap:** The basic ingredients are water and soil, which can be easily obtained in the vicinity of the construction site in most cases. The transportation cost will only consist of the cost of transporting the material used for the preparation of such mats.
8. **No concept of lifespan as compared to wood or steel:** Here lifespan is not an issue as it would be with wood or steel matting (Brischke & Meyer-Veltrup, 2015).

#### **Internal - Weakness:**

1. **Heavy initial investment:** Initial investment is high due to the cost of the refrigeration unit to perform ground freezing (based on the research done in this thesis). But in cold regions, the required capital cost will decrease as the temperature is already close to the freezing point.
2. **Temperature-dependent:** The mechanical properties of ice/frozen silt are temperature-dependent. However, this technology can be used in hot regions, provided there is sufficient insulation to prevent heat transfer.
3. **Low modulus of elasticity:** Ice has a low Young's modulus of elasticity. Young's modulus of elasticity of ice at  $-5^{\circ}\text{C}$  is only 9.0 MPa (Schulson, 1999). On the other hand, the modulus of elasticity of timber (wood) is between 9 GPa and 14.5 GPa (Zhiyong & Robert, 2010). The Young's modulus of frozen silt ranges from 2.1 to 10.6 GPa with the temperature range of  $0^{\circ}\text{C}$  to  $-11.6^{\circ}\text{C}$  (Yang et al., 2015). Timber mats withstand heavy loads without plastic deformation. The modulus of elasticity of concrete is about 14 GPa to 41 GPa, which is significantly higher than that of frozen soil (The Engineering Toolbox, 2017).
4. **Low Fracture Toughness:** The fracture toughness of ice is very low. It lies between  $50 \text{ KPa}\cdot\text{m}^{1/2}$  and  $150 \text{ KPa}\cdot\text{m}^{1/2}$  (Petrovic, 2003) The fracture toughness of eastern red spruce, by comparison, is about  $300 \text{ KPa}\cdot\text{m}^{1/2}$ , higher than that of ice (Mall, 1984). For Coastal Douglas-Fir, the average fracture toughness is about  $338 \text{ psi}\cdot\text{in}^{1/2}$  ( $371.41 \text{ KPa}\cdot\text{m}^{1/2}$ ) (Schiewind & Poznaik, 1971). As such, ice is vulnerable to fracture under loading.

5. **Flexural Strength (Modulus of Rupture):** The average modulus of rupture of ice beams in bending is about 22.5 kg/cm<sup>2</sup>. On the other hand, the modulus of rupture for pine is about 800 kg/cm<sup>2</sup>. With the addition of different pulp contents, the modulus of rupture of ice increases. If the pulp content is raised to 14%, the modulus of rupture increases to 66.7 kg/cm<sup>2</sup> (Perutz, 1997).
6. **Density anomalies of water with temperature:** The anomalies of water density with temperature is different from other materials. The density of water increases with the drop of temperature to 4°C, then the density of water decreases below 4°C. This means that ice melts under pressure, as discovered by Kirchhoff (1858) and Thomson (1873) (Bejan & Tyvand, 1992).

#### **External - Opportunity:**

1. **Can be used for heavy cranes and heavy loads:** Ice/frozen silt mats could be a good alternative solution for expensive matting (described in the previous chapter).
2. **Good market for cold-climate jurisdictions:** This technology could be particularly applicable for cold climates. The raw material for these mats is a combination of water and soil, which is temperature-dependent and works well even below the freezing point.
3. **Placement of Timber mats due to site constraints:** Mat manufacturing companies provide mats in standard sizes, and, if a special custom size mat is required, the price increases (Mats, 2017). This is not the case with ice/frozen silt mats, as they can be built to any size to fulfill the site requirement.
4. **Cost-effectiveness:** Initial cost is high, but the operational cost is lower (based on the research described above).

#### **External - Threats:**

1. **High ambient temperature:** Ice is temperature-sensitive, meaning that its density changes with temperature changes. The melting point of ice is 0°C. Therefore, high ambient temperature (above 0°C) will melt the ice/frozen silt.
2. **Sudden loading:** Sudden loading is related to flexural strength. Sudden loading can create cracks in ice sheets which can propagate easily and quickly.



3. **Change of bearing strength with respect to temperature:** With the increase of temperature, ice's tensile strength decreases. The compressive strength of ice also decreases with a rise in temperature. The range is 5 MPa to 25 MPa over the temperature range of  $-10^{\circ}\text{C}$  to  $-20^{\circ}\text{C}$  (Petrovic, 2003). Figure 40 shows the variation of frozen soil strength with respect to ambient temperature (Andersland & Ladanyi, 2004).

#### 6.4 Research Limitations and Assumptions

- This research can provide a guideline for the workability of frozen silt as crane ground support. The actual site and lab results may differ from the analysis in ANSYS described above.
- Only one type of soil (silt) is used for the analysis. Different soil parameters or types (clay, sand, etc.) may vary the results.
- Density anomalies of water with respect to ambient temperature are not incorporated in this research.
- Mechanical properties are considered uniform throughout the frozen silt mat. Usually, the mechanical properties vary with temperature variation, but in the interest of simplicity for the purpose of this research, it is taken as constant and uniform throughout the matting.
- Frozen silt mat cracking due to abnormal loading is not considered in this research. The impact of sudden loading is also not considered in this research.
- Pressure melting is not considered in the research.
- To avoid complexity, heat transfer from crane to frozen silt matting is not considered.
- The  $\text{CaCl}_2$  inlet temperature is considered uniform, which may not be the case in the actual freezing process.
- The heat transfer to the freezing mat may differ in actual practice from these ANSYS values and assumptions.
- Frozen silt mat requirement may differ from the actual project conditions.
- It is assumed that there is no rain on site throughout frozen silt mat usage.
- Assumed cost driver values are determined based on consultation with industry experts in crane and rigging<sup>1</sup>.

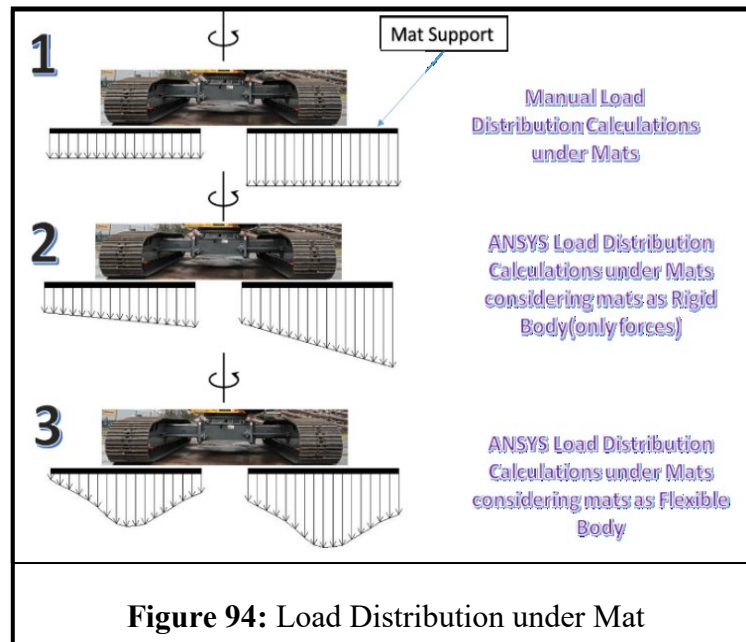
---

<sup>1</sup> NCSG – Northern Crane Services Group Engineering Department.

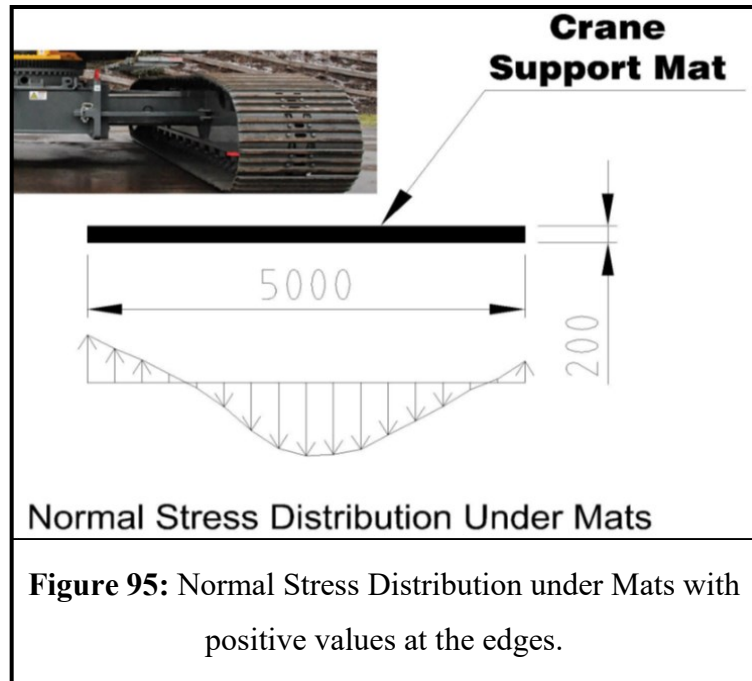
- The actual project parameters may differ from those assumed for the cost comparison between the frozen silt mat and traditional mat.
- All the cost estimation values are based on ANSYS freezing data. These may differ from the actual freezing data due to site constraints.
- The brine solution is corrosive in nature, so the lifespan of freezing pipes is taken as a maximum of one year maximum. It may be less than one year in actual practice.
- The mat cushion can be altered as per the site and actual requirements.

## 6.5. Conclusion

- This research provides a basis to measure the cost-effectiveness of frozen silt matting versus traditional crane matting.
- ANSYS has been used to calculate the GBP and compare it with the manual calculations. It can be used to re-check the calculations made by various GBP calculation software available in the market (Manitowoc, 2017) (Grove, 2017).
- The load distribution under the matting is not uniform; in fact the load distribution is non-uniform in nature. The maximum is right under the crawler and it decreases to the minimum value moving away from the crawler edge (see Figure 94). In the case of hydraulic cranes, the maximum is in the center of the outrigger.



- If the mat thickness is not sufficient, the GBP values (negative due to compression) on the edge of the mats could be zero or more than zero due to bending, meaning that the edges of the mat are not taking any load (see Figure 95).
- As per the results, ice/frozen silt can be used as the crane ground support provided that the load is fully distributed.



- Only a few physical properties are compared. Based on these physical properties, the results are favorable and feasible.
- Conditions for frozen silt mat workability:
  - Frozen silt matting can be used if the mat temperature is below  $-10^{\circ}\text{C}$  (as per the research findings described above). The mechanical properties of frozen silt mat under investigation are taken from the research done by Yang et al. (2015) on the specimens composed of silt from the Campbell Creek Bridge case project in Anchorage, AK (seasonally frozen soil) and the CRREL Permafrost Tunnel in Fox, AK (permafrost, frozen for two consecutive seasons) (Yang et al., 2015). The reader may refer to Section 3.3.2 for further details.
  - The Young's modulus ranges from 2.1 GPa to 10.6 GPa with the temperature ranging from  $0^{\circ}\text{C}$  to  $-11.6^{\circ}\text{C}$ . Compressive strength varies from 1.7 to 7.1 MPa (Yang et al., 2015; Wilson, 1982).
  - The assumed dry density of frozen silt for this research is considered to be within the range  $320\text{ kg/m}^3$  to  $941\text{ kg/m}^3$  (Yang et al., 2015).
  - The water content varies from 62% to 225% (Yang et al., 2015). However, in the present research, the impact of water content is not considered.

- The frozen silt mat is cost-effective in a hybrid system. Based on the assumed values of major cost drivers, the frozen silt can be a cost-effective solution if the brine chiller is being utilized in two simultaneous projects.

## 6.6. Future Research Recommendations

- This research provides a basis for future research on the practical use of frozen silt mat for crane ground support.
- ANSYS is used to calculate the results and compare them with manual calculations. They can be used to re-check the calculations made by various GBP calculation software available in the market. To make this workable, different crane model are required to be built and investigated using ANSYS or another suitable FEA application.
- The load distribution under the mat is non-uniform in nature. This phenomenon warrants further study to estimate the bending and stability of crane mats (see Figure 94).
- Only a few physical properties are compared. Future research can incorporate additional physical properties.
- Future research can investigate other soil types (sand, clay, loam, chalky soil, etc.) in order to establish an empirical relationship between mat strength, soil composition, water content, and mat temperature.
- The variation of Young's modulus on the strength of frozen silt mat warrants a detailed investigation.
- The dry density of frozen silt varies from 320 kg/m<sup>3</sup> to 940 kg/m<sup>3</sup> (Yang et al., 2015). The impact of density on the strength of mat needs to be investigated.
- The water content varies from 62% to 225% (Yang et al., 2015). The impact of density change on mat strength needs to be investigated.
- Density anomalies of water with respect to ambient temperature are not incorporated in this research. These anomalies and their impact on the strength of an ice/frozen silt mat can be investigated in future research.
- The frozen silt mat is cost-effective with a hybrid system. Based on the assumed values of major cost drivers, the frozen silt can be a cost-effective solution if two locations are operating simultaneously utilizing the same brine chiller (owned/rental). Still, the study is

hypothetical. Real-case scenarios need to be studied in order to ascertain actual cost-effectiveness.

- The use of mesh or reinforced bars to increase the stability and strength of ice/frozen silt mat also needs to be investigated. The same is the case of using pulp contents to increase the modulus of rupture of ice/frozen silt mat (Perutz, 1997).

### **6.7. Value Proposition for Frozen Silt Mat**

Based on the research presented in this thesis, the frozen silt mat can be an environmentally-friendly alternative for crane timber mats suitable for the climate of North America, with good performance with respect to technical and financial industry benchmarks.

## REFERENCES

- AHRI-550/590(I-P)-2015. 2015. "2015 Standard for Performance Rating of Water-chilling and Heat Pump Water-heating Packages Using the Vapor Compression Cycle." *AHRI Standard 550/590 (I-P)*. AHRI.
- Alberta-Government. 2018. *Alberta Major Projects*. Alberta Government. Accessed 05 14, 2018. [http://majorprojects.alberta.ca/#map/?sector=Oil-and-Gas,Pipelines&type=Oil-and-Gas\\_Gas,Oil-and-Gas\\_Oil-Sands:-In-Situ,Oil-and-Gas\\_Oil-Sands:-Mining,Oil-and-Gas\\_Upgrader](http://majorprojects.alberta.ca/#map/?sector=Oil-and-Gas,Pipelines&type=Oil-and-Gas_Gas,Oil-and-Gas_Oil-Sands:-In-Situ,Oil-and-Gas_Oil-Sands:-Mining,Oil-and-Gas_Upgrader).
- Al-Hussein, M., S. Alkass, and O. Moselhi. 2000. "D-CRANE: Database system for utilization of cranes." *Canadian Journal of Civil engineering* 27 (6): 1130-1138. doi:10.1139/cjce-27-6-1130.
- Al-Hussein, M., S. Alkass, and O. Moselhi. 2005. "Optimization algorithm for selection and on site location of mobile cranes." *Journal of Construction Engineering and Management* 131 (5): 579-590.
- Al-Hussein, Mohamed, Muhammad Athar Niaz, H. Yu, and H. Kim. 2005. "Integrating 3D visualization and simulation for tower crane operations on construction sites." *Automation in construction* 15 (5): 554-562.
- Andersland, Orlando B., and Branko Ladanyi. 2004. *Frozen Ground Engineering*. New Jersey: Wiley.
- Anlin, W., D. Tao, D. Yaning, and L. Fei. 2012. "Study on Structural Instability of Large Crawler Crane Boom Structure." *Proceedings of the 2009 3rd International Conference on Teaching and Computational Science (WTCS 2009)*. Berlin: Advances in Intelligent and Soft Computing. 401-406. doi:[https://doi.org/10.1007/978-3-642-11276-8\\_52](https://doi.org/10.1007/978-3-642-11276-8_52).
- AUC. 2018. *Current rates and terms and conditions*. Accessed 05 29, 2018. <http://www.auc.ab.ca/Pages/current-rates-electric.aspx>.
- Badry, Pallavi, and D. Neelima Satyam. 2013. "FINITE ELEMENT MODELLING TO STUDY SOIL STRUCTURE INTERACTION OF ASYMMETRICAL TALL BUILDING."

*TECHNICAL COMMITTEE 207 "SOIL-STRUCTURE INTERACTION AND RETAINING WALLS. 7.*

- Beavers, J. E., J. R. Moore, R. Rinehart, and W. R. Schriver. 2006. "Crane-related fatalities in the construction industry." *J. Constr. Eng. Manage.*, 132(9) 901-910.
- Bejan, A., and P. A. Tyvand. 1992. "The Pressure Melting of Ice Under a Body With Flat Base." *Journal of Heat Transfer* 114 (2): 529-531. doi:doi:10.1115/1.2911310.
- Belal, Adel, Nabil Nagy, and Ahmed Elshesheny. 2015. "Numerical Evaluation of Bearing Capacity of Square Footing on Geosynthetic Reinforced Sand." *International Conference on Civil, Structural and Transportation Engineering*. Ottawa. 143-1-9.
- B-Jahromi, Ali, Bryan Walford, J. Turner, A. M. Harte, Karen Bayne, A. Kermani, and Binsheng Zhang. 2006. "Influence of cross-section on the strength of timber beams." *Proceedings of The Institution of Civil Engineers-structures and Buildings*. Structures & Buildings . 103-114. doi:10.1680/stbu.2006.159.2.103.
- Boyer, Howard E., and Timothy L. Gall. 1985. *Metals Handbook*. OH: American Society for Metals, Materials Park.
- Braun, Bernd, and Alessandro Macchi. 1974. "Ground Freezing techniques at Salerno." *Tunnels and Tunneling Mag.*, March.
- Brischke, Christian, and Linda Meyer-Veltrup. 2015. "Moisture content and decay of differently sized wooden components during 5 years of outdoor exposure." *Eur. J. Wood Prod.* (Springer Berlin Heidelberg) 73 (6): 719–728. doi:https://doi.org/10.1007/s00107-015-0960-7.
- Canada, Government of. 2018. *Canadian Climate Normals*. 01 11. Accessed 2 1, 2018. [http://climate.weather.gc.ca/climate\\_normals/index\\_e.html](http://climate.weather.gc.ca/climate_normals/index_e.html).
- Cauer, W. 1885. "Gefrierverfahren beim Bau eines Tunnels in Stockholm." *Zentralblatt der Bauverwaltung* No51: 537-538.
- CISC. 2017. *Handbook of Steel Construction*. Canadian Institute of Steel Construction, 11th edition. Accessed 03 16, 2018. <http://www.webcivil.com/firmsteelproperty.aspx>.

- Commercial Energy Library. 2018. *Compare - O&M Costs - Chillers*. Accessed 05 29, 2018. <http://c03.apogee.net/contentplayer/?coursetype=ces&utilityid=northwestern&id=19018>.
- Coulton, J. 1974. "Lifting in Early Greek Architecture." *The Journal of Hellenic Studies* 94: 1-19.
- Dewaiker, D. M., and B. G. Mohapatro. 2003. "Computation of Bearing Capacity Factor  $N_{\gamma}$ —Terzaghi's Mechanism." *International Journal of Geomechanics* (American Society of Civil Engineers) 3 (1): 123-128. doi:10.1061/(ASCE)1532-3641(2003)3:1(123).
- Dharwadkar, Parmanand V., Koshy Varghese, James T. O'Connor, and Thomas M. Gatton. 1994. "Graphic Visualization for Planning Heavy Lifts." *3rd Congress on Computing in Civil Engineering*. New York: ASCE. 759-766.
- Dourado, N., M. F. S. F. de Moura, and S. Morel. 2015. "Wood fracture characterization under mode I loading using the three-point bending test. Experimental investigation of *Picea abies* L." *International Journal of Fracture* (Springer Netherlands) 194 (1): 1-9. doi:<https://doi.org/10.1007/s10704-015-0029-y>.
- Drucker, D. C., and W. Prager. 1952. "SOIL MECHANICS AND PLASTIC ANALYSIS OR LIMIT DESIGN." *Quarterly of Applied Mathematics* (Brown University) 10 (2): 157–165.
- Duerr, David. 2010. "Effective Bearing Length of Crane Mats." *Crane & Rigging Conference*. Houston: 2DM Associates, Inc. 1-8.
- DYNALENE. 2018. "Calcium Chloride Series Brine." Dynalene.
- Ekevad, M., P. Jacobsson, and G. Forsberg. 2011. "Slip between Glue-Laminated Beams in Stress-Laminated Timber Bridges: Finite-Element Model and Full-Scale Destructive Test." *Journal Of Bridge Engineering* 16 (2): 188-196. doi:10.1061/(ASCE)BE.1943-5592.0000153.
- Elfass, Sherif, Gary Norris, and Panchaligam Vimalaraj. 2007. "A Simple Bearing Capacity Equation." *Advances in Shallo Foundations*. Denver: Geo-Denver. 10.
- Enersion. 2017. *Cost of the current cooling technology*. Enersion. 04 14. Accessed 3 5, 2018. <http://enersion.com/cost-of-the-current-cooling-technology/#respond>.
- Eslami, A., and M. Gholami. 2005. "Bearing capacity analysis of shallow foundations from CPT data." *Proceedings of the 16th International Conference on Soil Mechanics and*



- Geotechnical Engineering*. Millpress Science Publishers/IOS Press. 1463-66.  
doi:10.3233/978-1-61499-656-9-1463.
- Farouki, Omar. 1986. *Thermal properties of soils*. Clausthal-Zellerfeld, Germany: Trans Tech. .
- FederalMetals. 2018. *Federal Metals in Calgary Sells A53 GR B Schedule 40 Welded Pipe*.  
Accessed 03 05, 2018. <http://www.federalmetals.ca/we-sell/pipe>.
- Gail, C. P. 1972. "TUNNEL DRIVEN USING SUBSURFACE FREEZING." *Civil Engineering*  
(American Society of Civil Engineers) 42 (N5): 37-40.
- Golden Environmental Mat Services, GEMS. 2015. "2014 ACCESS MAT RESEARCH:  
PERSPECTIVES ABOUT THE INDUSTRY AND ASSET TRACKING CONCEPT."  
Calgary.
- Goughnour, Roy R., and O. B. Andersland. 1968. "Mechanical Properties of a Sand-Ice System."  
*Journal of the Soil Mechanics and Foundations Division* 94 (4): 923-950.
- Green, David W., Jerrold E. Winandy, and David E. Kretschmann. 1999. "Mechanical Properties  
of Wood." In *Wood Handbook*, 4.1-45. U.S. Dept. of Agriculture, Forest Service, Forest  
Products Laboratory.
- Grevendonk, W., W. Herreman, and A. De Bock. 1970. "Measurement on the Viscosity of Liquid  
Nitrogen." *Physica* (Elsevier B.V.) 46 (4): 600-604.
- Grove. 2017. *Manitowoc Cranes*. 9 25.  
<https://www.manitowoccranes.com/en/Resources/tools/lift-planning/Outrigger-Pad-Load-Calculators/All-Terrain>.
- Gutkowski, Richard M., and William J. McCutcheon. 1987. "Comparative Performance of Timber  
Bridges." *Journal of Structural Engineering* 113 (7): 1468-1486.  
doi:10.1061/(ASCE)0733-9445(1987)113:7(1468).
- Han, SangHyeok, Ahmed Bouferguene, Mohamed Al-Hussein, and Ulrich (Rick) Herman. 2017.  
"3D-Based Crane Evaluation System for Mobile Crane Operation Selection on Modular-  
Based Heavy Construction Site." *Journal of Construction Engineering and Management*  
143 (9): 04017060, 12 Pages.
- Harris, J. 1995. *Ground Freezing in Practice*. London: Thomas Telford.

- Hasan, Shafiul, Mohamed Al-Hussein, U. H. Hermann, and Hassan Safouhi. 2010. "Interactive and Dynamic Integrated Module for Mobile Cranes Supporting System Design." *JOURNAL OF CONSTRUCTION ENGINEERING AND MANAGEMENT* 136 (2): 179-186. doi:10.1061/(ASCE)CO.1943-7862.0000121.
- Haynes, F. Donald, Charles M. Collins, and Walter W. Olson. 1992. *Bearing Capacity Tests on Ice Reinforced with Geogrid*. US Army Corps of Engineers, Cold Regions Research & Engineering Laboratory.
- Herbert, John A. 2009. *A Systems Approach for Total Cooling Design*. 03 09. Accessed 3 5, 2018. <http://www.johnherbert.hk/2009/03/09/system-cooling-design/>.
- Hindman, Daniel P., and Jong Nam Lee. 2007. "MODELING WOOD STRANDS AS MULTI-LAYER COMPOSITES: BENDING AND TENSION LOADS." *Wood and Fiber Science (The Society of Wood Science and Technology)* 39 (4): 516-526.
- Hornaday, W. C., C. T. Haas, J. T. O'Connor, and J. Wen. 1993. "Computer-Aided Planning for Heavy Lifts." *Journal of Construction Engineering and Management* 119 (3): 498-515.
- Howard, Isaac L., Chris L. Saucier, and Rubin Shmulsky. 2008. "Testing of Instrumented Construction Mats and Billets." *GeoCongress 2008: Characterization, Monitoring, and Modeling of GeoSystems*. 340-347. doi:10.1061/40972(311)43.
- Hu, Jun, Yong Liu, Hong Wei, and Wei Wang. 2017. "Finite-Element Analysis of Heat Transfer of Horizontal." *International Journal of Geomechanics (American Society of Civil Engineers)* 17 (10): 04017080.1-. doi:10.1061/(ASCE)GM.1943-5622.0000978.
- Hu, Xiangdong, and Shengjun Deng. 2016. "Ground freezing application of intake installing construction of an underwater tunnel." *Procedia Engineering*. 633-640.
- Implenia. 2017. "Ground Freezing." *Implenia Spezialtiefbau GmbH*. 3 3. [http://www.spezialtiefbau.implenia.com/fileadmin/con-spezialtiefbau/prospekte/englisch/Ground\\_Freezing.pdf](http://www.spezialtiefbau.implenia.com/fileadmin/con-spezialtiefbau/prospekte/englisch/Ground_Freezing.pdf).
- ISO. 1991. "Mobile crane - determination of stability. ISO4305:1991(E)." *International Organization for Standardization*. Geneva, Switzerland.

- Itterbeek, A. Van, and O. Verbeke. 1960. "Density of liquid nitrogen and argon as a function of pressure and temperature." *Physica* (Elsevier B.V.) 26 (11): 931-938.
- Jan, David. 2018. *Western Coal re-opens Willow Creek mine*. Accessed 03 12, 2018. <https://www.newswire.ca/news-releases/western-coal-re-opens-willow-creek-mine-544088022.html>.
- Jensen, J. E., W. A. Tuttle, R. B. Stewart, H. Brechna, and A. G. Prodell. 1980. *VI - Properties of Nitrogen*. Vol. 1, in *BROOKHAVEN NATIONAL LABORATORY SELECTED CRYOGENIC DATA NOTEBOOK*, by J. E. Jensen, W. A. Tuttle, R. B. Stewart, H. Brechna and A. G. Prodell, 45. New York: Brookhaven National Laboratory.
- Jessberger, H. L., and S. S. Vyalov. 1979. *General Report Session III: Engineering*. General Report, Amsterdam: Elsevier Scientific Publishing Company, 19-27.
- Jones, J. S. 1981. "State-of-the-art report - engineering practice in artificial ground freezing." *Engineering Geology* (Elsevier Scientific Publishing) 18 (1-4): 313-326.
- Kim, Young Seok, Jae-Mo Kang, Janguen Lee, Sung-Seo Hong, and Kwang-Jim Kim. 2012. "Finite Element Modeling and Analysis for Artificial Ground Freezing in Egress Shafts." *KSCE Journal of Civil Engineering* (Korean Society of Civil Engineers) 16 (6): 925-932. doi:10.1007/s12205-012-1252-y.
- Kováčiková, J., M. Ekevad, S. Berg, and O. Ivánková. 2016. "Finite element analysis of timber beams with flaws." *ECCOMAS Congress 2016 - Proceedings of the 7th European Congress on Computational Methods in Applied Sciences and Engineering*. (ECCOMAS Congress 2016 - Proceedings of the 7th European Congress on Computational Methods in Applied Sciences and Engineering, . Crete Island: National Technical University of Athens. 8606-8611. doi:10.7712/100016.2436.6566.
- Kretschmann, David. E. 2010. "Mechanical Properties of Wood, Chapter-5." In *Wood Handbook*, 5.1-46. U.S. Dept. of Agriculture, Forest Service, Forest Products Laboratory.
- Kudryavtsev, S. A. 2003. "Numerical investigations of thermophysical processes in seasonally frozen soils." *Kriosfera Zemli* 7 (4): 76-81.

- Kudryavtsev, S. A. 2004. "Numerical Modeling of The Freezing, Frost Heaving, And Thawing of Soils." *Soil Mechanics and Foundation Engineering* (Kluwer Academic Publishers-Consultants Bureau) 41 (5): 177-184. doi:<https://doi.org/10.1007/s11204-005-0005-z>.
- Kumbhojkar, A. S. 1993. "Numerical Evaluation of Terzaghi's Nγ." *Journal of Geotechnical Engineering* (American Society of Civil Engineers) 119 (3): 598-607. doi:10.1061/(ASCE)0733-9410(1993)119:3(598).
- Leung, Chris K. W., Ruppert K. Y. Leung, Anson K. K. Cheung, and W. L. Chan. 2012. "APPLICATION OF ARTIFICIAL GROUND FREEZING METHOD FOR TUNNEL CONSTRUCTION IN HONG KONG – A CONSTRUCTION CASE IN HARBOUR AREA TREATMENT SCHEME STAGE 2A." *Innovation and Creativity of infrastructure Developments for Quality Cities*. Hong Kong: Civil Division International Conference 2012. 1-12.
- liftinglogistics.com. 2017. *Ground Bearing Pressure Calculator*. Accessed 12 10, 2017. <http://liftinglogistics.com/gbp>.
- Lin, Kuo-Liang, and Carl T. Haas. 1996. "Multiple Heavy Lifts Optimization." *Journal of Construction Engineering and management* 122 (4): 354-362.
- Lin, Meng, Nguyet (Lisa) Duong, Lijun Deng, Ulrich (Rick) Hermann, Travis Zubick, Zhen Lei, and Samer Adeeb. 2017. "AN INVESTIGATION OF THE DISTRIBUTION OF MOBILE CRANE LOADS FOR CONSTRUCTION PROJECTS." *CSCE Leadership in Sustainable Infrastructure*. Vancouver. 10.
- Liu, Xiteng, Dave H. Chan, and Brian Gerbrandt. 2008. "Bearing capacity of soils for crawler crane." *Canadian Geotechnical Journal* 1282-1302.
- Madenci, Erdogan, and Ibrahim Guven. 2015. *The Finite Element Methods and Applications in Engineering Using ANSYS - 2nd Edition*. New York: Springer International Publishing. doi:0.1007/978-1-4899-7550-8\_1.
- Mahamid, Mustafa, Tom Brindley, Nicholas Triandafilou, and Slawomir Domagala. 2017. "Behavior and Strength Characteristics of Cross-Laminated Timber Mats: Experimental and Numerical Study ." *Structures Congress* 254-268.

- Mall, S. 1984. "The Fracture Toughness of Wood Under Impact Loading." *International Conference on Fracture*. New Delhi. 2881-2887. doi:<https://doi.org/10.1016/B978-1-4832-8440-8.50305-7>.
- Manitowoc. 2017. *Manitowoc Cranes*. 09 22. <https://www.manitowoccranes.com/en/Resources/tools/lift-planning/ground-bearing-pressure>.
- Mats, Quality. 2017. *Crane Mats*. 01 26. Accessed 12 10, 2017. <http://www.qmat.com/products/crane-mats/>.
- McNutt, Kristen. 1991. "SWOT Before you start." *Nutrition Today* 48-51.
- MEADinfo. 2015. *Material Properties of S355 Steel - An Overview*. 08 23. Accessed 03 16, 2018. <http://www.meadinfo.org/2015/08/s355-steel-properties.html>.
- Miniat, Bill. 2017. *Construction Business Owner*. 02 21. <http://www.constructionbusinessowner.com/safety/safety/january-2017-strategies-conquer-poor-ground-conditions>.
- Moretrench. 2018. *Ground Freezing Brochure*. 05 11. Accessed 05 11, 2018. <http://www.moretrench.com/brochures/>.
- Morrison, Jessica. 2013. *How Engineers Use Ground Freezing to Build Bigger, Safer, and Deeper*. 10 30. Accessed 03 07, 2018. <http://www.pbs.org/wgbh/nova/next/tech/artificial-ground-freezing/>.
- NDS. 2018. "National Design Specification for Wood Construction." Lessburg, VA: American Wood Council.
- Newman, Greg, Lori Newman, Denise Chapman, and Travis Harbicht. 2011. "Artificial Ground Freezing: An Environmental Best Practice at Cameco's Uranium Mining Operations in Northern Saskatchewan, Canada." *Rüde, Freund # Wolkersdorfer (Editors) (IMWA)* 113-118.
- Olearczyk, J., Z. Lei, B. Ofrim, S. Han, and M. Al-Hussein. 2015. "Intelligent Crane Management Algorithm for Construction Operation (iCrane)." *32nd International Symposium on Automation and Robotics in Construction*. Oulu, Finland. 8.

- OXYChem. 2018. "Calcium Chloride - A Guide to Physical Properties." OXYChem Publisher.
- Padilla, Francisco, and Jean-Pierre Villeneuve. 1992. "Modeling and experimental studies of frost heave including solute effects." *Cold Regions Science and Technology* (Elsevier Science Publishers B.V.) 20 (2): 183-194.
- Padilla, Francisco, Jean-Pierre Villeneuve, and Jean Stein. 1997. "Simulation and analysis of frost heaving in subsoils and granular fills of roads." *Cold Regions Science and Technology* (Elsevier Science B.V.) 25 (2): 89-99.
- Papakonstantinou, S., G. Anagnostou, and E. Pimentel. 2013. "Evaluation of ground freezing data from the Naples subway." *Proceedings of the ICE - Geotechnical Engineering* (Thomas Telford Services Ltd) 166 (3): 280-298. doi:10.1680/geng.10.00099.
- Pembina. 2017. *Pembina Pipeline Corporation Approves New Capital Projects and Announces 2018 Capital Program*. 11 29. Accessed 03 12, 2018. <http://www.pembina.com/media-centre/news-releases/news-details/?nid=135383>.
- Perutz, Max. F. 1997. *Science is not a quiet life : unravelling the atomic mechanism of haemoglobin*. Singapore: World Scientific Pub. Co.
- Petrovic, J. J. 2003. "Review Mechanical properties of ice and snow." *JOURNAL OF MATERIALS SCIENCE* (Kluwer Academic Publishers) 38 (1): 1-6. doi:<https://doi.org/10.1023/A:1021134128038>.
- Powers, Patrick J., Arthur B. Corwin, Paul C. Schmall, and Walter E Kaeck. 2007. *Construction Dewatering and Groundwater Control: New Methods and Applications*. 3. Hoboken, NJ: John Wiley & Sons. Inc. doi:10.1002/9780470168103.
- Qiyu, Li, Qin Yixiao, and Ming Yang. 2016. "Stability of Crane's Lifting Drum with Euler Distribution Forces." *International Journal of Mechanical Engineering and Applications* 4 (5): 176-181. doi:10.11648/j.ijmea.20160405.12 .
- RioTinto. 2018. *About Diavik*. Accessed 03 12, 2018. <http://www.riotinto.com/canada/diavik-2232.aspx>.

- Rodriguez-Ramos, Walter, and Richard L. Francis. 1983. "Single Crane Location Optimization." *Journal of Construction Engineering and Management* (American Society of Civil Engineers) 109 (4): 387-397.
- Sanger, F. J., and F. H. Sayles. 1979. "Thermal and Rheological Computations for Artificially Frozen Ground Construction." *Engineering Geology* (Elsevier Scientific Publishing Company) 13: 311-337.
- Schiewind, A. P., and R. A. Poznaik. 1971. "On the fracture toughness of Douglass-Fir wood." *Engineering Fracture Mechanics* 2 (3): 223-233. doi:[https://doi.org/10.1016/0013-7944\(71\)90026-9](https://doi.org/10.1016/0013-7944(71)90026-9).
- Schulson, Erland M. 1999. "The Structure and Mechanical Behavior of Ice." *JOM* (Springer-Verlag) 51 (2): 21-27. doi:<https://doi.org/10.1007/s11837-999-0206-4>.
- Sego, D. C., P. K. Robertson, S. Sasitharan, B. L. Kilpatrick, and V. S. Pillai. 1994. "Ground freezing and sampling of foundation soils at Duncan Dam." *Canadian Geotechnical Journal* 31 (6): 939-950.
- Selvadurai, A. P. S., J. Hu, and I. Konuk. 1999. "Computational modelling of frost heave induced soil–pipeline interaction: I. Modelling of frost heave." *Cold Regions Science and Technology* (Elsevier Science B.V. ) 29 (3). doi:[https://doi.org/10.1016/S0165-232X\(99\)00028-2](https://doi.org/10.1016/S0165-232X(99)00028-2).
- Shapiro, Lawrence K., and Jay P. Shapiro. 2011. *Cranes and Derricks*. New York: McGraw Hill.
- Singh, N. K., E. Cadoni, M. K. Singha, and N. K. Gupta. 2013. "Dynamic Tensile and Compressive Behaviors of Mild Steel at Wide Range of Strain Rates." *JOURNAL OF ENGINEERING MECHANICS* (ASCE) 139 (9): 1197-1206. doi:10.1061/(ASCE)EM.1943-7889.0000557.
- Song, Haiqing, Haibing Cai, Zhishu Yao, Chuanxin Rong, and Xiaojian Wang. 2016. "Finite element analysis on 3D freezing temperature field in metro cross passage construction." *15th International scientific conference "Underground Urbanisation as a Prerequisite for Sustainable Development"*. *Procedia Engineering* . 528-539. doi:10.1016/j.proeng.2016.11.729 .

- Stoss, K., and J. Valk. 1973. "Uses and Limitations of Ground Freezing with Liquid Nitrogen." *Elsevier Scientific Publishing Company* 485-494.
- Stueland, S. 1994. "The Otis Steam Excavator." *Technology and Culture* 35 (3): 571-574.
- Taborda, Joana. 2018. *Canada Inflation Rate*. 05 18. Accessed 05 29, 2018. <https://tradingeconomics.com/canada/inflation-cpi>.
- Tang, S. L., Irtishad U. Ahmad, Syed M. Ahmed, and Ming Lu. 2004. *Quantitative Techniques for Decision Making in Construction*. Hong Kong: Hong Kong University Press.
- Taylor, S. E., K. P. Keliher, J. D. Thompson, M. A. Ritter, and G. L. Murphy. 1995. "Portable Glulam Timber Bridge Design for Low-Volume Forest Roads." *Proceedings of the 6th International conference on low-volume roads*. Minneapolis: National Academy. 328-338.
- Terratest. 2018. *Ground Freezing*. Accessed 1 30, 2018. <http://www.terratest.com/ingles/products-ground-freezing.html>.
- Terzaghi, K. 1943. *Theoretical Soil Mechanics*. New York: John Wiley & Sons. doi:<http://dx.doi.org/10.1002/9780470172766>.
- The Engineering Toolbox. 2018. *Emissivity Coefficients of some common Materials*. Accessed 5 2, 2018. [https://www.engineeringtoolbox.com/emissivity-coefficients-d\\_447.html](https://www.engineeringtoolbox.com/emissivity-coefficients-d_447.html).
- . 2017. *Modulus of Rigidity of some Common Materials*. Accessed 12 5, 2017. [http://www.engineeringtoolbox.com/modulus-rigidity-d\\_946.html](http://www.engineeringtoolbox.com/modulus-rigidity-d_946.html).
- The-Canadian-Press. 2016. *Second coal mine to reopen in northeastern B.C.* December 29. Accessed 03 12, 2018. <http://vancouver.sun.com/news/local-news/second-coal-mine-to-reopen-in-northeastern-b-c>.
- Trane. 2012. *Price List*. 02 14. Accessed 05 29, 2018. <https://procure.ohio.gov/pricelist/800195revpricelist.pdf>.
- Turner, M. J., R. W. Clough, H. C. Martin, and L. J. Topp. 1956. "Stiffness and Deflection Analysis of Complex Structures." *Journal of Aeronautical Sciences* (Journal of Aeronautical Sciences) 23 (9). doi:10.2514/8.3664.



- U of T. 2018. *Liquid Nitrogen (LN2), 1L*. Accessed 03 05, 2018. [https://www.uoftmedstore.com/item\\_detail.sz?id=328&parent=12317](https://www.uoftmedstore.com/item_detail.sz?id=328&parent=12317).
- Wenyuan, Meng, and Guo Yingkui. 2015. "Experimental Study on Mechanical Properties of Ice." *AASRI International Conference on Industrial Electronics and Applications*. Atlantis Press. 192-196. doi:doi:10.2991/iea-15.2015.47.
- Wilson, Charles Ralph. 1982. "Dynamic Properties of Naturally Frozen Fairbanks Silt." *Master of Science Thesis in Civil Engineering*. Corvallis: Oregon State University, April 22.
- Wind, H. 1979. "The soil-freezing method for large tunnel constructions." *Engineering Geology* (Elsevier Scientific Publishing Company) 13 (1-4): 417-423.
- Wu, Di, Xin Wang, Yuanshan Lin, and Xiukun Wang. 2008. "Design and realization of crawler crane's lift simulation system." *ASME 2008 International Design Engineering Technical Conference & Computers and Information in Engineering Conference*. New York: ASME. 1-9. doi:10.1115/DETC2008-49581.
- Wu, Di, Yuanshan Lin, Xin Wang, Xiukun Wang, and Shunde Gao. 2011. "Algorithm of Crane Selection for Heavy Lifts." *JOURNAL OF COMPUTING IN CIVIL ENGINEERING* 25 (1): 57-65.
- Yang, Xiujuan, Zongxiang Xiu, Lisong Zhang, and Xiangzhen Yan. 2010. "3D simulation of weak foundation for good-sized oil storage tank." Wuhan. 1345-1348. doi:10.1109/MACE.2010.5536276.
- Yang, Z., Z. Jianzhi, and Y. Junjun. 2011. "Static structural finite-element analysis of tower crane based on FEM." *2011 IEEE 2nd International Conference on Computing, Control and Industrial Engineering*. Wuhan. 220-223. doi:10.1109/CCIENG.2011.6008106.
- Yang, Zhaohui (Joey), Benjamin Still, and Ziaoxuan Ge. 2015. "Mechanical properties of seasonally frozen and permafrost soils at high strain rate." *Cold Region Science and Technology* 113: 12-19. doi:doi.org/10.1016/j.coldregions.2015.02.008.
- Zaretsky, A. A., and H. I. Shapiro. 1997. "Overturning stability of a free standing crane under dynamic loading." *SAE Technical Paper Series, Society of Automotive Engineers* 972721: 1-9.

- Zhang, Helen, David Jin, and X. J. Zaho. 2013. "Analysis of Nonlinear Local Buckling of Crane Telescopic Boom." *Applied Mechanics and Materials* 387: 197-201. doi:10.4028/www.scientific.net/AMM.387.197.
- Zhao, Jiong, Qicai Zhou, Wenjun Li, and Zailei Zhou. 2015. "Lightweight Design for the Combinatorial Jib." *Proceedings of China Modern Logistics Engineering*. Springer-Verlag Berlin Heidelberg. 179-188. doi: DOI 10.1007/978-3-662-44674-4\_17.
- Zhao, Qi. 2011. "Cause Analysis of U.S. Crane-related Accidents (Master's Thesis)." Retrieved from <http://ufdc.ufl.edu/UFE0042972/00001>.
- Zhao, Qiong, and Shui-guang Tong. 2010. "Knowledge-based FEA system for combinatorial jib of portal crane." *The 2Nd International Conference On Information Science And Engineering, Information Science And Engineering (ICISE)*. 5147. doi:10.1109/ICISE.2010.5691317.
- Zhiyong, Cai, and J. Robert. 2010. "Mechanical Properties of Wood-Based Composite Materials." Chap. 12 in *Wood handbook*, 12.1-12.12. WI: U.S. Dept. of Agriculture, Forest Service, Forest Products Laboratory.
- Zimnisky, Paul. 2013. *The state of 2013 global rough diamond supply*. January 22. Accessed 03 12, 2018. <http://www.resourceinvestor.com/2013/01/22/the-state-of-2013-global-rough-diamond-supply>.

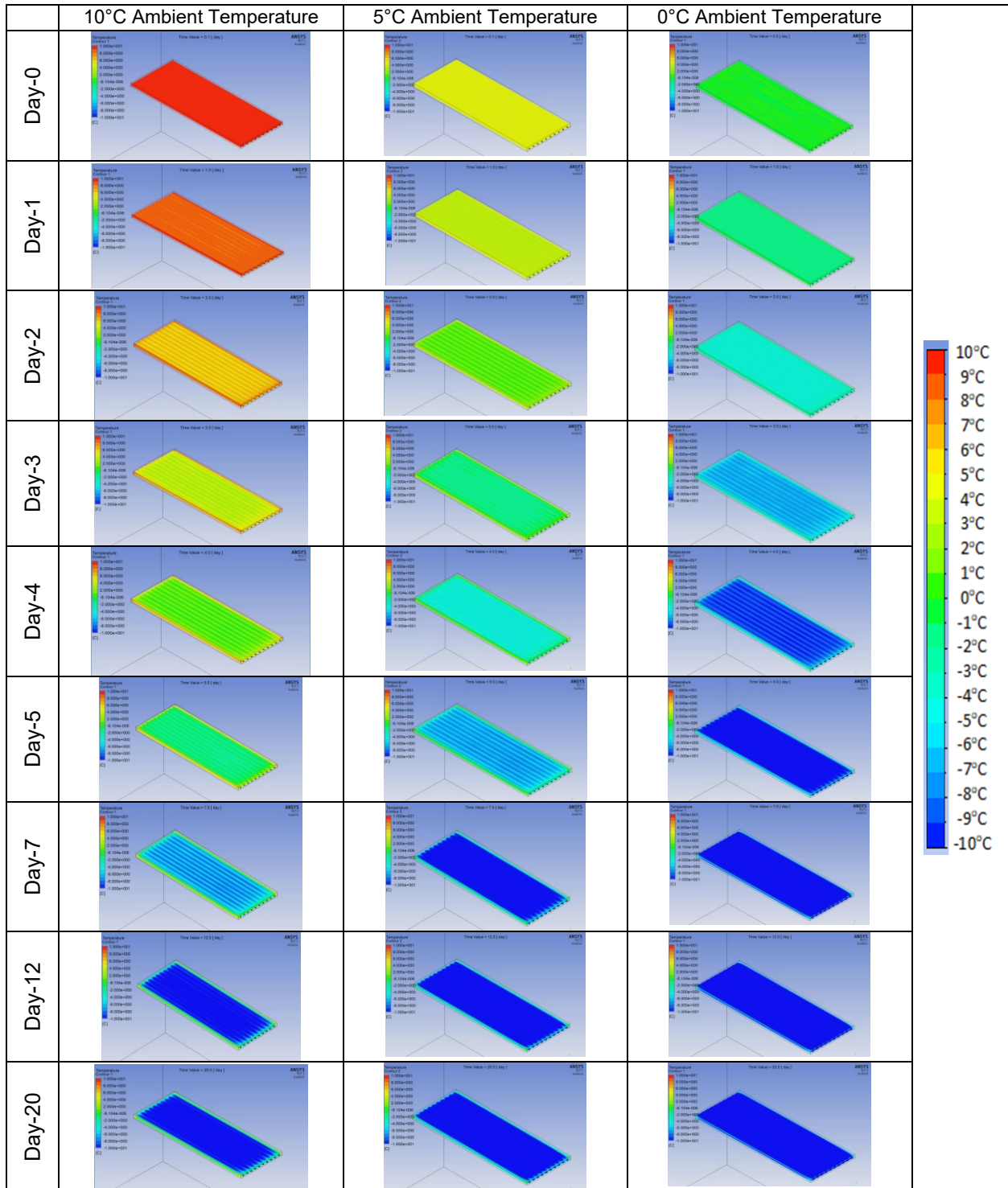
**Appendix A - Minimum Normal Stress Values for different mat materials Crawler Crane along boom rotation (0° to 90° from Front to Left Rear)**

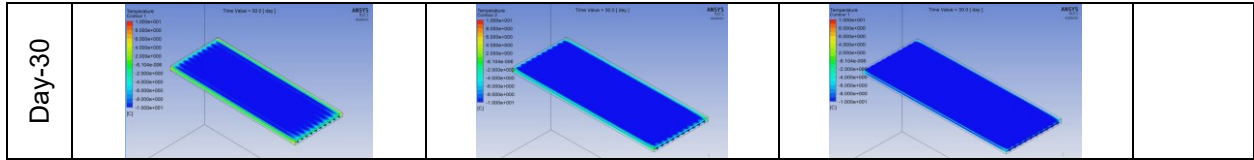
Boo m Slew Ang le	Normal Stress (Pa)									
	S355 Left Front	S355 Left Rear	G40.21 Left Front	G40.21 Left Rear	Coastal Douglas- Fir Left Front	Coastal Douglas- Fir Left Rear	Ice (0.8 m) Left Front	Ice (0.8 m) Left Rear	Frozen Silt Left Front	Frozen Silt Left Rear
0	-1.78E+05	-1.11E+05	-1.77E+05	-1.11E+05	-2.38E+05	-1.61E+05	-1.71E+05	-8.13E+04	-2.58E+05	-1.42E+05
3	-1.80E+05	-1.12E+05	-1.79E+05	-1.12E+05	-2.39E+05	-1.64E+05	-1.73E+05	-8.26E+04	-2.60E+05	-1.44E+05
6	-1.81E+05	-1.13E+05	-1.80E+05	-1.13E+05	-2.40E+05	-1.67E+05	-1.74E+05	-8.40E+04	-2.61E+05	-1.47E+05
9	-1.82E+05	-1.15E+05	-1.82E+05	-1.15E+05	-2.41E+05	-1.71E+05	-1.74E+05	-8.56E+04	-2.63E+05	-1.50E+05
12	-1.84E+05	-1.16E+05	-1.83E+05	-1.16E+05	-2.42E+05	-1.74E+05	-1.75E+05	-8.74E+04	-2.64E+05	-1.53E+05
15	-1.85E+05	-1.17E+05	-1.84E+05	-1.18E+05	-2.43E+05	-1.78E+05	-1.76E+05	-8.93E+04	-2.65E+05	-1.57E+05
18	-1.86E+05	-1.19E+05	-1.85E+05	-1.19E+05	-2.44E+05	-1.82E+05	-1.76E+05	-9.14E+04	-2.66E+05	-1.61E+05
21	-1.87E+05	-1.21E+05	-1.86E+05	-1.21E+05	-2.45E+05	-1.86E+05	-1.76E+05	-9.36E+04	-2.67E+05	-1.65E+05
24	-1.87E+05	-1.22E+05	-1.87E+05	-1.22E+05	-2.45E+05	-1.91E+05	-1.76E+05	-9.60E+04	-2.67E+05	-1.69E+05
27	-1.88E+05	-1.24E+05	-1.87E+05	-1.24E+05	-2.46E+05	-1.95E+05	-1.76E+05	-9.86E+04	-2.68E+05	-1.73E+05
30	-1.88E+05	-1.26E+05	-1.88E+05	-1.26E+05	-2.46E+05	-2.00E+05	-1.76E+05	-1.01E+05	-2.68E+05	-1.77E+05
33	-1.89E+05	-1.28E+05	-1.88E+05	-1.28E+05	-2.46E+05	-2.04E+05	-1.75E+05	-1.04E+05	-2.68E+05	-1.82E+05
36	-1.89E+05	-1.30E+05	-1.88E+05	-1.30E+05	-2.46E+05	-2.09E+05	-1.75E+05	-1.07E+05	-2.68E+05	-1.86E+05
39	-1.89E+05	-1.32E+05	-1.88E+05	-1.32E+05	-2.46E+05	-2.14E+05	-1.74E+05	-1.10E+05	-2.67E+05	-1.91E+05
42	-1.89E+05	-1.34E+05	-1.88E+05	-1.34E+05	-2.46E+05	-2.19E+05	-1.73E+05	-1.13E+05	-2.67E+05	-1.96E+05
45	-1.88E+05	-1.36E+05	-1.88E+05	-1.36E+05	-2.45E+05	-2.24E+05	-1.72E+05	-1.16E+05	-2.66E+05	-2.01E+05
48	-1.88E+05	-1.38E+05	-1.87E+05	-1.38E+05	-2.44E+05	-2.29E+05	-1.71E+05	-1.20E+05	-2.65E+05	-2.06E+05
51	-1.88E+05	-1.40E+05	-1.87E+05	-1.40E+05	-2.42E+05	-2.34E+05	-1.69E+05	-1.23E+05	-2.64E+05	-2.11E+05
54	-1.87E+05	-1.42E+05	-1.86E+05	-1.42E+05	-2.40E+05	-2.39E+05	-1.68E+05	-1.27E+05	-2.62E+05	-2.16E+05
57	-1.86E+05	-1.44E+05	-1.85E+05	-1.44E+05	-2.38E+05	-2.44E+05	-1.66E+05	-1.30E+05	-2.60E+05	-2.21E+05
60	-1.85E+05	-1.47E+05	-1.85E+05	-1.46E+05	-2.36E+05	-2.50E+05	-1.64E+05	-1.34E+05	-2.58E+05	-2.26E+05
63	-1.84E+05	-1.49E+05	-1.83E+05	-1.49E+05	-2.33E+05	-2.54E+05	-1.62E+05	-1.38E+05	-2.56E+05	-2.31E+05
66	-1.83E+05	-1.52E+05	-1.82E+05	-1.51E+05	-2.29E+05	-2.60E+05	-1.60E+05	-1.41E+05	-2.54E+05	-2.37E+05
69	-1.82E+05	-1.54E+05	-1.81E+05	-1.54E+05	-2.26E+05	-2.65E+05	-1.58E+05	-1.45E+05	-2.51E+05	-2.42E+05
72	-1.80E+05	-1.57E+05	-1.80E+05	-1.56E+05	-2.22E+05	-2.70E+05	-1.56E+05	-1.49E+05	-2.48E+05	-2.47E+05
75	-1.79E+05	-1.59E+05	-1.78E+05	-1.59E+05	-2.19E+05	-2.75E+05	-1.54E+05	-1.53E+05	-2.45E+05	-2.52E+05
78	-1.77E+05	-1.62E+05	-1.76E+05	-1.61E+05	-2.15E+05	-2.80E+05	-1.51E+05	-1.56E+05	-2.42E+05	-2.57E+05
81	-1.75E+05	-1.64E+05	-1.75E+05	-1.64E+05	-2.11E+05	-2.85E+05	-1.48E+05	-1.60E+05	-2.39E+05	-2.62E+05
84	-1.74E+05	-1.66E+05	-1.73E+05	-1.66E+05	-2.07E+05	-2.89E+05	-1.46E+05	-1.64E+05	-2.35E+05	-2.67E+05
87	-1.72E+05	-1.68E+05	-1.71E+05	-1.68E+05	-2.03E+05	-2.94E+05	-1.43E+05	-1.67E+05	-2.32E+05	-2.72E+05
90	-1.70E+05	-1.71E+05	-1.69E+05	-1.70E+05	-1.98E+05	-2.99E+05	-1.40E+05	-1.71E+05	-2.28E+05	-2.77E+05

**Appendix B - Minimum Normal Stress Values for different mat materials under Hydraulic Crane along boom rotation (0° to 90° from Rear to Right Front)**

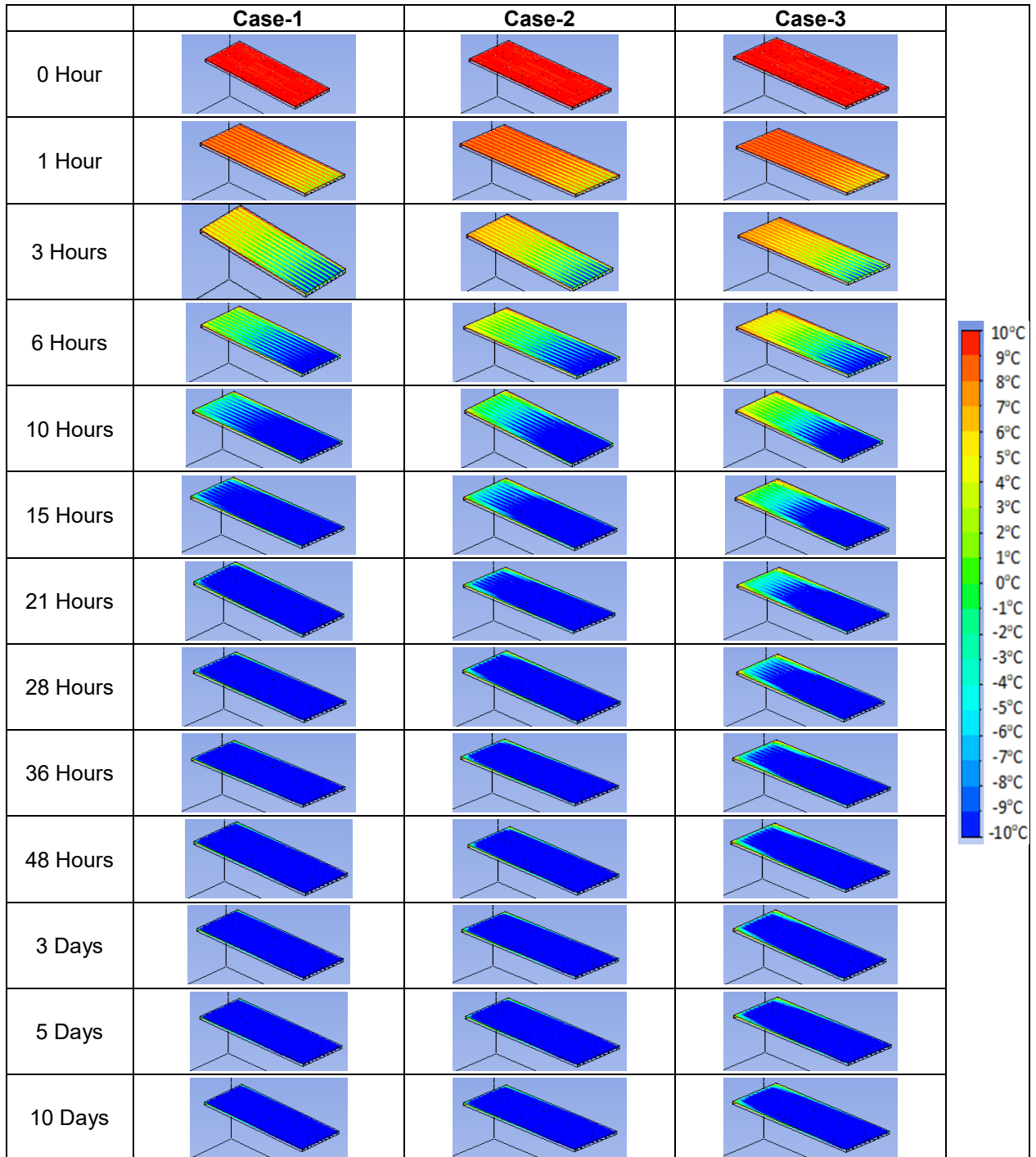
Boom Slew Angle	Normal Stress (Pa)									
	S355 Right Rear	S355 Right Front	G40.21 Right Rear	G40.21 Right Front	Coastal Douglas-Fir Right Rear	Coastal Douglas-Fir Right Front	Ice (1.3 m) Right Rear	Ice (1.3 m) Right Front	Frozen Silt Right Rear	Frozen Silt Right Front
0	-7.57E+04	-4.00E+04	-7.68E+04	-4.05E+04	-2.49E+05	-8.58E+04	-1.91E+05	-8.53E+04	-1.75E+05	-7.69E+04
15	-8.18E+04	-4.78E+04	-8.30E+04	-4.85E+04	-2.73E+05	-1.09E+05	-2.06E+05	-9.78E+04	-1.82E+05	-8.32E+04
30	-8.55E+04	-5.66E+04	-8.68E+04	-5.74E+04	-2.92E+05	-1.39E+05	-2.17E+05	-1.13E+05	-1.95E+05	-9.85E+04
45	-8.66E+04	-6.53E+04	-8.79E+04	-6.77E+04	-3.01E+05	-1.62E+05	-2.20E+05	-1.32E+05	-2.05E+05	-1.21E+05
60	-8.55E+04	-7.21E+04	-8.58E+04	-7.56E+04	-3.03E+05	-1.90E+05	-2.18E+05	-1.51E+05	-2.06E+05	-1.30E+05
75	-8.32E+04	-7.68E+04	-8.38E+04	-7.89E+04	-3.00E+05	-2.22E+05	-2.09E+05	-1.71E+05	-2.04E+05	-1.55E+05
90	-8.08E+04	-7.98E+04	-8.20E+04	-8.10E+04	-2.92E+05	-2.48E+05	-1.94E+05	-1.89E+05	-1.93E+05	-1.79E+05

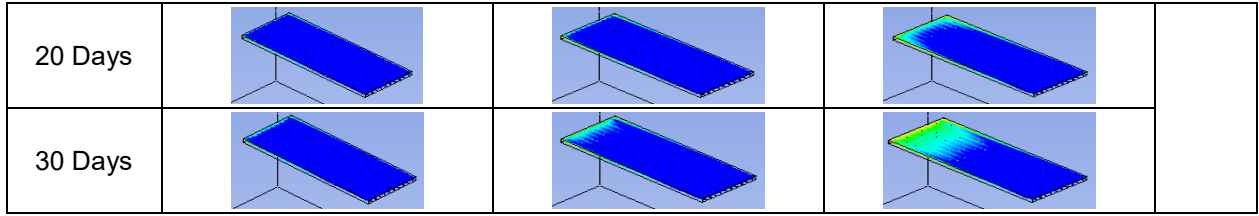
## Appendix C – Graphical Representation of Frozen Silt Mat freezing using Brine (30 days)



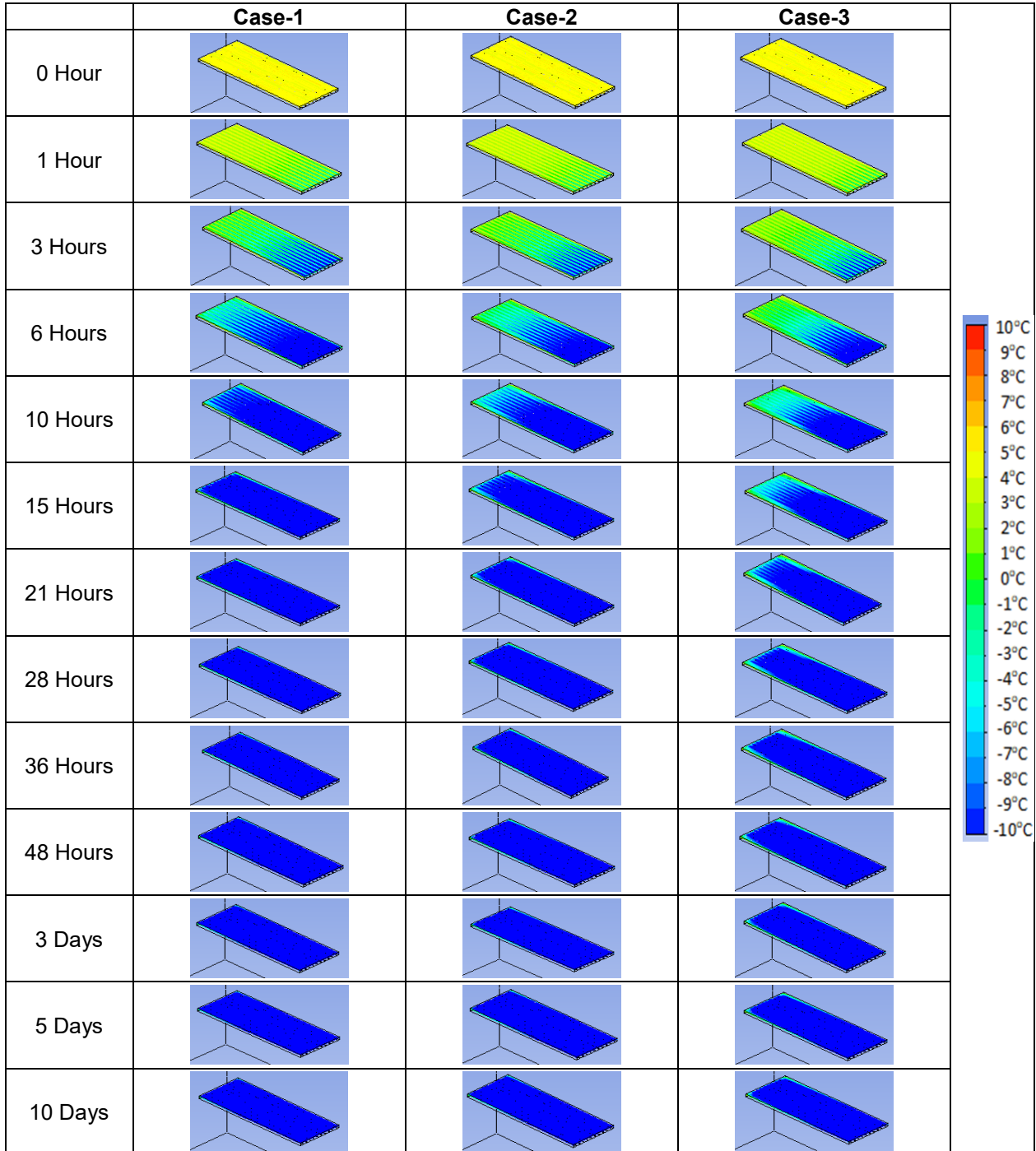


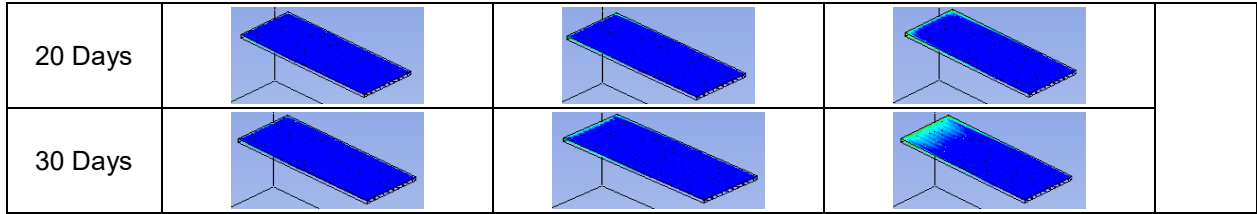
**Appendix D - Frozen Silt Mat (Liquid Nitrogen at 10°C Ambient Temperature, 30 days).**



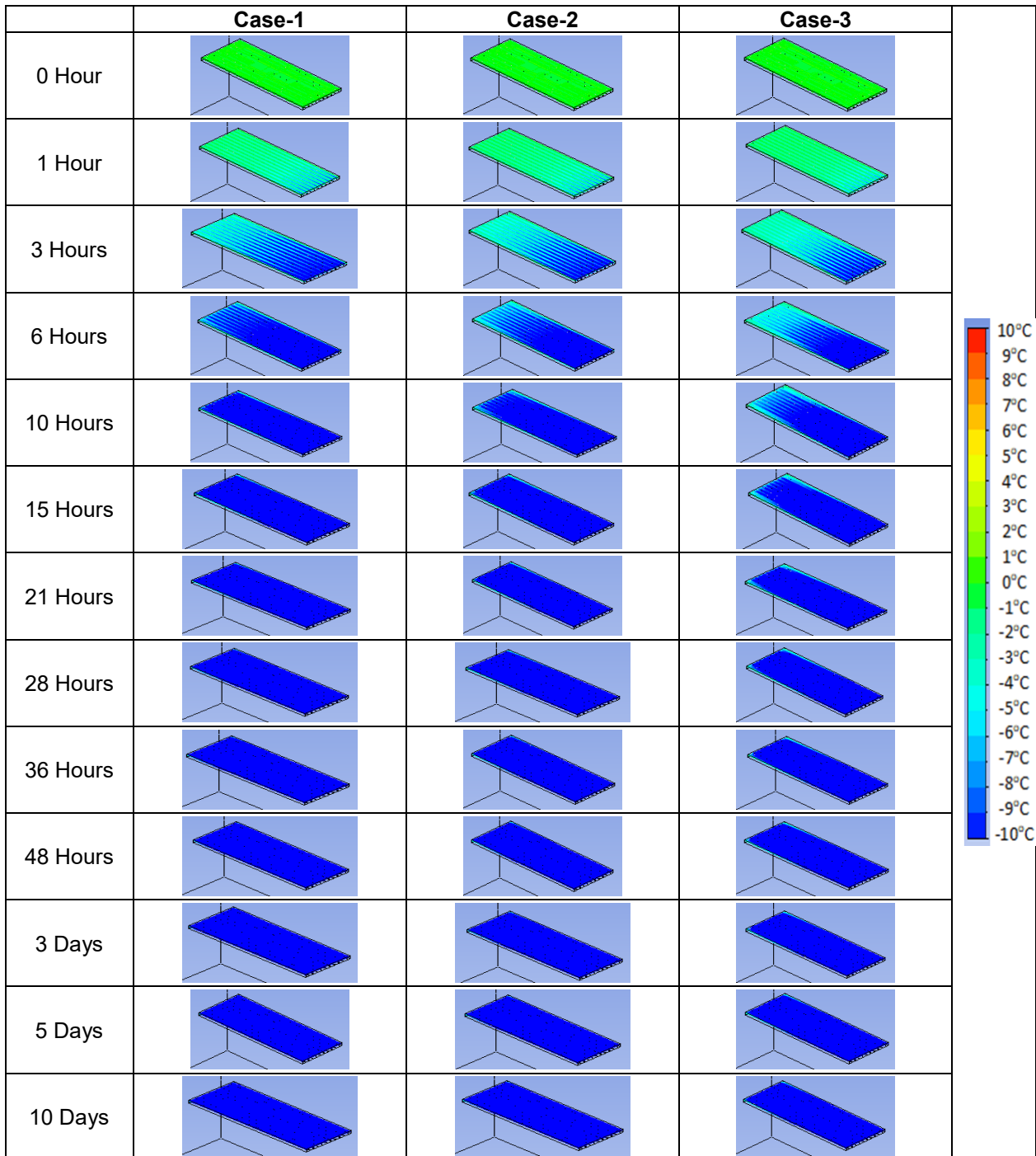


**Appendix E - Frozen Silt Mat (Liquid Nitrogen at 5°C Ambient Temperature, 30 days).**

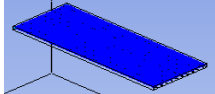
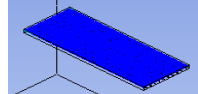
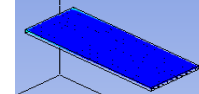
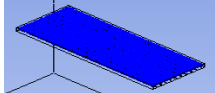
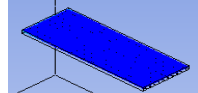
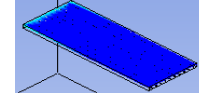




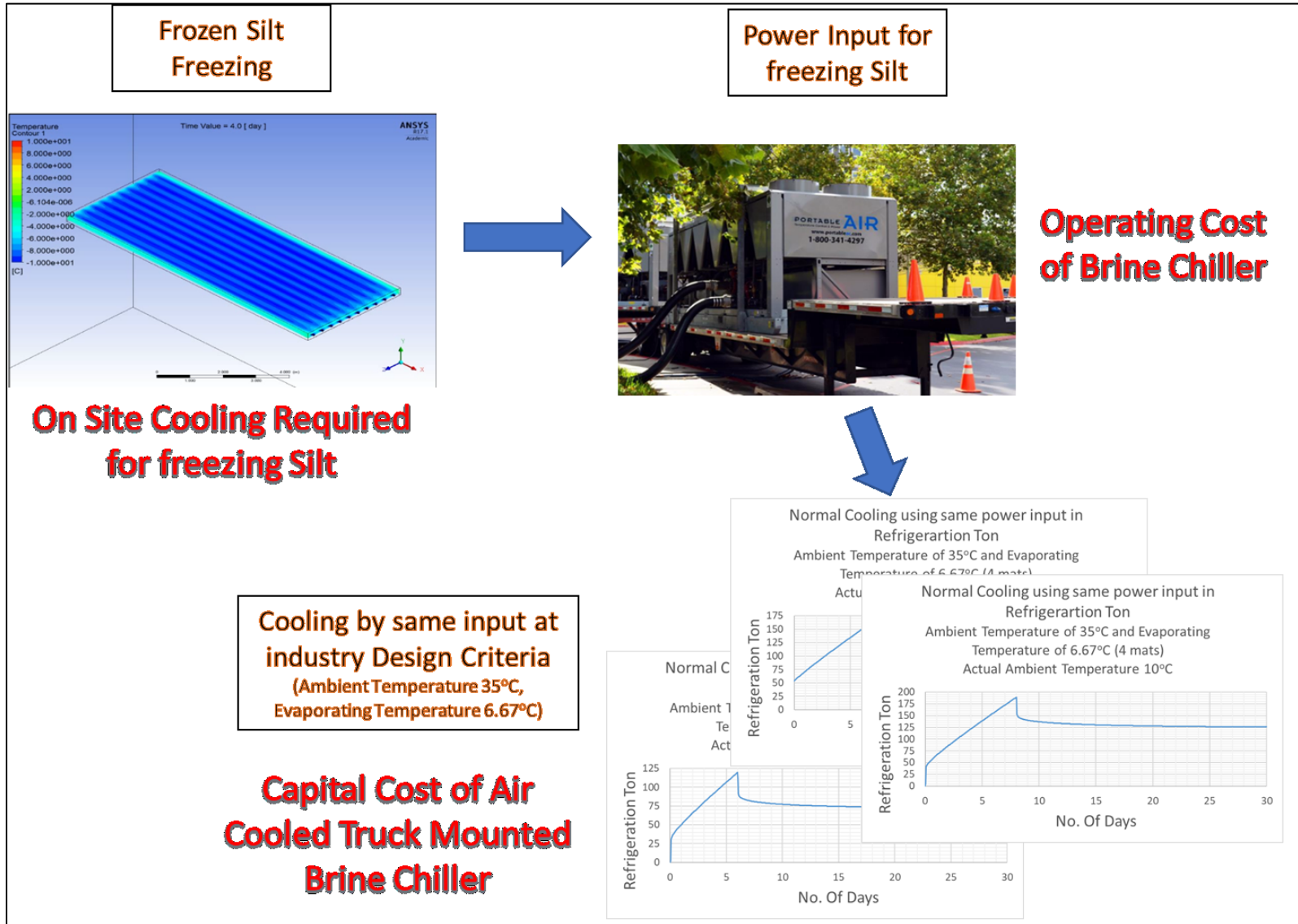
**Appendix F - Frozen Silt Mat (Liquid Nitrogen at 0°C Ambient Temperature, 30 days).**





20 Days				
30 Days				

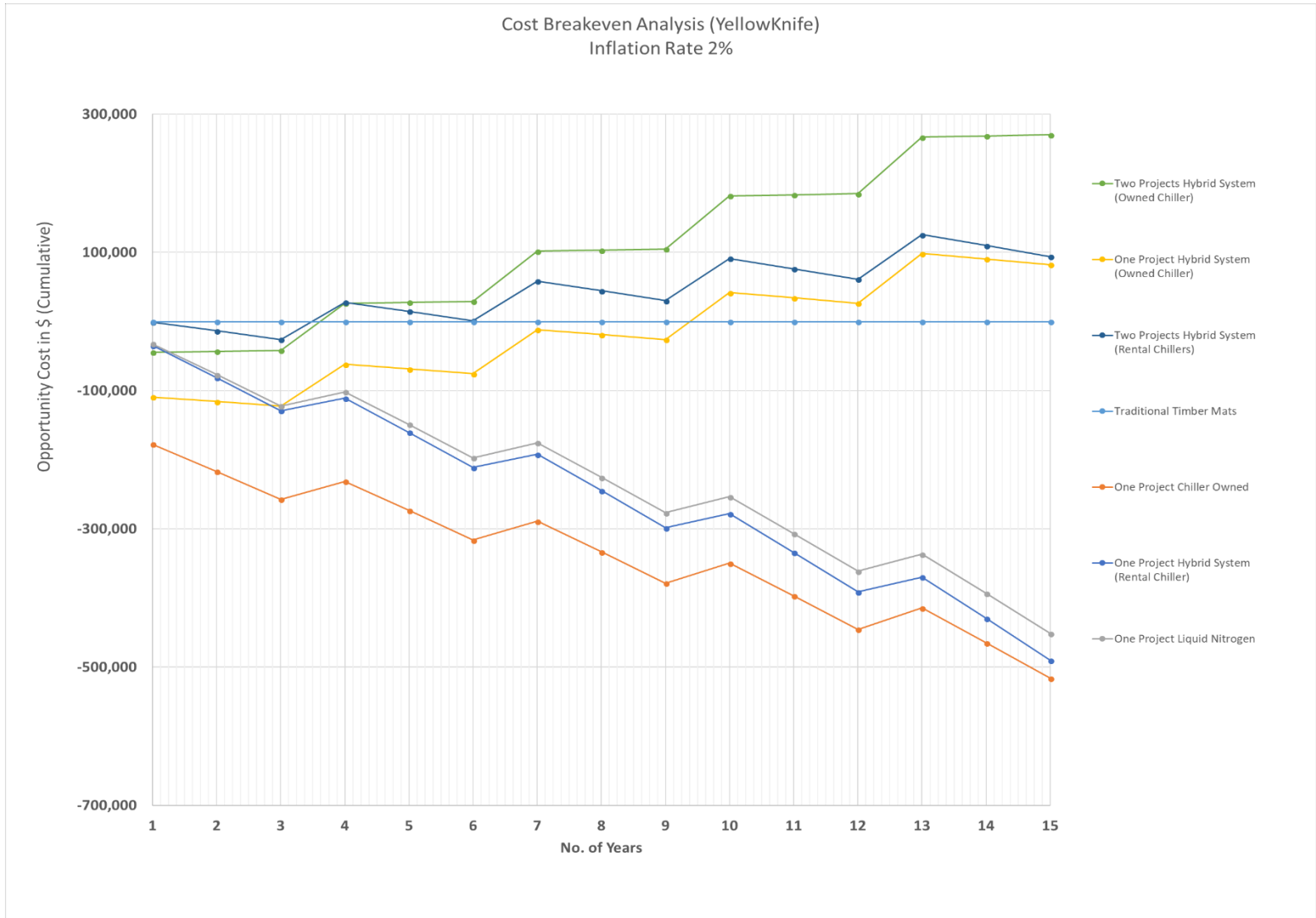
**Appendix G - Cost Estimation for Indirect Freezing (Brine chiller).**



**Appendix H - Cost Comparison – Traditional Mat versus Frozen Silt Mat.**

<b>Total Expenditures (\$)</b>															
Year	1	2	3	4	5	6	7	8	9	10	11	12	13	14	15
Traditional Timber Mats	138,023	216,414	296,404	444,751	528,040	613,028	770,644	859,137	949,436	1,116,900	1,210,922	1,306,863	1,484,790	1,584,687	1,686,623
One Project Chiller Owned	315,444	433,267	553,496	676,178	801,363	929,104	1,059,451	1,192,459	1,328,181	1,466,673	1,607,991	1,752,193	1,899,338	2,049,486	2,202,699
One Project Liquid Nitrogen	170,375	293,207	418,545	546,441	676,948	810,117	946,005	1,084,666	1,226,156	1,370,534	1,517,859	1,668,190	1,821,590	1,978,119	2,137,844
One Project Hybrid System (Owned Chiller)	247,327	332,054	418,509	506,729	596,750	688,608	782,340	877,985	975,582	1,075,171	1,176,793	1,280,488	1,386,299	1,494,270	1,604,445
One Project Hybrid System (Rental Chiller)	172,612	297,727	425,395	555,668	688,600	824,245	962,659	1,103,897	1,248,017	1,395,079	1,545,142	1,698,267	1,854,517	2,013,957	2,176,650
Two Projects Hybrid System (Owned Chiller)	182,625	259,643	338,233	418,426	500,256	583,757	668,961	755,904	844,622	935,150	1,027,525	1,121,786	1,217,970	1,316,118	1,416,268
Two Projects Hybrid System (Rental Chillers)	138,948	229,711	322,326	416,831	513,265	611,667	712,078	814,537	919,088	1,025,772	1,134,633	1,245,716	1,359,066	1,474,730	1,592,753
<b>Cost Difference Between Traditional Way and Ground Freezing Method (\$)</b>															
Traditional Timber Mats	0	0	0	0	0	0	0	0	0	0	0	0	0	0	0
One Project Chiller Owned	-177421	-216854	-257092	-231427	-273324	-316076	-288807	-333322	-378745	-349773	-397069	-445330	-414548	-464799	-516076
One Project Liquid Nitrogen	-32352	-76793	-122141	-101690	-148908	-197089	-175361	-225529	-276721	-253635	-306937	-361328	-336799	-393432	-451221
One Project Hybrid System (Owned Chiller)	-109304	-115640	-122105	-61979	-68710	-75580	-11696	-18848	-26147	41728	34129	26375	98491	90417	82178
One Project Hybrid System (Rental Chiller)	-34589	-81313	-128991	-110917	-160561	-211217	-192015	-244760	-298581	-278179	-334220	-391404	-369727	-429269	-490027
Two Projects Hybrid System (Owned Chiller)	-44602	-43229	-41829	26325	27783	29271	101683	103233	104814	181750	183397	185077	266820	268569	270354
Two Projects Hybrid System (Rental Chillers)	-925	-13297	-25922	27920	14774	1361	58566	44600	30348	91128	76289	61146	125724	109958	93869

**Appendix I - Cost Breakeven - Traditional Mat versus Frozen Silt Mat.**



**Appendix J – Research Path for Ice/Frozen Silt Mat.**

